T2R2 東京科学大学 リサーチリポジトリ
Science Tokyo Research Repository

論文 / 著書情報
Article / Book Information

題目(和文)	
Title(English)	Activation of Hydrogen Production in a Genetically Modified Cyanobacterium
著者(和文)	チョンスックサンテイクインアデイパー
Author(English)	Adipa Chongsuksantikul
出典(和文)	学位:博士（工学）, 学位授与機関:東京工業大学, 報告番号:甲第9765号, 授与年月日:2015年3月26日, 学位の種別:課程博士, 審査員:太田口　和久,ﾀﾝｻﾊﾟ ﾆﾁｬｸｰﾝ,伊東　章,大河内　美奈,吉川　史郎,下山　裕介
Citation(English)	Degree:, Conferring organization: Tokyo Institute of Technology, Report number:甲第9765号, Conferred date:2015/3/26, Degree Type:Course doctor, Examiner:,,,,,
学位種別(和文)	博士論文
Type(English)	Doctoral Thesis

Powered by T2R2 (Science Tokyo Research Repository)

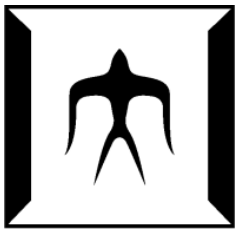

Graduate School of Science and Engineering

Department of Chemical Engineering

Doctoral Thesis

Activation of Hydrogen Production in a Genetically Modified Cyanobacterium

Ohtaguchi Laboratory

Adipa CHONGSUKSANTIKUL

12D51301

Acknowledgements

I would like to thank to my committee for their support and encouragement: Prof. Wiwut Tanthapanichakoon, Prof. Akira Ito, Prof. Mina Okochi, Assoc.Prof. Shiro Yoshikawa and Assoc.Prof. Yusuke Shimoyama.

My doctoral thesis completion could not have been accomplished without the support of my lab mates, Dr. Takashi Yamamoto, Matsuo Ryo and everyone in Ohtaguchi Laboratory for friendship and good time we have shared. I would like to thank to Assist. Prof. Asami Kazuhiro who always supports my experiment and gives me useful advices. I would like to express my gratefulness to my aunts, my grandmother and my friends. Thanks to my parents as well, Mr. and Mrs. Leethananont.

Finally, to my loving, respective and supportive sensei: Prof. Kazuhisa Ohtaguchi: my deepest gratitude for his valuable guidance, immense knowledge, extra time in the past 5 years. I would never expect better than this. I offer my sincere appreciation for the learning opportunities and financial support provided by Japanese Government.

Table of content

Nomenclature

c_A = acetate concentration	[µmol mL^{-1}]
c_E = ethanol concentration	[µmol mL^{-1}]
c_L = lactate concentration	[µmol mL^{-1}]
c_s = concentration of unreacted monosaccharides	[µmol mL^{-1}]
g = numbers of generations	[-]
g_C = numbers of generations from 0 h to t_C	[-]
G = numbers of generations from 0 h to t_f	[-]
I_o = photosynthetic photon flux density of incident light	[µmol $mL^{-1}s^{-1}$]
I_m = model parameter	[µmol $mL^{-1}s^{-1}$]
k = deactivation constant for H_2 production	[h^{-1}]
k^* = deactivation constant for H_2 production compared to control run	[-]
k_0 = rate constant of second order	[h^{-1}]
k_1 = rate constant of pseudo-first order	[h^{-1}]
k_i = model parameter of	[-]
k_G = degradation rate constant of glycogen content	[h^{-1}]
k_{OX} = rate constant of oxidant per dry weight	[h^{-1}]
k_{RED} = rate constant of reductant per dry weight	[h^{-1}]
K_d = specific death rate	[h^{-1}]
m_G = intracellular glycogen content per cell weight	[µmol mg^{-1}]
m^*_G = intracellular glycogen content per cell weight compared to control run	[µmol mg^{-1}]
m_GX = intracellular glycogen content per unit volume of reaction solution	[µmol mL^{-1}]
m_{OX} = number of moles of oxidant per dry weight (NAD(P)H)	[µmol mL^{-1}]
m_{RED} = number of moles of reductant per dry weight ($NAD(P)^+$)	[µmol mL^{-1}]
m_T = total amounts of NAD(P)H and $NAD(P)^+$ per dry weight	[µmol mL^{-1}]
q_{CO2} = specific CO_2 fixation rate	[µmol mL^{-1} h^{-1}]
q^*_{CO2} = specific CO_2 fixation rate compared to control run	[-]
q_{H2} = specific H_2 production rate	[µmol mL^{-1} h^{-1}]
q^*_{H2} = specific H_2 production rate compared to control run	[-]
q_S = specific monosaccharide consumption rate	[µmol mL^{-1} h^{-1}]
r_A = acetate production rate	[µmol mL^{-1} h^{-1}]
r_{H2} = H_2 production rate	[µmol mL^{-1} h^{-1}]

r_L = lactate production rate [µmol mL^{-1} h^{-1}]

r_S = monosaccharide consumption rate [µmol mL^{-1} h^{-1}]

r_X = growth rate [mg mL^{-1} h^{-1}]

R_G = specific production rate of endogenous glucose [µmol mg^{-1} h^{-1}]

$-R_G$ = specific consumption rate of endogenous glucose [µmol mg^{-1} h^{-1}]

R^*_G = specific production rate of endogenous glucose compared to control run [µmol mg^{-1} h^{-1}]

R_{G1} = specific production rate of endogenous glucose in logarithmically growing cells [µmol mg^{-1} h^{-1}]

R_{G2} = specific production rate of endogenous glucose in resting cells [µmol mg^{-1} h^{-1}]

R_{GAP} = generation rate of glyceraldehyde [µmol mg^{-1} h^{-1}]

R_GX = production rate of endogenous glucose [µmol mL^{-1} h^{-1}]

$-(R_GX)$ = consumption rate of endogenous glucose [µmol mL^{-1} h^{-1}]

t = time [h]

t_2 = doubling time [h]

t_C = critical time [h]

t_f = time in stationary phase [h]

t_{SHT} = time of acceleration (shift) [h]

X = cell mass concentration [mg mL^{-1}]

y_{H2} = total H_2 production per unit volume of reaction solution [µmol mL^{-1}]

$y_{H2,f}$ = attainable level of H_2 per culture volume Eq.(2.18) [µmol mL^{-1}]

$y^*_{H2,f}$ = attainable level of H_2 production per culture volume of reaction solution compared to control run [-]

Y = yield factor [-]

$Y_{A/G}$ = acetate production yield [-]

$Y_{L/G}$ = lactate production yield [-]

$Y_{H2/G}$ = H_2 production yield [-]

$Y_{X/S}$ = growth yield on monosaccharides [-]

σ_{HG} = specific activity of NiFe-hydrogenase [-]

ϕ = growth kinetic [-]

Subscript

0 = initial state

1 = at 96 h or 120 h (final time of experiment)

f = final state

Chapter 1

Introduction

1.1 Hydrogen production pathway

Hydrogen energy for sustainable development: Global energy consumption has increased since the worldwide spreading of industrial revolution doctrine. The fossil fuel combustion results in carbon dioxide (CO_2) emission that has led to an environmental problem. The increased concentrations of key greenhouse gases are a direct consequence of human activities. Man-made greenhouse gases accumulated in the atmosphere produce higher net warming by strengthening the natural "greenhouse effect". CO_2 concentrations in the atmosphere have been increasing over the past century compared to the rather steady level of the pre-industrial era. Atmospheric CO_2 level for November 2014 is 397.13 ppm (McGee, 2014).

CO_2 emission will continue to increase, as a result of continued growing consumption of fossil fuels in some of the large developing countries such as China and India. The link between climate change and energy is a part of a larger challenge of sustainable development. Since 1870, CO_2 emissions from fuel combustion have risen exponentially. Growing world energy demand from fossil fuels plays a key role in the upward trend in CO_2 emissions. Since the Industrial Revolution, annual CO_2 emissions from fuel combustion dramatically increased from near zero to more than 8.7 Pg y^{-1} ($P=10^{15}$; y=year) in 2008 (DOE-Carbon Dioxide Information Analysis Center, 2011). About 20% of total CO_2 emission is produced from burning gasoline for transportations. Primary consumption of energy is based on coal and oil, this kind of fossil fuel will inevitably deplete within the next century. This prompts us as urgent need to find a replacement for fossil fuel phase out era.

The most sustainable way to support the world economic growth in 21^{st} century is focusing on the development of renewable energy including solar energy, wind energy, geothermal energy, bioenergy, hydropower, ocean energy, green power and hydrogen (H_2) and fuel cells. Among them, considerable attention has been paid by automobile industry on hydrogen energy since hydrogen is high in energy (**Table 1.1**) and combustion of H_2 generates almost no pollution. Hydrogen was discovered in 1766 by Cavendish in UK. The element hydrogen is the simplest atom consisting of one proton and one electron. It is abundant in the space. Different from the distribution of element, molecular hydrogen is hardly observed in nature of the earth. Hydrogen atom always exists combining with other elements. Hydrogen represents very high heat of combustion per weight. Hydrogen stores about 3.02 times the energy per unit weight as gasoline. Due to the clean byproduct of hydrogen fuel, NASA has been utilizing liquid

hydrogen to launch the space shuttles since 1970. H_2 is one of the new sources of energy to be used as an alternative energy after deprivation of crude oil.

Hydrogen fuel vehicles: Hydrogen gas can be used as energy-carrier which can be installed into vehicle. **Figure 1.1** illustrates (a) H_2 fuel vehicle, (b) H_2 gas stand and (c) off-site liquid H_2 storage. The existing technology of fuel cell, storage and safety can support the practical use of hydrogen energy. Since the molecular weight of hydrogen is very low, the heat of combustion per mole shows an inverse relation. Liquid volume of hydrogen fuel is 3.47 times that of gasoline for a given amount of energy. A typical fuel cell vehicle (FCV) in Japan (Fig.1.1(a)) has a 156 L tank with upper limit pressure of 70 MPa (=109200L at 101300 Pa=4880 mole) for hydrogen fuel that can support a fuel of 1570MJ to drive 700 km (http://is-factory.com/post-4056/, 2014). Mileage of hydrogen fuel is 6.42 (=700/109) km m^{-3}. Price of hydrogen fuel is 100-150 yen Nm^{-3}. Fuel cost of hydrogen is 17-23 yen km^{-1}. In December 2014, the first industrial production of liquid H_2 (2.5 Mmol d^{-1}) was started in Japan. It can support 1000 FCVs. Expected prices are 30 yen per Nm^{-3} by 2025 and 20 yen per Nm^{-3} by 2050. A dispenser for H_2 is illustrated in Fig.1.1 (b). A typical station shown in Fig.1.1(c) has 10 m^3 (=708.5kg = (10 m^3)(70.85 kg m^{-3})=354000mole) liquid H_2 storage. That is 72.5(354000/(4880)) times that is required for 70MPa FCV. Gasoline fuel vehicle has a 60 L tank to support 400 km drive. Mileage of gasoline fuel is 10-15 km L^{-1}. Price of gasoline is 160 yen L^{-1}. Fuel cost of gasoline is 10-16 (=160/(10-15)) yen km^{-1}. H_2 can also be used efficiently for electricity generation due to prompted developed fuel cell technology (Momirlan and Veziroglu 2002).

Current industrial consumption of hydrogen: The current annual production of H_2 is about 55 Tg (=55 million tons). Ammonia synthesis utilizes about a half of industrially generated H_2. Petrochemical industry consumes another half to reduce heavy sources to lighter fractions. Resources of H_2 are 48% from natural gas, 30% from oil, 18% from coal and 4% from electrolysis of water. Sources are either fossil fuels or non-fossil fuels. The dominant source of current industrial production of H_2 is fossil fuels. If the number of the H_2 fueled vehicles increases, H_2 manufacturing industry will face the problem of supply of feedstock.

Available technologies for hydrogen production: **Figure 1.2** shows the overview of H_2 production technologies. Arcs shown by red are current main supply chain of H_2. Hydrogen production methods are classified into the methods from renewable sources (Appendix-1) and those from non-renewable sources (Appendix-2).

Technology with non-renewable sources includes (1) steam methane reforming, (2) partial oxidation of hydrocarbons, and (3) coal gasification. Technology with non-renewable sources is established and

represents a reasonable cost of H_2 for ammonia synthesis and heavy source treatment, however, currently we have found a great deal of difficulty in reproducing the same result in supporting H_2 fueled society since fuel market size is huge and production of H_2 from non-renewable sources always increases a cost of non-renewable source fuel. The additional problem of this pathway is the evolution of large volume of CO_2 from non-renewable resources. Although this technology can be applied to drive initial H_2 fueled society, there will be an urgent problem to solve those problems.

Technology with renewable sources includes (1) biomass gasification, (2) biomass pyrolysis, (3) electrolysis, (4) biocatalyzed electrolysis, (5) thermolysis, (6) photocatalytic water splitting, (7) dark fermentation, (8) direct biophotolysis, and (9) indirect biophotolysis. Technology with renewable sources is promising to solve those problems. Within technologies shown in Appendix-2, electrolysis, biocatalyzed electrolysis, photocatalytic water splitting method and thermolysis require the supply of electric power. Hence technology development of power plants without non-renewable resources is the underlying premise of such technologies. Biomass gasification and biomass pyrolysis generate CO_2, however the amount of CO_2 in this evolution is less than the amount of CO_2 assimilated by photosynthesis. Production of fuel H_2 requires the constant supply of H_2 and the huge amount supply, hence biomass gasification and biomass pyrolysis technologies face to solve these problems.

Other technologies shown in Appendix-2 utilize the microbial metabolism to generate H_2. The metabolism for H_2 production is classified as dark fermentation, direct biophotolysis and indirect biophotolysis. Dark fermentation of glucose to lactate by genetically modified anaerobic bacterium *Escherichia coli* generates 2 moles H_2 per mole of reacted glucose (**Figure A2.1**). The attainable level of H_2 for 120 h incubation reached 1.8 μmol mL^{-1}. One drawback of dark fermentation is the requirement of organic substrate for cell growth and metabolism.

A number of studies on direct or indirect biophotolysis have been reported beginning with the first work of Gaffron (Gaffron, 1939). Gaffron observed light-induced H_2 production (direct biophotolysis) in unicellular green algae *Scenedesmus* after dark incubation (Eq.(A2.7)). As shown in Appendix-2, unicellular green algae, purple non-sulfur bacteria (PNSB) and cyanobacteria have been tested for direct biophotolysis H_2 production. Cyanobacteria have been a model for photosynthesis-related H_2 production. Cyanobacteria are photosynthetic organism, acquiring energy from light, carbon from CO_2 and nitrogen from N_2, nitrate or ammonium ion. N_2-fixing cyanobacteria have nitrogenase and non N_2-fixing cyanobacteria have a bidirectional NiFe-hydrogenase. **Figure 1.3** shows an overview of cyanobacterial organization in the presence of light. Due to this light reaction, membrane of cyanobacteria under the

light actively generates NADPH, ATP and electrons, a large portion of which is utilized at the Calvin cycle to fix CO_2.

Figure 1.4 illustrates the Calvin cycle that is light-independent. The key enzyme is ribulose-1,5-bisphosphate carboxylase/oxygenase (RuBisCo) that fixes CO_2. The sum of the reactions in the Calvin cycle is given by

$$3CO_2+6NADPH+5H_2O+9ATP$$

$$\rightarrow \text{glyceraldehyde-3-phosphate}+2H^++6NADP^++9ADP+8Pi \quad (1.1)$$

The absorption of light energy at PSII (photosystem II) of thylakoid membrane (light-dependent reaction) by direct biophotolysis splits water and generates oxygen (O_2), H^+ and electron:

$$2H_2O \rightarrow O_2+4H^++2e^- \quad (1.2)$$

Electrons generated at thylakoid membrane during illumination are reduced in the form of NADPH by the Calvin cycle. Even though, solar energy conversion to electron production is high, H_2 production is inhibited by O_2 since O_2 generation during photosynthesis suppress NiFe-hydrogenase from H_2 production. A reversible hydrogenase accepts electron from reduced ferrodoxin to generate H_2 by the general reaction (Eq. (A2.8)).

Table 1.2 lists the H_2 production rate of non N_2-fixing cyanobacteria under the direct biophotolysis. The maximum H_2 production rate shown in this table is 1.38 μmol mg-chl a^{-1} h^{-1} that was obtained in run with *Gloebacter* PCC 7421. Chlorophyll a ($C_{55}H_{72}O_5N_4Mg$; molecular weight, 892.3 μg μmol^{-1}) content is variously reported. Cyanobacterium *Spirulina maxima* represents chlorophyll a content of 13.1 μg mg-DCW^{-1} at pH 9 and 9.5 μg mg-DCW^{-1} at 5 klx light intensity (Pandey and Tiwari,2010). Chlorophill a content and cell volume of unicellular cyanobacterium *Synechocystis* sp. strain PCC6803 for 72.5M cells mL^{-1} (OD_{750}=0.5) in a report (Lea-Smith et al., 2014) is 9.69 amol μm^{-3} and 4.34 μm^3.If dry cell weight concentration is 0.185 mg mL^{-1}, then chlorophyll a content is 14.7 μg mg^{-1} (= (892.3)(9.69)(4.34)(10^{-18})(10^6)(72.5)(10^6)/0.185). If chlorophyll a content is 14.7 μg mg^{-1}, then above highest H_2 production is 0.0932 μmol mg^{-1} h^{-1}.

Three years after the observation of direct biophotolysis, Gaffron and Rubin first observed H_2 evolution in indirect biophotolysis by adapting the green alga *Scenedesmus obliquus* in dark anaerobic condition (Gaffron and Rubin 1942). **Figure 1.5** shows indirect biophotolysis to generate H_2 in cyanobacteria (Carrieri, 2010). Different from green alga, cyanobacteria are reported to be organisms that prefer a dark auto-fermentation that follows the light-dependent photosynthetic stage to produce hydrogen. A 5-fold increase in H_2 production in *Synechococcus* sp. strain PCC7002 by eliminating genes coding for lactate dehydrogenase and pyruvate-ferredoxin oxidoreductase was achieved (McNeely, 2011). **Table 1.3** lists the typical results of previous works.

From Tables 1.2 and 1.3, highest H_2 production rate in previous works is found to be 0.0190 µmol mg^{-1} h^{-1} from *Synechococcus* PCC 6830. Indirect biophotolysis is promising for H_2 production because there is no O_2 generation to suppress hydrogenase. The specific H_2 evolution activities of bidirectional hydrogenases are higher than those of nitrogenase-based H_2 production. Therefore systems based on bidirectional hydrogenases present the most likely approach to practical development.

For indirect biophotolysis, photosynthesis stage is important to prepare cellular states suitable for dark anaerobic H_2 production. If this technology is promising, cyanobacterial fuel is renewable, clean and sustainable for future. It can be genetically modified to produce valuable substance such as isoprene, ethanol, sugar, and lactate (Ducat et al. 2011). However, several obstacles must be overcome to put cyanobacteria to be economically commercialized. From recent knowledge, cyanobacteria have been known as origin of photosynthesis organism. Fossil stromatolites (microbial communities mat) can be dated back to 3.5 Gya (Giga years ago) (Blankenship 1992). Photosynthetic organisms may have been among the very earliest life forms on the primitive earth. Global oxygen accumulation in the atmosphere and oceans are from production of O_2 by photosynthesis. Photosynthesis of cyanobacteria still recently plays a major role in the conversion of carbon dioxide to biological energy storage materials on earth. Photosynthesis efficiency calculated by the combination of energy losses in light absorption and the initial chemical reactions results in a maximal overall energetic efficiency estimated at about 11% (Brenner et al. 2006) which is much higher than plants (mostly less than 1%)

To create a general method toward increasing H_2 production utilizing model species is also important. Cyanobacteia are known to produce H_2 mainly via indirect biophotolysis. Unicellular cyanobacterium *Synechosystis* cells work as a solar power collector through bioconversion of ambient CO_2 into cell constituting materials. Exposure of cells to dark anaerobic condition or sulfur-limiting condition triggers the conversion of energy-rich components to energy-lean compounds and H_2. This allows the formation of secondary products such as ethanol, acetate, lactate and succinate. Thus, this indirect biophotolysisis

consisted of two stages in series, photosynthesis for carbohydrate storage, and cells switched into specific condition allowing for stored carbon to be turned into H_2 production.

1.2 Hydrogen production in a glucose tolerant mutant of unicellular cyanobacterium *Synechocystis* sp. strain PCC 6803 through indirect biophotolysis

Besides the works of N_2-fixing cyanobacteria, indirect biophotolysis to produce H_2 has been studied utilizing non N_2-fixingcyanobacteria.

Figure 1.6 is a method of indirect biophotolysis for H_2 production in *Synechocystis* sp. strain PCC 6803. It was shown to be important to eliminate nitrate ion when photosynthetically grown cells were inoculated into dark anaerobic condition.

Unicellular cyanobacterium *Synechocystis* sp. PCC 6803 is a fresh-water and non-nitrogen fixing organism. Among cyanobacteria, *Synechocystis* sp. PCC 6803 is the most well studied species and, defined its robust growth characteristic, therefore the organism has been selected for this work. This study concerned with the hydrogen production on a bidirectional NiFe-hydrogenase (HoxEFUYH hydrogenase) in the Glucose Tolerance strain (GT) of cyanobacterium *Synechocystis* sp. strain PCC 6803. H_2 production on bidirectional NiFe-hydrogenase is shown by

$$NAD(P)H + H^+ \rightarrow NAD(P)^+ + H_2 \quad (1.3).$$

When reductive form of co-enzyme NADH or NADPH binds to NiFe-hydrogenase, it transfers reductive potential to NiFe-hydrogenase, which then transfer electrons to proton. Protons then change to molecular hydrogen.

This strain's genome has been fully sequenced and all of its open reading frames (ORFs) have been annotated (Kaneko et al. 1996). Database can be retrieved on line. It is naturally competent for DNA transformation and can take up naked DNA as plasmids or as linear DNA for homologous recombination. GT strain is able to consume extracellular glucose in dark anaerobic condition which allows an observation in H_2 enhancement and cell growth in dark anaerobic condition (Cournac et al. 2004; Yamamoto et al. 2012b).

1.3 Objectives of this research

Previous works have suggested that hydrogen production is largely limited by availability of intracellular reduction equivalents in the form of NAD(P)H rather than hydrogenase availability for cells. Methyl viologen is used in the experiment as an infinite reductant dissolving in cell solution; H_2 is produced at high rate. A recent work has argued if ferrodoxin is also a prime reductant to NiFe-hydrogenase in *Synechocystis* sp. strain PCC 6803 (Gutekunst et al. 2014). This knowledge supports a H_2

production enhancement method of decreasing intracellular reductant consumption. In Tables 1.2 and 1.3. *Synechocystis* sp. strain PCC 6803 is not a top range in H_2 producer; however, its well research works and complete DNA sequence have allowed us to handle it.

If manipulation of redox homeostasis is the keyword to elevate H_2 production, a roadmap to create a method to increase H_2 production with unicellular cyanobacteria is outlined as shown in **Figure 1.7**. Availability of this roadmap is confirmed in this study where a glucose tolerant mutant of unicellular cyanobacterium *Synechocystis* sp. strain PCC6803 (GT strain) is utilized as a model organism. Indirect biophotolysis is performed in which cells of GT strain are photoautotrophically grown in the first stage, and then cells are dark anaerobically incubated in HEPES buffer solution for H_2 production. To activate H_2 production in GT strain, this study focuses on the dark anaerobic H_2 production in GT strain and derivatives. In vew of three platforms of research in Fig.1.7, the primary purposes of this study are:

(1) to select a monosaccharide additive to increase initial amount of reductive compounds,

(2) to formulate a mathematical model to interpret kinetics for H_2 production,

(3) to characterize photoautotrophic growth phase effect on the subsequent H_2 production,

(4) to manipulate DNA to supply more electrons to NiFe-hydrogenase,

and

(5) to integrate three platforms to create a method to activate H_2 production

Significance of cyanobacterial H_2 production is also briefed based on empirical findings.

1.4 Outline of this thesis

Outline of this thesis is shown in **Figure 1.8**. The thesis is composed with 6 chapters. Contents of the chapters are briefed as follows:

Chapter 1: Introduction

Objectives and scopes of this research is described.

Chapter 2: Monosaccharide Effects on Hydrogen Production

To define the baseline of this research, dark anaerobic H_2 production in GT strain in HEPES buffer solution is first studied. A mathematical model to interpret kinetics for H_2 production is formulated. Second, to increase cellular content of NAD(P)H, which is normally generated by glycolysis or glycogen breakdown, H_2 production in the presence of monosaccharide is studied. Tested monosaccharides are glucose, fructose, galactose, mannose and xylose. Relations between the production of H_2 and the

consumption of monosaccharide, consumption or production of endogenous glucose and dry cell weight and production of lactate, acetate, succinate and ethanol are analyzed. Second and third mathematical models to predict attainable level of the number of moles of H_2 per culture volume from initial H_2 production rate and to relate final level of the number of moles of H_2 per culture volume and that of endogenous glucose are developed.

Chapter 3: Growth Phase Effects on Hydrogen H_2 Production

To find out the effect of cellular state, prior to dark anaerobic incubation, on H_2 production, cells from logarithmic growth phase, late-logarithmic growth phase and stationary phase are utilized for dark anaerobic fermentation. Cellular state during photosynthesis is analyzed by monitoring dry cell weight reproduction and endogenous accumulation. The activity of the Calvin cycle that is a big electron sink is evaluated for cells from each growth phase.

Chapter 4: Genetic Modification Effects on Hydrogen Production

To remove pathways that compete NAD(P)H with NiFe-hydrogenase, metabolic engineering approach is made. The mutant defective of the genes coding for D-lactate dehydrogenase (Δddh mutant) and that defective of the genes coding for both alcohol dehydrogenase and D-lactate dehydrogenase (ΔadhΔddh mutant) are constructed. Dark anaerobic H_2 production of newly constructed mutants are compared with that of GT strain in HEPES buffer solution without or with glucose.

Chapter 5: Fructose Effects on Hydrogen Production

Studies prior to this chapter select fructose as a key additive monosaccharide to elevate dark anaerobic H_2 production. First, effect of fructose concentration on dark anaerobic H_2 production in GT strain is investigated. Mathematical model for H_2 production kinetics is re-evaluated. Second, combined effect of fructose addition and genetic modification is studied. Third, conceptual design for dark anaerobic bioreactor to produce fuel H_2 is challenged. Integration of all data has been concluded to draw a protocol for developing a dark anaerobic H_2 production enhancement method with unicellular cyanobacterium.

Chapter 6: Concluding Remarks

The overall conclusion of this thesis and future aspects of this study are described.

Table 1.1 Heat of combustion for fuels

Fuel	Heating value		Molecular weight	Liquid density	Liquid volume per combustion energy
	kJ g^{-1}	kJ mol^{-1}	g mol^{-1}	kg L^{-1}	mL kJ^{-1}
Hydrogen	141.8	283.6	2	0.071	0.0993
Gasoline	47.0	4700	100	0.745	0.0286
Petroleum diesel	43.1	1985	46.07	0.832	0.0279
Ethanol	29.7	1370	46	0.789	0.0427
Propane	49.9	2220	44	0.582	0.0344
Butane	49.5	2877	58.12	0.601	0.0337
Wood	15.0	-	-	-	-
Coal(Lignite)	28.5	-	-	-	-
Coal(Anthracite)	35.3	-	-		-
Natural gas	54	866	16.04	0.46	0.0403

Table 1.2 Summarization of literature survey of direct biophotolysis H_2 production in non-nitrogen-fixing unicellular cyanobacteria (Dutta et al. 2005).

Cyanobacteria	Maximum H_2 evolution rate (calculated in μmol mg-DCW^{-1} h^{-1})	Growth in photosynthesis	H_2 evolution assay condition	Reference
Synechococcus PCC 602	0.66 μmol mg chl a^{-1}h^{-1} (0.00970)	Air; photon fluence rate 20 μE m^{-2} s^{-1}	Ar with CO (13.4 μmol); photon fluence rate 20–30 μE m^{-2} s^{-1}	Howarth and Codd, 1985
Synechococcus PCC 6307	0.02 μmol mg chl a^{-1}h^{-1} (0.000294)	Air; photon fluence rate 20 μE m^{-2} s^{-1}	Ar (100%) with photon fluence rate 20–30 μE m^{-2} s^{-1}	Howarth and Codd, 1985
Synechoccus PCC 6301	0.09 μmol mg chl a^{-1}h^{-1} (0.00132)	Air; photon fluence rate 20 μE m^{-2} s^{-1}	Ar with C_2H_2 (1.34 μmol); fluence rate 20–30 μE m^{-2} s^{-1}	Howarth and Codd, 1985
Microcystis PCC 7820	0.16 μmol mg chl a^{-1}h^{-1} (0.00235)	Air; photon fluence rate 20 μE m^{-2} s^{-1}	Ar with CO (13.4 μmol), C_2H_2 (1.34 μmol); photon fluence rate 20–30 μE m^{-2} s^{-1}	Moezelaar et al.,1996
Gloebacter PCC 7421	1.38 μmol mg chl a^{-1}h^{-1} (0.0203)	Air; photon fluence rate 20 μE m^{-2} s^{-1}	Ar with CO (13.4 μmol), C_2H_2 (1.34 μmol); photon fluence rate 20–30 μE m^{-2} s^{-1}	Moezelaar et al., 1996
Synechocystis PCC 6308	0.13 μmol mg chl a^{-1}h^{-1} (0.00191)	Air; photon fluence rate 20 μE m^{-2} s^{-1}	Ar with CO (13.4 μmol), C_2H_2 (1.34 μmol); photon fluence rate 20–30 μE m^{-2} s^{-1}	Howarth and Codd, 1985
Synechocystis PCC 6714	0.07 μmol mg chl a^{-1}h^{-1} (0.00103)	Air; photon fluence rate 20 μE m^{-2} s^{-1}	Ar with CO (13.4 μmol); photon fluence rate 20–30 μE m^{-2} s^{-1}	Howarth and Codd, 1985
Aphanocapsa montana	0.40 μmol mg chl a^{-1}h^{-1} (0.00588)	Air; photon fluence rate 20 μE m^{-2} s^{-1}	Ar (100%); photon fluence rate 20–30μE m^{-2} s^{-1}	Howarth and Codd,1985

Table 1.3 Summarization of literature survey of indirect biophotolysis H_2 production in non-nitrogen-fixing unicellular cyanobacteria

Cyanobacteria	Maximum H_2 evolution rate (calculated in μmol mg-DCW^{-1} h^{-1})	Growth in photosynthesis	H_2 evolution assay condition	Reference
Synechococcus PCC 6830	0.26 μmol mg chl a^{-1}h^{-1} (≈0.00382 μmol mg^{-1} h^{-1})	Air; photon fluence rate 20 μE m^{-2} s^{-1}	Ar with CO (13.4 μmol), C_2H_2 (1.34 μmol); darkness.	Howarth and Codd, 1985
Synechococcus leopoliensis	0.130 μmol mL^{-1} h^{-1}	6% CO_2 in air, MDM medium, 313K, 12klx	DEC solution without nitrate, darkness	Ohtaguchi et al., 1995
Synechocystis PCC 6803	0.0190 μmol mg^{-1} h^{-1}	6% CO_2 in air, BG-11medium、adapted to BG-11 without nitrate source for 24 h, 100 μmol m^{-2} s^{-1}	N_2 (100%); 50 μmol HEPES solution; darkness	Yamamoto et al., 2012a

(a) (b)

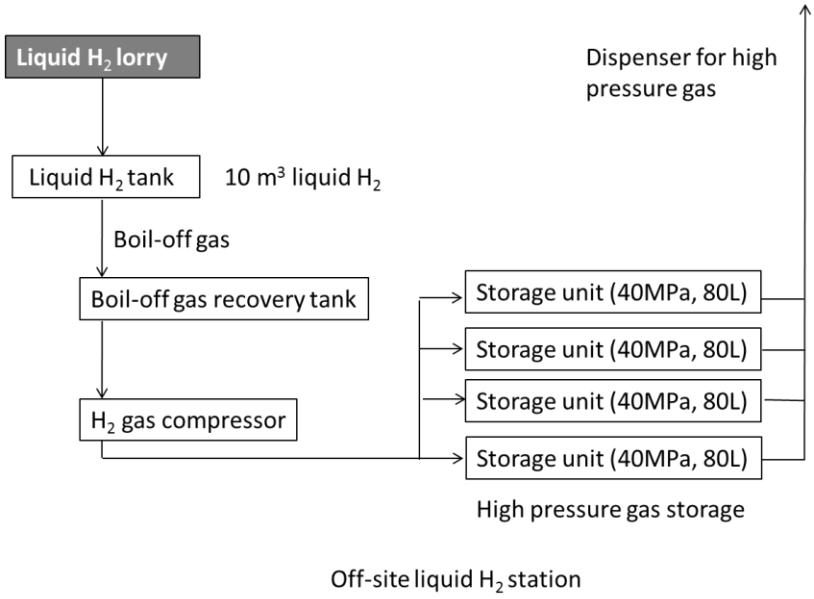

Figure 1.1 Hydrogen fuel vehicle and gas station

(a) Hydrogen fuel vehicle, http://www.h2euro.org/wp-content/uploads/2014/08/toyota-fuel-cell.jpg

(b) Hydrogen gas stand, http://i.ytimg.com/vi/64NaZNh3O_w/0.jpg

(c) Off-site liquid H_2 station, modified graph from http://www.jari.or.jp/portals/0/jhfc/e/station/kanto/ariake.html

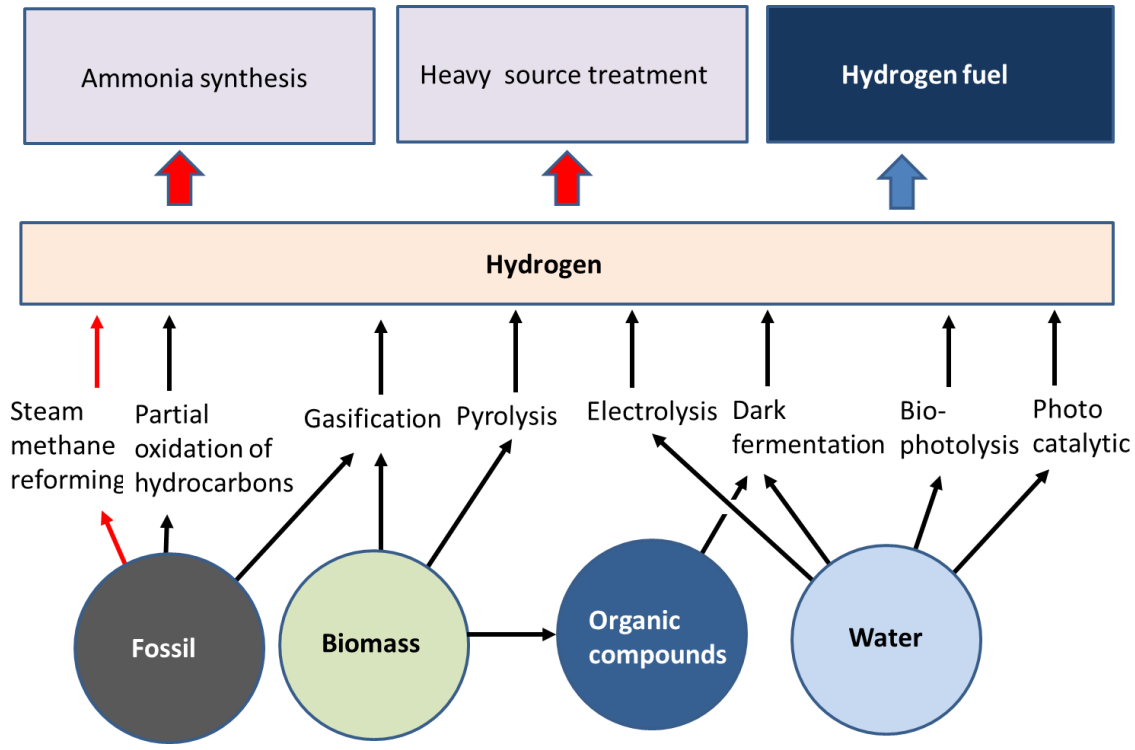

Figure 1.2 Overview of ongoing hydrogen production technologies

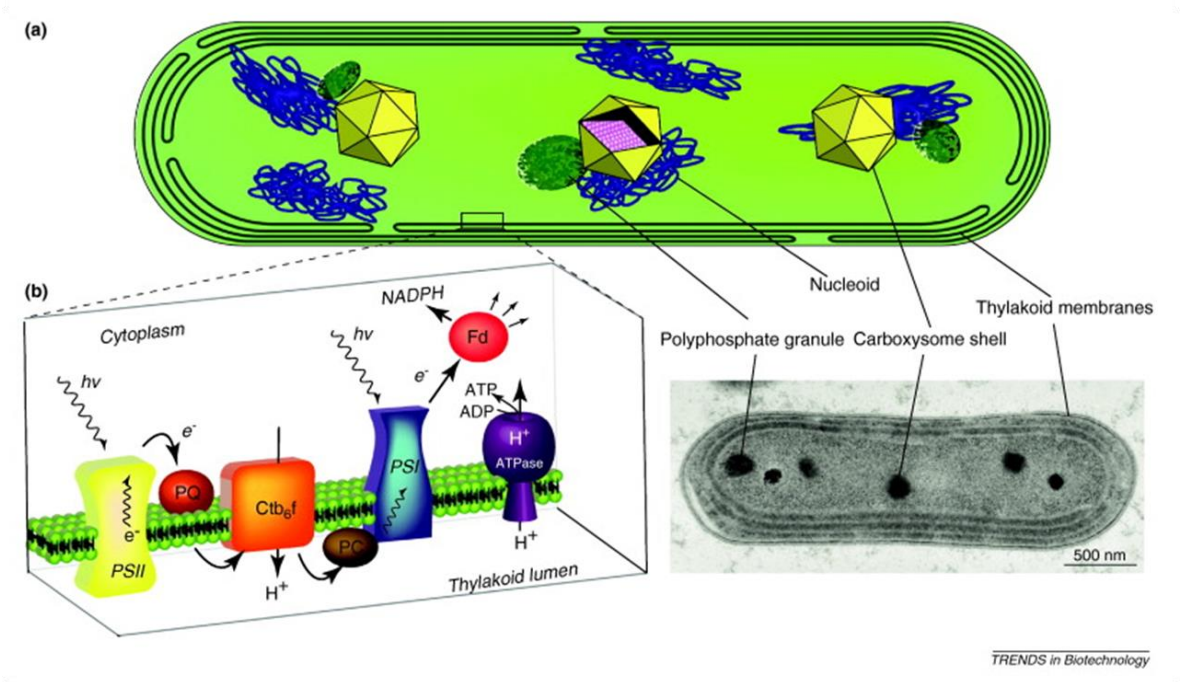

Figure 1.3 Outline of cell organization of unicellular cyanobacterium *Synechococcus elongates* (Ducat et al. 2011)

(a) Cross-section of a cell. Carboxysome shell contains CO_2 fixation machinery. Mutiple chromosomes, which diffuse throughout the cytoplasm, exist in a cell. Thylakoid membrane absorbs radiant energy.

(b) Electron transport chain. PSII (Photosystem II) absorbs 680 nm light to oxidize and split water molecules, generating electrons, protons and O_2. Electron potential is lowered. PQ (plastoquinone) receives electrons from PSII and transfer them to the cytochrome b6-f complex. Electrons are then passed to PSI (photosystem I) through PC (plastocyanin). PSI absorbs 700 nm light and lowers the electron potential. FNR (ferredoxin-NADP reductase), which receives electrons from PSI through Fd (ferredoxin), produces NADPH from $NADP^+$ and proton. Proton gradient drives ATP synthase to generate ATP from ADP and Pi. Protons in the thylakoid lumen are returned to the cytoplasm through ATP synthase.

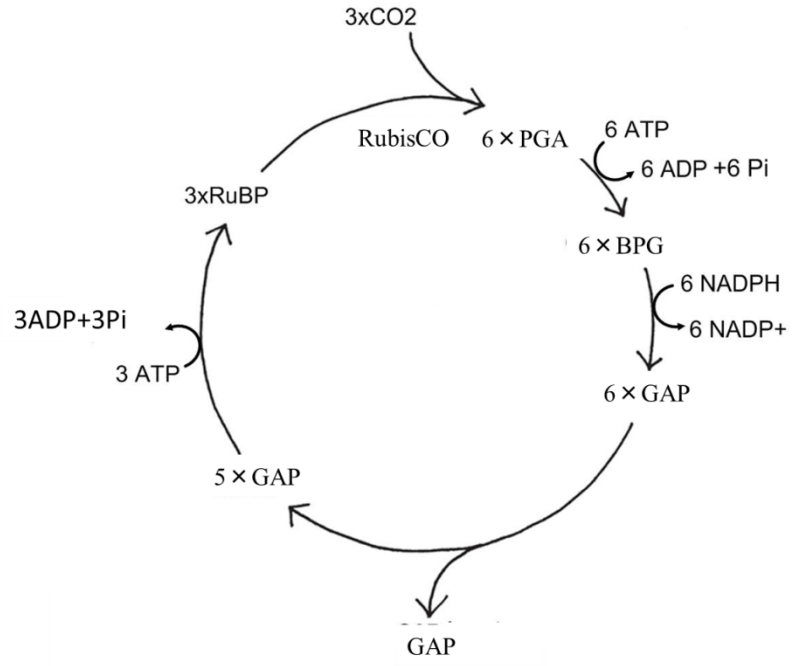

Figure 1.4 The Calvin cycle

RuBP,ribulose-1,5-bisphosphate; GAP,glyceraldehyde 3-phosphate; PGA, 3-phosphoglycerate; BPG,1,3-bisphosphoglycerate; RubisCO, ribulose-1,5-bisphosphate carboxylase/oxygenase

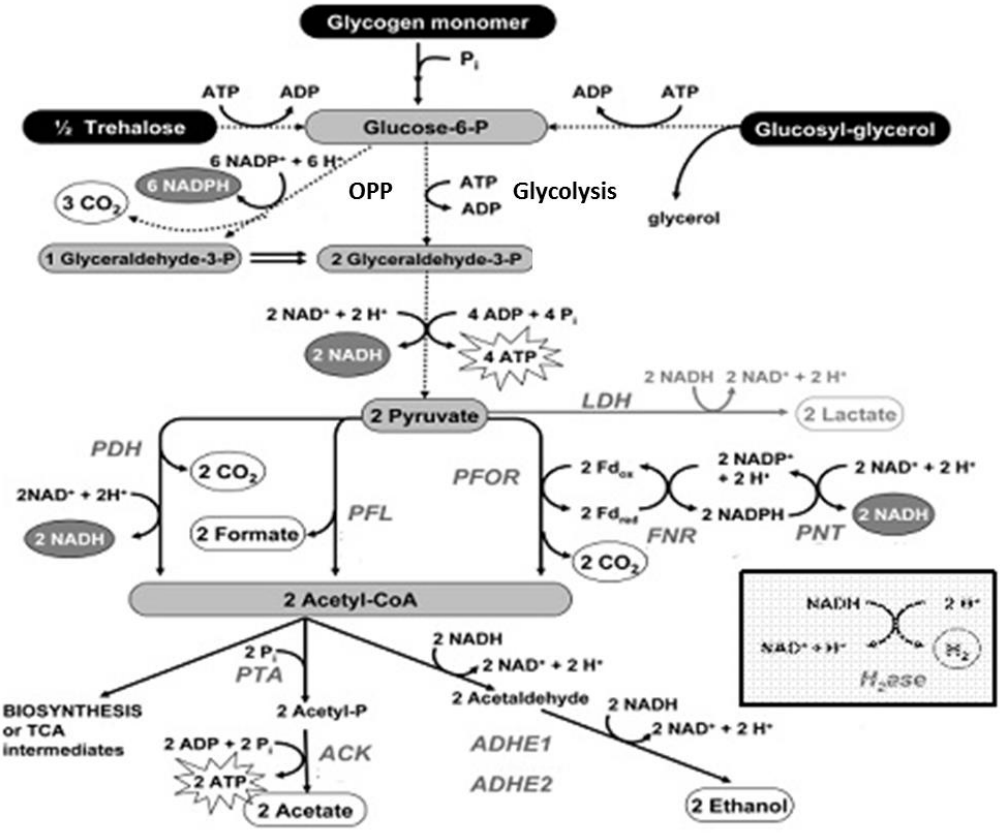

Figure 1.5 Dark fermentative metabolism with H_2 production in cyanobacteria based on indirect biophotolysis (Carrieri,2010) http://dismukeslab.99k.org/bioenergy.html

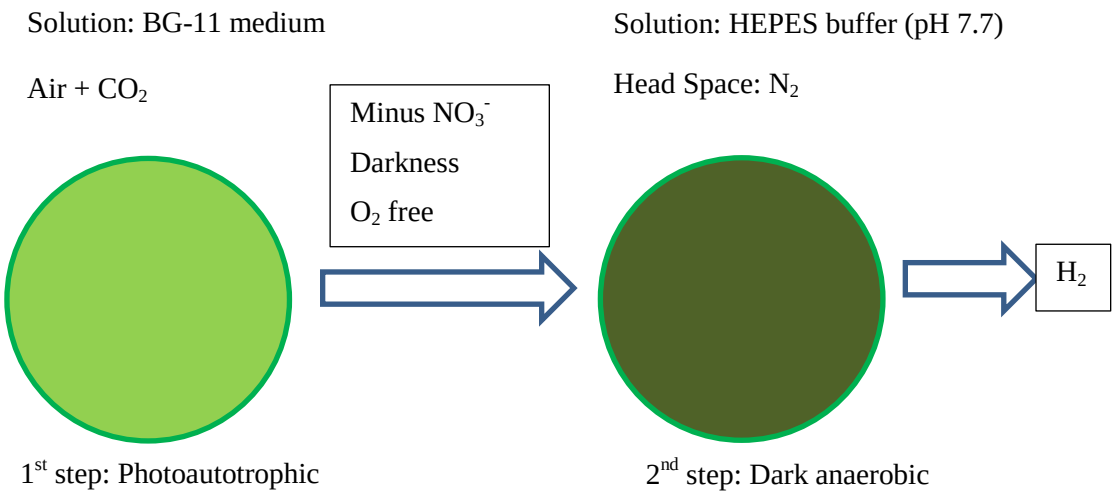

Figure 1.6 Indirect biophotolysis to generate H_2 in a glucose tolerant mutant of *Synechocystis* sp. strain PCC6803

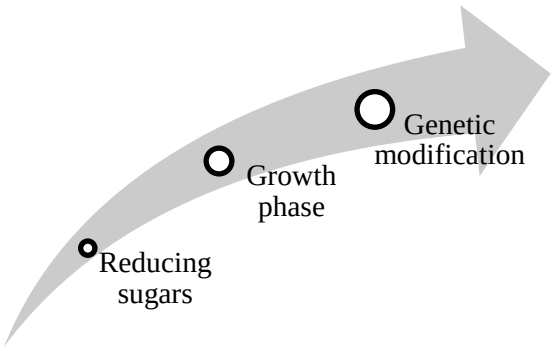

Figure 1.7 Roadmap: using 3 platforms to draw the protocol of how to adjusting reaction for the best hydrogen production from cyanobacteria.

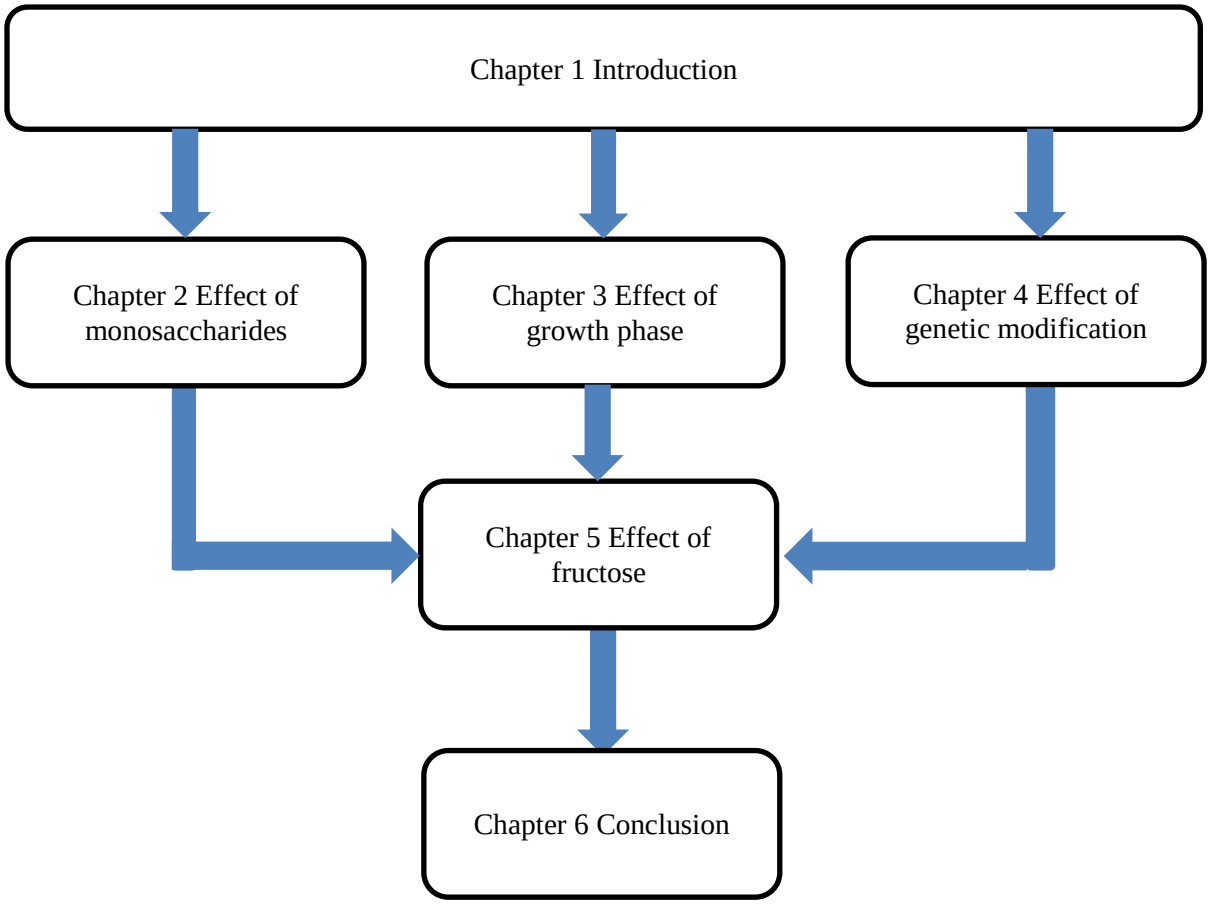

Figure 1.8 Illustration of H_2 production enhancement strategy used in this thesis to draw a protocol of how to enhance H_2 production from cyanobacteria.

Chapter 1: References

Blankenship R (1992) Origin and early evolution of photosynthesis. Photosyntheis Research 33(2):91-111.

Brenner MP, Bildsten L, Dyson F, Fortson N, Garwin R, Grober R, Hemley R, Hwa T, Joyce G, Katz J (2006) Engineering microorganisms for energy production. DTIC Document

Carrieri, D., Momot, D., Brasg, I. A., Ananyev, G., Lenz, O., Bryant, D. A., & Dismukes, G. C. (2010). Boosting autofermentation rates and product yields with sodium stress cycling: application to production of renewable fuels by cyanobacteria. Applied and Environmental Microbiology, 76(19), 6455-6462

Cournac L, Guedeney G, Peltier G, Vignais PM (2004) Sustained photoevolution of molecular hydrogen in a mutant of *Synechocystis* sp. strain PCC 6803 deficient in the type I NADPH-dehydrogenase complex. Journal of Bacteriology 186 (6):1737-1746

Ducat DC, Way JC, Silver PA (2011) Engineering cyanobacteria to generate high-value products. Trends in Biotechnology 29 (2):95-103

Dutta D, De D, Chaudhuri S, Bhattacharya S (2005) Hydrogen production by Cyanobacteria. Microbial Cell Factories 4 (1):36

Gaffron H (1939) Reduction of carbon dioxide with molecular hydrogen in green algae. Nature 143 (3614):204-205

Gaffron H, Rubin J (1942) Fermentative and Photochemical Production of Hydrogen in Algae The Journal of General Physiology 26 (2):219-240

Gutekunst K, Chen X, Schreiber K, Kaspar U, Makam S, Appel J (2014) The Bidirectional NiFe-hydrogenase in *Synechocystis* sp. PCC 6803 Is Reduced by Flavodoxin and Ferredoxin and Is Essential under Mixotrophic, Nitrate-limiting Conditions. Journal of Biological Chemistry 289 (4):1930-1937

Howarth DC, Codd GA (1985) The Uptake and Production of Molecular Hydrogen by Unicellular Cyanobacteria. Journal of General Microbiology 131 (7):1561-1569.

Kaneko T, Sato S, Kotani H, Tanaka A, Asamizu E, Nakamura Y, Miyajima N, Hirosawa M, Sugiura M, Sasamoto S, Kimura T, Hosouchi T, Matsuno A, Muraki A, Nakazaki N, Naruo K, Okumura S, Shimpo S, Takeuchi C, Wada T, Watanabe A, Yamada M, Yasuda M, Tabata S (1996) Sequence Analysis of the Genome of the Unicellular Cyanobacterium *Synechocystis* sp. Strain PCC6803. II. Sequence Determination of the Entire Genome and Assignment of Potential Protein-coding Regions. DNA Research 3 (3):109-136

McGee Laboratory, Atmospheric CO_2 for November 2014, http://co2now.org/, accessed 25 December 2014

Moezelaar R, Bijvank SM, Stal LJ (1996) Fermentation and sulfur reduction in the mat-building cyanobacterium Microcoleus chthonoplastes. Applied and Environmental Microbiology 62 (5):1752-1758

Momirlan M, Veziroglu TN (2002) Current status of hydrogen energy. Renewable and Sustainable Energy Reviews 6 (1–2):141-179

Ohtaguchi K OA, Takahashi N, Ogawa M and Koide K (1995) Kinetics of hydrogen production by the photolithotroph *Synechococcus leopoliensis*, . IONICS 21:69-72

Pandey JP and Tiwari A (2010) Optimization of biomass production of *Spirulina maxima*. Journal of Algal Biomass Utilization. 1:20-32

Yamamoto T, Asami K, Ohtaguchi K (2012a) Anaerobic production of hydrogen in the dark by *Synechocystis* sp. strain PCC 6803: effect of photosynthesis media for cell preparation. Journal of Biochemical Technology 3 (4):344-348

Yamamoto T, Chongsuksantikul A, Asami K, Ohtaguchi K (2012b) Anaerobic Production of Hydrogen in the Dark by *Synechocystis* sp. strain PCC 6803 supplemented with D-glucose. Journal of Biochemical Technology 4 (1):464-468

Chapter 2

Monosaccharide Effects on Hydrogen Production

2.1 Problem Definition and General Consideration

The purpose of the study in this chapter is to elucidate the effect of exogenous monosaccharide on production of molecular hydrogen (H_2) in a glucose-tolerant mutant of unicellular cyanobacterium *Synechocystis* sp. strain PCC6803 (GT strain) in HEPES buffer solution in darkness and to analyze H_2 production kinetics with a mathematical model. GT strain has been isolated from the culture of wild type *Synechocystis* sp. strain PCC6803 (WT strain) (Williams 1988). WT strain and GT strain are known to generate H_2 on bidirectional NiFe-hydrogenase through indirect biophotolysis. GT strain is capable of growing mixotrophically under the light and light-activated heterotrophically in the dark (Anderson and McIntosh 1991). Dark anaerobic H_2 production in HEPES buffer solution is limited not by enzyme activity but by availability of NAD(P)H.

To increase the reductive potential of HEPES buffer solution, in a preceding work, a colleague of the author has elucidated the effects of reductive compounds on initial H_2 production rate (Yamamoto, 2012). The tested reductive compounds are 250 μmol mL^{-1} amino acids (aspartate, leucine, proline, tryptophan, isoleucine, asparagine, valine, phenylalanine, tyrosine, serine, threonine, methionine, alanine, glycine, glutamine, glutamate, histidine, lysine, arginine, and cysteine), 0.25 or 1.0 μmol mL^{-1} organic acids (butyrate, citrate) and 0.25 or 1.0 μmol mL^{-1} glucose (α-D-glucose) on dark anaerobic H_2 production in GT strain. Yamamoto reported that the additives that give no less than 1.4-fold increase in initial H_2 production rate were aspartate, glutamate and glucose. Glucose effect shown in his work reveals that initial H_2 production rates of GT strain in 0, 5.6, 28, 56 μmol mL^{-1} glucose solution are 0.035, 0.042, 0.033 and 0.033 μmol mL^{-1} h^{-1}, respectively, and that production of lactate and acetate is high when glucose concentration is no less than 28 μmol mL^{-1}. The highest initial H_2 production rate is 0.104 μmol mL^{-1} h^{-1} that is seen in run with 5.6 μmol mL^{-1} exogenous glucose. Heterotrophic growth on glucose was reported by Yamamoto but increase in dry cell weight concentration was not high as suggested from increase in H_2 production. Addition of small amount of glucose to insure curbing the fermentation of lactate and acetate appears to elevate H_2 production. No more than 0.8-fold initial H_2 production rate was observed in histidine solution. The mechanism of the added compounds on H_2 production is not yet known.

Glucose is a reducing sugar, hence the reductive environment provided by glucose has a possibility to increase H_2 production. **Figure 2.1** shows conversion of α-D-glucopyranose, acylic form (open chain) D-glucose and β-D-glucopyranose. The hydroxyl on carbon 1 represents a high reductive potential. Reducing sugars are other candidates of additives to increase H_2 production, however, no such works have been reported. The present investigation in this chapter extends the above work of Yamamoto and concerns the effect of reducing monosaccharides glucose, fructose, galactose, mannose and xylose on dark anaerobic H_2 production in GT strain. **Table 2.1** tabulates physical property data of above monosaccharides.

Shown in **Figure 2.2** is a cyanobacterial cell envelope consisting with all layers surrounding the cytoplasm. The 60-70% of outer membrane (LIV) is composed of mannose, glucose, galactose and other carbohydrate. External layer (EL) contains galactose, hexose, glucose and xylose. Hence reducing sugars selected above are important for cyanobacterial cell envelope.

There is a classic work (Stal and Moezelaar 1997) that lists up the dark anaerobic chemoorganotrophic growth of cyanobacteria involving the growth of *Anabaena azollae* AaN or *Nostoc* sp. A12 on glucose or fructose (De Philippins et al., 1996), *Microcystis aeruginosa* 7806 on glucose (Moezelaar and Stal, 1994), *Nostoc* sp. on glucose, fructose or sucrose (Hoare *et al*.,1917) and *Oscillatoria terebriformis* on glucose or fructose (Richardson et al., 1987). Except for *M. aeruginosa* 7806, all species reported for dark anaerobic chemoorganotrophic growth are N_2-fixing filamentous cyanobacteria. There are remarkably few data available on the dark anaerobic metabolism on monosaccharides. Stal et al. also reported the detection of fermentation products H_2, lactate, acetate and ethanol from endogenous glycogen and exogenous glucose in cyanobacteria *Synechocystis* sp, strain PCC 6714, *Synechocystis* sp, strain PCC 6308 and *Synechococcus* sp. strain PCC 6301**.**

Some works have reported that GT strain is capable of generating more H_2 in dark anaerobic glucose-supplemented solution than in dark anaerobic solution without glucose (Cournac et al. 2004; Yamamoto et al. 2012). Glucose-supplemented culture of this strain shows a small increase in dry cell weight concentration in darkness (Anderson and McIntosh 1991). Trophic modes of cyanobacteria are shown by complete autotrophy at one end and complete heterotrophy at the other end, and mixotrophy at a mixed utilization mode of CO_2 and organic substrate.

NiFe-hydrogenase of GT strain is important for mixotrophic growth on glucose under dark anaerobic condition because mutant lacking hydrogenase gene (Δ*hoxH*) impairs ability to grow on glucose (Gutekunst et al. 2014). This has suggested that hydrogenase is one of important electron sink in dark

anaerobic condition. The other sink is nitrate reductase (Baebprasert et al. 2011). Effect of glucose on mixotrophic growth of GT strain under the light has been variously reported. One work shows that glucose inhibits the growth in the absence of herbicide DCMU ((3-(3,4-dichlorophenyl)-1,1-dimethylurea) (Flores and Schmetterer 1986). The other work shows that glucose stimulates the growth in the absence of DCMU (Yoo et al. 2007).

Figure 2.3 represents metabolism of carbon dioxide (CO_2) and exogenous glucose by a mixotrophically growing cells of unicellular cyanobacterium *Aphanocapsa* 6714 in the light (2000 lx) in BG-11 medium (Pelroy et al., 1976). The Calvin cycle (Fig.1.4) is shown by the closed path from RuBP to RuBP via PGA, GAP, Pentose Phosphate cycle and Ru5P. RuBP is the only sugar phosphate that is unique to the Calvin cycle. During photosynthesis, CO_2 incorporated into the Calvin cycle is converted to glycogen. Peloy et al. showed the accumulation of RuBP under the light, inhibition of glucose-6-phosphate dehydrogenase by RuBP and rapid consumption of RuBP in darkness. This event relieves glucose-6-phosphate dehydrogenase from allosteric inhibition of RuBP, and initiate the conversion of glucose-6-phosphate to 6-PGl (6-phosphogluconate). This change activates the oxidative pentose phosphate (OPP) pathway and the cellular glycogen is decomposed. In the presence of glucose, cells of *Aphanocapsa* 6714 under the light with 0.01 μmol mL^{-1} DCMU convert about 28% and 65% of carbon in exogenous glucose to CO_2 and cell constituting materials, respectively, and they under the dark convert about 37% and 64% of it to CO_2 and cell constituting materials, respectively. The carbon metabolism of GT strain during dark anaerobic H_2 production by indirect biophotolysis (Yamamoto et al., 2014) is slightly different from that shown in Fig.2.3, since photosynthesis of the work of Yamamoto et al. was performed not mixotrophically but autotrophically and exogenous glucose was added at the time of shift from photosynthesis mode to dark anaerobic incubation mode. In the absence of oxygen (O_2) cells are required to activate NiFe-hydrogenase as an alternative of electron sink. In darkness, where OPP pathway turns to be active, consumption of exogenous glucose on OPP pathway generates additional electrons that contribute to increase H_2 production activity.

CyanoBase for *Synechocystis* sp. strain PCC6803 is the total genome database of this strain, which outputs 21 genes against the search word of "glucose". The glycolysis metabolism of WT strain is shown in **Fig.A3.1** of Appendix-3 (KEGG pathway database). Lines in the graph are drawn based on the defined genes coding for corresponding enzymes and conversions shown by green box are specific to WT strain. This map shows the reversible pathway between glycogen and glucose via glucose-1-P. Glucose is converted to pyruvate by glycolysis pathway (**Fig.A3.2**) or to glyceraldehyde 3-phosphate pentosephosphate by pathway (**Fig.A3.3**). Glyceraldehyde 3-phosphate is converted to pyruvate by

glycolysis pathway. Pyruvate is converted to lactate (D-lactate) by D-lactate dehydrogenase (ddh) that is specific to WT strain (**Fig.A3.4**). Pyruvate is also converted to acetate via acetyl CoA by GT strain specific enzymes (Fig.A3.4), and to ethanol via acetaldehyde (Fig.A3.2).

Photoheterotrophic growth of this strain is possible on glucose and impossible on fructose (Rippka et al., 1979). Fructose is a reducing sugar and a glucose isomer which expresses a reactivity different from glucose (Laroque et al. 2008). Fructose is a bactericidal for GT strain, of which growth in glucose aqueous solution under the light is inhibited by 10 $\mu mol \cdot mL^{-1}$ fructose (Flores and Schmetterer 1986; Joset et al. 1988). Fructose enters the cell via glucose transporter (Zhang et al. 1989). Deactivation of the expression of *glcP* (glucose-transporter gene) makes cells to be resistant to fructose. CyanoBase for *Synechocystis* sp. strain PCC6803 is the total genome database of this strain, which outputs 5 genes against the search word of "fructose". Besides four genes that are closely related to photosynthesis, L-glutamine: D-fructose-6-P amidotransferase is listed. Fructose metabolism in GT strain is not detailed in previous works, while isolated genes suggest the pathway from fructose to glyceraldehyde 3-phosphate via fructose 1-phosphate (**Fig.A3.5**). Glycogen is synthesized from fructose 1-phosphate via fructose 6-phosphate, glucose 6-phosphate, and glucose 1-phosphate (Fig.A3.1). When glycolysis is dominant, pyruvate is produced from fructose 1-phosphate via glyceraldehyde 3-phosphate (Fig.A3.4). The fructose resistant strain has less affinity to glucose (Zhang et al. 1989; Kahlon et al. 2006). In the presence of glucose, concentration of NAD(P)H increases significantly in the dark adapted cells of GT strain (Lee et al. 2007).

Galactose is a C-4 epimer of glucose. Galactose metabolism and fructose and mannose metabolism in GT strain are presented in KEGG (**Fig.A3.6**). CyanoBase for *Synechocystis* sp. strain PCC6803 is the total genome database of this strain, which outputs no genes against the search word of "galactose". Experimental data on galactose metabolism in WT strain is not seen in previous works but the metabolic map of Fig.A3.6 based on genes suggests that galactose is converted to glucose 6-phosphate via galactose 1-phosphate and glucose 1-phosphate.

Mannose is a C-2 epimer of glucose. Isolated genes suggest the pathway from mannose to fructose 6-phosphate via mannose-6-phosphate (Fig.A3.5). CyanoBase for *Synechocystis* sp. strain PCC6803 is the total genome database of this strain, which outputs 9 genes against the search word of "mannose". Five genes among them are related to mannose-1-phosphate guanyltransferase. No reports have shown the mannose utilization in WT strain.

Xylose is an aldopentose monosaccharide. No report shows consumption of xylose in WT strain, while isolated genes assume the metabolism shown in Appndix-3 (7) (**Fig.A3.7**). CyanoBase for *Synechocystis* sp. strain PCC6803 is the total genome database of this strain, which outputs no genes against the search word of "xylose". If these gene products expresses, xylose is converted to pyruvate via xylonolactone. High sequence conservation with the xylose transporter of *Escherichia coli* (Schmetterer, 1990 Plant Molecular Biology, 14:697-706) is found in WT strain DNA.

This chapter also concerns the kinetics of dark anaerobic H_2 production in GT strain. When cells of GT strain are inoculated from photoautotrophic condition into dark anaerobic HEPES buffer solution, they generate molecular hydrogen (H_2) on bidirectional NiFe-hydrogenase by receiving sufficient amount of electrons in terms of NAD(P)H as shown by

$$NAD(P)H+H^{+}\rightarrow NAD(P)^{+}+H_2 \qquad (2.1)$$

This technique is an indirect biophotolysis to generate H_2. The reductive compound NAD(P)H is reported to be generated from the breaking-down of stored glycogen (glycolysis). **Figure 2.4** is cited from the work of Yamamoto (Yamamoto, 2012). This graph shows the time course of the moles of H_2 per anaerobic HEPES buffer solution (y_{H2}) in the darkness, oxygen-free and nitrate-free are reported to be prerequisites for H_2 production. This work proposed a following kinetic model for H_2 production:

$$r_{H2}=\frac{dy_{H2}}{dt}=q_{H2}X \qquad (2.2),$$

$$q_{H2}=k_1 m_{RED} \qquad (2.3),$$

and

$$k_1=k_0\sigma_{HG} \qquad (2.4).$$

For initiating a kinetic approach, following models were also assumed:

$$\frac{dm_{RED}}{dt}=(a_1k_G m_G+a_2K_d-k_1m_{RED})+K_d m_{RED} \qquad (2.5),$$

$$m_G=m_{G0}\exp\{(K_d-k_G)t\} \qquad (2.6)$$

and

$$X = X_0 \exp(-K_d t) \tag{2.7}$$

in which r_{H2} and q_{H2} are the H_2 production rate and specific H_2 production rate, respectively, m_{RED} is the number of moles of reductant(s) NAD(P)H per dry weight, m_G is the number of moles of endogenous glucose per dry weight, σ_{HG} is the specific activity of NiFe-hydrogenase, X is the dry cell weight concentration, m_{G0} and X_0 are the initial values of m_G and X, respectively, k_0 is the rate constant of second order reaction, k_1 is the rate constant of pseudo-first order reaction and K_d is the specific death rate. Broken line in Fig.2.4 shows the calculated value of y_{H2} in the work of Yamamoto that fits well with experimental data. Despite this fact, further work is required since Eq.(2.5) assumed the reductants for NiFe-hydrogenase are supplied only by glycolysis and cell death, and Eq.(2.6) assumed the exponential decline of the amount of endogenous glucose with time.

This study assumes that reductants NADH and NADPH are supplied by reduction of oxidants NAD^+ and $NADP^+$, that reductants are assimilated by oxidation of reductants including NiFe-hydrogenase reaction, and that synthesis and decomposition of $NAD(P)^+$ plus NAD(P)H are absent under dark anaerobic incubation. These assumption lead the following equations instead of Eq.(2.5), when dry cell weight concentration decreases with time at the specific death rate of K_d (Eq.(2.7)):

$$\begin{aligned} \frac{dm_{RED}}{dt} &= (-k_{RED} m_{RED} + k_{OX} m_{OX} - k_1 m_{RED}) + K_d m_{RED} \\ &= k_{OX} m_T - (k_{RED} + k_{OX} + k_1 - K_d) m_{RED} \end{aligned} \tag{2.8}$$

where

$$m_T = m_{RED} + m_{OX} = \text{constant} \tag{2.9},$$

in which m_{OX} is the number of moles of oxidants per dry weight, and m_T is the total amounts of NAD(P)H and $NAD(P)^+$ per dry cell weight. Eq.(2.8) is the same as Eq.(2.5) under the stoichiometric relations for redox reaction.

When, right after dark anaerobic incubation, cell grows with the specific growth rate of μ as:

$$X = X_0 \exp(\mu t) \tag{2.10},$$

Eq.(2.8) is replaced by:

$$\frac{dm_{RED}}{dt} = (-k_{RED} m_{RED} + k_{OX} m_{OX} - k_1 m_{RED}) - \mu m_{RED}$$
$$= k_{OX} m_T - (k_{RED} + k_{OX} + k_1 + \mu) m_{RED} \quad (2.11).$$

During H_2 production, the term $k_{RED}+k_{OX}+k_1$ is apparently not zero. The following two cases are assumed.

i) Case where $k_{RED}+k_{OX}+k_1-K_d$ is not zero (cell population effect is large).

Eq.(2.8) or (2.11) results in that

$$m_{RED} = \frac{k_{OX}}{k_{RED} + k_{OX} + k_1 - K_d} m_T + (m_{RED,0} - \frac{k_{OX}}{k_{RED} + k_{OX} + k_1 - K_d} m_T) \exp\{-(k_{RED} + k_{OX} + k_1 - K_d)t\} \quad (2.12)$$

or

$$m_{RED} = \frac{k_{OX}}{k_{RED} + k_{OX} + k_1 + \mu} m_T + (m_{RED,0} - \frac{k_{OX}}{k_{RED} + k_{OX} + k_1 + \mu} m_T) \exp\{-(k_{RED} + k_{OX} + k_1 + \mu)t\} \quad (2.13)$$

Eq.(2.12) or (2.13) results in that

$$\frac{dy_{H2}}{dt} = k_1 m_{RED} X = k_1 m_T X_0 [\frac{k_{OX}}{k_{RED} + k_{OX} + k_1 - K_d} \exp(-K_d t) + (\frac{m_{RED,0}}{m_T} - \frac{k_{OX}}{k_{RED} + k_{OX} + k_1 - K_d}) \exp\{-(k_{RED} + k_{OX} + k_1)t\}] \quad (2.14)$$

or

$$\frac{dy_{H2}}{dt} = k_1 m_{RED} X = k_1 m_T X_0 [\frac{k_{OX}}{k_{RED} + k_{OX} + k_1 + \mu} \exp(\mu t) + (\frac{m_{RED,0}}{m_T} - \frac{k_{OX}}{k_{RED} + k_{OX} + k_1 + \mu}) \exp\{-(k_{RED} + k_{OX} + k_1)t\}] \quad (2.15).$$

From Eq.(2.14) or Eq.(2.15), it is found that

$$r_{H2,0} = k_1 m_{RED,0} X_0 \quad (2.16).$$

Eq.(2.16) is constructed to support an idea that H_2 production at early state in dark anaerobic condition is very much dependent to initial reductive compound ($m_{RED,0}$). This initial reductive compound sets the value of initial H_2 production rate ($r_{H2,0}$) which is highest at the beginning then declines over time. Eq.(2.14) or Eq.(2.15) suggests that H_2 production rate decreases with time from the initial value shown by Eq.(2.16) and approaches to zero, hence it can be approximated to:

$$\frac{dy_{H2}}{dt} \approx r_{H2,0} \exp(-kt) \tag{2.17}$$

in which k is a model parameter which is constant value assumed to be all factors involved in H_2 production, presumably changes of reductive and oxidative compounds, cell death or growth (k_{RED}, k_{OX}, k_1, K_d or μ). If k is not zero, integrating Eq.(2.17) results in that

$$\begin{aligned} y_{H2} &= \frac{r_{H2,0}}{k}\{1-\exp(-kt)\} \\ &= y_{H2,f}\{1-\exp(-kt)\} \end{aligned} \tag{2.18}$$

The attainable level of H_2 production ($y_{H2,f}$) can now be predicted by initial H_2 production rate and deactivation constant.

ii) Case where $k_{RED}+k_{OX}+k_1$ is extremely greater than K_d or μ (cell population effect is small).

Eq.(2.12) or (2.13) results that

$$m_{RED} = \frac{k_{OX}}{k_{RED}+k_{OX}+k_1} m_T \tag{2.19}$$

The H_2 production rate is given by:

$$\frac{dy_{H2}}{dt} = k_1 m_{RED} X = k_1 m_T X_0 \frac{k_{OX}}{k_{RED}+k_{OX}+k_1} = k_1 m_{RED,0} X_0 \tag{2.20}$$

The initial H_2 production rate of this equation satisfies Eq.(2.16).

$$y_{H2} = r_{H2,0} t \tag{2.21}$$

Solid line in Fig.2.4 shows the y_{H2} value estimated by Eq.(2.18) with $r_{H2,0}$ at 0.0310 μmol $mL^{-1}h^{-1}$ and k at 0.0108 h^{-1}. Even though this model contains only two parameters $r_{H2,0}$ and k, simulated curve can reproduce the experimental results satisfactory. Hence experimental data of H_2 production in this work is interpreted by Eqs. (2.18) and (2.21).

If NiFe-hydrogenase in *Synechocystis* sp. strain PCC 6803 works as an electron sink for NAD(P)H or reduced ferredoxin/flavodoxin, and if exogenous reducing sugar provides reductive environment to the cell, the possibility exists that H_2 production is enhanced by reducing sugar supplementation under nitrate limiting condition. The effect of exogenous electron donors in terms of reducing sugars such as glucose, fructose, galactose, mannose and xylose upon the H_2 production in GT strain in the dark anaerobic nitrate free condition is analyzed utilizing Eq.(2.20).

2.2 Materials and Methods

2.2.1 Culture technique and fermentation

A glucose tolerant mutant of *Synechocystis* sp. strain PCC6803 (GT strain) was utilized in the experiments of this chapter. For both pre-culture and main culture, clear cylindrical photobioreactors (pyrex glass made; inner diameter, 27 mm; outer diameter, 29 mm) were utilized. Single nozzle sparger (inner diameter, 4 mm; outer diameter, 8 mm) was equipped for gas sparging. For pre-culture, cells were grown photoautotrophically for 3 days in BG-11 medium (**Table 2.2**), initial pH 7.8, at 34ºC, aerated by air containing 6% CO_2 with a flow rate of 80 mL min^{-1}, illuminated by fluorescent lamps with photosynthetic photon flex density (*PPFD*) at 100 μmol-photons m^{-2} s^{-1}. Superficial gas velocity was 8.39 m h^{-1}.

Dry cell weight concentration (X) was monitored by measuring OD_{730}: optical density at 730 nm. One unit absorbance was equivalent to 0.369 mg mL^{-1}. When X increases with time, growth rate (r_X) and specific growth rate (μ) are calculated as:

$$r_X = \frac{dX}{dt} = \mu X \tag{2.22}$$

When X decreases with time, death rate ($-r_X$) and specific death rate (K_d) are calculated as:

$$(-r_X) = -\frac{dX}{dt} = K_d X \tag{2.23}$$

Pre-culture cells were grown for 3 d to logarithmic growth phase before transferring to main culture. The main culture used the same condition as pre-culture. Cells of late-logarithmic growth phase in main culture (OD_{730}, 7) were collected by centrifugation at 3000 rpm and 25 ºC for 10 min. The cell pellets were washed by 50 μmol mL^{-1} HEPES buffer solution (pH 7.8) and collected by centrifugation to remove nitrate. Cells were re-suspended and incubated with or without 28 μmol mL^{-1} glucose, fructose, galactose, mannose or xylose in 10 mL of 50 μmol mL^{-1} HEPES buffer solution (pH 7.8) in 32 mL glass test tube with butyl rubber cap. The initial dry cell weight concentration was set at 2.13±0.06 mg mL^{-1} and cell suspension was purged with N_2 gas for a few minutes to remove oxygen molecules. Incubation was carried out under dark anaerobic conditions with shaking at 145 rpm on a reciprocating shaker. The reciprocating distance was 40 mm and the horizontal angle was about 30º.

2.2.2 Measurement of H_2 production

The amount of molecular H_2 in the gas phase in 32 mL test tube was monitored by withdrawing 500 μL sample and measuring with a gas chromatograph equipped with a molecular sieve column and a thermal conductivity detector (GC-320, GL science Inc.; column, Molecular sieve 13X; column temperature, 37ºC; injector temperature, 45ºC; detector temperature 80ºC) with nitrogen gas as the carrier gas. The number of moles of H_2 per culture volume (y_{H2}) is first analyzed, and then the rate of H_2 production per culture volume (r_{H2}) and the specific rate of H_2 production (q_{H2}) were calculated as:

$$r_{H2} = \frac{dy_{H2}}{dt}$$
$$q_{H2} = \frac{1}{X}\frac{dy_{H2}}{dt} = \frac{r_{H2}}{X} \tag{2.24}$$

2.2.3 Determination of metabolic product distribution

Metabolites in a 500 μL portion of supernatants were analyzed by HPLC (JASCO PU-2080 Plus and UV-2075 Plus). Mobile phase was 18 μmol mL^{-1} KH_2PO_4, pH of which was adjusted at 2.3 with H_3PO_4. Flow rate of mobile phase was 0.7mL min^{-1}. Column temperature was 30°C. A 10 μL of supernatant

sample was injected by using 10 µL syringes. The wave length of 210 nm was used for detection of metabolites. To confirm molecular mass of acid, sample was analyzed by a liquid chromatography-electrospray ionization-time-of-flight-mass spectrometry (LC-ESI-TOF-MS) (microTOF Ⅱ, Bruker Daltonics Co.) utilizing 1% formate as mobile phase. LC column of the system was XBridge C18 HPLC Column 3×150 mm 3.5 µm.

The concentrations of lactate (c_L), acetate (c_A), and succinate (c_{SUC}) were first analyzed, and then the rate of production of lactate, acetate and succinate per culture volume (r_L, r_A, r_{SUC}) were calculated as:

$$r_L = \frac{dc_L}{dt},\ r_A = \frac{dc_A}{dt},\ r_{SUC} = \frac{dc_{SUC}}{dt} \tag{2.25}$$

When metabolite is consumed, its consumption rates are calculated as:

$$(-r_L) = -\frac{dc_L}{dt},\ (-r_A) = -\frac{dc_A}{dt},\ (-r_{SUC}) = (-\frac{dc_{SUC}}{dt}) \tag{2.26}$$

2.2.4 Measurement of reducing sugar consumption

Residual reducing sugars in cell suspensions were analyzed by a high performance liquid chromatography (HPLC) (Shimadzu LC-10AD and RID-6A). Column equipped was SZ5532, φ6.0 × 150 mm (Showa Denko Co.). Column temperature was set at 50°C. Mobile phase was 70% acetonitrile. Mobile phase flow rate was 0.7 mL min^{-1}. A 10 µL of supernatant sample was injected by using a 10 µL syringe.

The concentration of unreacted monosaccharide (c_S) is first analyzed, and then the rate of monosaccharide consumption rate ($-r_S$) and the specific rate of monosaccharide consumption (q_S) was calculated as:

$$\begin{aligned} (-r_S) &= -\frac{dc_S}{dt} \\ q_S &= -\frac{1}{X}\frac{dc_S}{dt} = \frac{(-r_S)}{X} \end{aligned} \tag{2.27}$$

2.2.5 Measurement of endogenous glycogen consumption and production

The amount of glycogen per culture volume was determined as follows: cell pellets were collected by centrifugation at 25ºC, 3000 rpm for 10 min then washed 3 times by deionized water to eliminate extracellular carbon sources; intracellular glycogen was extracted and decomposed to glucose in 50 μL of 6 N HCl at 80ºC for 30 min; glucose amount was determined by using Glucose CII Test Wako (Wako Pure Chemical Ind., Ltd.).

The number of moles of endogenous glucose per dry cell weight is shown by m_G. The number of moles of endogenous glucose per culture volume ($m_G X$) is first analyzed, and then, when $m_G X$ decreases with time, the consumption rate of endogenous glucose ($-R_G X$) was calculated as:

$$(-R_G X) = -\frac{d(m_G X)}{dt} \tag{2.28}$$

When $m_G X$ increases with time, the generation rate of endogenous glucose ($-R_G X$) was calculated as:

$$R_G X = \frac{d(m_G X)}{dt} \tag{2.29}$$

In Eqs.(2.28) and (2.29), ($-R_G$) and R_G show the specific consumption rate and specific production rate of endogenous glucose, respectively.

2.3 Results and discussion

The LC-ESI-TOF-MS and HPLC analysis of supernatant of cell suspended dark anaerobic HEPES buffer solution with glucose confirmed production of acetate, lactate and succinate. MS analysis has suggested that fumarate and malate possibly presented in buffer solution. Main metabolic products of the dark incubated culture of the runs with or without monosaccharide other than glucose were identified by GC and HPLC to be H_2, acetate, lactate and succinate as shown in **Figure 2.5**.

Culture variables were monitored. **Figure 2.6** shows the time courses of dark anaerobic incubation variables measured in runs without monosaccharide (○) and with glucose (■), fructose (▲), galactose (●), mannose (◆) and xylose (▼). Quantities plotted include (a) the mole of H_2 per culture volume (y_{H2}), (b) the concentration of exogenous reducing sugars (c_S), (c) the amount of endogenous glycogen per culture volume (c_G), (d) the concentration of cell mass (X), (e) pH of cell suspension, (f) the concentration of acetate, (g) the concentration of lactate and (h) the concentration of succinate

Figure 2.6(a) shows that the production of H_2 starts right after inoculation. Prior to dark anaerobic incubation, cells of GT strain were photoautotrophically grown on BG-11 medium in the presence of oxygen. NiFe-hydrogenase of GT strain is found to be synthesized in the presence of oxygen. This observation differs from NiFe-hydrogenase sysnthesis in *Eschericha coli*, transcription of which is reported to be blocked by oxygen (Richard et al., 1999). Our observation is supported by previous works (Appel et al.,2000; Gutekunst et al.,2005). In WT strain, higher levels of NiFe-hydrogenase transcripts have been detected under micro-aerobic or anaerobic conditions. These works suggest that under the photoautotrophic culture, NiFe-hydrogenase transcripts are prepared but blocked for expression by oxygen. H_2 production rate (r_{H2}) is highest at initial and clearly decelerated with time, hence time course of y_{H2} can be fitted by Eq.(2.18). NiFe-hydrogenase is inhibited to produce H_2 by oxygen during photosynthesis, is found to be active when cells are inoculated into oxygen-free dark environment.

The data for H_2 production (y_{H2}) are well fitted by Eq.(2.18) as shown in the dotted lines of Fig 2.5a. No data in this graph represents the time course of y_{H2} that is suggested by Eq.(2.21). Not only H_2 production in GT strain in HEPES buffer solution without monosaccharides, that with glucose, fructose, galactose, mannose and xylose can be fitted by Eq.(2.18).

Figure 2.7 shows the relation between $y_{H2,1}$ and $y_{H2,f}$. There seems to be a relation shown by:

$$y_{H2,f} = k_2 y_{H2,1}^{k_3} \tag{2.30}$$

Best fits to the data results that the parameters are k_2,1.47 μmol mL^{-1}; and k_3, 0.752.

In this study, subscript 0 and f show the initial state and the final state, respectively. Although the state of inocula are kept as constant as possible, the initial rate $r_{H2,0}$, calculated from Eq.(2.18), is affected by variation in reducing sugars. Calculated data has been tabulated in **Table 2.3**. If the initial rate $r_{H2,0}$ represents the reductive state of the inocula, reductive potential is found to be highest in glucose, second highest in fructose, third highest in galactose, fourth highest in mannose and lowest in xylose. The reductive potential of cells in buffer solution without monosaccharide is lower than that in xylose. The attainable level of amount of H_2 per culture volume ($y_{H2,f}$) is highest at 3.26 μmol·mL^{-1} in the solution containing glucose, which is 1.50 times that without reducing sugar.

To investigate the relation between initial cellular content of NAD(P)H and attainable level of the number of moles of H_2 per culture volume, relative parameters are defined as:

$$y^*_{H2} = \frac{y_{H2}}{(y_{H2,f})_{ref}},\ q^*_{H2} = \frac{q_{H2}}{(q_{H2,0})_{ref}},\ m^*_{RED} = \frac{m_{RED}}{(m_{RED,0})_{ref}},\ X^* = \frac{X}{(X_0)_{ref}},$$

$$y^*_{H2,f} = \frac{y_{H2,f}}{(y_{H2,f})_{ref}},\ q^*_{H2,0} = \frac{q_{H2,0}}{(q_{H2,0})_{ref}},\ m^*_{RED,0} = \frac{m_{RED,0}}{(m_{RED,0})_{ref}},\ X^*_0 = \frac{X_0}{(X_0)_{ref}} \qquad (2.30)$$

in which subscript ref specifies the results of reference run that, throughout this thesis, is defined as the dark anaerobic H_2 production in GT strain in HEPES buffer solution without monosaccharide that is performed with cells from the cell suspension of OD_{730} at 7 when cells are in late-logarithmic growth phase in photoautotrophic cultures.

Figure 2.8 is a plot similar to the Hammett equation (Hammett, 1937). Data of Table 2.2 are plotted. The result shows that exposure of inoculum cells to glucose, fructose and galactose elevates the reductive potential of GT cells ($q^*_{H2,0}$ >1), and that

$$y^*_{H2,f} > q^*_{H2,0} \qquad (2.31)$$

for runs with glucose, fructose and galactose. Dark anaerobic H_2 production by inoculum with higher reductive state is found to shift up the attainable level of H_2. This plot also shows that

$$y^*_{H2,f} < q^*_{H2,0} \qquad (2.32)$$

for runs with mannose and xylose. The plots in Fig.2.7 with Eq.(2.3) lead to the following relation:

$$y^*_{H2,f} = (q^*_{H2,0})^{k_4} \qquad (2.33).$$

In a preliminary experiment utilizing methyl viologen (dimethyl-4,4'-bipyridim dichloride), H_2 production rate of GT strain is found to be independent from NiFe-hydrogenase activity. Hence, from Eq.(2.4), rate constant k_1 is assumed to be constant. This assumption leads to

$$m^*_{RED,0} = q^*_{H2,0} \qquad (2.34).$$

The linear line in Fig.2.7 without run with mannose results in that k_4 is 0.619. This relation shows that the attainable level of H_2 can be estimated by the number of mole of reductive compounds right after the inoculation of cells of GT strain into dark anaerobic HEPES buffer solution without or with monosaccharides.

To elucidate the effect of reductive compounds on H_2 production, additional experiments were performed in which dark anaerobic incubation of GT strain was performed in HEPES buffer solution with reductive compound 5 μmol mL^{-1} $FeCl_3$ or 5 μmol mL^{-1} ascorbic acid sodium. H_2 production of GT strain was not affected by $FeCl_3$ or ascorbic acid sodium. Effect of non-reductive compound is also studied by adding 28 μmol mL^{-1} disaccharide sucrose to HEPES buffer solution. The initial H_2 production rate of this was comparable with that of run without monosaccharide (data not shown). The results of experiments in this chapter negates the working assumption that effect of reducing sugar for H_2 production is due to the effect of the increase in reductive potential in the cellular environment.

Numerically, deactivation constants for H_2 production (k) in runs with glucose, fructose and galactose are nearly the same and higher than that in runs with mannose and xylose and without monosaccharide. Roughly dark anaerobic incubation of high r_{H2} production results in high k value. Oxidation of NAD(P)H by NiFe-hydrogenase generates not only H_2 but also $NAD(P)^+$ that appears to inactivate NiFe-hydrogenase.

Combination of Eqs.(2.26),(2.28) and (2.31) results in that

$$\begin{aligned} m_{RED}^{*} &= \frac{m_{RED}}{(m_{RED,0})_{ref}} = \frac{m_{RED,0}}{(m_{RED,0})_{ref}} \frac{m_{RED}}{m_{RED,0}} = \frac{q_{H2,0}}{(q_{H2,0})_{ref}} \exp(-kt) \\ &= q_{H2,0}^{*} \exp(-kt) \end{aligned} \tag{2.35}$$

Figure 2.9 is the time courses of calculated m_{RED}^{*} utilizing Eq.(2.34) and parameters $q_{H2,0}^{*}$ and k in Table 2.3. This graph shows that inoculum cells in glucose, fructose and galactose have high reductive potential at the beginning of dark anaerobic incubation, and rapidly consumes those compounds. Eq.(2.34) is important since m_{RED} is a key parameter representing the redox potential of cells in dark anaerobic incubation.

Amount of reductive compounds per culture volume is given by

$$\begin{aligned} m_{RED}^{*} X^{*} &= q_{H2,0}^{*} \exp(-kt) X_0^{*} \exp(-K_d t) \\ &= q_{H2,0}^{*} X_0^{*} \exp\{-(k + K_d)t\} \end{aligned} \tag{2.36}$$

The amount of H_2 per culture volume is shown by

$$y_{H2}^{*} = \frac{y_{H2}}{(y_{H2,f})_{ref}} = \frac{\frac{q_{H2,0}X_0}{k}\{1-\exp(-kt)\}}{(\frac{q_{H2,0}X_0}{k})_{ref}}$$
$$= q_{H2,0}^{*}X_0^{*}\{1-\exp(-kt)\} \quad (2.37)$$
$$= q_{H2,0}^{*}X_0^{*}[1-\{\frac{1}{q_{H2,0}^{*}}m_{RED}^{*}\}^{k/(k+K_d)}]$$

Figure 2.10 is the plots of y_{H2}^{*} against m_{RED}^{*} which are estimated by Eq.(2.35) and parameters $q_{H2,0}$ and k in Table 2.2. The amount of H_2 and the amount of reductive compound are related by this equation.

When dark anaerobic incubation is performed in 28 μmol mL^{-1} monosaccharide solution, during the first 48 h, cells of GT strain are unable to assimilate exogenous reducing sugars other than glucose (Fig. 2.6(b). Despite the fact that glucose and fructose share common transport system in *Synechocystis* sp. strain PCC 6803 (Zhang et al. 1989), cells are unable to assimilate exogenous fructose for cell division under the dark anaerobic condition at least during first 48 h. Fructose has a potential to enter into the intracellular environment and reduce the redox potential inside the cells. However, fructose consumption curve suggests that this change blocks additional transport of fructose. Galactose transporter is not reported in previous works. Fig. 2.6(b) suggests that galactose is also transported into cell as fructose but mannose cannot utilize the glucose transporter.

The H_2 production that is most active right after inoculation is found to be effected by monosaccharide as shown by $q_{H2,0}/(q_{H2,0})_{w/o}$ in Table 2.3. Despite this fact, Fig.2.6 (b) represents quite low level of consumption of monosaccharides except for glucose. GT strain assimilates more than 6 μmol mL^{-1} exogenous glucose assimilation in the first 24 h. The elevated production of H_2 in the first 48 h of the run with fructose is independent from fructose uptake.

H_2 production is nearly always accompanied by glycogen degradation except for run with glucose (Fig. 2.6(c)). In all experiments, the initial amount of endogenous glycogen per culture volume was fixed at 0.2±0.04 μmol mL^{-1}. The run without sugar shows that the decrease of glycogen from 0.21 μmol mL^{-1} to 0.06 μmol mL^{-1} results in the increase of y_{H2} from zero to 1.79 μmol mL^{-1} during 96 h. Decomposition of 1 mol glucose in glycogen and associated decomposition of other biomaterials are found to generate 12 mols of H_2. For run without monosaccharide, Eq.(2.6) is applicable as a rough approximation, while for runs with monosaccharides, Eq.(2.6) cannot interpret the change of endogenous glucose concentration. Approximated 0.20 μmol mL^{-1} increase in endogenous glucose in glycogen is observed in the first 24 h of

run with glucose. Decrease in endogenous glucose in glycogen of the cell in run with glucose is also seen after 24 h. Curves for the amount of glycogen per culture volume shows that glycogen assimilation is inactivated at 48 h.

Contact of exogenous monosaccharide with cells of GT strain is found to trigger to activate enzymes in endogenous glucose decomposition pathways. The highest final $y_{H2,f}$ is seen in run with glucose. The comparable highest glycogen amount hence highest $y_{H2,f}$ is seen in run with fructose. Glucose is found to be useful to elevate the level of endogenous glucose in glycogen. Fructose is found to be useful to inhibit the decomposition of endogenous glucose in glycogen. Even after 48 h, H_2 production possibly proceeds for additional 96 h. Hence endogenous glycogen decomposition cannot make up the bulk source of the reductive potential for H_2 production.

The dry cell weight concentration of the run with fructose is stable. Stability of dry cell weight in the presence of fructose is quite different from the observation in a previous report (Flores and Schmetterer 1986) which concerns the photoheterotrophic incubation of WT strain on BG-11 medium with 20 μmol mL^{-1} fructose to evaluate the fructose toxic that is the degree to which fructose exerts damage to WT strain. The 0.1% survival after 2 d was reported. We find that the dark anaerobic incubation of GT strain in nitrate free solution with fructose supports cell survival.

The dry cell weight concentration of run with glucose increases during the first 72 h with the specific growth rate of 0.0038 h^{-1}. The doubling time of this run is 182 h that is 0.4 times that observed on 28 μmol mL^{-1} glucose in the previous work (Anderson and McIntosh 1991). The K_d values for run without monosaccharide, with xylose, and for runs after 48 h with galactose and mannose are 1.08, 2.49, 1.52 and 2.13 h^{-1}, respectively.,

The assimilated glucose appears to be utilized for glycogen synthesis (Fig. 2.6(c)), cell growth (Fig. 2.6(d)) and acid production (Fig. 2.6(f),(g),(h)). Galactose and mannose also support to keep cell viability in the first 48h, while cannot support cell survival after 48 h. Dry cell weight concentration decreases with time in xylose or in solution without reducing sugars.

The pH of runs without or with monosaccharide other than glucose decreases from 7.7 at initial to 7.5 at 96 h. The decreases in pH of these runs are undefined while that of run with glucose is remarkable. The pH of run with glucose drops linearly with time from 7.7 at initial to 6.8 at 96 h. The decrease of pH is a result of production of organic acids by cells.

Major metabolic products other than H_2 and CO_2 are lactate, acetate (Fig. 2.6(f)), lactate (Fig. 2.6(g)) and succinate (Fig. 2.6(h)). If the amount of total acid is defined by the summation of amounts of acetate, lactate and succinate, if the amount of total glucose is defined by the summation of amounts of exogenous glucose and endogenous glucose, then H_2 production, total acid production and total glucose consumption in the first 48 h of run with glucose are 2.29, 17.7, and 7.98 $\mu mol \cdot mL^{-1}$, respectively. Complete theoretical conversion of glucose to these acids through only EMP pathway estimates the production of 16 $\mu mol \cdot mL^{-1}$ acids and H_2. Hence it turns out that some portion of carbon in total acid is supplied from metabolisms other than glycolysis. Except for the run with glucose, the production of H_2 is very active during the first 48 h, whereas the production of lactate, acetate and succinate are extremely low.

A previous study reports that the accumulation of acetate, which is produced via pyruvate:flavodoxin/ferredoxin Oxidoreductase (PFOR), leads to increase reductive flavodoxin/ferrodoxin to provide excess electrons for hydrogenase (Gutekunst *et al*. 2014). According to the previous work (Das and Veziroğlu 2001), the increase in acetate production leads the increase in NAD(P)H production, followed by the increase in H_2 production. This mechanism is different from our observation that H_2 production is high at the beginning of dark incubation where acetate production is low, and that H_2 production is inactivated when acetate production becomes active after 48h. In presence of fructose, electron supply to hydrogenase is not from acetate production via PFOR.

Metabolic product distribution analysis shows that succinate in incomplete tricarboxylic acid (TCA) cycle that lacks 2-oxoglutarate dehydrogenase is a major end-product on glucose fermentation. The supply of 2-oxaglutarate from glycolysis, decompositions of amino acids from proteins, membrane lipids and PHB in *Synechocystis* sp. strain PCC6803-GT by dark anaerobic shift with nitrate starvation results in a high level of succinate. The enzyme for this mechanism is not yet well elucidated (Cooley *et al*. 2000). *Synechococcu*s sp. PCC 7002 possessing incomplete TCA cycle have succinic semiadehyde as a shortcut from the missing step (Zhang and Bryant 2011). Presence of all metabolites (malate, fumarate and succinate) in reductive branch of TCA cycle suggested NADH oxidation to elevate succinate in reductive TCA arm. The enzymes of reductive branch are phosphoenolpyruvate (PEP) carboxylase, malate dehydrogenase, fumarase and succinate dehydrogenase. The anoxic glucose-fermentation of *E.coli* also produced succinate by reductive TCA cycle. This result has suggested that TCA cycle had a role in anoxia glucose metabolism.

Except for run with glucose, the production of H_2 is very active during the first 48 h, whereas the production of lactate, acetate and succinate are extremely low. Hence early H_2 production is found to be catalyzed on NiFe-linked hydrogenase, utilizing not reductive flavodoxin/ferredoxin but NAD(P)H, the

bulk of which is not provided by acid production pathways but by initial stock and by catabolism of intracellular storage compound including proteins, membrane lipids and poly-β-hydroxybutyrate (PHB). Acetate and succinate are observed after 48 h. The proportion of the total amount of acetate and succinate in total acid in the run with glucose at 96 h is 92.6%. Such large proportion of acid is produced through PFOR. The major source of electrons for NiFe-hydrogenase in this system is found to shift from NAD(P)H to reductive flavodoxin/ferredoxins.

From Eq.(2.36), the relative consumption rate of reductive compounds ($-r_{\mathrm{RED}}^{*}$) is shown by

$$-r_{RED}^{*} = \frac{d}{dt}(m_{RED}^{*} X^{*}) = (k + K_d) q_{H2,0}^{*} X_0^{*} \exp\{-(k + K_d)t\} \tag{2.38}$$

for no cell growth case or

$$-r_{RED}^{*} = \frac{d}{dt}(m_{RED}^{*} X^{*}) = (k - \mu) q_{H2,0}^{*} X_0^{*} \exp\{-(k - \mu)t\} \tag{2.39}$$

for cell growth case.

Time course of reaction rates of run without monosaccharide is shown in **Figure 2.11**. Graph (a) shows the time course of NAD(P)H consumption rates r_{H2}, $R_G X$, r_X, r_L, r_A, r_{SUC} and (b) NAD(P)H production rates, ($-r_S$), ($-R_G X$), ($-r_X$). The order of magnitude of NAD(P)H consumption rates is found to be higher than that of NAD(P)H production rate. Glycolysis provides about 10% of NAD(P)H for H_2 production. The remaining amount of NAD(P)H is supplied by other pathways of which reactions are accompanied by glycolysis at the beginning of dark anaerobic incubation. Decrease in the consumption rate of endogenous glucose with time and decrease in the production of H_2 with time are similar trends, however, NAD(P)H generated by glycolysis is insufficient to support the high rate of H_2 production which less than 10 time. This has suggested that there is other pathways providing NAD(P)H to hydrogenase. The ($-R_G X$) versus time data resemble that of the r_{SUC} versus time data. The r_L is smaller than ($-R_G X$).

Figure 2.12 shows the time courses of (a) NAD(P)H consumption rates r_{H2}, $R_G X$, r_X, r_L, r_A, r_{SUC} and (b) NAD(P)H production rates, ($-r_S$), ($-R_G X$), ($-r_X$) in run with glucose. Decrease in the consumption rate of endogenous glucose with time and decrease in the production of H_2, acetate and succinate with time are similar. The NAD(P)H generated by glycolysis from uptake of exogenous glucose is comparable to that for supporting the high rate of H_2 production, succinate production, acetate production The r_{H2} is lower than ($-r_S$), however, the r_{H2} of this run is similar to that of run with fructose of which ($-r_S$) is very small.

The r_{H2} and the r_L are comparable order. The r_A and $r_{SUC}/2$ are higher than r_L and comparable with $(-r_S)$. Dry cell weight increases for 72 h. The large portion of assimilated exogenous glucose appears to be converted to dry cell weight, succinate and acetate. Lower amount appears to be converted to lactate and in early stage to endogenous glucose.

Figure 2.13 shows the results of run with fructose. The r_{H2} is higher than that of run without monosaccharide. The r_A, r_L and r_{SUC} are not zero but lower than those shown in Fig.2.11. The $(-r_G)$ is smaller than r_{H2}, however, there seems to be a cross talk between endogenous glucose consumption and H_2 production. Reductive compounds for H_2 production is assumed to be supplied not by glycolysis of exogenous glucose and endogenous fructose consumption but by decomposition of other macro molecules.

Figure 2.14 shows the results of run with galactose. The relation between reaction rates of this run is similar to that shown in Fig.2.13, however, r_{H2} is lower than that of run with fructose. The r_{SUC} versus time data resemble to the $(-r_S)$ versus time data. Acetate production seems to the main carbon sinks from galactose as they show the same consumption and production.

Figure 2.15 shows the results of run with with mannose. The relation between reaction rates of this run is similar to that shown in Fig.2.13, however, r_{H2} is lower than that of run with fructose. The $(-r_S)$ for mannose is extremely high so that supply of NAD(P)H from mannose appears to support the need for H_2 production.

Figure 2.16 shows the results of run with xylose. The relation between reaction rates of this run is similar to that shown in Fig.2.14.

As viewed on Figs. 2.11-2.16, there seems to be an indirect relation between decomposition of endogenous glucose and H_2 production. Glycolysis appears to be a marker reaction for global generation of NAD(P)H. Eq.(2.33) implies that the initial cellular content of NAD(P)H defines the attainable level of the number of moles of H_2 per culture volume. If the initial cellular content of NAD(P)H also defines the attainable level of the number of moles of endogenous glucose per culture volume ($(m_G X)_f$), then Eq.(2.33) suggests that the attainable level $y_{H2,f}$ is able to be referred to $(m_G X)_f$. After 48h, no remarkable variation is seen in m_G and X with time and $y_{H2,f}$ is able to be referred to $y_{H2,1}$ (Fig.2.7), hence, instead of studying a relation in a pair of $(m_G X)_f$ and $y_{H2,f}$, a relation in a pair of $(m_G X)_1$ and $y_{H2,1}$ is elucidated.

Figure 2.17 shows plots of $y_{H2,1}$ against $(m_G X)_1$. It is found that the increase in the number of moles of H_2 per culture volume at 96 h is accompanied by the increase in the number of moles of endogenous glucose per culture volume at 96 h. Solid line in the graph is correlated by

$$y_{H2,1} = k_5 (m_G X)_1^{k_6} \quad (2.40)$$

in which subscript 1 shows the state at 96 h, and k_5 and k_6 are model constants. Curve fitting results in that the parameters are k_5,5.21; and k_6, 0.379 $\mu mol^{0.621}$ $mL^{-0.621}$. To keep high level of amount of endogenous glucose per culture volume is found to be important to increase H_2 production.

Since there are several dehydrogenase-pathways involved in dark anaerobic metabolism by *Synechocystis* sp. strain PCC6803, this study focused only on measurable parameters which are believed to be important. Observation of monitored parameters suggests that main mechanisms for NAD(P)H production are decomposition of dry cell weight, degradation of glycogen and turnover of other biochemical compounds in run without monosaccharides. If available monosaccharide exists in cellular environment, its consumption also contributes to the main mechanism of NAD(P)H production. Major consumption of NAD(P)H is H_2 production on NiFe-hydrogenase in runs without monosaccharide, with mannose or xylose. Acetate production is the main NAD(P)H consumption in runs with glucose, fructose and galactose. The most interesting point is the highest succinate production when glucose is present. Succinate appears to be an important electron sink for dark anaerobic glucose metabolism. Succinate production is peculiar to glucose fermentation and it doesn't occur from the assimilation of other monosaccharides that results acetate as an electron sink. The amount of lactate produced in runs w/o monosaccharide, with fructose, galactose, mannose, xylose are comparable except for run with glucose. Lactate production is not affected by monosaccharide. Carbon sources for lactate are found to be intracellularly accumulated compounds.

Figure 2.18 shows a proposal of conceivable mechanism of dark H_2 production of GT strains in nitrate free solution. Before dark incubation, GT strains are grown on CO_2 under the light and the bulk of chemical energy is stored in glycogen, protein, membrane lipid and PHB (Montagud et al. 2010). Nitrate starvation at the beginning of dark incubation appears to trigger the instantaneous sudden accumulation of reductive compounds NAD(P)H. The shift of cellular environment from illuminated culture in BG-11 medium to dark nitrate free solution also appears to trigger the decomposition of glycogen, protein, membrane lipid and PHB. This reaction produces additional reductants. The excess NADH, NADPH and reductive ferredoxin are utilized for hydrogen on NAD(P)H-linked hydrogenase throughout the reaction and on reductive ferredoxin-linked hydrogenase after 48 h.

2.4 Summary

The dark anaerobic H_2 production of GT strain in HEPES buffer solution without or with monosaccharide (glucose, fructose, galactose, mannose or xylose) has been studied by following the time courses of the number of moles of H_2 per solution, the concentration of unreacted monosaccharide, the number of moles of endogenous glucose, and concentrations of dry cell weight, lactate, acetate and succinate. The highlights of this chapter are as follows.

1. The addition of exogenous reducing sugar to dark anaerobic HEPES buffer solution is useful to increase initial H_2 production activity of NiFe-hydrogenase in GT strain.

2. A mathematical model to interpret dark anaerobic H_2 production kinetics was formulated.

3. The H_2 production of GT strain in dark anaerobic HEPES buffer solution is found to be elevated by limiting glycogen decomposition, cell breakage and hydrogenase deactivation under stresses (nitrate deprivation and dark anaerobic). The more glycogen storage, the more H_2 production was observed.

4. Relations between the attainable level of the number of moles of H_2 per culture volume and the initial H_2 production rate, and between the final level of the number of moles of H_2 per culture volume and the final level of the number of moles of endogenous glucose per culture volume are developed. The H_2 production of GT strain in dark anaerobic HEPES buffer solution is found to be elevated by limiting glycogen decomposition, cell breakage and hydrogenase deactivation under stresses (nitrate deprivation and dark anaerobic). The shift-up the amount of stored glycogen is of utmost importance to elevate H_2 production

5. Glucose and fructose are characterized as monosaccharides that bring cells to produce higher amount of H_2 per culture volume. Different from glucose, fructose elevates attainable level of H_2 without assimilation of fructose. The mechanism by which these monosaccharides exact this effect remains to be elucidated.

6. Reductive wing of incomplete TCA cycle is important in mixotrophic growth under dark anaerobic condition.

7. A large portion of electrons for H_2 production on NiFe-hydrogenase are supplied not only by glycolysis to generate acetate but also by other degradation reactions, the progress of which can be roughly monitored by that of glycolysis. Glycolysis is available as a marker reaction of global decomposition of cell constituting materials after incubation of cells into dark anaerobic HEPES buffer solution with or without monosaccharide.

Table 2.1 Physical property data of monosaccharides.

ΔH_f^0: Enthalpy of formation of solid at standard conditions

	Glucose	Fructose	Galactose	Mannose	Xylose
Chemical structure	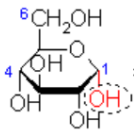	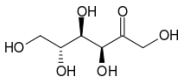	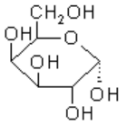	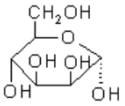	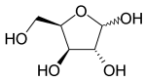
Molar mass [μg μmol^{-1}]	180.16	180.16	180.16	180.16	150.13
ΔH_f^0 [mJ μmol^{-1}]	-1274.43(aq.; α-D-glucose	-1265.6(S)	-1271.50	-1263.4(S)	-750.5

Table 2.2 Composition of BG-11 medium

	Compound	Amount per milliliter
Stock1	$NaNO_3$	1.5 mg
	$MgSO_4 \cdot 7H_2O$	0.075mg
Stock2	$CaCl_2 \cdot 2H_2O$	0.036mg
Stock3	Citric acid	0.00656mg
	Ferric ammonium	0.006mg
	EDTA·2Na	0.00114mg
Stock4	Trace metal mix A5	1.0μL
Stock5	K_2HPO_4	0.04mg
Stock6	Na_2CO_3	0.02mg

Trace metal mix A5

Compound	Amount per milliliter
H_3BO_3	2.86mg
$MnCl_2 \cdot 4H_2O$	1.81mg
$ZnSO_4 \cdot 7H_2O$	0.222mg
$Na_2MoO_4 \cdot 2H_2O$	0.39mg
$CuSO_4 \cdot 5H_2O$	0.079mg
$Co(NO_3)_2 \cdot 6H_2O$	0.0494mg

Table 2.3 Kinetic parameters for H_2 production in GT strain in HEPES buffer solution without or with reducing sugars. $q^*_{H2,0}$, $q_{H2,0}/(q_{H2,0})_{w/o}$; $y^*_{H2,f}$, $y_{H2,f}/(y_{H2,f})_{w/o}$; and $k^*=k/(k)_{w/o}$. $y_{H2,1}$, c_{L1}, c_{A1}, observed number of moles of H_2, lactate and acetate per culture volume at 96 h. m_{G1}, X_1, observed m_G and X at 96h; $\Delta(m_GX)_1$, observed decrease in m_GX during 96 h H_2 production; $Y_{H2/G}=y_{H2,1}/\Delta(m_GX)_1$

	w/o	Glucose	Fructose	Galactose	Mannose	Xylose
X_0 [mg·mL^{-1}]	2.09	2.17	2.14	2.06	2.13	2.15
$r_{H2,0}$ [μmol·mL^{-1}·h^{-1}]	0.0405	0.0730	0.0674	0.0527	0.0369	0.0305
$q_{H2,0}$ [μmol·mg^{-1}·h^{-1}]	0.0194	0.0336	0.0315	0.0256	0.0173	0.0142
$q^*_{H2,0}$ [-]	1	1.73	1.62	1.32	0.892	0.732
$y_{H2,f}$ [μmol·mL^{-1}]	2.18	3.26	3.05	2.33	2.51	2.06
$y^*_{H2,f}$ [-]	1	1.50	1.40	1.07	1.15	0.945
k [h^{-1}]	0.0186	0.0224	0.0221	0.0226	0.0147	0.0148
k^* [-]	1	1.20	1.19	1.22	0.790	0.796
K_d [h^{-1}]	0.0011	0	0	0.0015	0.0019	0.0025
$y_{H2,1}$ [μmol·mL^{-1}]	1.79	2.81	2.62	2.03	1.85	1.52
m_{G1} [μmol·mg^{-1}]	0.032	0.080	0.072	0.050	0.037	0.023
X_1 [mg·mL^{-1}]	1.86	2.55	2.12	1.77	1.68	1.65
$(m_GX)_1$ [μmol·mL^{-1}]	0.0595	0.204	0.153	0.0885	0.0622	0.0380
$c_{L,1}$ [μmol·mL^{-1}]	0.258	3.12	0.210	0.225	0.293	0.235
$c_{A,1}$ [μmol·mL^{-1}]	0.208	15.3	3.02	1.50	0.479	0.507
$\Delta(m_GX)_1$ [μmol·mL^{-1}]	0.151	-0.025	0.076	0.075	0.156	0.154
$Y_{H2/G}$ [-]	11.8	-	34.6	27.3	11.9	9.9

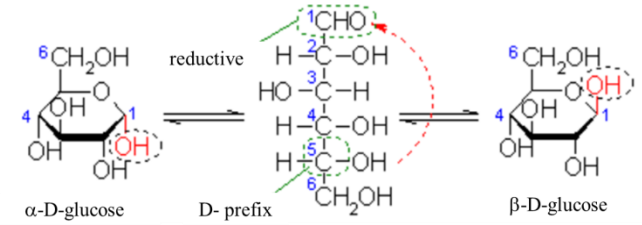

Figure 2.1 Conversion of acylic forms and glucopyranososes.

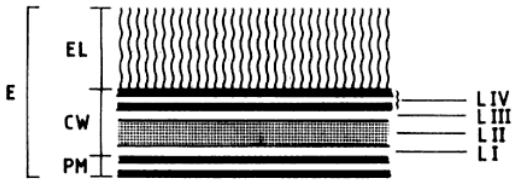

Figure 2.2 Cyanobacterial cell envelope, E, cell envelope; PM, plasma membrane; CW, cell wall; EL, external layer; LII, peptidoglycan layer; LIV, outer membrane; LI, LIII, space between layers (Drews et al.,1982)

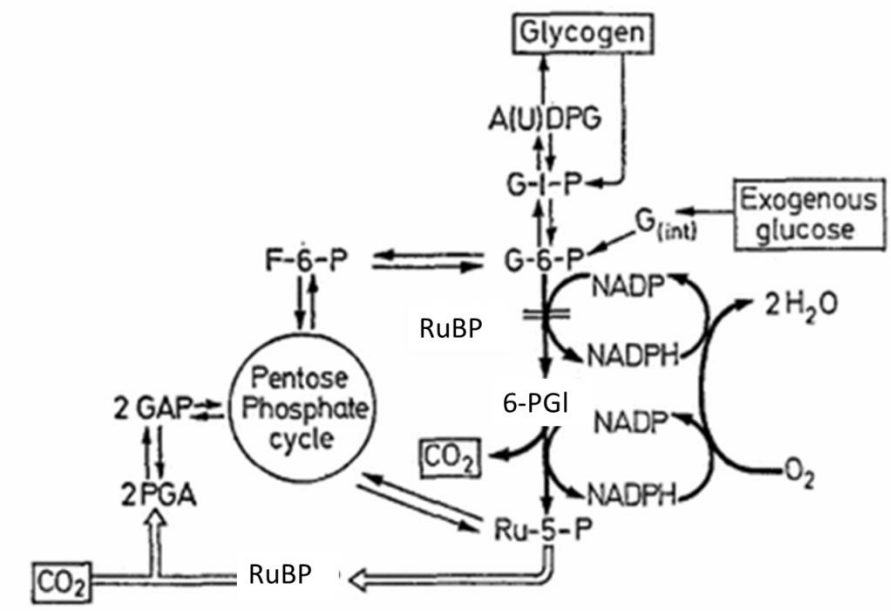

Figure 2.3 A simplified metabolic map to show carbon metabolism of *Aphanocapsa* 6714 in the light (Pelroy et al., 1976). White arrows, reactions specify to photosynthetic CO_2 assimilation; heavy dark arrows, reactions specific both to dark endogenous respiration and to the respiratory metabolism of glucose. A(U)DPG, ADP-glucose or UDP-glucose; G-1-P, glucose-1-phosphate; G-6-P, glucose-6-phosphate; $G_{(int.)}$, endogenous glucose; F-6-P, fructose-6-phosphate; 6-PG, 6-phosphogluconate; Ru-5-P, ribulose-5-phosphate; RuBP, ribulose-1,5-diphosphate; PGA, 3-phosphoglycerate; GAP, glyceraldehyde-3-phosphate

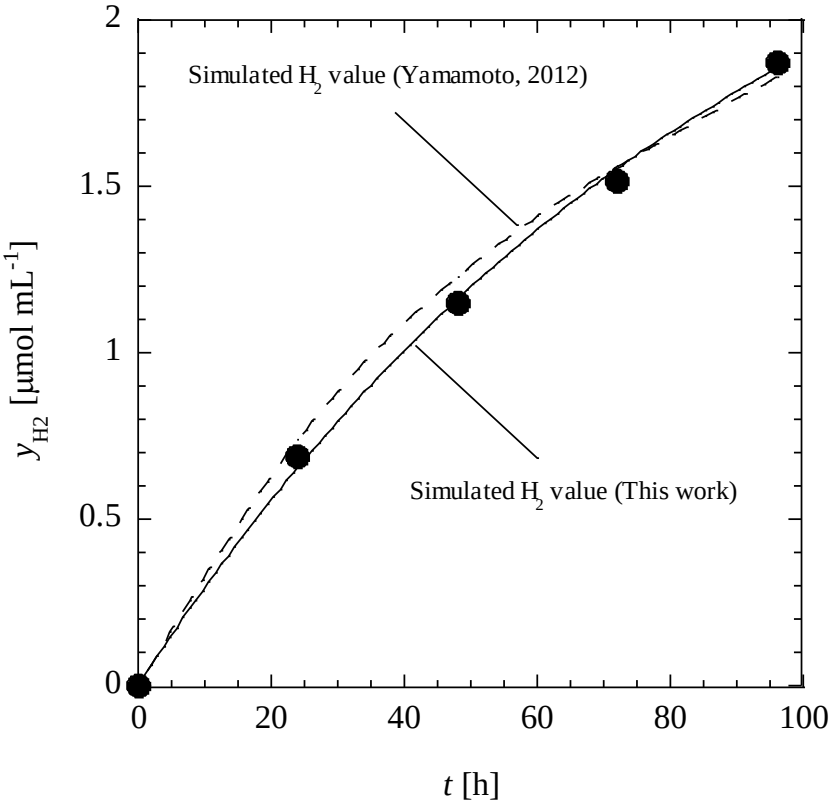

Figure 2.4 Time course of the amount of H_2 per culture volume shown in a previous work (Yamamoto, 2011). Broken line, simulated y_{H2} value by Yamamoto; solid line, simulated y_{H2} value utilizing Eq.(2.17) in this work

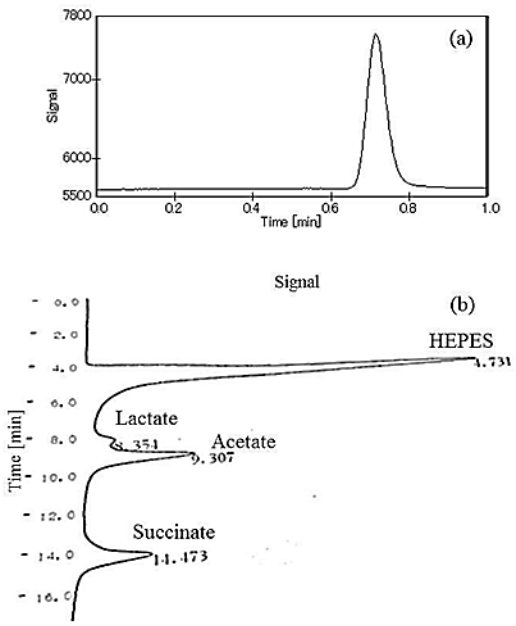

Figure 2.5 Peaks of metabolic products under dark anaerobic incubation of *Synechocystis* sp. strain PCC6803-GT. Cells were suspended in nitrate-free HEPES buffer supplemented with 28 μmol mL^{-1} glucose. (a) Single peak represents H_2 detected from Gas Chromatography analysis, GC-320, GL science Inc.; column, Molecular sieve 13X; column temperature, 37 ºC; injector temperature, 45 ºC; detector temperature 80 ºC with nitrogen gas as the carrier gas. (b) Four peaks are HEPES, lactatic acid, acetate and succinate detected from HPLC analysis (JASCO PU-2080 Plus and UV-2075 Plus). Mobile phase was 18 mmol L^{-1} KH_2PO_4, pH of which was adjusted at 2.3 with H_3PO_4. Flow rate of mobile phase was 0.7 mL min^{-1}. Column temperature was 30 °C

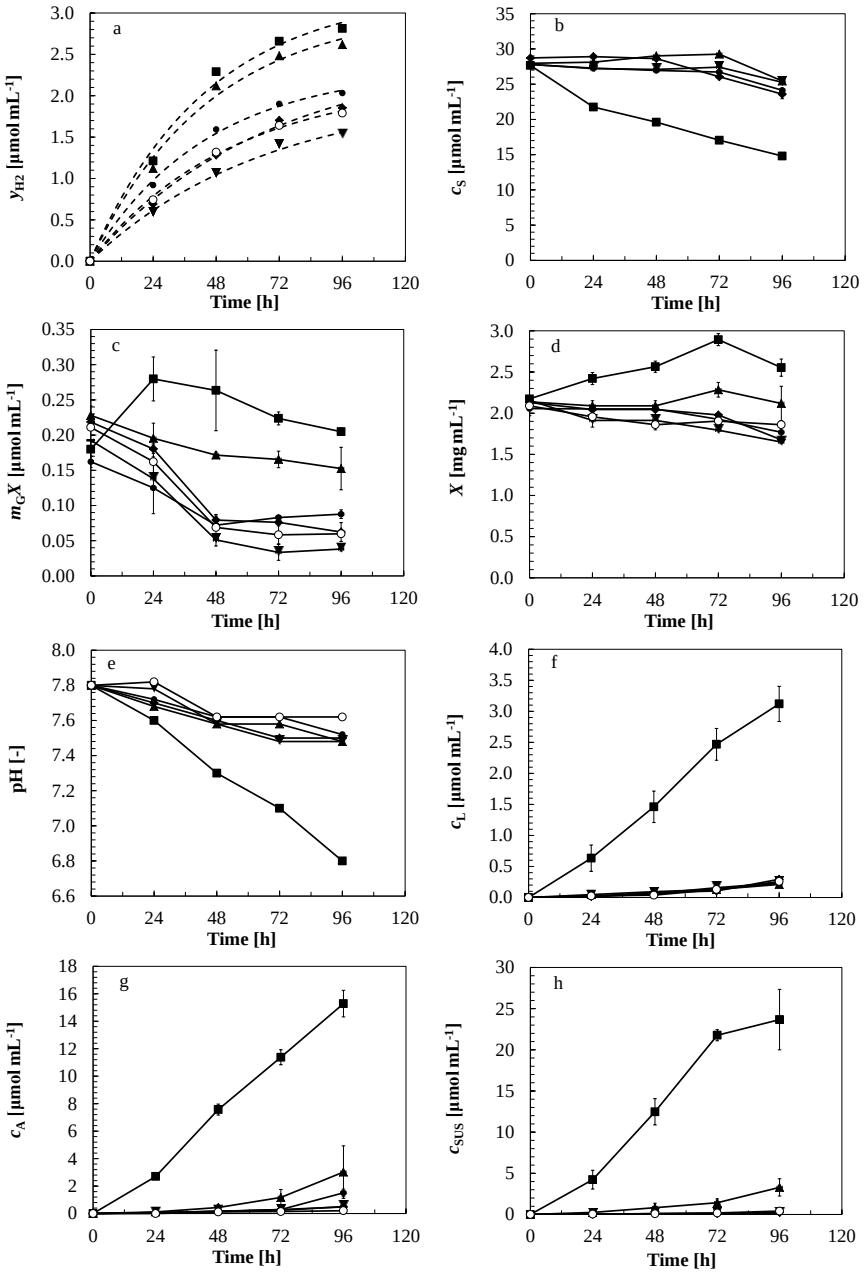

Figure 2.6 Time courses of culture variables measured in runs without (○) or with 28 µmol mL^{-1} reducing sugars (glucose (■), fructose (▲), galactose (●), mannose (◆) and xylose (▼)). Quantities analyzed are (a) the mole of H_2 per culture volume (y_{H2}), (b) the concentration of exogenous reducing sugars (c_S), (c) the amount of endogenous glucose per culture volume (c_G), (d) the concentration of dry cell weight (X), (e) pH of cell suspension, (f) the concentration of lactate, (g) the concentration of acetate and (h) the concentration of succinate under dark anaerobic incubation.

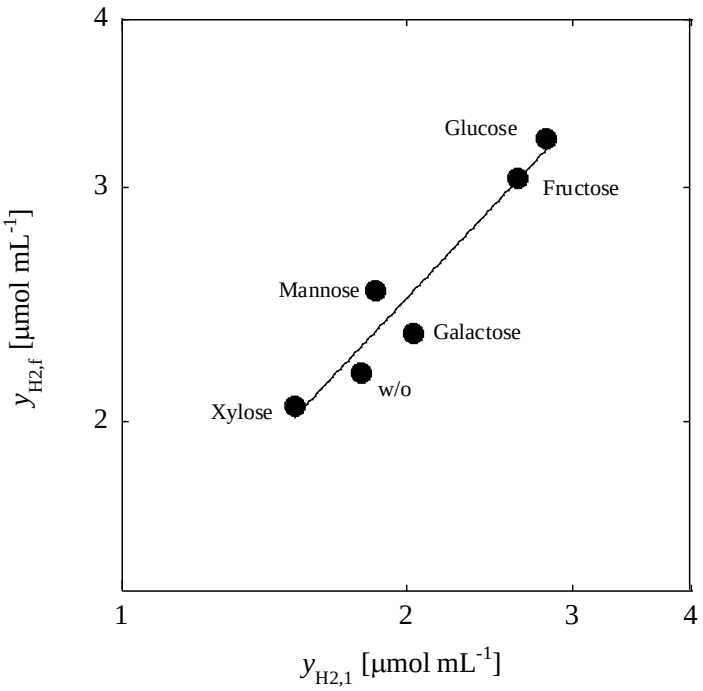

Figure 2.7 relation between observed $y_{H2,1}$ and estimated $y_{H2,f}$

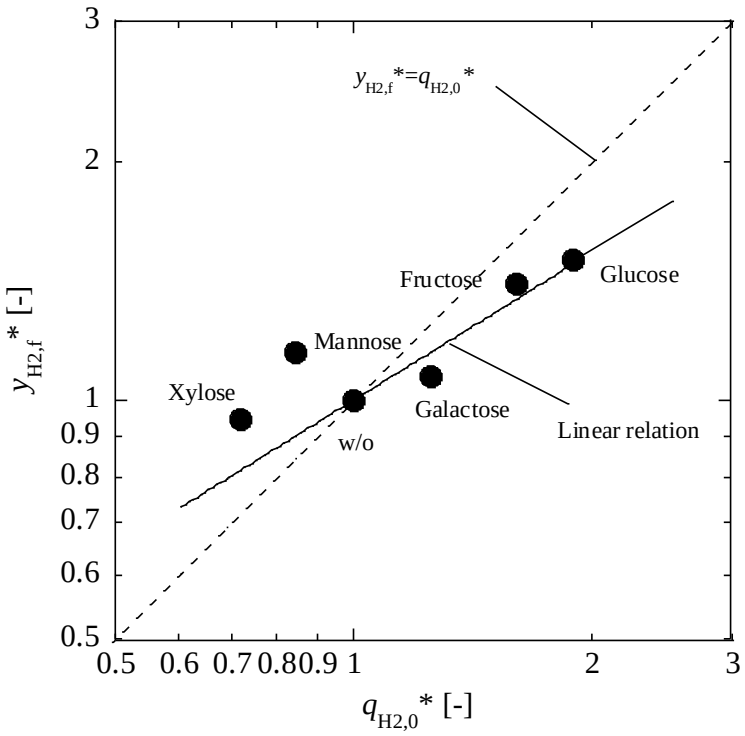

Figure 2.8 Relation between initial specific H_2 production rate and attainable level of H_2

$q_{H2,0}$*=$q_{H2,0}$/($q_{H2,0}$)$_{ref}$; $y_{H2,f}$*=$y_{H2,f}$/($y_{H2,f}$)$_{ref}$; Reference run, without monosaccharide

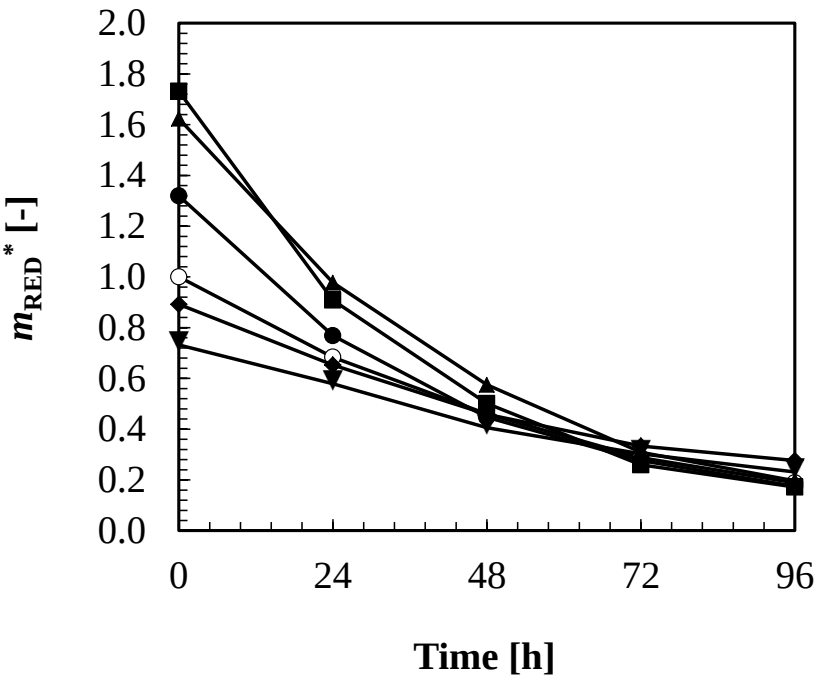

Figure 2.9 Time courses of the calculated m_{RED}* in runs without (○) or with 28 μmol mL^{-1} reducing sugars, (glucose (■), fructose (▲), galactose (●), mannose (◆) and xylose (▼)).

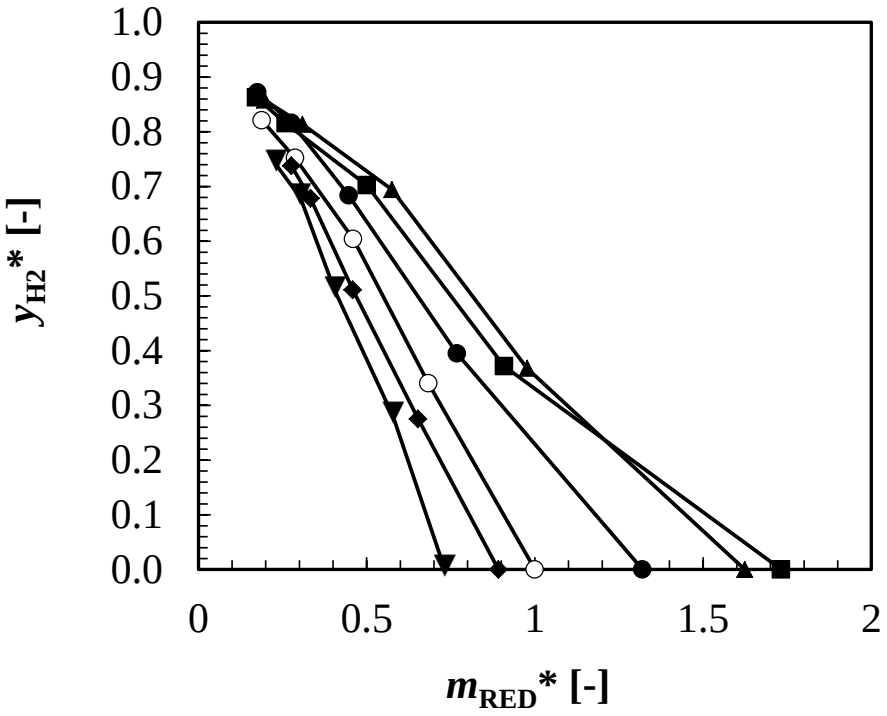

Figure 2.10 Relation between y_{H2}^{*} and m_{RED}^{*}

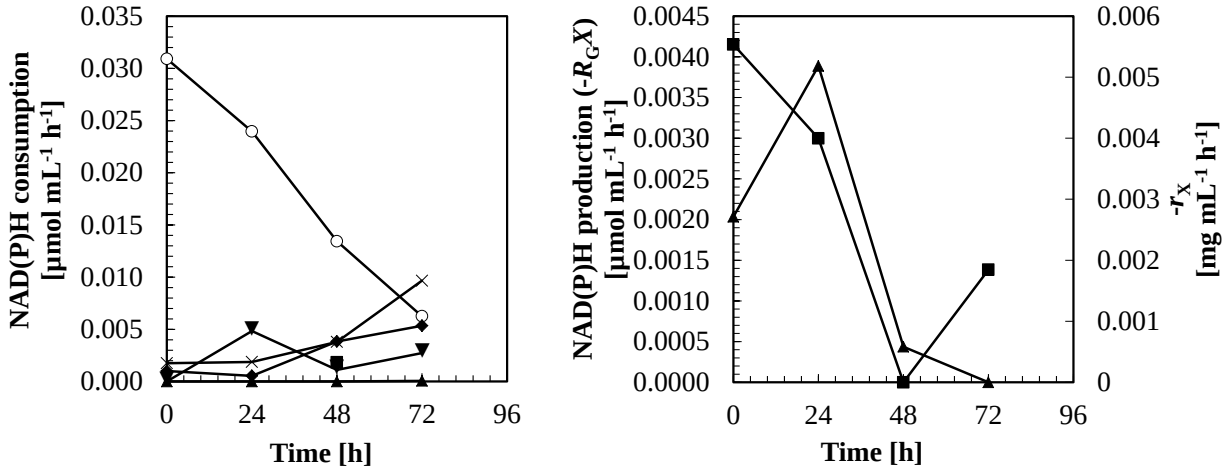

(a) (b)

Figure 2.11 Time courses of the rates for (a) NAD(P)H consumption (r_{H2}, R_GX (>0), r_X(>0), r_L, r_A, r_{SUC}), and (b) NAD(P)H production (($-R_GX$)(>0), ($-r_X$)(>0)) for run without monosaccharide (r_{H2} (○); R_GX,($-R_GX$)(▲); r_X ,($-r_X$)(■), r_L (◆), r_A (▼),r_{SUC} (✕)).

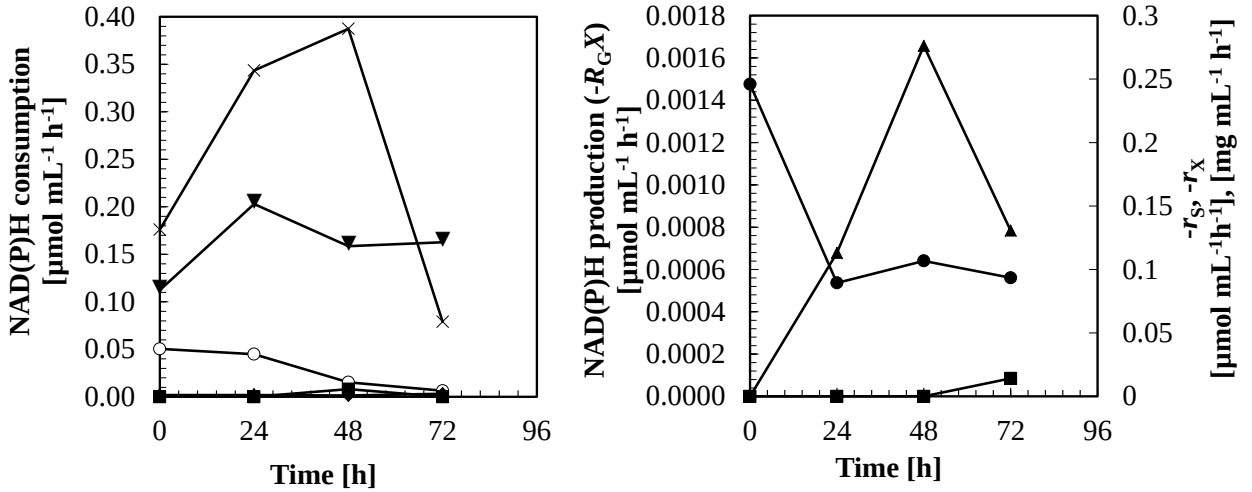

(a) (b)

Figure 2.12 Time courses of the rates for (a) NAD(P)H consumption (r_{H2}, R_GX (>0), r_X(>0), r_L, r_A, r_{SUC}), and (b) NAD(P)H production (($-r_S$), ($-R_GX$)(>0), ($-r_X$)(>0)) for run with glucose (r_{H2} (○); ($-r_S$) (●); R_GX,($-R_GX$)(▲); r_X ,($-r_X$)(■), r_L (◆), r_A (▼),r_{SUC} (✕)).

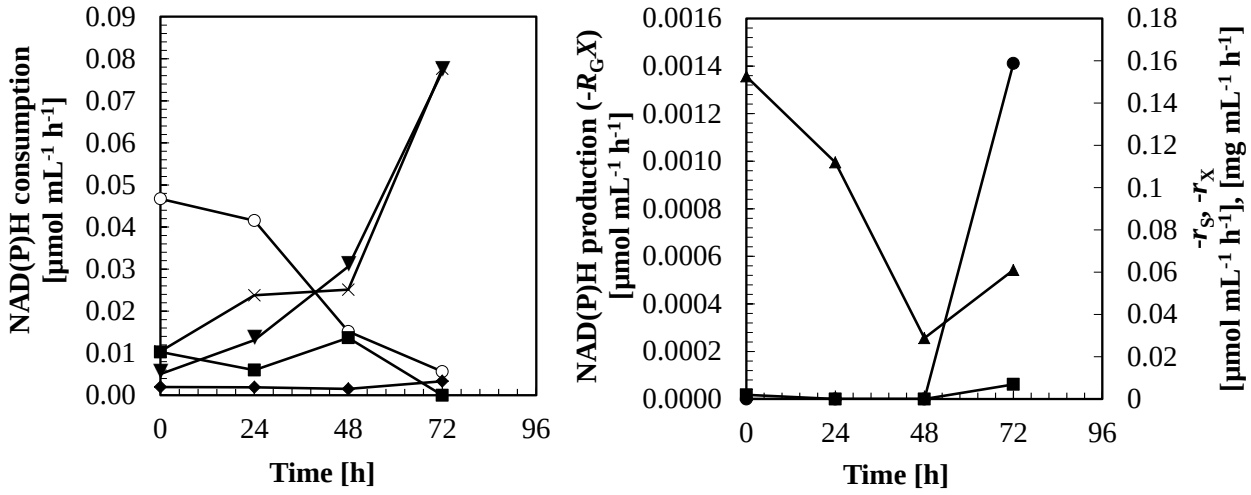

(a) (b)

Figure 2.13 Time courses of the rates for (a) NAD(P)H consumption (r_{H2}, R_GX (>0), r_X(>0), r_L, r_A, r_{SUC}), and (b) NAD(P)H production ((-r_S), (-R_GX)(>0), (-r_X)(>0)) for run with fructose (r_{H2} (○); (-r_S) (●); R_GX,(- R_GX)(▲); r_X ,(- r_X)(■), r_L (◆), r_A (▼),r_{SUC} (✕)).

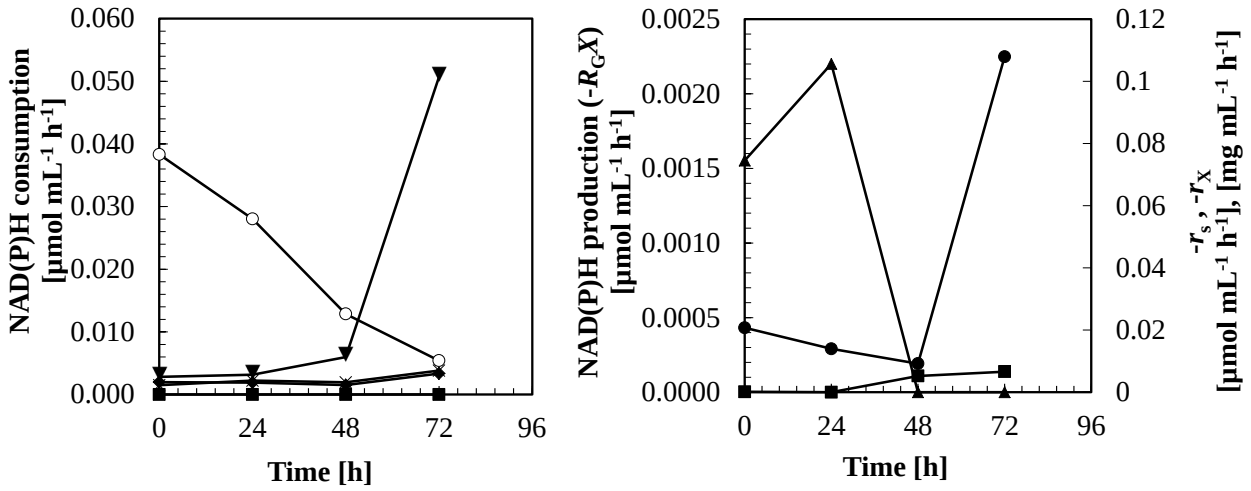

(a) (b)

Figure 2.14 Time courses of the rates for (a) NAD(P)H consumption (r_{H2}, R_GX (>0), r_X(>0), r_L, r_A, r_{SUC}), and (b) NAD(P)H production ((-r_S), (-R_GX)(>0), (-r_X)(>0)) for run with galactose (r_{H2} (○); (-r_S) (●); R_GX,(- R_GX)(▲); r_X ,(- r_X)(■), r_L (◆), r_A (▼),r_{SUC} (✕)).

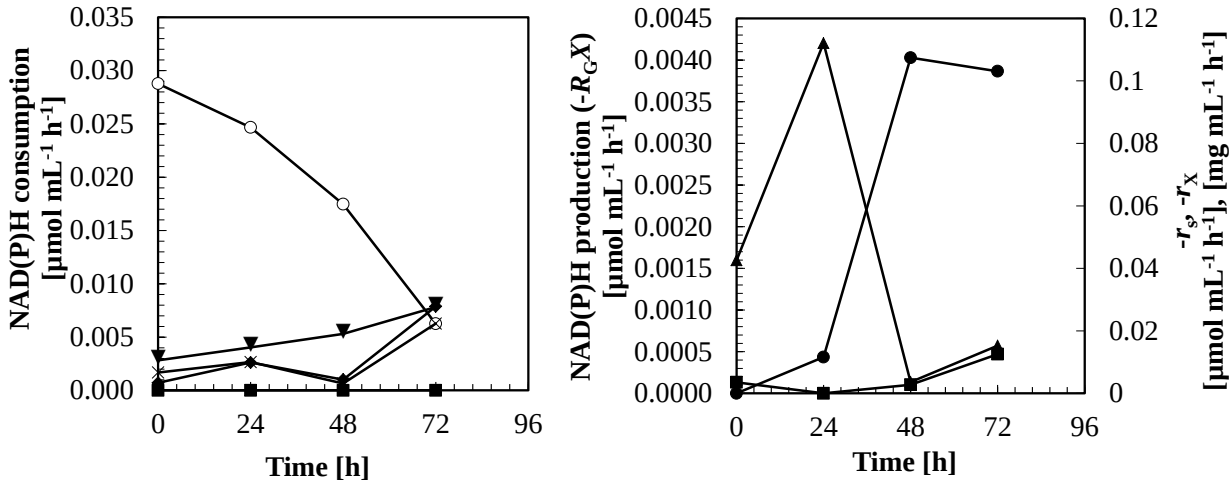

(a) (b)

Figure 2.15 Time courses of the rates for (a) NAD(P)H consumption (r_{H2}, R_GX (>0), r_X(>0), r_L, r_A, r_{SUC}), and (b) NAD(P)H production (($-r_S$), ($-R_GX$)(>0), ($-r_X$)(>0)) for run with mannose (r_{H2} (○); ($-r_S$) (●); R_GX,($-R_GX$)(▲); r_X ,($-r_X$)(■), r_L (◆), r_A (▼),r_{SUC} (✕)).

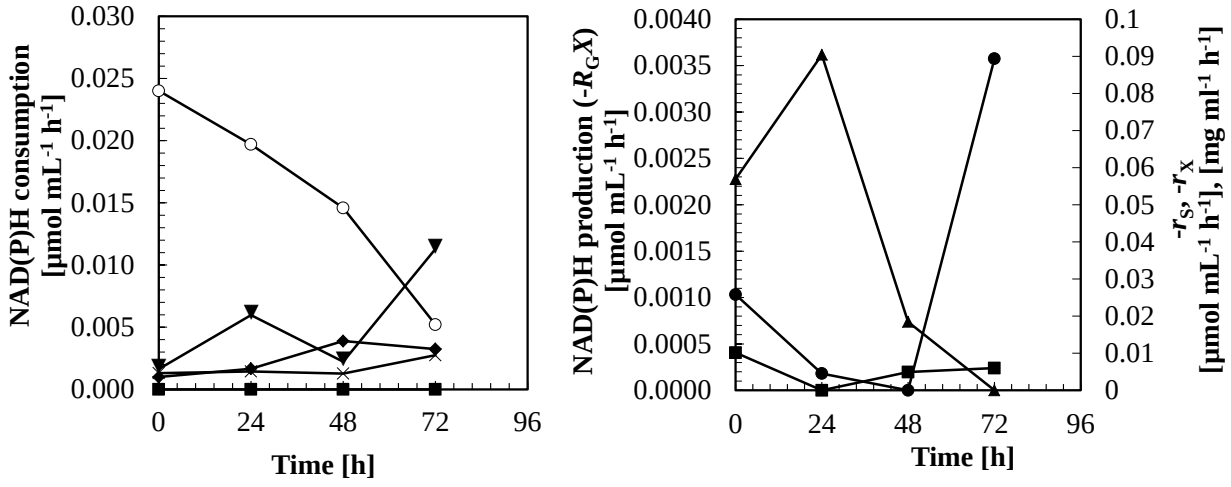

(a) (b)

Figure 2.16 Time courses of the rates for (a) NAD(P)H consumption (r_{H2}, R_GX (>0), r_X(>0), r_L, r_A, r_{SUC}), and (b) NAD(P)H production (($-r_S$), ($-R_GX$)(>0), ($-r_X$)(>0)) for run with xylose (r_{H2} (○); ($-r_S$) (●); R_GX,($-R_GX$)(▲); r_X ,($-r_X$)(■), r_L (◆), r_A (▼),r_{SUC} (✕)).

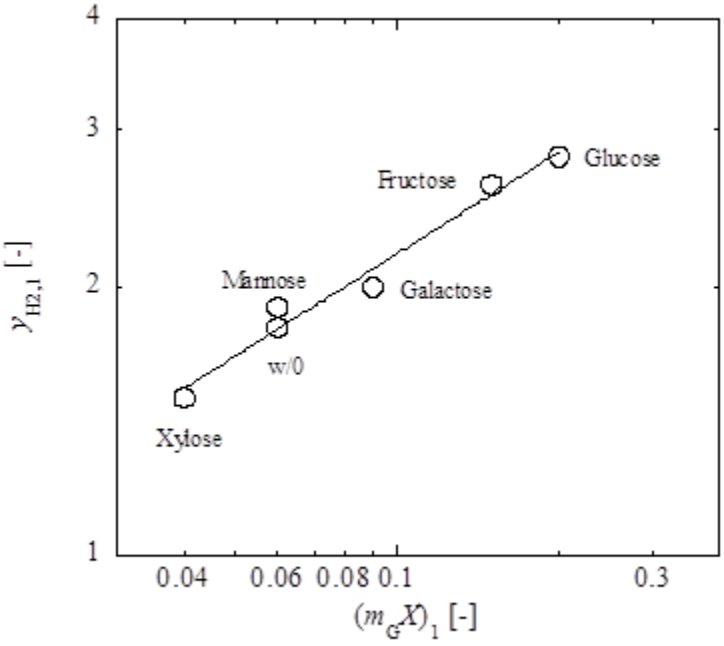

Figure 2.17 Relation between $(m_G X)_1$ and $y_{H2,1}$ of dark anaerobic incubation of GT strain, from late-logarithmic growth phase, in HEPES buffer solution with or without monosaccharides.

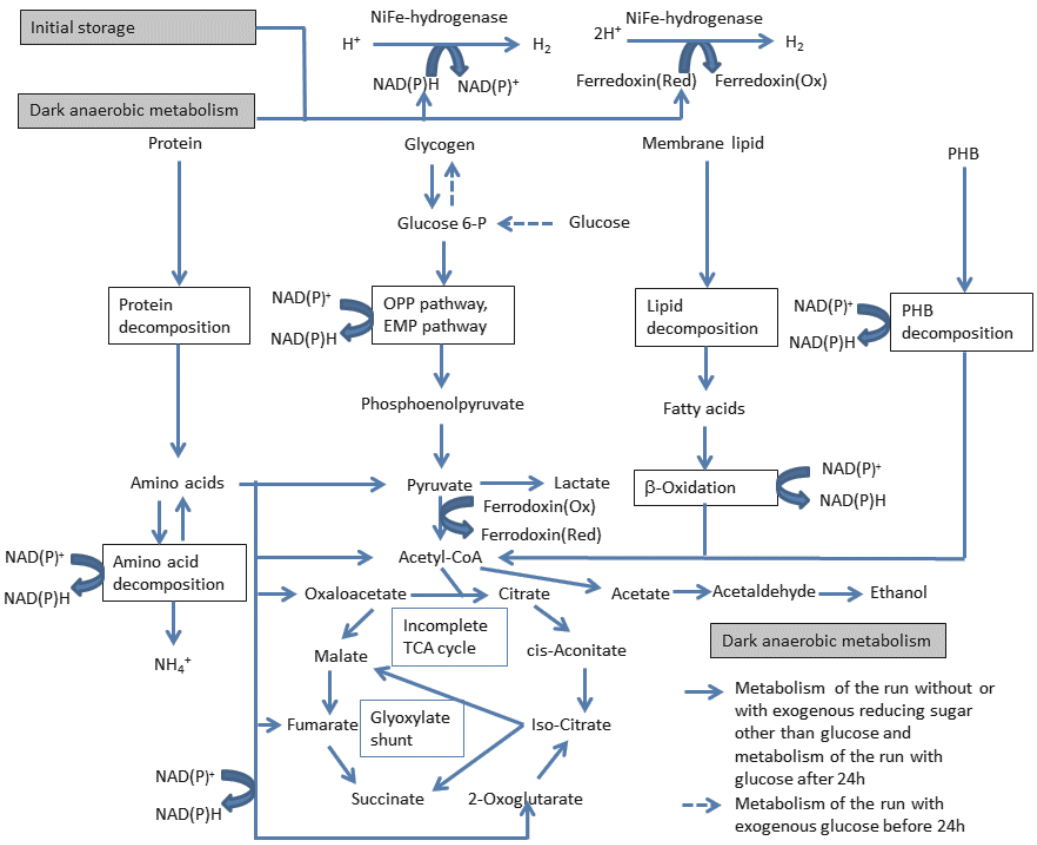

Figure 2.18 Proposed fermentative schemes for a glucose tolerant mutant of *Synechocystis* sp. strain PCC6803 under the dark anaerobic condition on HEPES buffer solution with or without exogenous glucose.

Chapter 2: References

Anderson SL, McIntosh L (1991) Light-activated heterotrophic growth of the cyanobacterium *Synechocystis* sp. strain PCC 6803: a blue-light-requiring process. Journal of Bacteriology 173 (9):2761-2767

Appel J, Phunpruch S, Steinmuller K,Schulz R(2000) The bidirectional hydrogenase of *Synechocystis* sp. PCC 6803 works as an electron valve during photosynthesis. Archive of Microbiology. 173 :333-338

Baebprasert W, Jantaro S, Khetkorn W, Lindblad P, Incharoensakdi A (2011) Increased H_2 production in the cyanobacterium *Synechocystis* sp. strain PCC 6803 by redirecting the electron supply via genetic engineering of the nitrate assimilation pathway. Metabolic Engineering 13 (5):610-616

Cooley JW, Howitt CA, Vermaas WFJ (2000) Succinate:Quinol Oxidoreductases in the Cyanobacterium *Synechocystis* sp. Strain PCC 6803: Presence and Function in Metabolism and Electron Transport. Journal of Bacteriology 182 (3):714-722

Cournac L, Guedeney G, Peltier G, Vignais PM (2004) Sustained photoevolution of molecular hydrogen in a mutant of *Synechocystis* sp. strain PCC 6803 deficient in the type I NADPH-dehydrogenase complex. Journal of bacteriology 186 (6):1737-1746

Das D, Veziroğlu TN (2001) Hydrogen production by biological processes: a survey of literature. International Journal of Hydrogen Energy 26 (1):13-28

De Philippins R, Margheri MC, Vincenzini M (1996) Fermentation in symbiotic and free-living cyanobacteria. Arch. Hydrobiol. Algol. Stud. 83:459-468

Drews G, Weckesser J (1982) Function, structure and composition of cell walls and external layers. in The biology of cyanobacteria, Carr N, Whitton BA eds. Blackwell Scientific Pub., Oxford

Flores E, Schmetterer G (1986) Interaction of fructose with the glucose permease of the cyanobacterium *Synechocystis* sp. strain PCC 6803. Journal Bacteriology 166 (2): 693-696

Gutekunst K, Phunpruch S, Schwarz C, Schuchardt S, R-Friedrich S, J. Appel(2005) LexA regulates the bidirectional hydrogenase in the cyanobacterium *Synechocystis* sp. PCC 6803 as a transcription activator. Molecular Microbiology 58:810-823

Gutekunst K, Chen X, Schreiber K, Kaspar U, Makam S, Appel J (2014) The Bidirectional NiFe-hydrogenase in *Synechocystis* sp. PCC 6803 Is Reduced by Flavodoxin and Ferredoxin and Is Essential under Mixotrophic, Nitrate-limiting Conditions. The Journal of Biological Chemistry 289 (4):1930-1937

Hammett LP (1937) The effect of structure upon the reactions of organic compounds. Benzene derivatives". Journal of the American Chemical Society 59 (1): 96.

Hoare DS, Igram LO, Thurston EL, Walkup R(1917) Dark heterotrophic growth of an endophytic blue-green alga. Arch Mikrobiol 78:310-321

Joset F, Buchou T, Zhang CC, Jeanjean R (1988) Physiological and genetic analysis of the glucose-fructose permeation system in two *Synechocystis* species. Archives of Microbiology 149 (5):417-421

Kahlon S, Beeri K, Ohkawa H, Hihara Y, Murik O, Suzuki I, Ogawa T, Kaplan A (2006) A putative sensor kinase, Hik31, is involved in the response of *Synechocystis* sp. strain PCC 6803 to the presence of glucose. Microbiology 152 (3):647-655

Laroque D, Inisan C, Berger C, Vouland É, Dufossé L, Guérard F (2008) Kinetic study on the Maillard reaction. Consideration of sugar reactivity. Food Chemistry 111 (4):1032-1042

Lee S, Ryu J-V, Kim SY, Jeon J-H, Song JY, Cho H-T, Choi S-B, Choi D, de Marsac NT, Park Y-I (2007) Transcriptional Regulation of the Respiratory Genes in the Cyanobacterium *Synechocystis* sp. PCC 6803 during the Early Response to Glucose Feeding. Plant Physiology 145: 1018-1030

Moezelaar R, Stal LJ (1994) Fermentation in the unicellular cyanobacterium *Microcystis* PCC7806. Archives of Microbiology 163:63-69

Montagud A, Navarro E, Fernandez de Cordoba P, Urchueguia J, Patil K (2010) Reconstruction and analysis of genome-scale metabolic model of a photosynthetic bacterium. BMC Systems Biology 4 (1):156

Pelroy, R. A., Levine, G. A., & Bassham, J. A. (1976). Kinetics of light-dark CO_2 fixation and glucose assimilation by Aphanocapsa 6714. Journal of bacteriology, 128(2), 633-643.

Richard DJ, Sawers G, Sargent F,McWalter L, Boxer DH(1999) Transcriptional regulation in response to oxygen and nitrate of operons rncoding the [NiFe] hydrogenases 1 and 2 of *Escherichia coli*. Microbiology. 145:2903-2912

Richardson LL, Castenholz RQ (1987)Enhanced survival of the cyanobacterium *Oscillatoria terebriformis* in darkness under anaerobic conditions. Applied Environmental Microbiolology 53:2151-2158

Rippka, R., Deruelles, J., Waterbury, J. B., Herdman, M., & Stanier, R. Y. (1979). Generic assignments, strain histories and properties of pure cultures of cyanobacteria. Journal of General microbiology, 111(1), 1-61

Stal LJ, Moezelaar R(1997)Fermentation in cyanobacteria. FEMS Microbiology Reviews. 21:179-211.

Williams JG (1988) [85] Construction of specific mutations in photosystem II photosynthetic reaction center by genetic engineering methods in *Synechocystis* 6803. Methods Enzymol 167:766-778

Yamamoto T (2012) Analysis and activation of hydrogen production Reaction by Cyanobacteria. Doctoral thesis in Engineering. Tokyo Institute of Technology

Yamamoto T, Chongsuksantikul A, Asami K, Ohtaguchi K (2012) Anaerobic Production of Hydrogen in the Dark by *Synechocystis* sp. strain PCC 6803 supplemented with D-glucose. Journal Biochemical Technology 4 (1):464-468

Yoo S-H, Keppel C, Spalding M, Jane J-l (2007) Effects of growth condition on the structure of glycogen produced in cyanobacterium *Synechocystis* sp. PCC6803. International Journal of Biological Macromolecules 40 (5):498-504

Zhang C-C, Durand M-C, Jeanjean R, Joset F (1989) Molecular and genetical analysis of the fructose-glucose transport system in the cyanobacterium *Synechocystis* PCC6803. Molecular Microbiology 3 (9):1221–1229

Zhang S, Bryant DA (2011) The Tricarboxylic Acid Cycle in Cyanobacteria. Science 334 (6062):1551-1553

Chapter 3

Growth Phase Effects on Hydrogen Production

3.1 Introduction

Cyanobacterial cells utilize radiated energy on photosystems and assimilate the thylakoid membrane photosynthetic products, NADPH and ATP, for carbon reduction and glycogen synthesis via the Calvin cycle. When the photosynthetic photon flux density (PPFD) of incident light is fixed, as a growth phase of photosynthetic cells proceeds, low cell density culture of inoculum changes to dense culture due to dry cell weight reproductions and cells in the suspension are exposed to low intensity light. Structure of cyanobacterial thylakoid membrane is associated with light intensity (van de Meene et al. 2012), hence it is rational to suppose that the activities of carbon dioxide fixation and glycogen synthesis per dry cell weight are affected by growth phase.

The hydrogen (H_2) production in GT strain is comprehended by a cellular response to the redox unbalance stress caused by the change in cellular environment from radiated aerobic nitrate-containing solution to dark anaerobic nitrate-free solution. Growth phase effects on dark anaerobic H_2 production have been suggested in previous works with *Arthrospira* (Spirulina) *maxima* (Ananyev et al. 2008), *Aphanothece halophytica* (Taikhao et al. 2013) and *Synechocystis* sp. strain PCC6803 (WT strain) (Baebprasert et al. 2010) , while, as yet, few author has presented the experimental results on the related parameters such as the amounts of glycogen and products in dark anaerobic condition. Apart from dark anaerobic H_2 production, a report shows that carbohydrate content is at peak during stationary phase in cyanobacteria, green algae and diatoms (Henderson et al. 2008). The increase in carbohydrate content in *Synechococcus* sp. on BG-11 medium with late growth phase was reported (Phlips et al. 1989). Other report shows that glycogen content and glycogen chain length of WT strain is varied not only by medium but also by growth phase (Yoo et al. 2007). Searching the growth phase of the inoculum suited for use in dark anaerobic nitrate-free H_2 seems to be a good possibility to elevate H_2 production of GT strain.

This study concerns an indirect biophotolysis for H_2 production in a glucose tolerant mutant of *Synechocystis* sp. strain PCC6803 (GT strain). Cells photoautotrophically grown in the first stage are harvested and inoculated into dark anaerobic culture in the second stage to generate H_2. To optimize cellular NAD(P)H in selecting growth phase of cells in photosynthesis, dark fermentation of cells from various growth phase have been monitored.

Under sufficient supply of radiant energy, cells of cyanobacterium grow logarithmically. This period is called logarithmic growth phase. If X is the dry cell weight concentration, change of cellular concentration in the logarithmic growth phase is shown by:

$$\frac{dX}{dt} = \mu X \qquad (3.1),$$

in which μ is the specific growth rate. In a classic work (Steele, 1962), the specific growth rate of logarithmically growing cells is modeled by Steele as:

$$\mu = \mu_m \frac{I_0}{I_m} \exp(1 - \frac{I_0}{I_m}) \qquad (3.2)$$

in which I_0 is the photosynthetic photon flux density (*PPFD*) of incident light, and μ_m and I_m are model parameters. **Figure 3.1** is the relationship of Eq.(3.2) for a unicellular cyanobacterium *Synechococcus* sp. strain PCC6301 with the model constants of μ_m, 0.112 h^{-1} ; and I_m, 294 μmol m^{-2} s^{-1}. (Ohtaguchi and Wijanarko, 2002).

If I is the *PPFD* of transmitted light, then drop of *PPFD* of light passing through cell suspension is given by the equation (Ohtaguchi and Wijanarko, 2002):

$$\frac{I}{I_0} = \exp(-\frac{k_1 X}{1 + k_2 X^{k3}}) \qquad (3.3).$$

If light path length is 27 mm and diameter of cell is 1.29 μm, then above work suggests the constants k_1, 353 mL mg^{-1}; k_2, 256 $mL^{0.605}$ $mg^{-0.605}$; and k_3, 0.605. **Figure 3.2** shows the effect of dry cell weight concentration on transmittance of light through cell suspension in above reference.

Increase in dry cell weight concentration according to Eq.(3.1) reduces the PPFD inside the bioreactor according to Eq.(3.3). Above work also shows that, when cell suspension of *Synechococcus* sp. strain PCC6301 is illuminated by 165 μmol m^{-2} s^{-1} light, transmitted light intensity I is 97 μmol m^{-2} s^{-1} right after inoculation and drops to 9.0 μmol m^{-2} s^{-1} at 144 h. If radiation cannot support logarithmic growth of whole cells in suspension, and support a fraction of whole cells, Eq.(3.1) changes to

$$\frac{dX}{dt} = \mu \phi X \qquad (3.4)$$

for ϕ between 0 and 1. This period is called late-logarithmic growth phase. If dry cell weight concentration further increases and cell suspension becomes dense culture, cell growth ceases. This period is called stationary phase. Dense culture at 144h in stationary phase indicates that cells are exposed to the light of which *PPFD* is 165 μmol m^{-2} s^{-1} at illuminated surface and 9.0 μmol m^{-2} s^{-1} at transmitted surface.

A classic work (Allen, 1968) is cited in **Figure 3.3** that shows an electron microscopic observation of a ultrastructure of a unicellular cyanobacterium *Synechococcus* sp. strain PCC7942 (*Anacystis nidulans*) at different light intensities. Cells under higher light intensity shown in graph (A) have two concentric lamellae and contains lower amount of pigments per dry cell weight (carotenoid, 15.7 μg mg^{-1}; chlorophyll, 42 μg mg^{-1}; phycocyanin, 195 μg mg^{-1}). Those under lower light intensity shown in graph (B) have three concentric lamellae and contains higher amount of pigments per dry cell weight (carotenoid, 18.1 μg mg^{-1}; chlorophyll, 61 μg mg^{-1}; phycocyanin, 281 μg mg^{-1}). Generation times of cells under higher and lower light intensities are 16 h and 4 h, respectively. Cell suspension in logarithmic growth phase is diluting that provides the environment for high transmittance of light (Fig.3.2). Graph (A) of Fig.3.3 represents the ultrastructure of such cells. Cell suspension in stationary phase is dense that provides the environment for low transmittance of light (Fig.3.2). Graph (B) of Fig.3.3 represents the ultrastructure of such cells. Pigment enzyme contents appear to be higher in stationary phase cells than in late-logarithmic growth phase cells, and in late-logarithmic growth phase cells than in logarithmic growth phase cells. If synthesis of pigment protein is activated as transparency of culture decreases, the assimilation of NAD(P)H in dense culture proceeds by this reaction. Similarly synthesis of endogenous glycogen seems to be a good possibility in dense cultures that offers not darkness but dim light illuminated condition.

A recent work reported the degradation of glycogen in GT strain in darkness (Hanai et al.,2014). Electron micrographs of ultrathin sections of the GT strain cells shows the decrease in glycogen granules under dark condition for 12 h. Dense culture represents the very low light transmittance condition, however, it seems to be quite different from darkness since life of cyanobacteria is supported by illumination. If decomposition of pigment proteins, glycogen and other photosynthesis-supported materials in darkness offers NAD(P)H that is a substrate for H_2 production on NiFe-hydrogenase, and if synthesis of those macromolecules in the light is activated in dense culture, the possibility exists that the cells from stationary phase generates high amount of H_2 in darkness.

Therefore, the research in this chapter was aimed at the elucidation of effect of growth phase of GT strain in photosynthesis upon H_2 production under dark anaerobic condition. The H_2 production kinetics is related to endogenous glucose degradation, cell death, lactate and acetate productions.

3.2 Materials and methods

A glucose tolerant mutant of unicellular cyanobacterium *Synechocystis* sp. strain PCC6803 (GT strain) was utilized. Growth phase of cells of GT strain in the first stage for indirect biophotolysis was changed. Cells of GT strain were grown photoautotrophically on BG-11 medium at 303K under the illumination of 100 μmol photons m^{-2} s^{-1} fluorescent lamp as described in Chapter 2. Pre-culture for the first stage main culture was performed for 3 d to logarithmic growth phase before transferring the harvested cells to main culture. The main cultures were performed in the same condition as pre-cultures. The dry cell weight concentration at initial for photosynthetic cell preparation (X_0) was set at 0.0118 $mg \cdot mL^{-1}$ (OD_{730}, 0.02). Cells of logarithmic growth phase (OD_{730}, 3), late-logarithmic growth phase (OD_{730}, 7) and stationary phase (OD_{730}, 12) in main cultures were collected by centrifugation at 3000 rpm and 298K for 10 min.

Cells in different growth phases were then inoculated into dark anaerobic HEPES buffer solution for H_2 production. H_2 production experiments were performed as described in Chapter 2.

3.3 Results and discussion

Prior to dark anaerobic H_2 production in the second stage of indirect biophotolysis, GT strain cells were grown on BG-11 medium under illumination in the first stage of indirect biophotolysis. Optical density at 730 nm was observed over time. One unit absorbance was equivalent to 0.369 mg-$DCW \cdot mL^{-1}$. **Figure 3.4** shows the time courses of culture variables measured during photosynthesis. Quantities measured include (1) the dry cell weight concentration of GT strain (X) and (2) the number of moles of endogenous glucose per dry cell weight (m_G). There is no lag phase on this growth curve because inoculum cells were taken from logarithmic growth phase of preculture. Cyanobacterial growth is in general limited not by carbon dioxide (CO_2) supply but radiation energy supply (Ohtaguchi and Wijanarko, 2002), hence logarithmic growth is observed in the first 55 h where sufficient radiation energy to support logarithmic growth is supplied by illumination because of low dry cell weight concentration.

Critical time (t_C) from logarithmic growth phase to late-logarithmic growth phase, when growth rate declines with time, is 55 h. Integration of Eq.(3.1) results that

$$\ln X = \ln X_0 + \mu t \qquad \text{for } t<t_C \tag{3.5}$$

The time course data of X from 0 to 55 h gives μ of 0.104 h^{-1}. The doubling time ($t_2=\ln 2/\mu$) is calculated to be 6.66 h.

After t_C, as transparency of cell suspension changes from dilute culture to dense culture, decrease in the slope of ln$X$ versus time curve is observed. If t_f is the transition time from the late-logarithmic growth phase to the stationary phase, growth curve of Fig.3.1 gives 80 h for t_f. The highest dry cell weight concentration (X_f) of 6.37 mg mL^{-1} that is kept constant with time is seen in the stationary phase (after t_f).

For late-logarithmic growth phase, growth kinetics are interpreted by Eq.(3.4) with $\phi\,(0<\phi<1)$. A previous work assumed the following model (Ohtaguchi et al.,1987):

$$\phi = 1 \qquad \text{for } 0 \le t \le t_C \tag{3.6},$$

$$\phi = \frac{1-\dfrac{g}{G}}{1-\dfrac{g_C}{G}} \qquad \text{for } t_C \le t \le t_f \tag{3.7},$$

and

$$\begin{aligned} X &= X_0 2^g \\ X_C &= X_0 \exp(\mu t_C) = X_0 2^{g_C} \\ X_f &= X_0 2^G \end{aligned} \tag{3.8},$$

in which g, g_C and G represent the number of generations from 0 h to t, from 0 h to t_C and from 0 h to t_f, respectively. Growth curve of Fig.3.1 results in that X_0 and X_C are 0.00548 and 1.67 mg mL^{-1}, respectively, and that g_C and G are 8.25 and 10.2, respectively. Insertion of Eqs.(3.4) to (3.6) to Eq.(3.3) results that

$$\ln X = \ln X_f + \left(\ln \frac{X_C}{X_f}\right) \exp\left(\frac{\mu(t-t_C)}{\ln \dfrac{X_C}{X_f}}\right) \qquad \text{for } t_C \le t < t_f \tag{3.9}.$$

Solid line for growth curve in Fig.3.4 is calculated utilizing Eqs.(3.5) and (3.9). The calculated values shown by the curve are in fair agreement with the experimental values.

From Eqs. (3.7) and (3.9), the fraction of growing cells (ϕ) in the late logarithmic growth phase is related to time by

$$\phi = \exp\{\frac{\mu(t - t_C)}{(g_C - G)\ln 2}\} \quad (3.10).$$

Figure 3.5 shows the time course of ϕ for parameters μ, 0.104 h^{-1}; t_C, 55h; g_C, 8.25; and G, 10.2.

CO_2 is a sole carbon source of the photoautotroph *Synechocystis* sp. strain PCC6803, and the cell formula of this strain shown in a reference is $CH_{1.62}N_{0.22}O_{0.40}P_{0.11}$ (Yu et al. 2013), hence, if the fixed CO_2 is totally converted to cell constituting materials, the specific carbon dioxide fixation rate (q_{CO2}) during logarithmic growth phase is calculated by

$$q_{CO2} = \frac{10^3}{X}\frac{d(X/23.1)}{dt} = 43.3\frac{d\ln X}{dt} = (43.3)(0.104)$$

$$= 4.50\ \mu\text{mol mg}^{-1}\ \text{h}^{-1} \quad (3.11).$$

During photosynthesis, the electron generated by photon absorption on the thylakoid membrane converts $NADP^+$ to NADPH, which is utilized in the Calvin cycle (Fig.1.4) according to Eq.(1.1).

CO_2 also reacts with ribulose-1,5-bisphosphate (RuBP) on ribulose-1,5-bisphosphate carboxylase/oxygenase (RubisCO) and form 2-phosphoglycolate that is further converted to glycine, serine, glycerate and CO_2. It is called photorespiration. Central carbon metabolism in *Synechocystis* sp. strain PCC6803 in a reference with $^{13}CO_2$ labelling experiment (Huege et at., 2011) shows that CO_2 incorporated into glyceraldehyde 3-P formation versus photorespiration at the RubisCO is 0.09-fold. Considering this, present study ignores the carbon conversion via photorespiration. Other detected photosynthesis products in this reference includes glyceraldehyde 3-P (GAP), phosphoenolpyruvate (PEP), citrate, malate, aspartate, ornithine, glycerate, glycine, serine, glycerate and glucose 6-P. A key product of photosynthesis in GT strain is endogenous glucose in glycogen. Broken line in Fig.3.4 shows the amount of glucose per dry cell weight (m_G) in logarithmically growing cells at 0.102 μmol mg^{-1} (=0.0184 mg mg^{-1}). One mole glucose is synthesized from 2 moles glyceraldehyde 3-P. Another key product from CO_2 in WT strain is poly-β-hydroxybutyrate (PHB) that is 2.3% of dry cell weight, and the NADPH content in a mutant defective of PHB synthesis is up to 1.85-fold higher than that in WT strain

(Xie et al., 2011). Contents of all these intracellular photosynthesis products are involved in the formula of dry cell weight: $CH_{1.62}\ N_{0.22}O_{0.40}P_{0.11}$.

In logarithmic growth phase, the yield factor $Y_{X/CO2}$ is determined as

$$Y_{X/CO2} = \frac{\mu}{q_{CO2}} = \frac{0.104}{4.46} = 0.0233 \text{ mg } \mu\text{mol}^{-1} = 0.530 \text{ mg mg}^{-1} \quad (3.12).$$

About a half weight of assimilated CO_2 is found to be incorporated into cell constituting materials. From the stoichiometry of Eq.(1.1), the NADPH consumption in the Calvin cycle during logarithmic growth phase is calculated to be 9.00 $\mu\text{mol}\cdot\text{mg}^{-1}\cdot\text{h}^{-1}$. Generation rate of glyceraldehyde 3-P in the Calvin cycle (R_{GAP}) is calculated to be 1.49 $\mu\text{mol}\cdot\text{mg}^{-1}\cdot\text{h}^{-1}$.

If R_{G1} is the specific production rate of glucose in logarithmically growing cells, the mass balance for endogenous glucose in logarithmic growth phase is shown by

$$\frac{d(m_G X)}{dt} = R_{G1} X \quad (3.13)$$

or

$$\frac{dm_G}{dt} = R_{G1} - \mu m_G \quad (3.14).$$

Data of m_G in logarithmic growth phase in Fig.3.4 are constant (=0.102μmol mg^{-1}=0.0184 mg mg^{-1}) with time. Thus the rate R_{G1} is calculated as

$$R_{G1} = \mu m_G = (0.104)(0.102) = 0.0107 \ \mu\text{mol}\cdot\text{mg}^{-1}\text{h}^{-1} \quad (3.15).$$

Gluconeogenesis from glyceraldehyde 3-P to glucose is shown by the equations:

Glyceraldehyde 3-P $\leftrightarrow$ Dihydroxyacetone (3.16)

Glyceraldehyde 3-P+ Dihydroxyacetone $\leftrightarrow$ Fructose 1,6-bisphosphate (3.17)

Fructose 1,6-bisphosphate+H_2O $\rightarrow$ Fructose 6-P+Pi (3.18)

Fructose 6-P $\leftrightarrow$ Glucose 6-P (3.19)

Glucose 6-P+H_2O $\rightarrow$ Glucose +Pi (3.20)

The irreversible reaction of Eq.(3.18) is mediated by fructose-1,6-bisphosphatase. Net reaction is shown by

2 Glyceraldehyde 3-P+2H_2O $\rightarrow$ Glucose+2Pi (3.21).

Glucose 6-P is further utilized as follows:

$$\text{Glucose 6-P} \leftrightarrow \text{Glucose 1-P} \tag{3.22}$$

$$\text{Glucose 1-P+ATP} \rightarrow \text{ADP-Glucose+PPi} \tag{3.23}$$

$$\text{ADP-Glucose+}(\alpha\text{-1,4-Glycosyl}) \rightarrow (\alpha\text{-1,4-Glycosyl})_2\text{+ADP} \tag{3.24}$$

$$\text{ADP-Glucose+}(\alpha\text{-1,4-Glycosyl})_2 \rightarrow (\alpha\text{-1,4-Glycosyl})_3\text{+ADP} \tag{3.25}$$

$$\text{ADP-Glucose+}(\alpha\text{-1,4-Glycosyl})_{n-1} \rightarrow (\alpha\text{-1,4-Glycosyl})_n\text{+ADP} \tag{3.26}$$

The formula $(\alpha\text{-1,4-Glycosyl})_n$ shows glycogen. For glycogen synthesis from glyceraldehyde 3-P, ATP requirement is shown in Eqs.(3.16)-(3.26) .

In photosynthesis, majority of ATP in Eq.(3.23) is synthesized at thylakoid membrane as follows:

$$12H_2O+12NADP^+ \rightarrow 6O_2+12NADPH+12H^+ \tag{3.27}$$

$$72H^+ + 24ADP + 24Pi \rightarrow 72H^+ + 24ATP \tag{3.28}.$$

Radiation is a requirement of these reactions.

The observed yield of moles of endogenous glucose from 2 moles of glyceraldehyde 3-P ($Y_{G/GPA}$) for logarithmically growing cells is estimated as:

$$Y_{G/GAP} = \frac{R_G}{\frac{R_{GAP}}{2}} = \frac{0.0107}{\frac{1.49}{2}} = 0.0144 \tag{3.29}.$$

The yield of endogenous glucose from CO_2 ($Y_{G/CO2}=R_{G1}/(q_{CO2}/6)=(0.0107)(6)/4.46$) is 0.0144 in logarithmic growth phase. The large portion of the Calvin cycle product is found to be converted to cell constituting materials and byproduct CO_2.

When mode of cell growth proceeds to late-logarithmic growth phase, there appears non-growing cells. If dry cell weight concentration is shown by

$$X = \phi X + (1-\phi)X \tag{3.30},$$

Eq.(3.4) shows the growth of dividing cells (ϕX). Dry cell mass concentration $(1-\phi)X$ shows the concentration of resting cells. When $\phi=1$, all cells are in resting state. If R_{G2} is the specific production rate of glucose in resting cells, the mass balance for endogenous glucose in late-logarithmic growth phase is shown by

$$\frac{d(m_G X)}{dt} = R_{G1}\phi X + R_{G2}(1-\phi)X \tag{3.31}$$

or

$$\begin{aligned}\frac{dm_G}{dt} &= R_{G1}\phi + R_{G2}(1-\phi) - \mu\phi m_G \\ &= R_{G2} + \phi(R_{G1} - R_{G2} - \mu m_G)\end{aligned} \tag{3.32}$$

The factor ϕ is 1 at t_C and 0 after t_f (Fig.3.5). Broken line in Fig.3.4 shows that he data of m_G in late-logarithmic growth phase and stationary phase increases linearly with time. From this observation it is obtained that

$$R_{G2} = 0.00128 \text{ μmol mg}^{-1} \text{ h}^{-1} \tag{3.33}$$

and

$$\begin{aligned}m_G &= 0.0379 + 0.00128t \\ \phi(R_{G1} - R_{G2} - \mu m_G) &\approx 0\end{aligned} \tag{3.34}$$

Figure 3.4 shows that calculated m_G is in fair agreement with the observed m_G. The m_G at 96 h is 0.160 μmol mg^{-1}(=0.0289 mg mg^{-1}) that is 1.57 (=0.160/0.102) times that in logarithmically growing cells. Inversely glucose production rate of resting cells (R_{G2}) drops to 12.0 % (=0.00128/0.0107) of dividing cells because there is no need for carbon flow to new born cells.

The level of m_G in this work is supported by a previous work reporting that the glycogen content of GT strain on BG-11 medium under 50 μmol photons m^{-2}·s^{-1} illumination for 15 d (=360 h) was 11% (= 0.611 μmol glucose equivalent mg^{-1}) (Joseph et al. 2014). The predicted m_G at 360 h by Eq.(3.9) is 0.499 μmol·mg^{-1}, that agrees well with above value. Glycogen content in another work is varied according to how cells are grown. A reported glycogen content of *Synechocystis* sp. strain PCC 6803 grown on BG-11 medium at 25º C for a week is approximately 1.5–4.5 mg glycogen per g wet cell mass, of which variation is resulted depending on whether glucose is supplied. If dry cell mass is 20% of wet cell mass, then glycogen content is 0.042-0.125 μmol·mg^{-1} (Yoo et al. 2007), which also supports the m_G level of this report. A recent wok (Hanai et al., 2014) shows m_G/OD$_{730}$ at 4.3 μg mL OD^{-1} that corresponds to the m_G at 0.0647 (=4.3/180/0.369) μmol mg^{-1}. Glucose content of *Synechocystis* sp. strain PCC6803 in previous works and this work is extremely low when it is compared with another model cyanobacterium *Synecoccus* sp. strain PCC6301 of which glucose content m_G is 2.78 μmol mg^{-1}(Mustaqim and Ohtaguchi, 1997).

Balance of elements C, H, N, O and P and electrons from 0h to t_f results in a growth reaction equation as:

$$CH_{1.62}N_{0.22}O_{0.40}P_{0.11} + 9.2CO_2 + 2.02NO_3^- + 1.12HPO_4^{2-} + 64.3H^+ + 60.04e^-$$

$$\rightarrow 10.2CH_{1.62}N_{0.22}O_{0.40}P_{0.11} + 25.26H_2O \quad (3.35).$$

This equation relates the states of cultures at inoculation time and t_f. The yield factor $Y_{X/CO2}$ during batch cultivation is calculated as

$$Y_{X/CO2} = \frac{(10.2-1)(26.5)}{(9.2)(10^3)} = 0.0265 \text{ mg } \mu\text{mol}^{-1} = 0.602 \text{ mg mg}^{-1} \quad (3.36).$$

Comparison of Eq.(3.12) and Eq.(3.36) suggests that the conversion of CO_2 to dry cell weight that is 53% in logarithmic growth phase increases in late-logarithmic growth phase.

In late-logarithmic growth phase, carbon balance at glyceraldehyde 3-P is interpreted by

$$\frac{q_{CO2}X}{6} = \frac{R_{GAP}X}{2} = \frac{1}{Y_{G/GAP,1}}R_{G1}\phi X + \frac{1}{Y_{G/GAP,2}}R_{G2}(1-\phi)X \quad (3.37)$$

or

$$q_{CO2} = 4.50\phi + \frac{0.00128}{Y_{G/GAP,2}}(1-\phi)\} \quad (3.38)$$

with parameters R_{G1},0.0107 μmol mg^{-1} h^{-1}; R_{G2}, 0.00128 μmol mg^{-1} h^{-1};$Y_{G/GAP,1}$,0.0144. **Figure 3.6** is the calculated q_{CO2} for $Y_{G/GAP2}$ at 0.0144(=$Y_{G/GAP,1}$) and 1. Conversion of glyceraldehyde 3-P to glucose shows very small effect on CO_2 fixation rate. It is found that glucose accumulation rate in stationary phase is weakly affected by CO_2 fixation rate.

Figure 3.4 also shows the time course of the q_{CO2} that is calculated by Eq. (3.38) with perfect conversion of glyceraldehyde 3-P to glucose. The q_{CO2} was maximum ($q_{CO2,max}$) and constant at 4.46 μmol mg^{-1}h^{-1} in logarithmic growth phase and decreased drastically in late-logarithmic growth phase to extremely low value at 120 h. Growth is not seen at 120 h since PPFD of transmitted light is only 10% of incident light. Photosynthesis pigments appear to be developed as shown in Fig.3.3 (b).

Although the q_{CO2} of cells in stationary phase is extremely low, Eq.(3.33) shows the occurrence of glycogen synthesis. If carbon of glycogen synthesis in stationary phase comes from the fixed CO_2 at the Calvin cycle (Eq.(1.1),(3.16)-(3.26)), and the yield of glucose from glyceraldehyde 3-P is same as Eq.(3.29), then

CO_2 fixation rate of resting cells is calculated as 0.544 μmol mg^{-1} h^{-1}.

Figure 3.7 shows a conceivable mechanism of CO_2 assimilation, glycogen synthesis, cell constituting material synthesis and decomposition and redox buffering systems in GT strain during logarithmic growth phase and stationary phase. Reducing compound NAD(P)H is mainly supplied by thylakoid membrane (Eq(1.1)). Majority of NADPH is consumed for CO_2 fixation and majority of photosynthesis product glyceraldehyde 3-P is utilized for synthesis of biomaterials of new born cells during logarithmic growth phase. Cell suspension is dilute in this phase, hence high PPFD radiation supports this mechanism for 55 h. To keep a homeostasis a small portion of glyceraldehyde 3-P is converted to endogenous glucose. Production of dry cell weight seems to be accompanied by evolution of CO_2 that is reproduced from the pathways from glyceraldehyde 3-P. Growth arrest signal is triggered at 55 h, when cell suspension becomes dense culture. This growth arrest was reported in a previous work that showed an arrest of the growth of *Synechococcus* sp. strain PCC6301 at the transmitted light intensity (I_b) of 38.6 μmol m^{-2} s^{-1}.(Ohtaguchi and Wijanarko, 2002). After entering late-logarithmic growth phase at 55 h, cell suspensions receive constant radiation energy that corresponds to the drop of PPFD from I_0 to I_b. Generated NADPH is utilized in the Calvin cycle to fix CO_2 with a low fixation rate. A portion of produced glyceraldehyde 3-P is converted to glycogen. Other macromolecules to store radiant energy appear to be synthesized in this period. Content of carotenoid, chlorophyll and phycocyanin shown by Allen (Allen, 1968) is 1.81%, 6.1% and 28.1%, that of PHB shown by Xie et al is is 2.3% (Xie et al., 2011) , and that of glycogen shown in Fig.3.4 is 1.84-2.89%. The GT strain under growth arrest likely utilized the synthesis reaction of these macromolecule for discharging NADPH generated by absorption of highest light energy corresponding to I_0-I_b. Cell suspension in late-logarithmic growth phase appear to contain both logarithmic growth phase cells and stationary phase cells.

H_2 production in the second stage of indirect biophotolysis was performed by inoculating cells of GT strain from photoautotrophic culture at different growth phases to dark anaerobic HEPES buffer solution. **Table 3.1** shows the cellular states of GT strain, utilized for dark anaerobic H_2 production. If the specific CO_2 consumption rate q_{CO2} of each run is referred to that of late-logarithmically growing cells, the q_{CO2} of logarithmically growing cells and stationary phase cells are 3.08 and 0.631 times that of late-logarithmically growing cells, respectively. If the m_G of each run is referred to that of late-logarithmically growing cells, the m_G of logarithmically growing cells and stationary phase cells are 0.75 and 1.89 times that of late-logarithmically growing cells, respectively. If m_G represents the cellular content of energy-stored chemicals and q_{CO2} represents the cellular production capability of NAD(P)H, logarithmically growing cells are found to be low level in m_G but high level in q_{CO2}, and stationary phase cells are found to be low level in q_{CO2} but high level in m_G.

Figure 3.8 shows the time courses of culture variables measured in three dark anaerobic runs made utilizing cells from (1) logarithmic growth phase (●), (2) late-logarithmic growth phase(■) and (3) stationary phase(▲). Growth phase of inoculum cells is found to have a major impact on subsequent dark anaerobic H_2 production and cellular metabolism in darkness. Results of run with late-logarithmically growing cells are re-plots of the data of run without monosaccharide in Fig.2.6. Culture variables shown in Fig.3.8 are (a) the number of moles of H_2 per culture volume (y_{H2}); (b) the number of moles of endogenous glucose per dry cell weight (m_G) in solid line and the number of moles of endogenous glucose per culture volume in broken line ($m_G X$); (c) the dry cell weight concentration (X); (d) the lactate concentration; (e) the acetate concentration; (f) the lactate production rates in broken line (r_L), the acetate production rates in solid line (r_A) and the H_2 production rate in long short broken line (r_{H2}); gas phase, nitrogen gas; inoculum cells, washed to ensure there is no nitrogen source in fermentation system.

Graph (a) in Fig.3.8 shows that H_2 production is largely affected by the growth phase of inoculum cell. The curve of the number of moles of H_2 per culture volume (y_{H2}) versus time of run with logarithmically growing cells is similar to the curve of run with late-logarithmically growing cells. The results of three runs show that the r_{H2} was highest at $r_{H2,0}$ right after inoculation and then decreased with time (Fig.3.2f).

The H_2 production curve of run with stationary phase cells shows high production rate of which kinetics can be interpreted by either Eqs.(2.18) or (2.20). If inoculum cells are obtained from stationary phase, after dark anaerobic incubation, there seems to be a reaction which generates NAD(P)H, even though NiFe-hydrogenase consumes NAD(P)H.

The curves shown in Fig.3.8(a) are calculated by Eq.(2.18) with the model constants $r_{H2,0}$ and k shown in **Table 3.2**. These curves resulted in a relatively good fit to the measured variables. The $r_{H2,0}$ is highest in run with inoculum from late-logarithmic growth phase. The $r_{H2,0}$ values of cells from logarithmic growth phase and stationary phase are 0.806 times and 0.871 times that from late-logarithmic growth phase. The highest number of moles of H_2 per culture volume at 96 h ($y_{H2,1}$) was achieved from cells inoculated from stationary phase. The conclusion reached from this observation is that it is important to shift up the cellular content of energy reserved chemicals to elevate dark anaerobic H_2 production.

The lowest H_2 production is seen in the result of run with cells from logarithmic growth phase. The calculated y_{H2} shown by broken lines in Fig.3.8(a) fits well with observed y_{H2}. The order of model parameter $y_{H2,f}$ is found to be same as the order of observed variable $y_{H2,1}$. The relation represents that the $y_{H2,f}$ increases as the $r_{H2,0}$ is higher or the k is lower.

Figure 3.9 shows the relation between initial H_2 production rate ($q_{H2,0}$) and attainable level of H_2 ($y_{H2,f}$). Reference values $(q_{H2,0})_{ref}$ and $(y_{H2,f})_{ref}$ are the data of run with late-logarithmically growing cells that are same as $(q_{H2,0})_{w/o}$ and $(y_{H2,f})_{w/o}$ utilized in chapter 2. Solid line shows the relation between $y_{H2,f}$* and $q_{H2,0}$* of runs with logarithmically growing cells in HEPES buffer solution with monosaccharide (Eq.(2.33)). The plot of data with logarithmically growing cells is approximated by this relation; however, that with stationary phase cells cannot be represented by this relation. Time course of H_2 production with stationary phase cells is found to be dependent not only on the initial amount of NAD(P)H but also on mechanism of NAD(P)H reproduction during the fermentation. This viewpoint is supported by the m_G versus time curve of graph (b) of Figure 3.8 that shows no change or increase in m_G. If initial specific H_2 production rate represents NAD(P)H content, right after inoculation to dark anaerobic HEPES buffer solution, cells from both logarithmic growth phase and stationary phases show lower amount of NAD(P)H than those from late-logarithmic growth phase. Late-logarithmically growing cells are found to be very sensitive to the change of cellular environment from illuminate BG-11 medium with oxygen to dark HEPES buffer solution without oxygen.

Table 3.2 shows that the k is lowest with inoculum from stationary phase, second lowest with inoculum from late-logarithmic growth phase and highest with inoculum from logarithmic growth phase. The ascending order of $y_{H2,f}$ is same as the descending order of k in Table 3.2. The GT strain in dark anaerobic incubation with inoculum from stationary phase is found to be most stable for dark anaerobic H_2 production. The redox balance after dark anaerobic incubation in GT strain from stationary phase is characterized by the activation of reproduction of NAD(P)H.

The q_{CO2} is proportional to NADPH consumption rate of the Calvin cycle, hence the decrease in q_{CO2} of inoculum cells appears to increase $r_{H2,0}$, while q_{CO2} in Table 3.1 shows that the q_{CO2} of late-logarithmically growing cells is second lowest. The m_G represents the amount of reactants for generating NAD(P)H, hence the increase in m_G of inoculum cells appears to increase $r_{H2,0}$, while the m_G in Table 3.1 shows that the m_G of late-logarithmically growing cells is second highest. For these reasons, late-logarithmically growing cells seems to exhibit high initial H_2 production rate. Although the ascending order of $r_{H2,0}$ is different from ascending order of $y_{H2,f}$, the descending order of k is same as ascending order of $y_{H2,f}$,. The attainable level of number of moles of H_2 per culture volume is found to depend more on stability of H_2 production rate than initial H_2 production rate.

Comparison of curves in Figures 3.8(a) and (b) shows that, during dark anaerobic H_2 production, H_2 production is more stable when the level of m_G is high. Table 3.1 shows that the m_G of inoculum cells from stationary phase is highest, that from late-logarithmic growth phase the second highest and that from logarithmic growth phase is lowest. This order is the same as the descending order of k in Table 3.2. The

increase in the m_G is found to increase the stability of H_2 production during dark anaerobic incubation. Our results show that stationary phase cells that accumulate glycogen are most suitable for inoculum of dark anaerobic H_2 production. The m_G of inoculum cells from stationary phase is 0.195 μmol mL^{-1}, which is 2.52 times that from logarithmic growth phase.

The solid line curves of m_G versus time in Fig. 3.8(b) show that, except for the changes between 0 and 24 h of run with inoculum from logarithmic growth phase and between 72 and 96 h of run with inoculum from stationary phase, the m_G of cells in dark anaerobic incubation decreased with time. The broken line curves of m_GX versus time in Fig. 3.8(b) show that, except for the m_GX between 0 and 24 h of run with inoculum from logarithmic growth phase, m_GX always decreased with time. Glycogen degradation occurred in dark incubation with inocula from late-logarithmic growth phase and stationary phase. The m_GX curve of run with inoculum from logarithmic growth phase shows glycogen synthesis between 0 and 24 h and glycogen degradation after 24 h. The decrease in m_G between 72 h and 96 h of run with inoculum from stationary phase was brought by the decrease in X. No change in m_G is seen in the first 24 h of runs with late-logarithmic growing cells. The cellular content of glycogen of runs with inocula from late-logarithmic growth phase and stationary phase dropped drastically during 96 h.

During photosynthesis, specific glycogen accumulation rate (R_G) shown in Table 3.1 is highest at 0.106 μmol·mL^{-1}·h^{-1} for cells from logarithmic growth phase, second highest in run with inoculum from late-logarithmic growth phase and lowest in run with inoculum from stationary phase. Glycogen synthesis in the dark is seen between 0 and 24 h in the m_GX curve of run with inoculum from logarithmic growth phase, while glycogen consumption is seen after 24 h of this run and after 0 h of runs with inocula from late-logarithmic growth phase and stationary phase. As shown by R_G*, the R_G of logarithmically growing cells is 2.23 times that of late-logarithmically growing cells. The ATP production rate of logarithmically growing cells are so high that, right after dark anaerobic incubation, the generated large amount of ATP appears to be utilized for the glycogen synthesis for 24 h. Of special interest is that the decrease in the m_GX is not affected by the growth phase of inoculum cells (Table 3.2). Growth phase dependent production of dark anaerobic production of H_2 is found to be caused not by endogenous glucose decomposition but by turnover of cell constituting components.

Figure 3.8 (c) shows that cell death occurred in dark anaerobic incubation. The specific death rate (K_d) is highest in run with stationary phase cells, second highest in run with late-logarithmically growing cells and lowest in run with logarithmically growing cells (Table 3.2). The ascending order of K_d is the same as the ascending order of $y_{H2,f}$. Activation of turnover of cell constituting components is found to be important for shifting-up H_2 production. Observed cell death shows that inoculum from stationary phase suits for increasing K_d.

Figures 3.8 (d) and (e) shows that H_2 production is accompanied by the production of lactate and acetate. Previous report also shows a detectable level of lactate and acetate in the culture of *Synechocystis* sp. strain PCC6803 (Troshina et al. 2002). Dark anaerobic production of acetate increased drastically when cells from stationary phase were incubated. At 96 h, lactate concentration that was 0.20 μmol mL^{-1} in run with logarithmically growing cells increased to 0.48 μmol mL^{-1} in run with stationary phase cells. Acetate production was roughly parallel to lactate production. Acetate concentration that was 0.05 μmol mL^{-1} in run with logarithmically growing cells increased to 0.8 μmol mL^{-1} in run with stationary phase cells Interestingly, cells from stationary phase resulted in higher ratio of acetate concentration to lactate concentration. These ratios of acetate concentration to lactate concentration at 96 h of runs with cells from logarithmic growth phase, late-logarithmic growth phase and stationary phase were 0.25, 0.80 and 1.67 respectively. The ascending order of this ratio is similar to that of the yield of H_2 on endogenous glucose ($Y_{H2/G}$) of Table 3.2. Dark anaerobic H_2 production of stationary phase cells is found to be highly dependent on NAD(P)H formation at incomplete TCA cycle. The highest $Y_{H2/G}$ is 19.1 that is a result of run with cells from stationary phase. This yield is about double of that with cells from logarithmic growth phase.

The amount of lactate or acetate at 96 h is the 1% order of it in run with glucose (Fig.2.6). Considering that 2 moles lactate or acetate is produced from 1 mole consumption of glucose, the yield of lactate or acetate on endogenous glucose is defined by:

$$Y_{L/G} = \frac{\frac{c_{Lf}}{2}}{-\Delta(m_G X)} \tag{3.39}$$

or

$$Y_{A/G} = \frac{\frac{c_{Af}}{2}}{-\Delta(m_G X)} \tag{3.40}.$$

These yields are shown in Table 3.2 .Those yields are less than 1 when inoculum cells are obtained from logarithmic growth phase or late-logarithmic growth phase; however, they are greater than for run with stationary phase cells. Cells of GT strain from stationary phase are found to produce lactate and acetate not only from endogenous glucose but also from other endogenous carbonaceous compounds. Decomposition of such compounds appears to supply NAD(P)H to NiFe-hydrogenase from $NAD(P)^+$.

Figure 3.10 shows a relation between $(m_G X)_1$ and $y_{H2,1}$ of experiments in this chapter. The linear line is calculated using Eq.(2.40). The $(m_G X)_1$ of run with cells from logarithmic growth phase is the same as

that from late-logarithmic growth phase, whereas the $y_{H2,1}$ of run with cells from logarithmic growth phase is smaller than that from late-logarithmic growth phase. The $(m_G X)_1$ of run with cells from stationary phase results in high $(m_G X)_1$ value, whereas the $y_{H2,1}$ of run with cells from stationary phase is comparable with that from late-logarithmic growth phase. Growth phase is confirmed to be important for H_2 production.

3.4 Summary

H_2 production in indirect biophotolysis is composed of photosynthesis in the first stage and dark fermentation in the second stage. Research in this chapter concerns the effect of growth phase in the first stage to the H_2 production in the second stage. The highlights of this chapter are as follows.

1. Dark anaerobic H_2 production in NiFe-hydrogenase of the glucose tolerant mutant of *Synechocystis* sp. strain PCC6803 (GT strain) in nitrate-free HEPES buffer solution, is strongly dependent on the growth phase of inoculum cells in the first stage.

2. Cell death during dark anaerobic incubation can be limited by the use of cells from logarithmic growth phase

3. Cells from stationary phase contain high amount of endogenous glucose and they are useful to achieve high amount of stored glycogen at the end of H_2 production. Different from expectation, H_2 production is not affected by glycogen content. Glycogen content effect is found to be a growth phase dependent phenomenon

4. The amount of H_2 production is 9.6-19.1 times higher than amount of endogenous glucose consumption. The amount of reductive compounds generated by glycolysis is insufficient to make up those utilized for H_2 production. Despite this fact, H_2 production is indirectly traceable by glycolysis.

   Glycolysis appears to be an indicator of dark anaerobic decomposition of cell constituting materials.

5. The inoculum cells from stationary phase are most suitable for dark anaerobic H_2 production in GT strain in HEPES buffer solution.

Third point is the result of experiment with GT strain in HEPES buffer solution. More definitive experiments with genetically modified strain or with monosaccharide solution are needed before the exact growth phase effect is known.

Table 3.1 Physiological state of cells in photoautotrophic cultures that are performed prior to dark anaerobic H_2 production in indirect biophotolysis. GT strain was obtained from different growth phases. ref, cellular state in late-logarithmic growth phase. $q^*_{CO2,0}$, $q_{CO2,0}/(q_{CO2,0})_{ref}$; and m^*_G, $m_G/(m_G)_{ref}$.

	Logarithmically growing cells	Late-logarithmically growing cells	Stationary phase cells
Harvesting time [h]	44-47	65	89
X[mg·mL^{-1}]	1.11-1.48	2.58	4.43
g[-]	6.56-6.97	7.77	8.55
q_{CO2} [μmol·mg^{-1}·h^{-1}]	4.50	1.46	0.921
q^*_{CO2} [-]	3.08	1	0.631
m_G [μmol·mg^{-1}]	0.0773	0.103	0.195
m^*_G [-]	0.750	1	1.89
R_G [μmol·mg^{-1}·h^{-1}]	0.0106	0.00475	0.00128
R^*_G [-]	2.23	1	0.269

Table 3.2 Kinetic parameters for H_2 production in GT strain in HEPES buffer solution. GT strain was obtained from different growth phases.

ref, run with cells from late-logarithmic growth phase. $q^*_{H2,0}$, $q_{H2,0}/(q_{H2,0})_{ref}$; $y^*_{H2,f}$, $y_{H2,f}/(y_{H2,f})_{ref}$; and $k^*=k/(k)_{ref}$. $y_{H2,1}$, c_{L1}, c_{A1}, observed number of moles of H_2, lactate and acetate per culture volume at 96 h. m_{G1}, X_1, observed m_G and X at 96h; $\Delta(m_GX)_1$, observed decrease in m_GX during 96 h H_2 production; $y_{H2/G}=y_{H2,1}/\Delta(m_GX)_1$; $Y_{L/G}=(c_{Lf}/2)/\Delta(m_GX)$; $Y_{A/G}=(c_{Af}/2)/\Delta(m_GX)$

	Logarithmically growing cells	Late-logarithmically growing cells	Stationary phase cells
X_0[mg·mL^{-1}]	2.07	2.03	1.95
$r_{H2,0}$ [μmol·mL^{-1}·h^{-1}]	0.0316	0.0405	0.025
$q_{H2,0}$[μmol·mg^{-1}·h^{-1}]	0.0121	0.0200	0.0138
$q^*_{H2,0}$ [-]	0.605	1	0.69
$y_{H2,f}$ [μmol·mL^{-1}]	1.86	2.18	4.24
$y^*_{H2,f}$ [-]	0.853	1	1.94
k [h^{-1}]	0.017	0.0186	0.006
k^*[-]	0.914	1	0.326
K_d [h^{-1}]	0.00076	0.0011	0.0026
$y_{H2,1}$[μmol·mL^{-1}]	1.48	1.79	1.97
m_{G1} [μmol·mg^{-1}]	0.0308	0.0323	0.188
X_1[mg·mL^{-1}]	1.95	1.86	1.49
$(m_GX)_1$[μmol·mL^{-1}]	0.0601	0.0601	0.280
$c_{L,1}$[μmol·mL^{-1}]	0.20	0.26	0.48
$c_{A,1}$[μmol·mL^{-1}]	0.05	0.21	0.80
$\Delta(m_GX)_1$[μmol·mL^{-1}]	0.10	0.15	0.10
$Y_{H2/G}$[-]	9.6	11.8	19.1
$Y_{L/G}$[-]	1.0	0.867	4.8
$Y_{A/G}$[-]	0.25	0.7	8

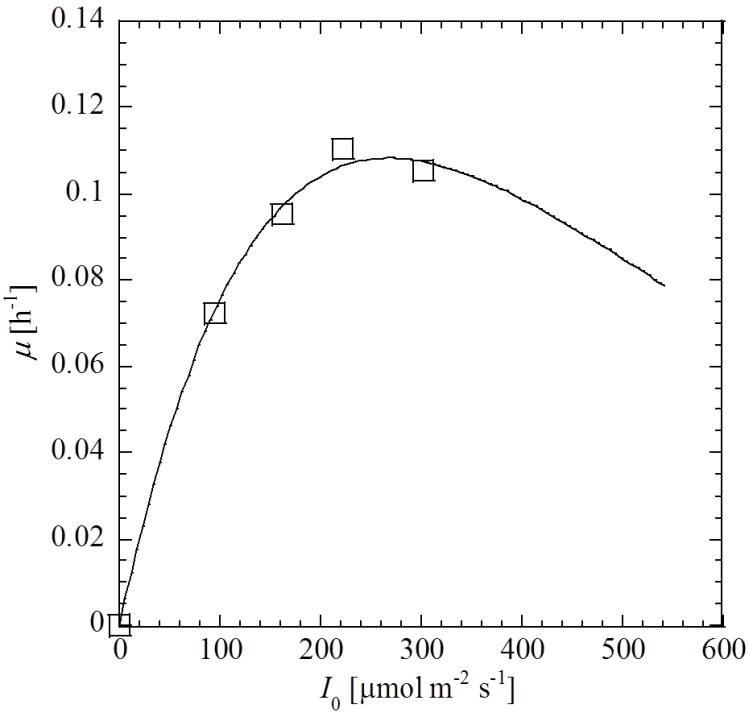

Figure 3.1 Effect of incident light intensity on the specific growth rate of logarithmically growing cells of a unicellular cyanobacterium *Synechococcus* sp. strain PCC6301. Solid line, calculated by the Steele's model (Ohtaguchi and Wijanarko, 2002).

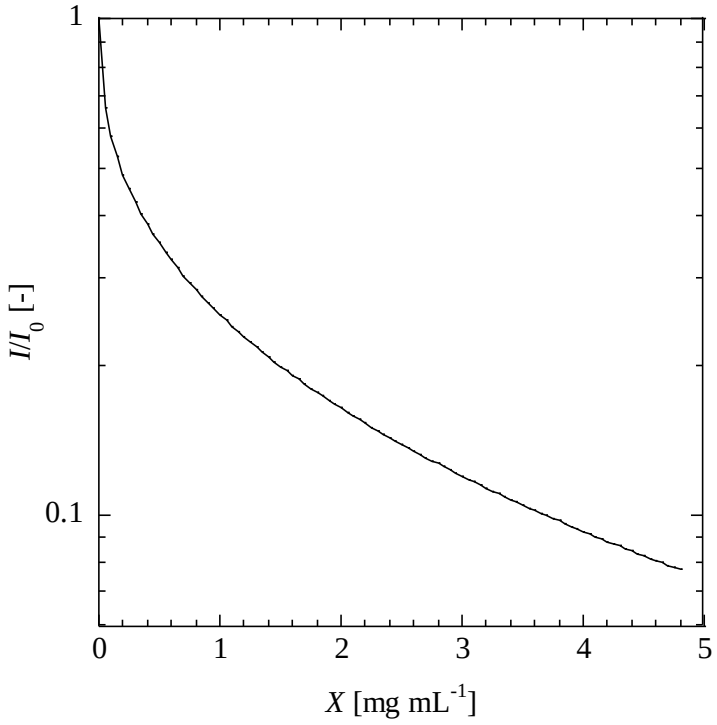

Figure 3.2 Correlation of the estimation of the transmittance of the light (I/I0) at the back of culture suspension for *Synechococcus* sp. strain PCC6301. Light path length, 27 mm.(Ohtaguchi and Wijanarko,2002).

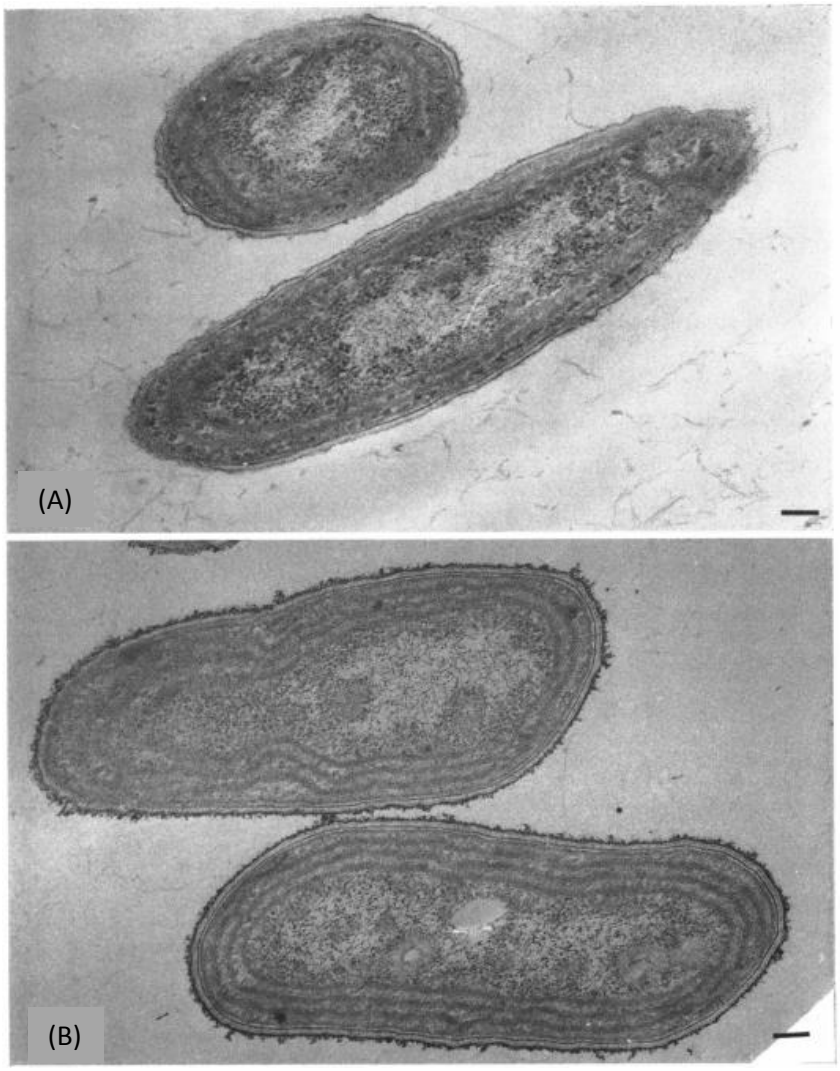

Figure 3.3 Ultrastructure of *Synechococcus* sp. strain PCC7942 (*Anacystis nidulans*) (Allen, 1968)

(A) Cells grown with 1000 ft-c illumination (roughly 150 μmol m^{-2} s^{-1}) at 308K

(B) Cells grown with 100 ft-c illumination (roughly 15 μmol m^{-2} s^{-1}) at 308K

X60,000. All markers indicate 0.1 μm.

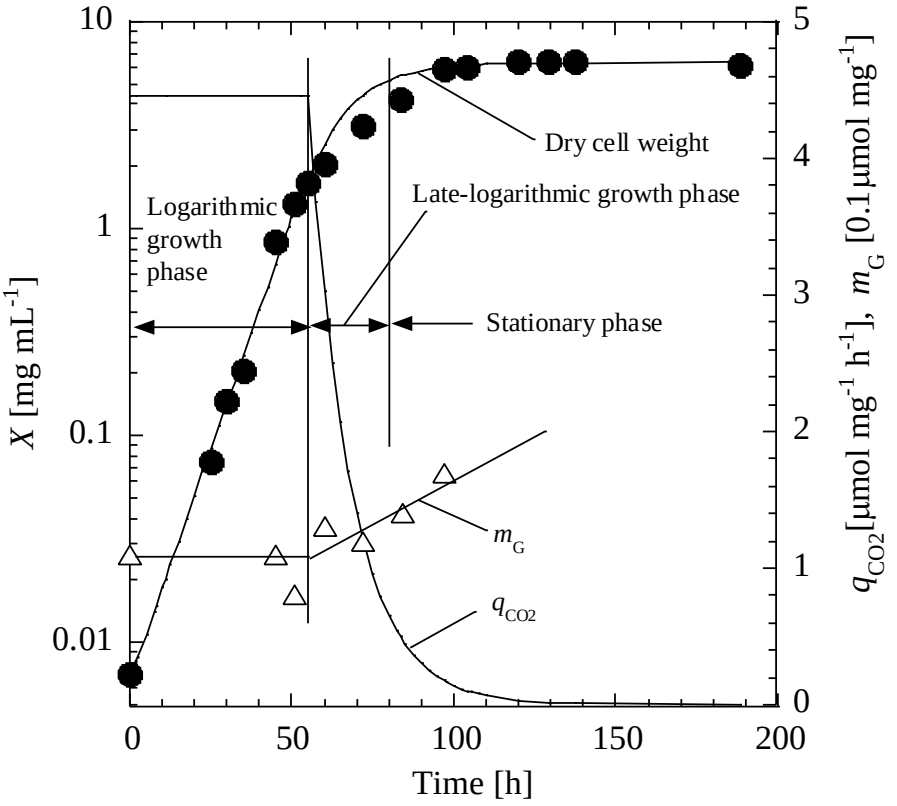

Figure 3.4 Time courses of culture parameters for photoautotrophic growth of GT strain in BG-11 medium, aerated by 6% CO_2 in air and continuously illuminated at 100 μmol photons·m^{-2}·s^{-1} photosynthetic photon flux density (*PPFD*). Inoculum size, OD_{730} at 0.02; dry cell weight concentration, measured by optical density of wavelength at 730 nm (●); specific carbon dioxide fixation rate, calculated from growth curve; m_G, number of moles of endogenous glucose per dry cell weight (△); the m_G at 0 h, glycogen content from pre-culture analysis.

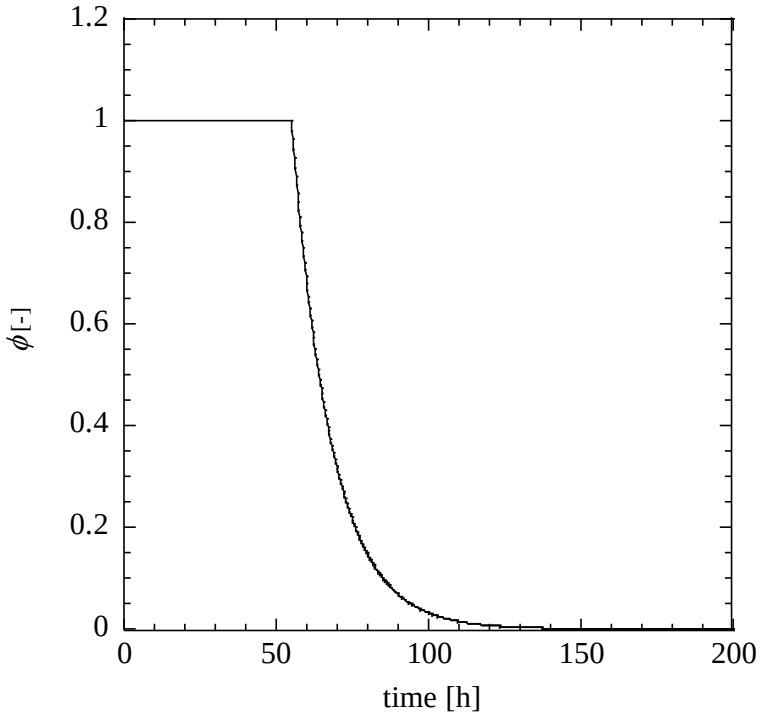

Figure 3.5 Calculated time course of the factor ϕ of the photoautotrophically growing cells of GT strain on BG-11 medium under the illumination of 100 μmol m^{-2} s^{-1} *PPFD* light.

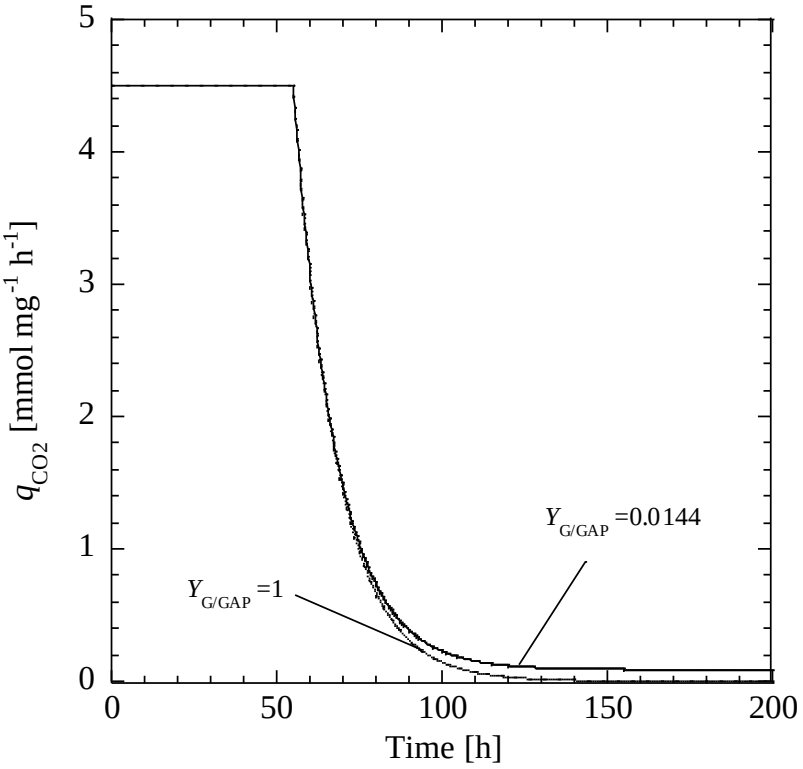

Figure 3.6 Time course of CO_2 for yield factor $Y_{G/GAP}$ at 0.0144 and 1

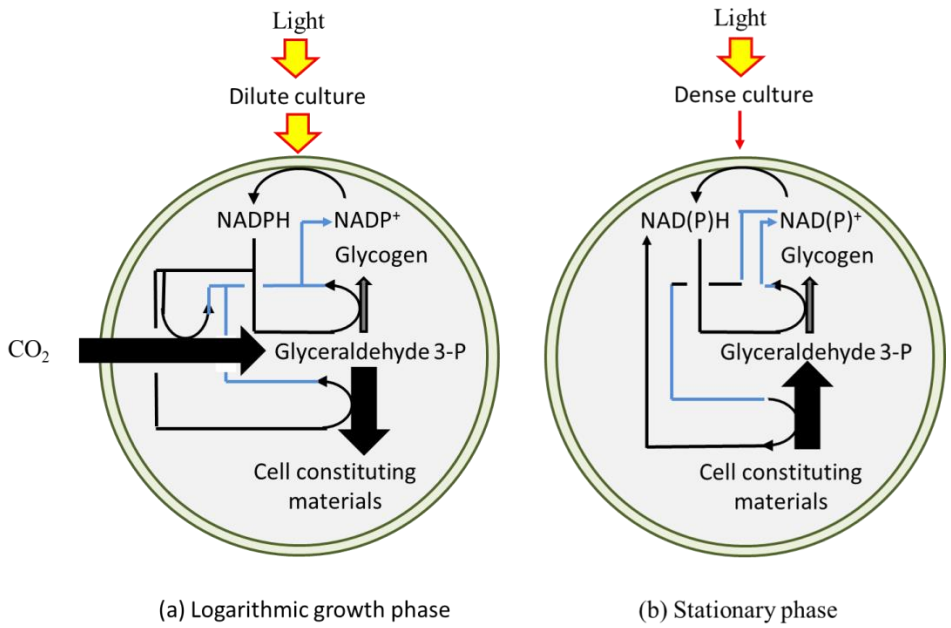

Figure 3.7 Conceivable mechanism of CO_2 assimilation, glycogen synthesis, cell constituting material synthesis and decomposition and redox buffering systems in GT strain during logarithmic growth phase and stationary phase.

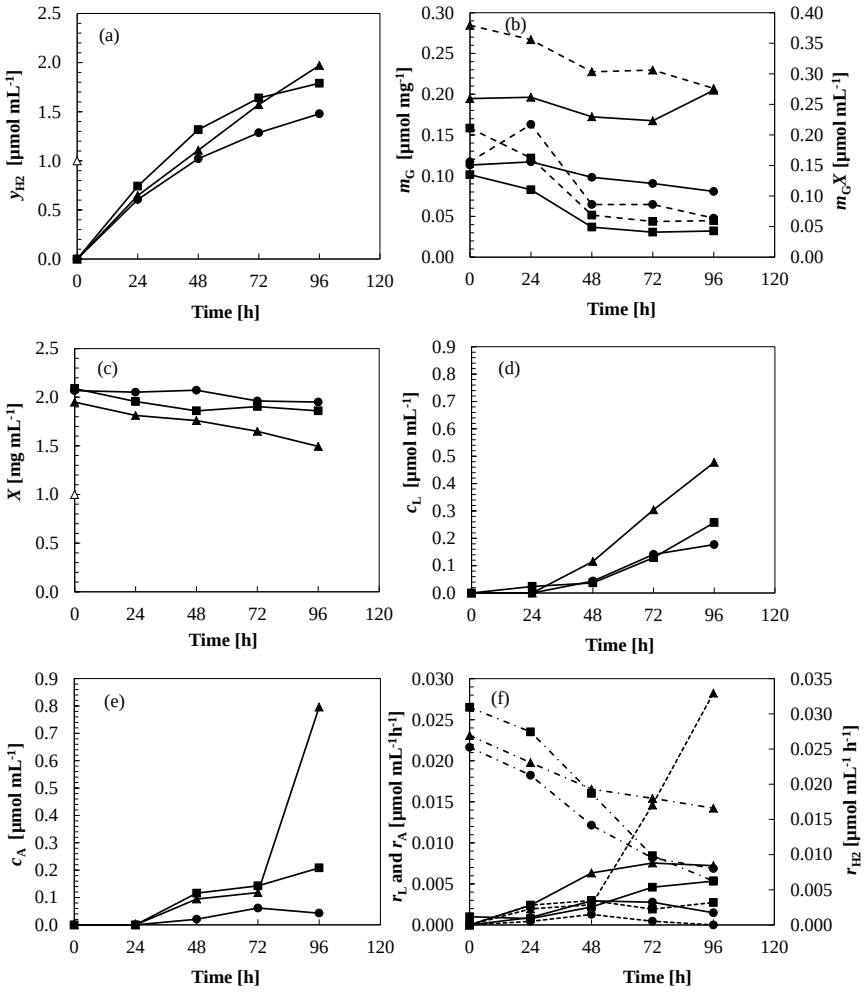

Figure 3.8 Time courses of culture variables measured in three dark anaerobic runs made utilizing cells from (1) logarithmic growth phase (●), (2) late-logarithmic growth phase(■) and (3) stationary phase(▲). (a) the number of moles H_2 per culture volume (y_{H2}); (b) the number of moles of endogenous glucose per dry cell weight (m_G) in solid line and the number of moles of endogenous glucose per culture volume in broken line (m_GX); (c) the dry cell weight concentration (X); (d) the lactate concentration; (e) the acetate concentration; (f) the lactate production rates in broken line (r_L), the acetate production rates in solid line (r_A) and the H_2 production rate in long short broken line (r_{H2}); gas phase, nitrogen gas; inoculum cells, washed to ensure there is no nitrogen source in fermentation system.

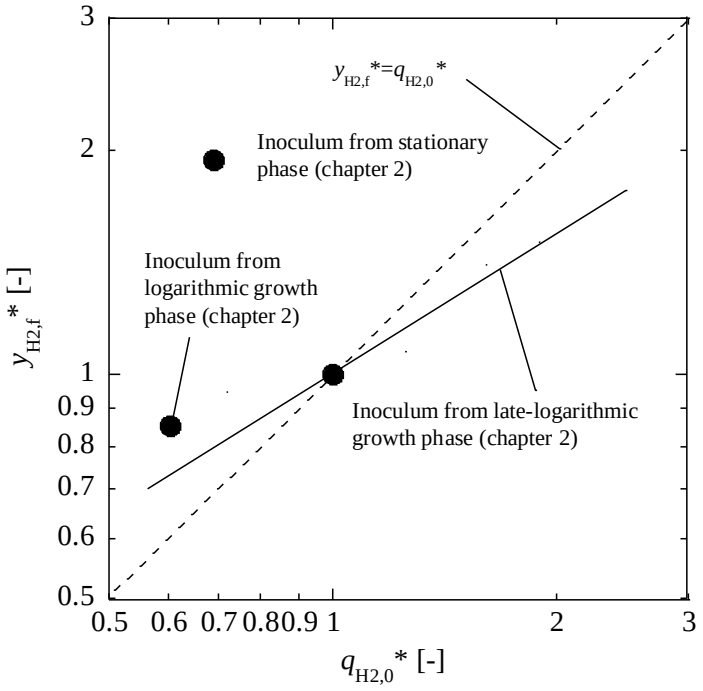

Figure 3.9 Relation between initial specific H_2 production rate and attainable level of H_2

$q_{H2,0}$*=$q_{H2,0}$/($q_{H2,0}$)$_{ref}$; $y_{H2,f}$*=$y_{H2,f}$/($y_{H2,f}$)$_{ref}$; ref, run with late-logarithmically growing cells

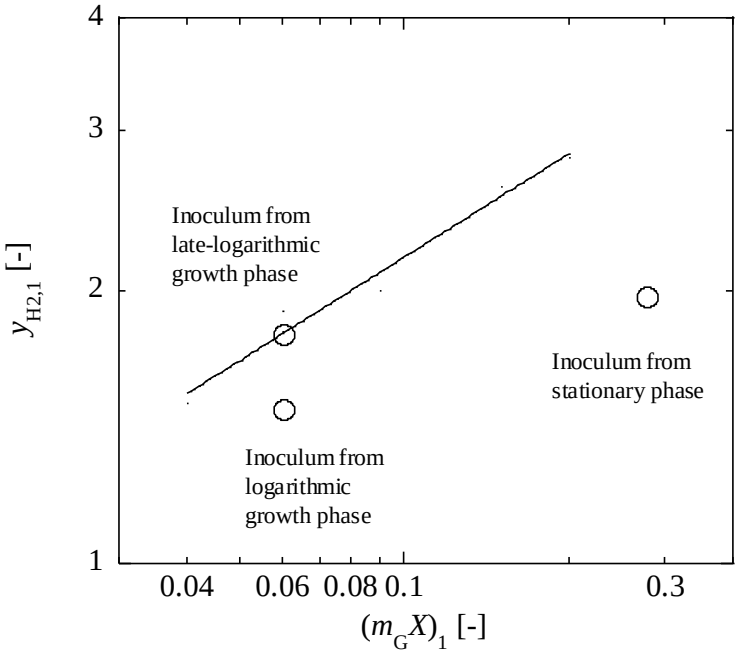

Figure 3.10 Relation between $(m_G X)_1$ and $y_{H2,1}$ of dark anaerobic incubation of GT strain, from logarithmic growth phase, late-logarithmic growth phase and stationary phase, in HEPES buffer solution.

Solid line is calculated for cells, from late-logarithmic growth phase, in HEPES buffer solution with monosaccharides. Calculation was made utilizing equation and parameters in chapter 2

Chapter 3: References

Allen MM (1968) Photosynthetic membrane system in *Anacystis nidulans*. Journal of Bacteriology. 96(3):836-841

Ananyev G, Carrieri D, Dismukes GC (2008) Optimization of Metabolic Capacity and Flux through Environmental Cues To Maximize H_2 Production by the Cyanobacterium "*Arthrospira* (Spirulina) *maxima*". Applied and Environmental Microbiology 74 (19):6102-6113

Baebprasert W, Lindblad P, Incharoensakdi A (2010) Response of H_2 production and Hox-H2ase activity to external factors in the unicellular cyanobacterium *Synechocystis* sp. strain PCC 6803. International Journal of Hydrogen Energy 35 (13):6611-6616

Hanai M, Sato Y, Miyagi A, Kawai-Yamada M, Tanaka K, Kaneko Y, Nishiyama Y, Hihara Y(2014)The effects of dark incubation on cellular metabolism of the wild type cyanobacterium *Synechocystis* sp. PCC6803 and a mutant lacking the transcriptional regulator cyAbrB2. Life. 4:770-787

Henderson RK, Baker A, Parsons SA, Jefferson B (2008) Characterisation of algogenic organic matter extracted from cyanobacteria, green algae and diatoms. Water Research 42 (13):3435-3445. Huege J, Goetze J, Schwarz D, Bauwe H, Hagemann M, Kopka J(2011)Modulation of the major paths of carbon in photorespiratory mutants of *Synechocystis*. PLos One. 6(1)e16278

Joseph A, Aikawa S, Sasaki K, Matsuda F, Hasunuma T, Kondo A (2014) Increased biomass production and glycogen accumulation in apcE gene deleted *Synechocystis* sp. PCC 6803. AMB Express 4 (1):17

Mustaqim D, Ohtaguchi K(1997) A synthesis of bioreactions for the production of ethanol.Energy. 22:353-356

Ohtaguchi K, Nasu A, Koide K , Inoue I (1987) Effects of size structure on batch growth of lactic acid bacteria. Journal of Chemical Engineering of Japan. 20(6):557-562

Ohtaguchi K, Wijanarko A (2002) Elevation of the efficiency of cyanobacterial carbon dioxide removal by monoethanolamine solution. Technology 8:267-286

Phlips E, Zeman C, Hansen P (1989) Growth, photosynthesis, nitrogen fixation and carbohydrate production by a unicellular cyanobacterium, *Synechococcus* sp. (Cyanophyta). Journal of Applied Phycology 1 (2):137-145

Steele JH (1962) Environmental control of photosynthesis in the sea. Limnol Oceanogr. 7: 137–150

Taikhao S, Junyapoon S, Incharoensakdi A, Phunpruch S (2013) Factors affecting bioH2 production by unicellular halotolerant cyanobacterium *Aphanothece halophytica*. Journal of Applied Phycology 25 (2):575-585.

Troshina O, Serebryakova L, Sheremetieva M, Lindblad P (2002) Production of H_2 by the unicellular cyanobacterium *Gloeocapsa alpicola* CALU 743 during fermentation. International Journal of Hydrogen Energy 27 (11–12):1283-1289

van de Meene AML, Sharp WP, McDaniel JH, Friedrich H, Vermaas WFJ, Roberson RW (2012) Gross morphological changes in thylakoid membrane structure are associated with photosystem I deletion in *Synechocystis* sp. PCC 6803. Biochim Biophys Acta - Biomembranes 1818 (5):1427-1434

Xie J, Zhou J, Zhang H, Li Y (2011) Incresing redactant NADPH content via metabolic engineering of PHB synthesis pathway in *Synechocystis* sp. PCC6803. Sheng Wu Gong Cheng Xue Bao.27(7):998-1004

Yoo S-H, Keppel C, Spalding M, Jane J-l (2007) Effects of growth condition on the structure of glycogen produced in cyanobacterium *Synechocystis* sp. PCC6803. International Journal of Biological Macromolecules 40 (5):498-504

Yu Y, You L, Liu D, Hollinshead W, Tang YJ, Zhang F (2013) Development of *Synechocystis* sp. PCC 6803 as a phototrophic cell factory. Marine drugs 11 (8):2894-291

Chapter 4

Genetic Modification Effects on Hydrogen Production

4.1 Problem Definition and General Consideration

(a) General remarks

Experimental results in chapters 2 and 3 show that hydrogen (H_2) production in a glucose tolerant mutant of *Synechosystis* sp. strain PCC 6803 (GT strain) in the dark anaerobic HEPES buffer solution is accompanied by the decomposition of endogenous glucose, and production of H_2, lactate and acetate. In the presence of glucose or fructose, it also produces succinate and ethanol (Figure 2.6). The reductive compound NAD(P)H (=NADH plus NADPH) is the substrate for H_2 production on NiFe-hydrogenase, hence association of above products with NAD(P)H is briefed.

Glucose catabolism in is known to start by the glycolysis to fructose 6-P and glyceraldehyde 3-P through the oxidative pentose phosphate (OPP) pathway (Figure A3.2). Overall stoichiometry is shown by:

$$3\ \text{Glucose 6-P}+6\text{NADP}^{+}+2\text{ADP}\rightarrow 2\text{Fructose 6-P}+\text{Glyceraldehyde 3-P}+3\text{CO}_2$$

$$+6(\text{NADPH}+\text{H}^{+})+2\text{ATP}+\text{Pi} \qquad (4.1)$$

The two monosaccharide-phospates in products are further converted to pyruvate:

$$\text{Fructose 6-P}+\text{ATP}\rightarrow 2\text{Glyceraldehyde 3-P}+\text{ADP}$$

$$\text{Glyceraldehyde 3-P}+2\text{ADP}+\text{NAD}^{+}\rightarrow \text{Pyruvate}+2\text{ATP}+\text{NADH}+\text{H}_2\text{O} \qquad (4.2).$$

These equations show that breaking down of 1 mol glucose 6-P to 2 moles pyruvate results in the production of 5/3 moles pyruvate and 2 moles NADPH plus 10/3 moles NADH. If reductive compound is shown by NAD(P)H (NADH plus NADPH), these equation result that conversion of glucose 6-P to pyruvate produces 16/3 moles NAD(P)H.

Conversion of pyruvate to lactate or ethanol consumes NADH or NAD(P)H. Hence, the pathways to generate lactate and ethanol compete for the reductive compound with H_2 generating NiFe-hydrogenase. Genes coding for lactate dehydrogenase (*ddh*) or alcohol dehydrogenase *(adh*) appear to be possible targets to be eliminated to increase H_2 production. Conversion of pyruvate to lactate is shown by

$$\text{Pyruvate} + \text{NADH} + H^+ \longrightarrow \text{Lactate} + NAD^+ \quad (4.3).$$

Hence 1 mole decrease in lactate production has a potential to elevate 1 mole H_2 production. Conversion of pyruvate to ethanol is shown by

$$\text{Pyruvate} + \text{NAD(P)H} + H^+ \longrightarrow \text{Ethanol} + \text{NAD(P)}^+ \quad (4.4).$$

If both lactate and ethanol productions are knocked out, additional increase in H_2 production can be predicted. GT strain is challenged to evaluate the potential of the work that has focused on *ddh* and *adh* deletions for H_2 production enhancement. Succinate pathway of incomplete tricarboxylic acid (TCA) cycle (**Figure 4.1**) of *Synechocystis* sp. strain PCC 6803 is also an interesting reaction which should have been targeted to be another way to enhance H_2 production if it is not due to the fact that succinate and succinate dehydrogenase (*sdh*) have a major role on respiratory electron transfer and thereby in redox poising (Cooley and Vermaas 2001). However, this research ignores the knocking out of *sdh* genes since H_2 production in this study is performed only in completely oxygen (O_2) free environment.

(b) Lactate dehydrogenase as a target of metabolic engineering approach

Lactate dehydrogenase (*ddh*) is an enzyme that consumes NADH during lactate production. To elevate the level of intracellular NADH for bidirectional NiFe-hydrogenase, in Chapter 4, the genes coding for *ddh* were disrupted in GT strain. The modified strain was referred as Δddh mutant. Redirection of NAD(P)H to bidirectional hydrogenase is found to be a very promising engineering approach to elevate H_2 production. Main fermentative products in dark anaerobic condition of GT strain are lactate and acetate. There are some research works which show increases in H_2 production by a deletion of lactate dehydrogenase genes in a cyanobacterium *Synechococcus* sp. strain PCC 7002 (McNeely 2010) and in gut bacillus *Escherichia coli*. Genes in GT strain coding for lactate dehydrogenase, which catalyzes the reaction of Eq.(4.3), is cloned in slr1556 (lactate dehydrogenase gene).

First experiment in Chapter 4 is designed to disrupt the *ddh* genes in a glucose tolerant mutant of *Synechocytis* sp. strain PCC 6803 (GT strain) to increase the amount of NADH that limits the H_2 production rate of bidirectional hydrogenase. This mutant is referred as Δddh strain.

(c) Alcohol dehydrogenase genes as a second target of metabolic engineering approach

GT strain can naturally produce small amount of ethanol as a byproduct in dark anaerobic condition. Pyruvate is converted to acetaldehyde and CO_2. Acetaldehyde is then reduced to ethanol by alcohol dehydrogenase (*adh*, EC 1.1.1.2). One of metabolites appears during dark anaerobic condition is detected

to be ethanol. The disruption of alcohol dehydrogenase for H_2 enhancement in cyanobacteria is first carried out using a model cell for study. The *adh* gene is selected and targeted to be deleted in order to save NADPH for hydrogenase pathway. A mutant lacking both *adh* genes and *ddh* genes is referred as a double knocking out mutant. Second experiment in chapter 4 is to derive the double knocking out mutant by disrupting both *ddh* genes and *adh* genes. It has a potential to further elevate H_2 production. This chapter draws a construction method on ΔadhΔddh double mutant.

According to CyanoBase (http://genome.kazusa.or.jp/cyanobase/) and Kyoto Encyclopedia of Genes and Genomes (KEGG, http://www.genome.jp/kegg/), alcohol dehydrogenase genes in *Synechocystis* sp. strain PCC 6803 are distributed in 4 genes as shown in **Table 4.1**. There are multiple genes involving in alcohol production. Clone slr0942 contains $NADP^+$ [EC.1.1.1.2] dependent alcohol dehydrogenase and clone slr1192 contains probable zinc-containing alcohol dehydrogenase. Clone slr1192 was previously knocked out to study stress response. Clone slr1192 contains NADP dependent alcohol dehydrogenase for aromatic compounds. This enzyme uses medium-chain aliphatic aldehyde as oxidants (Vidal et al. 2009). Those enzymes on slr0942 and slr1192 were previously knocked out to study reduction of ketone.

Only the deletion mutant from slr0942 exhibited a change in reaction while that from slr1192 gave no effect to ketone reaction. (Takemura et al. 2009). No report confirms specific role in dark anaerobic condition on both genes. The highly possible pathways involves in ethanol production in heterotrophic of GT strain are alcohol dehydrogenase-NAD^+ [EC.1.1.1.1] and alcohol dehydrogenase-NADP+ [EC.1.1.1.2] enzymes. This work selects the clone slr0942 as a target because the gene is classified as a gene for short chain alcohol dehydrogenase and GT strain cells produce ethanol (short chain alcohol) in dark anaerobic condition. The other genes were not selected because the sll0990 is class III alcohol dehydrogenase which has virtually no activity for ethanol oxidation but exhibits high activity for oxidation of long-chain primary alcohols and oxidation of S-hydroxymethyl-glutathione, a spontaneous adduct between formaldehyde and glutathione in human (National Center for Biotechnology Information 2012). There was a study of slr1192 as an aromatic–medium chain alcohol dehydrogenase in *Synechocystis* sp. strain PCC 6803 therefore slr1192 was not likely to catalyze ethanol production. There are reports that show a construction of a mutant by inserting pyruvate decarboxylase (*pdc*) of *Zymomonas mobilis* into *Synechocystis* sp. strain PCC 6803 make cells to be able to yield a production of 120 μmol mL^{-1} ethanol phototrophically via cyanobacterium *adh* (Gao et al. 2012; Dehring et al. 2012). Although aldehyde is toxic to *Synechocystis* sp. strain PCC6803, cells are protected by converting it to ethanol. It is known that fermentation products of cyanobacteria are CO_2, H_2, acetate, lactate and ethanol. The selected clone slr0942 fits to an assumption of gene that involves in ethanol production as shown in Eq.(4.4).

Thus, the primary purposes of the study in this chapter were (1) to construct the Δddh mutant and ΔadhΔddh mutant from GT strain by genetic modification techniques, and (2) to evaluate the generic modification effects on H_2 production.

4.2 Materials and methods

(a) Mutagenesis

Organisms, plasmids, growth media and primers

The competent cells of *Escherichia coli* X1-Blue were used for transformation purposes. In general, *E.coli* cells were cultured in Lysogeny broth (LB) at 37°C and 220rpm in a shaking incubator. A pUC19 plasmid was selected to be used for vector for homologous DNA recombination (Yanisch-Perron et al. 1985)

Overall experimental design to construct a vector to disrupt *ddh* genes

Table 4.2 shows pUC4K and pUC19. Plasmid pUC4K was used as a donor of kanamycin fragment. Plasmid pUC19 was used as a vector.

Host organism used was *Synechocystis* sp. strain PCC6803-GT. Lactate dehydrogenase gene (*ddh*) sequence of cyanobacterium *Synechocystis* sp. strain PCC6803 was retrieved from Kyoto Encyclopedia of Genes and Genomes (KEGG). Primers used in this experiment were as shown

Forward primer: 5'GCCTATGATCGTCAATTTTTCC3'

Reverse primer: 5'TTCAGCAATATTTGCCAGTGTC3'

Figure 4.2 shows the strategy to construct a vector pUC19-*ddh*-Km^r to disrupt the lactate dehydrogenase gene (*ddh*) of GT strain. The *ddh* gene on the fragment slr1556 from chromosomal DNA of wild-type *Synechocystis* sp. strain PCC6803 was prepared by a PCR amplification using above primers forward and reverse.

Overall experimental design to construct a vector to disrupt both *ddh* genes and *adh* genes

Table 4.3 shows plasmid DNA for the construction of DNA for ΔadhΔddh. The 2.692 kb DNA pMD19 was used as a vector. The 4.3 kb DNA pHP45-Ωconferring streptomycin (Sm) and spectinomycin

(Sp) cassette (Ω fragment) was used as a donor of the genes coding for antibiotic fragment (Prentki and Krisch 1984).

The slr0942 gene sequence of cyanobacterium *Synechocystis* sp. strain PCC 6803 was retrieved from KEGG. Primers used in this experiment were as shown

Forward primer: 5' CAAAAGCATTGTCCGCCTCACC3'

Reverse primer: 5' GCTTCCGCTTGGGAGTGCC3'

Figure 4.3 shows the strategy to construct a vector pMD19-*adh*-Ω to disrupt the alcohol dehydrogenase gene (*adh*). The deletion of alcohol dehydrogenase-$NADP^+$ (slr0942) was performed by a PCR amplification of slr0942 gene fragment using primer forward and reverse from chromosomal DNA of wild-type *Synechocystis* sp. strain PCC6803. PCR-amplified *adh* fragment was ligated into *Eco*RV restriction site of plasmid pMD19 (T-vector) from Takara company. The streptomycin/spectinomycin cassette (Sm/Sp) from plasmid pHP45-Ω was inserted into the *Eco*RV restriction site at slr0942 gene fragment. Transformant colony (ΔadhΔddh) was selected from Sm^+/Km^+ plate and continuously re-streaked to new plates. Sm resistant cell were grown at increasing Sm concentrations and finally transferred into liquid BG-11 medium.

Transformation (homologous recombination) of GT strain with pUC19-*ddh*-Km^r

By adding 3.5 µg vector to cells on membrane surface, cells replaced its original DNA with new constructed one in order to survive on Km^+ plate. Transformant colony was selected from Km^+ plate. Km resistant cells were continuously at week interval re-streaked to new plates at increasing Km concentrations to 120 µg mL^{-1}. Transformant was grown on agar plate with high concentration Km. A successful complete segregation was confirmed by PCR using above primers.

Transformation (homologous recombination) of GT strain and Δ*ddh* strain with pMD-*adh*-Ω

GT strain and Δddh were transformed with pMD19-*adh*-Ω plasmid on agar plate with Sm and Sm/Km antibiotic(s). Transformations were carried out as described below.

1. Δddh strain and GT strain cells were grown to reach OD_{730} of 0.5.
2. 1500 µL cell cultures were harvested by centrifugation and re-suspended in 200 µL fresh BG-11 medium.
3. 3.5 µg of pMD-19-*adh*-Ω was added and incubated at room temperature for 30 min.
4. Previous mixtures were spread on BG-11 plates containing membranes on surfaces.

5. Membranes were move to new BG-11 plate containing appropriate antibiotic (Sm) after 24 h.
6. Plates were observed after 2 weeks.

(b) Segregation of mutant

Transformation of GT strain with pUC19-ddh-Km^+ and Transformation of GT strain and Δadh strain with pMD19-adh-Ω were performed as described (Yamamoto et al. 2012; Chongsuksantikul et al. 2014).

(c) Indirect biophotolysis for dark anaerobic H_2 production

Strain

A glucose-tolerant strain of cyanobacterium *Synechosystic* sp. strain PCC6803-GT was used as a host strain Cells of GT strain were kept shaking in L-tube glass, and grown on BG-11 medium under constant illumination of fluorescent light, at constant room temperature prior to cell growth. Mutant cells of GT strain were also kept in L-tube. GT strain, Δddh mutant and ΔadhΔddh mutant were performed on BG-11 medium containing 60 µmol mL^{-1} kanamycin and BG-11 medium containing 60 µmol mL^{-1} kanamycin and 2.5 µmol mL^{-1} streptomycin.

Culture technique and fermentation

Cells of GT strain grown in L-tube were pre-cultured in 60 mL BG-11 medium containing HEPES buffer at pH = 7.7, in 100 mL clear Pyrex glass column. The culture was bubbled from the bottom of column at 80 mL min^{-1} by the air containing 6% CO_2 that was filtered through 0.45µm filter. Photosynthetic photon flux density (*PPFD*) of incident light by fluorescent light was maintained at approximately 100 µmol m^{-1} s^{-1}. Cells of Δddh mutant and ΔadhΔddh mutant were pre-cultured in BG-11 mediium with 60 µmol mL^{-1} kanamycin and both 60 µmol mL^{-1} kanamycin and 2.5 µmol mL^{-1} streptomycin, respectively, 60 µmol mL^{-1} kanamycin and 2.5 µmol mL^{-1} streptomycin for 3-4 d until logarithmic growth phase. Preculture growth of mutant cells in BG-11 medium with antibiotic required longer time to reach a turbid state than that of GT strain on BG-11 medium without antibiotics.

Logarithmically growing cells of GT strain, Δddh mutant and ΔadhΔddh mutant in precultures were inoculated into 60 mL BG-11 medium (pH, 7.7) without antibiotics. The apparatus (100 mL clear Pyrex glass column) and the conditions for aeration and illumination were the same as those for precultures. The initial dry cell weight concentration was set at 0.103 ± 0.027 mg mL^{-1}. Growth was monitored by measuring OD_{730} of cell suspension. One of OD_{730} represents the dry cell weight concentration (*X*) of 0.369 mg mL^{-1}. Cells were harvested in late logarithmic phase when *X* reached 2.58 mg mL^{-1} (OD_{730}=7).

Dark anaerobic H_2 production was performed as described in the section 2.2.1.

4.3 Results and discussion

(a) Construction of Δddh mutant and ΔadhΔddh mutant

GT strain was transformed with pUC19-*ddh*-Km^r plasmid on agar plate with Km antibiotic as shown in **Table 4.4**. Many colonies were observed after 6 d. It took around 6 months to complete segregation due to short homologous segments (200,700 bp) of *ddh* gene. It is known that, when the homologous segments are less than 400 bp, the efficiency drops significantly.

Results of transformation of GT strain and Δadh strain with pMD19-adh-Ω are shown in **Table 4.5**. Large number of colonies appeared on Sm^r plate. The mutant of GT strain that is knocked down *adh* genes is obtained. This strain is referred as Δadh strain. The Δddh strain was transformed with pMD19-*adh*-Ω to eliminate both *adh* genes and *ddh* genes from GT strain. Slight growth on Sm^r and Km^r selection medium is confirmed. Colonies were tiny in this run. Mutant lacking *adh* genes and *ddh* genes is successfully constructed. This mutant is referred as Δ*adh*Δ*ddh* strain.

Photographs in **Figure 4.4** show results of agarose-gel electrophoretic analyses of PCR products for evaluating the achievement of deletion of (a) *ddh* genes and (b) both *adh* and *ddh* genes. Photograph (a) shows Lane 1: size marker DNA, Lane 2: PCR product for ddh primers and pUC19-slr1556:Km^r, Lane 3: PCR product for ddh primers and genomic DNA from GT strain, and Lane 4:PCR product with ddh primers and genomic DNA from Δ*ddh* mutant. Photograph (b) shows Lane 1: size marker DNA, Lane 2: PCR product for ddh primers and pUC19-slr1556:Km^r, Lane 3: PCR product for adh primers and pMD19-slr0942::Sp^{r}Sm^r, Lane 4: PCR product for ddh primers and genomic DNA from GT strain, Lane 5: PCR product for adh primers and genomic DNA from GT strain, Lane 6: PCR product for *ddh* primers and DNA from ΔadhΔddh mutant and Lane 7: PCR product for adh primers and genomic DNA from ΔadhΔddh mutant. The successful segregation of Δddh is confirmed, ((a) Lane 4 or (b) Lane 6) is the same size as that for primers and DNA fragment from pUC19-slr1556:Km^r ((a) or (b) Lane 2). Double mutation is also confirmed by the result showing that the size of PCR product for primers and genomic DNA from ΔadhΔddh mutant ((b) Lane 7) is the same size as that for primers and DNA fragment from pMD19-slr0942::Sp^r/Sm^r ((b) Lane 3).

(b) Cellular state prior to dark anaerobic incubation

Precultures for photoautotrophic growth of GT strain, Δddh mutant and ΔadhΔddh mutant were performed on BG-11 medium, BG-11 medium containing 60 μmol mL^{-1} kanamycin and BG-11 medium containing 60 μmol mL^{-1} kanamycin and 2.5 μmol mL^{-1} streptomycin, respectively. At 96 h of precultures, cells were harvested, washed and then inoculated into main cultures in which cells were grown photoautotrophically in antibiotic-free BG-11 medium. Growth of cells on BG-11 was monitored by optical density at 730 nm wavelength. Growth curves for GT strain, Δddh mutant and ΔadhΔddh mutant show that cells of GT strain and Δddh mutant were in logarithmic growth phase from 0 h to 24 h and from 0 h to 40 h, respectively, while ΔadhΔddh mutant was in lag phase from 0 h to 24 h and in logarithmic growth phase from 24 h to 48 h (**Figure 4.5**).

The lag time for the growth of ΔadhΔddh mutant appears to represent a period for adaptation of the mutant from antibiotic containing preculture medium to antibiotic-free main culture medium. After one week cultivation, dry cell weight concentrations of Δddh mutant and ΔadhΔddh mutant reached the same level as GT strain.

Carbon dioxide (CO_2) is a single carbon source for cell growth, hence the slope of growth curve represents the activity of carbon dioxide fixation. Total amount of carbon dioxide incorporated into dry cell weight during 168 h cultivation is found not to be affected by deletion of *adh* or *ddh* genes. The inoculum cells of GT strain, Δddh mutant and ΔadhΔddh mutant for dark anaerobic hydrogen production were harvested at 36, 45, and 60 h, respectively. **Table 4.6** shows the state of cells prior to dark anaerobic H_2 production experiments.

The OD_{730} at the cell harvesting time was fixed at 7, hence inoculum cells for hydrogen production experiment were confirmed to be exposed to same PPFD from incident light to transmitted light. The slope of growth curves ($d\ln X/dt$) of GT strain, Δddh mutant and ΔadhΔddh mutant of the X at 2.58 mg mL^{-1} are 0.0187, 0.0318 and 0.0238 h^{-1}, respectively. The cell formula of *Synechocystis* sp. strain PCC6803 shown in a reference is $CH_{1.62}N_{0.22}O_{0.40}P_{0.11}$ (Yu et al. 2013), hence the rates of CO_2 assimilation by inocula of GT strain, Δddh mutant and ΔadhΔddh mutant are calculated as 2.09, 3.55 and 2.66 μmol mL^{-1} h^{-1}, respectively and the rates of NADPH consumption at the Calvin cycle are calculated as 4.18, 7.10 and 5.32 μmol mL^{-1} h^{-1}, respectively.

(c) Characteristics of dark anaerobic nitrate-free H_2 production in the absence of exogenous glucose

In the first series of H_2 production experiments, photoautotrophic cells of GT strain, Δddh mutant or ΔadhΔddh mutant in late-logarithmic growth phase was incubated at 2.58 mg mL^{-1} dry cell weight concentration in dark anaerobic nitrate-free HEPES buffer solution without glucose. H_2 production

characteristics in the absence of glucose were studied. **Figure 4.6** shows the time courses of culture variables during dark anaerobic H_2 production in GT strain Δddh mutant and ΔadhΔddh mutant. Quantities measured include the moles per culture volume of (a) hydrogen and (b) the moles of endogenous glucose in glycogen, and the concentrations of (c) dry cell weight, (d) lactate and (e) acetate. Similar to photoautotrophic culture, the solution for hydrogen production was free from antibiotics.

Table 4.7 shows the characteristics of dark anaerobic H_2 production in GT strain, Δddh mutant and ΔadhΔddh mutant in dark anaerobic HEPES buffer solution without glucose. If subscript 1 shows the state at 96 h, the $y_{H2,1}$ values of runs with GT strain, Δddh mutant and ΔadhΔddh mutant are 1.8, 2.0 and 1.5 μmol mL^{-1}, respectively. The $y_{H2,1}$ of Δddh mutant is 1.11 times that of GT strain. The $y_{H2,1}$ of Δddh mutant shown in our previous report (Yamamoto et al. 2012) was 1.5 times that of GT strain. Previous work and present work utilized the inocula from logarithmic growth phase and late-logarithmic growth phase, respectively. As concluded in chapter 3, growth phase is of utmost important factor for H_2 production.

The elimination of adh activity resulted to decrease $y_{H2,1}$ that was 0.83 times that of GT strain, The highest $y_{H2,1}$ was observed in run with Δddh mutant, second highest is in run with GT strain and the lowest is in run with ΔadhΔddh mutant. This descending order is same as the ascending order of the modified DNA size shown in Table 4.6. The DNA size of ΔadhΔddh mutant is 0.56 kb larger than that of GT strain, hence expression of increased DNA size appears to increase the NAD(P)H consumption for protein and amino acid synthesis and reduce the hydrogen production. On the other hand, the DNA size of Δddh mutant is 0.459 kb smaller than that of GT strain, hence expression of decreased DNA size appears to decrease the NAD(P)H consumption for protein and amino acid synthesis and increase the hydrogen production.

The curves in Figure 4.6 (a) for GT strain, Δddh mutant and ΔadhΔddh mutant are calculated with the values of $y_{H2,f}$ and k in Table 4.7. The calculated y_{H2} agrees well with the observed y_{H2}. The descending order of $y_{H2,f}$ in Table 4.7 is same as the descending order of the $y_{H2,1}$. **Figure 4.7** is the plots of observed $y_{H2,1}$ against change in expressed DNA size. Experimental data fit well with the equation:

$$y_{H2,1} = 1.78 - 0.475(\text{change in expressed DNA size}) \quad (4.5)$$

An increase in the expressed DNA size has a potential to reduce the reductive compounds during dark anaerobic H_2 production.

The $r_{H2,0}$ of Table 4.7 is highest for run with Δddh mutant, second highest for run with ΔadhΔddh mutant and lowest for run with GT strain. The descending order of $r_{H2,0}$ is similar to that of the consumption rate of NAD(P)H in the Calvin cycle just before inoculation (Table 4.6). Shift of cellular

environment from illuminated aerobic nitrate-containing BG-11 medium to dark anaerobic nitrate-free HEPES buffer solution appears to redirect the accumulated NAD(P)H molecules in the Calvin cycle to NiFe-hydrogenase.

The elimination of ddh activity or both adh and ddh activities results in 1.16-fold increase or 1.15-fold increase in the $r_{H2,0}$. Considering that the NiFe-hydrogenase converts 1 μmol NAD(P)H to form 1 μmol hydrogen, this result shows that the amount of NADH consumed by lactate dehydrogenase of GT strain is about 16% of the total amount of NADH and NADPH consumed by NiFe-hydrogenase of GT strain. The initial lactate production rate was 0.000833 μmol mL^{-1} h^{-1} in GT strain and almost 0 μmol mL^{-1} h^{-1} in Δddh and ΔadhΔddh mutants (Figure 4.6d). Stoichiometry of D-lactate dehydrogenase and NiFe-hydrogenase suggests that the elimination of above lactate production rate potentially increases hydrogen production rate from 0.0309 μmol mL^{-1} h^{-1} to 0.0359 μmol mL^{-1} h^{-1}. The observed increase is 6 times more than the estimated increase by ddh elimination. Redirection of carbon metabolism at pyruvate from lactate production to acetyl-CoA production is found to amplify NAD(P)H production.

A 1.28-fold increase in Δddh mutant and a 2.19-fold increase in ΔadhΔddh mutant over GT strain in the deactivation constant *k* are seen in the results (Table 4.7). The presence of dehydrogenases in GT strain appears to be important to stabilize the dynamical redox adaptation of cells against continuous consumption of NAD(P)H on NiFe-hydrogenase.

The attainable level of y_{H2} by Δddh mutant is comparable with that of GT strain, while that by ΔadhΔddh mutant is 0.65 times that of GT strain. For H_2 production in the absence of exogenous glucose, stabilization is of first importance for high production of hydrogen by ΔadhΔddh mutant. Our result of Δddh mutant in *Synechocystis* sp. strain PCC 6803 differs from that of ΔddhA mutant in *Synechococcus* sp. strain PCC7002 (McNeely et al., 2010) which shows 5-fold increase in hydrogen production from wild type strain; however the attainable level of hydrogen ($y_{H2,f}$) in this experiment is 10 times that shown by their experiment.

Graph (b) of Figure 4.6 shows endogenous glucose consumption characteristics in the absence of glucose. The $m_G X$ of runs with three strains decreased or kept constant with time. Although H_2 productions in three strains were highest at initial, extremely low decrease in the $m_G X$ at initial was seen in run with Δddh mutant. The initial rates of endogenous glucose consumption of GT strain, Δddh mutant and ΔadhΔddh mutant were 0.00208, 0.000417 and 0.00125 μmol mL^{-1} h^{-1}, respectively. The initial H_2 production of mutants is unrelated to endogenous glucose consumption. The decrease in the $m_G X$ with time is highest from 24 to 48 h in runs with GT strain and Δddh mutant, and from 0 to 24 h in run with ΔadhΔddh mutant. The yields of hydrogen on endogenous glucose ($Y_{H2/G}$) in GT strain and in Δddh

mutant evaluated in this period are 6.67 and 10.0, respectively. The $Y_{H2/G}$ in ΔadhΔddh mutant is constant at 26 from 0 to 72 h.

No decrease in $m_G X$ is seen from 48 to 96 h in run with GT strain, from 0 to 24 h and 48 to 72 h in run with Δddh mutant and from 24 to 72 h in run with ΔadhΔddh mutant. The molecules of NAD(P)H for NiFe-hydrogenase are found to be mainly supplied by oxidative reactions other than glycolysis such as turnover of proteins, membrane lipids and PHB.

The decrease in $m_G X$ with time is highest from 24 to 48 h in runs with GT strain and Δddh mutant, and from 0 to 24 h in run with ΔadhΔddh mutant. The yields of H_2 on endogenous glucose ($Y_{H2/G}$) in GT strain and in Δddh mutant evaluated in this period are 6.67 and 10.0, respectively. The $Y_{H2/G}$ in ΔadhΔddh mutant is constant at 26 from 0 h to 72 h.

The present results are obtained in runs with inocula from late-logarithmic growth phase. If logarithmically growing cells are inoculated into dark anaerobic nitrate-free HEPES buffer solution, the $m_G X$ increases in the first 24 h and then decreases after 24 h (data not shown). The inoculum $m_G X$ levels of GT strain, Δddh mutant and ΔadhΔddh mutant were 0.21, 0.17 and 0.14 μmol·mL^{-1}, respectively. Figure 4.6 (b) shows that the $m_G X$ at 96 h of runs with GT strain, Δddh mutant and ΔadhΔddh mutant were 0.06, 0.07, and 0.07 μmol mL^{-1}, respectively. The $m_G X$ of ΔadhΔddh mutant is relatively stable with time.

Dry cell weight consumption characteristic in the absence of glucose is shown in Figure 4.6(c). Concentration of dry cell weight of GT strain slightly decreased with time, while that of Δddh mutant or ΔadhΔddh mutant was almost not varied with time. The K_d of Table 4.7 shows that cell survival in dark anaerobic nitrate free solution increased in Δddh and ΔadhΔddh mutants. The K_d values of those mutants are almost zero.

Lactate production characteristics in the absence of glucose is shown in Figure 4.6(d).: The production of lactate in GT strain started right after dark incubation Although the deletion of ddh genes is confirmed, the time courses of lactate concentration of runs with Δddh mutant and with ΔadhΔddh mutant show the production of trace amount of lactate. Lactate concentrations of runs with Δddh and Δadhddh mutants at 96 h were extremely low as 0.03 and 0.01 μmol mL^{-1}, respectively. These trace amount represent the generation of Δddh phenotype deficient cells from Δddh mutant and ΔadhΔddh mutant during photosynthesis on antibiotic-free BG-11 medium and dark incubation on antibiotic-free HEPES buffer solution.

The specific production rate of lactate by GT strain in the first 24 h was 0.000397 μmol mg^{-1} h^{-1}. The increases in lactate concentration in the incubation of Δddh mutant and ΔadhΔddh on glucose in the first

24 h were 0.01 μmol mL^{-1} and 0 μmol mL^{-1}, respectively, hence the fraction of Δddh photype deficient cells in Δddh cells and ΔadhΔddh cells are analyzed to be 0.5 and 0, respectively. Lactate concentrations at 96 h of runs with Δddh and Δadhddh mutants were extremely low as 0.03 and 0.01 μmol mL^{-1}, respectively. The initial yield of lactate on endogenous glucose of GT strain was 0.4, which shows that the relatively large portion of degraded-glycogen is utilized not for the synthesis of lactate. Although hydrogen production rate and endogenous glucose consumption rate decreased with time, lactate production rate was accelerated after 48 h. The carbon for lactate production after 48 h appears to be supplied from not only endogenous glucose but also other carboneous compounds.

Acetate production characteristic in the absence of glucose is shown in Figure 4.6(e). Acetate concentration is about one-tenth of lactate concentration. Acetate is not detected in the incubation of ΔadhΔddh mutant. The production of acetate delays for 24 h in the incubations of GT strain and Δddh mutant. No difference is observed in the acetate production in GT strain and in Δddh mutant from 24 h to 72 h. The acetate production rate in this period was 0.00417 μmol mL^{-1} h^{-1}. After 72 h, acetate production was activated in GT strain but turned to consumption in Δddh mutant. The acetate consumption after 72 h in Δddh mutant appears to show an oxidation of acetate to carbon dioxide in incomplete TCA cycle. In Δddh mutant, acetate appears to be redirected to compensate the damaged cell constituting materials for survival. Acetate consumption in Δddh mutant after 72 h is not seen in GT strain that represents high activity in endogenous glucose consumption. In GT strain, degradation of endogenous glucose likely contributes to be directed to biochemical synthesis for survival. Different from mutant, GT strain actively processed in glycolysis by converting glycogen to lactate and acetate.

Ethanol production characteristics in the absence of glucose: Ethanol concentration at 96 h of runs with GT strain, Δddh mutant and ΔadhΔddh mutant was extremely low as 0.7, 1.0 and 0.4 μmol mL^{-1}, respectively. These results show that the specific rates of ethanol production by GT strain and Δddh mutant were 0.00283 and 0.00404 μmol mg^{-1} h^{-1}, respectively. The ethanol production of Δddh mutant was higher than that of GT strain. The excess NADH molecule that was generated by elimination of lactate hydrogenase activity appears to be redirected to alcohol dehydrogenase. Drop of ethanol concentration of run with ΔadhΔddh mutant from that with Δddh mutant partially verifies the successful deletion of the genes coding for adh. Incomplete elimination of ethanol production in run with ΔadhΔddh mutant shows the generation of Δadh phenotype deficient cells from ΔadhΔddh mutant

(d) Characteristics of Dark Anaerobic Nitrate-Free Hydrogen Production in the Presence of Glucose

In the second series of H_2 production experiments, photoautotrophic cells of GT strain, Δddh mutant and ΔadhΔddh mutant in late-logarithmic growth phase were harvested and incubated with X at 2.58 mg mL^{-1} in dark anaerobic nitrate-free antibiotic-free HEPES buffer solution with 5 mmol mL^{-1} exogenous glucose. The number of moles per culture volume of H_2 (y_{H2}), exogenous glucose (c_S), endogenous glucose ($m_G X$), lactate (c_L) and acetate (c_A) and dry cell weight concentration (X) are analyzed. Time courses of y_{H2}, c_S, $m_G X$, X, c_L and c_A are shown in **Figure 4.8**. Different from curves in Figure 4.6, curves in Figure 4.8 represent the heterotrophic growth of GT strain, Δddh mutant and ΔadhΔddh mutant on exogenous glucose. Production of lactate, acetate and ethanol in GT strain were also become eminent.

Figure 4.8(a) shows that the y_{H2} versus time data of runs with exogenous glucose are fitted by Eq.(2.18). The parameters $r_{H2,0}$, k and $y_{H2,f}$ for curve-fittings are tabulated in **Table 4.8**. The calculated y_{H2} agrees relatively well with the observed y_{H2}. The $y_{H2,f}$ of glucose-supplemented runs with GT strain, Δddh mutant and ΔadhΔddh mutant were 5.61, 3.48 and 2.45 μmol mL^{-1}, respectively, which were 2.46, 1.50 and 1.65-fold, respectively over runs without glucose. It becomes eminent that exogenous glucose elevates dark anaerobic hydrogen production in GT strain, Δddh mutant and ΔadhΔddh mutant.

The relation shown in Fig.4.7 is not seen in Table 4.8. Glucose effect on H_2 production is extremely high, hence genetic modification effect in the absence of glucose becomes to be missing in the presence of glucose. For elevating H_2 production, it is important to elucidate the interrelated effect of monosaccharide, growth phase and genetic modification.

The $r_{H2,0}$ of Table 4.8 is highest for run with GT strain, lowest for run with Δddh mutant and second lowest for run with ΔadhΔddh mutant. This order is quite different from that of runs without glucose. Intracellular electrons increased at the dark anaerobic inoculation is likely directed to NiFe-hydrogenase in the absence of glucose, however, they are directed not only NiFe-hydrogenase but also many metabolic pathways including cell growth, acid fermentation that are triggered in the presence of glucose. Hence $r_{H2,0}$ of Δddh mutant under exogenous glucose solution couldn't show highest activity.

Highest $y_{H2,f}$ is found to be achieved utilizing GT strain in the presence of exogenous glucose. The attainable level of y_{H2} by Δddh mutant and ΔadhΔddh is less than that of GT strain. When glucose was present, the highest $y_{H2,1}$ was GT strain , second highest is Δddh strain and the lowest is ΔadhΔddh mutant. The elimination of adh activity resulted to decrease $y_{H2,1}$ that was 0.49 times that of GT strain in runs with exogenous glucose.

Exogenous glucose consumption is shown in Fig.4.8(b). Time course of the concentration of exogenous glucose (c_S) shows that consumption activity of exogenous glucose by Δddh mutant and ΔadhΔddh mutant are extremely low when it is compared with that by GT strain. Glucose consumption of

GT strain was active in the first 48 h as shown in chapter 2, while that of Δddh mutant and that of ΔadhΔddh mutant were inactive in the first 72 h. Genetic elimination of lactate dehydrogenase activity is found to block the assimilation of glucose. It is known that lactate inhibits glucose uptake (Brown and Whitely, 2009), however, there are remarkably few data available on the cross talk between lactate dehydrogenase and glucose consumption. Conversions of glucose at 96 h by GT strain, Δddh mutant and ΔadhΔddh mutant were 0.76, 0.19 and 0.23, respectively. The observed block of exogenous glucose assimilation by the disruption of ddh genes was not anticipated.

Fig.4.8(c) shows the time courses of the number of moles of endogenous glucose per culture volume ($m_G X$) in the presence of glucose: Right after dark anaerobic incubation of GT strain, Δddh mutant and ΔadhΔddh mutant, no decrease in $m_G X$ is seen in this graph. Inoculum cells for dark anaerobic incubation were obtained from logarithmic growth phase, hence NAD(P)H synthesis rate is so high that generated NAD(P)H is ready to be redirected for glycogen synthesis. The $r_{H2,0}$ and the initial glucose production rate r_{G0} (=d($m_G X$)/dt) of GT strain is highest among three strains. Since H_2 production and glycogen synthesis are NAD(P)H and ATP consumption rate, GT strain in the presence of glucose is found to be rich in reductive compounds and ATP. The time courses of $m_G X$ show that, during 96 h incubation, $m_G X$ of mutant increased during first 24 h, decreased from 24 to 48 h and then become constant after 48 h, whereas $m_G X$ of GT strain shows accumulation of endogenous glucose from the beginning to 72 h and then decreased. Endogenous glucose of run with GT strain shows the accumulation of glucose right after dark anaerobic incubation, when exogenous glucose is also assimilated.

The initial production of H_2 production in GT strain was highest at initial time, an increase in $m_G X$ at initial was seen in run with GT strain. The initial rate of endogenous glucose accumulation of GT, Δddh mutant and ΔadhΔddh mutant were 0.00384, 0.00250 and 0.00032 μmol mL^{-1} h^{-1}, respectively. The decrease in $m_G X$ with time is not observed from 48 to 96 h in runs with Δddh mutant and ΔadhΔddh mutant, they were constant. The endogenous glucose of GT strain was increasing during fermentation with a sharp drop after 72 h. The present results are obtained in runs with inocula from late-logarithmic growth phase.

Figure 4.8 (d) shows that dry cell weight concentration (X) of GT strain, Δddh mutant and ΔadhΔddh mutant increased in the first 24 h, and decreased after 24 h. As shown in Table 4.7, those 3 strains represent same specific growth rate at 0.0101h^{-1} from 0 to 24h. The curve of GT strain shows that the initial increase in X is associated with the reduction in exogenous glucose concentration. This association confirms the heterotrophic growth of GT strain on glucose. Growth of Δddh mutant and ΔadhΔddh mutant appears to be triggered by exogenous glucose. Combination of the time courses of exogenous glucose, endogenous glucose and dry cell weight suggests that carbon source for cell growth of Δddh

mutant is not exogenous glucose or endogenous glucose but unidentified intracellular organic compounds. Carbonaceous compounds, other than glucose, that is contained in cell suspended HEPES buffer solution with glucose is CO_2, HCO_3^- and those evolved from cell at the beginning of dark anaerobic incubation. The rate of decrease in dry cell weight concentration after 48 h is comparable with the initial decrease in dry cell weight concentration of run without glucose. The time course of dry cell weight concentration of ΔadhΔddh mutant is comparable with that of Δddh mutant.

Time course of lactate concentration (c_L) in the presence of glucose (Fig. 4.8 (e)) shows that c_L at 96 h of run with GT strain was 4.74 μmol mL^{-1} which is 18 times more than that in the absence of glucose. This result shows that exogenous glucose is converted to lactate by GT strain. The yield of lactate on dry cell weight in the first 24 h is 3.95 μmol mg^{-1}. The increases in c_L in the incubation of Δddh mutant and ΔadhΔddh mutant on glucose in the first 24 h were 0.03 μmol mL^{-1}, and 0.07 μmol mL^{-1}, respectively, hence the fraction of Δddh photype deficient cells in Δddh mutant and ΔadhΔddh mutant are analyzed to be 0.00362 and 0.00844, respectively. Concentrations (c_L) at 96 h of runs with with Δddh and Δadhddh mutants were extremely low at 0.05 and 0.06 μmol mL^{-1}, respectively. The deletion of ddh genes in this work possibly altered the intracellular balance between NAD(P)H and $NAD(P)^+$ towards shifting-up NAD(P)H level. This NAD(P)H shifting-up is important because NADH and NADPH are essential reductive compounds for hydrogen production on NiFe-hydrogenase. The increase in the level of NAD(P)H results in the increase in the level of ATP and subsequently inactivates phosphofructokinase. Assimilation of exogenous glucose by Δddh mutant appears to be blocked by the inactivation of phosphofructokinase, brought by the elimination of the genes coding for ddh.

Time course of acetate concentration (c_A) in the presence of glucose (Fig. 4.8 (f)) shows that acetate production is highly activated by exogenous glucose in GT strain. Exogenous glucose stimulated acetate production also in Δddh mutant and ΔadhΔddh mutant. After 96 h, acetate concentrations of runs with GT strain, Δddh mutant and Δadhddh mutant in the presence of exogenous glucose were 17.19, 8.66 and 4.83 μmol mL^{-1}, respectively, that were about more than 100 times those in the absence of exogenous glucose. Acetate is one of the terminal carbon release compound from glucose consumption. Glucose consumption and acetate production of GT strain were higher than those of Δddh and ΔadhΔddh mutants.

Time course of ethanol concentration (c_E) in the presence of glucose (Fig. 4.8 (g)) shows that c_E at 96 h of runs with GT strain, Δddh mutant and ΔadhΔddh mutant was extremely low as 0.70, 1.01 and 0.47 $\mu mol \cdot mL^{-1}$, respectively. Extremely low production of ethanol by the incubation of ΔadhΔddh mutant from antibiotic-free photoautotrophic culture verifies the successful deletion of the genes coding for *adh*. The yield of ethanol on dry cell weight of GT strain in the first 24 h is 0.45 μmol mg^{-1}. The increase in

ethanol concentration in the incubation of ΔadhΔddh mutant on glucose in the first 24 h was 0.17 μmol mL^{-1}, hence the fraction of Δadh photype deficient cells in ΔadhΔddh cells are analyzed to be 0.180.

If stability of H_2 production is evaluated in low value of the parameter k shown in Table 4.9, incubation of Δddh mutant in the presence of exogenous glucose represents the most stable H_2 production condition. This stabilization is not harnessed in the attainable level of H_2 ($y_{H2,f}$), which is highest in run with GT strain in the presence of exogenous glucose. When viewed over the parameters in this study, the increase in the initial hydrogen production rate ($r_{H2,0}$) is found to be crucial to elevate the level of $y_{H2,f}$. Elimination of ddh and adh genes is effective to increase the level of $r_{H2,0}$ in the absence of exogenous glucose, however, it becomes ineffective in the presence of exogenous glucose. Redox balance in the presence of exogenous glucose is found to be different from that in the absence of exogenous glucose.

(e) Effect of redox perturbation in genetically modified strains on H_2 production

Parameters $q_{H2,0}$* and $y_{H2,f}$* defined by Eq.(2.30) are calculated and listed in Tables 4.7 and 4.8. **Figure 4.9** shows plots of $y_{H2,f}$* against $q_{H2,0}$*. The plots shows that genetic modification results in an increase in the initial content of NAD(P)H. The presence of glucose affects to elevate initial content of NAD(P)H. The attainable level of the amount of H_2 per culture volume in GT strain and Δddh mutant increases in the presence of glucose, while it decreases in ΔadhΔddh mutant in the presence of glucose. The $y_{H2,f}^*$ in terms of $q_{H2,0}^*$ of data in this chapter is slightly higher than that predicted by Eq.(2.33) with k_{H2} at 0.619. The initial specific H_2 production rate ($q_{H2,0}$) of GT strain in run with glucose shown in Table 2.3 was 0.0336 μmol $mg^{-1}h^{-1}$, while that shown in Table 4.8 is 0.0410 μmol $mg^{-1}h^{-1}$ that is 1.22 times that in Table 2.3. The $y_{H2,f}$ of GT strain in run with glucose shown in Table 2.3 was 3.26 μmol mL^{-1}, while that shown in Table 4.8 is 5.61 μmol mL^{-1} that is 1.72 times that in Table 2.3. About 20% shift in the initial content of NAD(P)H is found to results in about 70% variation in attainable level in y_{H2}.

In Fig.4.9, results of runs with GT strain, Δddh mutant and ΔadhΔddh mutant are plotted by two points from runs with and without glucose. Pair points are connected by straight lines. Slope of the straight lines $d\ln y_{H2,f}^*/d\ln q_{H2,0}^*$ is highest in ΔadhΔddh mutant, second highest in Δddh mutant and lowest in GT strain. Sensitivity analysis to glucose concludes that genetic modification elevates the sensitivity of H_2 production to glucose. Increase in the initial NAD(P)H content by utilizing exogenous glucose affects to increase the attainable level of amount of H_2 per culture volume in GT strain, to largely increase it in Δddh mutant and to decrease in ΔadhΔddh mutant.

Figure 4.10 shows a relation between $(m_G X)_1$ and y_{H1} in runs with GT strain, Δddh mutant and ΔadhΔddh mutant in HEPES buffer solution with or without glucose. Solid line without keys is calculated utilizing data of chapter 2 and Eq.(2.40). Plots of data with and without glucose of runs with Δddh mutant

and ΔadhΔddh mutant are connected by straight lines. Slope of lines indicates the sensitivity of $y_{H2,1}$ against $(m_G X)_1$. Sensitivity is found to be highest in ΔadhΔddh mutant, second highest in Δddh mutant and lowest in GT strain. Plotted data in this graph utilize the experimental data with glucose for inoculum from late-logarithmic growth, hence it is still an open question whether the initial increase in cellular content of NAD(P)H in two mutants can results in the increase in $y_{H2,1}$ when inoculum is obtained from logarithmic phase and incubated in solution of monosaccharide other than glucose.

4.4 Summary

Research in this chapter concerns a DNA modification of a glucose tolerant mutant of *Synechocystis* sp. strain PCC6803 for H_2 production. The highlights of this chapter are as follows.

1. Mutants that are defective of the genes coding for lactate dehydrogenase (Δddh mutant) and both lactate dehydorogenase and alcohol dehydrogenase (ΔadhΔddh mutant) are constructed.
2. Metabolic engineering approach to introduce a perturbation in redox homeostasis of GT strain is made. Mutants defective the genes coding for lactate dehydrogenase (Δddh mutant) and for both lactate dehydrogenase and alcohol dehydrogenase (ΔadhΔddh mutant) are constructed. The initial H_2 production of mutants are slightly higher than that of GT strain.
3. Among GT strain, Δddh mutant and ΔadhΔddh mutant in HEPES buffer solution with or without glucose, GT strain in the presence of glucose is capable of producing the highest attainable level of the number of moles of hydrogen per culture volume due to heterotrophic growth by assimilating exogenous glucose and producing endogenous glucose, lactate and acetate.
4. Glucose elevates H_2 production in GT strain and Δddh mutant, while lowers it in ΔadhΔddh mutant. Glucose is assimilated by GT strain. Assimilation of glucose is blocked by the elimination of the genes coding for lactate dehydrogenase.
5. Deletion of NAD(P)H-consuming dehydrogenase pathways redirects more NAD(P)H to NiFe-hydrogenase and affects to increase hydrogen production rate. Successful mutant constructions are confirmed by a drastic drop in lactate production and ethanol production by corresponding mutants.
6. Attainable level of the amount of H_2 per culture volume in GT strain and Δddh mutant is defined by the initial cellular content of NAD(P)H.

Table 4.1 *Synechocystis* sp. strain PCC 6803 genes relating to a function of ethanol production.

Gene	Function
slr0942	Alcohol dehydrogenase-$NADP^+$ [EC.1.1.1.2]
slr1192	Zinc-containing alcohol dehydrogenase like protein[EC.1.-.-.-]
sll0990	S-(hydroxymethyl)glutathione dehydrogenase (GSH) [EC.1.1.1.284]/ Alcohol dehydrogenase-NAD^+ [EC.1.1.1.1]
slr2124	Short chain dehydrogenase (SDR)/Short chain alcohol dehydrogenase

Table 4.2 Plasmids used for constructing the vector DNA to disrupt genes *ddh* in GT strain to derive Δddh mutant strain

Restriction enzyme cleavage map	
Kanamycin fragment:pUC4K	Vector: pUC19
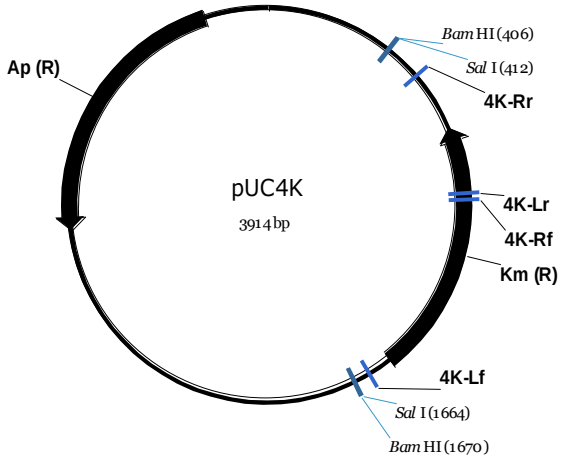	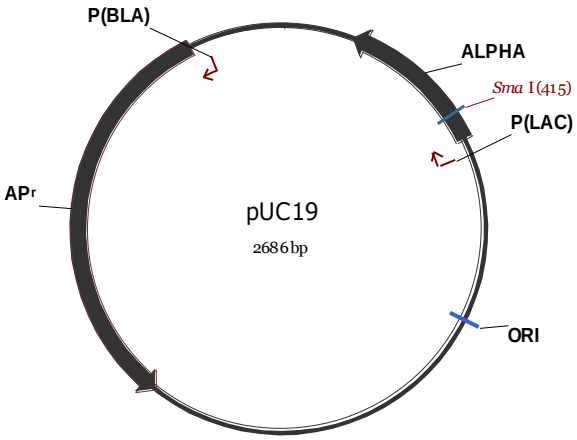

Table 4.3 Plasmids used for constructing the vector DNA to disrupt genes adh in Δddh mutant to derive Δadh Δddh mutant strain

Restriction enzyme cleavage map	
Streptomycin and spectinomycin fragement (Sm/Sp or Ω): pHP45-Ω	Vector: pMD19 (Takara)
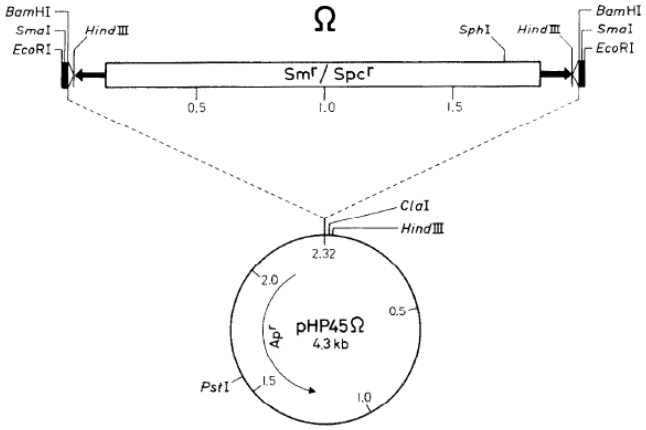	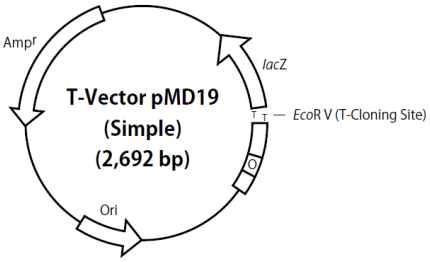

Table 4.4 Condition used for pUC19-*ddh*-Km^r transformation into GT strain

Control	**Δddh transformation**
GT cells were grown to OD_{730} = 1.48	
3.5µg vector **Plate: Km^- (no antibiotic)**	3.5µg vector Plate: 60 µmol mL^{-1} Km^+
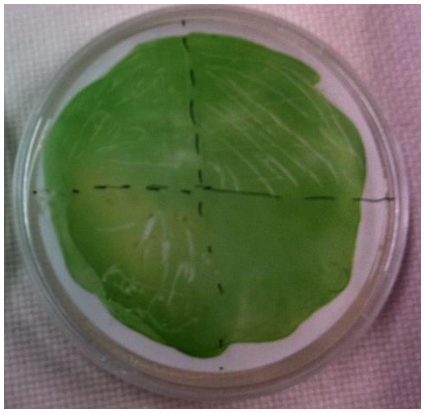	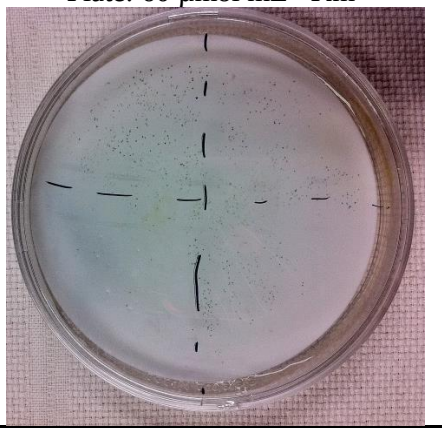

Table 4.5 Condition used for pMD19-adh-Ω transformation into GT strain

Control	**Δadh transformation**	**ΔadhΔddh transformation**
GT cells were grown to OD_{730} = 0.984		Δddh cells were grown to OD_{730} = 0.48 with 60µmol/mL Km
3.5µg vector **Plate: Sm^- (no antibiotic)**	3.5µg vector Plate: 5µmol/mL Sm^+	3.5µg vector Plate: 5 Sm^+, 60 Km^+ in µmol/mL
	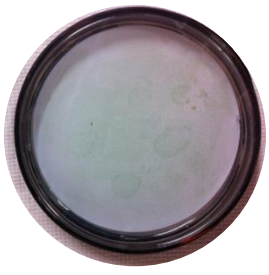	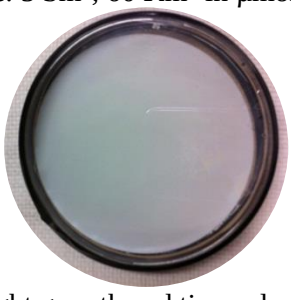
	Large number of colonies appeared	Slight growth and tiny colonies

Table 4.6 Physiological state of cells in photoautotrophic cultures that are performed prior to dark anaerobic H_2 production in indirect biophotolysis. GT strain, Δddh mutant and ΔadhΔddh mutant were obtained from different growth phases (ref, cellular state of GT strain in late-logarithmic growth phase. $q^*_{CO2,0}$, $q_{CO2,0}/(q_{CO2,0})_{ref}$;and m^*_G, $m_G/(m_G)_{ref}$.).

	GT strain		Δddh mutant		ΔadhΔddh mutant	
	w/o Glucose	with Glucose	w/o Glucose	with Glucose	w/o Glucose	with Glucose
Increase in DNA size [kb]	0		-0.495		0.56	
Harvesting time [h]	37		46		60	
X_0[mg·mL^{-1}]	1.14		1.26		1.16	
X_f[mg·mL^{-1}]	17.2		18.3		16.8	
G[-]	7.81		7.14		7.37	
g[-]	5.08		4.31		4.66	
$\mu\phi$[h^{-1}]	0.0187		0.0318		0.0238	
q_{CO2} [μmol·mg^{-1}·h^{-1}]	2.09		3.55		2.66	
q^*_{CO2} [-]	1		1.70		1.27	
NAD(P)H production rate in the Calvin cycle before inoculation [μmol mL^{-1} h^{-1}]	4.18		7.10		5.32	
m_G [μmol·mg^{-1}]	0.101		0.0815		0.0676	
m^*_G [-]	1		0.806		0.669	
R_G [μmol·mg^{-1}·h^{-1}]	0.00170		0.00273		0.00227	
R^*_G [-]	1		1.61		1.34	

Table 4.7 Kinetic parameters for H_2 production in GT strain, Δddh mutant and ΔadhΔddh mutant in HEPES buffer solution without glucose. Inoculum cells were obtained from late-logarithmic growth phase (ref, run with GT strain cells from late-logarithmic growth phase. $q^*_{H2,0}$, $q_{H2,0}/(q_{H2,0})_{ref}$; $y^*_{H2,f}$, $y_{H2,f}/(y_{H2,f})_{ref}$; $k^*=k/(k)_{ref}$; $y_{H2,1}$, c_{L1}, c_{A1}, observed number of moles of H_2, lactate and acetate per culture volume at 96 h. m_{G1}, X_1, observed m_G and X at 96h;$\Delta(m_GX)_1$, observed decrease in m_GX during 96 h H_2 production; $y_{H2/G}=y_{H2,1}/\Delta(m_GX)_1$;$Y_{L/G}=(c_{Lf}/2)/\Delta(m_GX)$; $Y_{A/G}=(c_{Af}/2)/\Delta(m_GX)$)

	GT strain	Δddh mutant	ΔadhΔddh mutant
X_0[mg·mL^{-1}]	2.10	2.10	2.10
$r_{H2,0}$ [μmol·mL^{-1}·h^{-1}]	0.0309	0.0359	0.0355
$q_{H2,0}$[μmol·mg^{-1}·h^{-1}]	0.0147	0.0171	0.0169
$q^*_{H2,0}$ [-]	1	1.16	1.15
$y_{H2,f}$ [μmol·mL^{-1}]	2.28	2.31	1.48
$y^*_{H2,f}$ [-]	1	1.01	0.649
k [h^{-1}]	0.0167	0.0213	0.0365
k^*[-]	1	1.28	2.19
K_d [h^{-1}]	0.00105	0.000620	0.000620
$y_{H2,1}$[μmol·mL^{-1}]	1.80	2.0	1.5
m_{G1} [μmol·mg^{-1}]	0.0316	0.035	0.035
X_1[mg·mL^{-1}]	1.9	2.0	2.0
$(m_G X)_1$[μmol·mL^{-1}]	0.0600	0.0700	0.0700
$c_{L,1}$[μmol·mL^{-1}]	0.26	0.03	0.01
$c_{A,1}$[μmol·mL^{-1}]	0.2	0	0
$-\Delta(m_GX)$[μmol·mL^{-1}]	0.15	0.10	0.07
$Y_{H2/G}$[-]	12	20	21.4
$Y_{X/S}$[mg μmol^{-1}]	0	0	0
$Y_{L/G}$[-]	1.73	0.3	0.143
$Y_{A/G}$[-]	1.33	0	0

Table 4.8 Kinetic parameters for H_2 production in GT strain, Δddh mutant and ΔadhΔddh mutant in HEPES buffer solution with glucose. Inoculum cells were obtained from logarithmic growth phase.

ref, run with GT strain cells from logarithmic growth phase. $q^*_{H2,0}$, $q_{H2,0}/(q_{H2,0})_{ref}$; $y^*_{H2,f}$, $y_{H2,f}/(y_{H2,f})_{ref}$; $k^+=k/(k)_{ref}$; $y_{H2,1}$, c_{L1}, c_{A1}, observed number of moles of H_2, lactate and acetate per culture volume at 96 h. m_{G1}, X_1, observed m_G and X at 96h; $\Delta(m_GX)_1$, observed decrease in m_GX during 96 h H_2 production; $y_{H2/G}=y_{H2,1}/\Delta(m_GX)_1$; $Y_{L/G}=(c_{Lf}/2)/\Delta(m_GX)$; $Y_{A/G}=(c_{Af}/2)/\Delta(m_GX)$

	GT strain	Δddh mutant	ΔadhΔddh mutant
X_0[mg·mL^{-1}]	2.20	2.10	2.10
c_{S0}[μmol·mL^{-1}]	5.0	4.8	4.7
$r_{H2,0}$ [μmol·mL^{-1}·h^{-1}]	0.0901	0.0430	0.0502
$q_{H2,0}$[μmol·mg^{-1}·h^{-1}]	0.0410	0.0205	0.0239
$q^*_{H2,0}$ [-]	2.79	1.39	1.63
$y_{H2,f}$ [μmol·mL^{-1}]	5.61	3.48	1.07
$y^*_{H2,f}$ [-]	2.46	1.53	0.469
k [h^{-1}]	0.0184	0.0145	0.0299
k^*[-]	1.12	0.868	1.79
μ[h^{-1}]	0.0100(0-24h)	0.00890(0-24h)	0.0105(0-24h)
K_d [h^{-1}]	0(24-96h)	0.00170(24-96h)	0.00217(24-96h)
$y_{H2,1}$[μmol·mL^{-1}]	4.7	2.6	2.3
c_{S1}[μmol·mL^{-1}]	1.2	3.9	3.6
m_{G1} [μmol·mg^{-1}]	0.0963	0.0478	0.0435
X_1[mg·mL^{-1}]	2.7	2.3	2.3
$(m_G X)_1$[μmol·mL^{-1}]	0.260	0.110	0.100
$c_{L,1}$[μmol·mL^{-1}]	4.74	0.05	0.06
$c_{A,1}$[μmol·mL^{-1}]	17.2	8.66	4.83
$c_{E,1}$[μmol·mL^{-1}]	0.70	1.01	0.47

$-\Delta c_S$[μmol·mL^{-1}]	3.8	0.9(after 48h)	1.1(after 72h)
$(-\Delta c_S)_0$[μmol·mL^{-1}]	2.6	0	0
$\Delta(m_G X)_0$[μmol·mL^{-1}]	0.14 (0-48h)	0.06 (0-24h)	0.01 (0-24h)
$-\Delta(m_G X)_1$[μmol·mL^{-1}]	0.08 (72-96h)	0.13(24-48h)	0.11(24-48h)
$-\Delta c_{SG}$[μmol·mL^{-1}]	3.74	0.97	1.20
$(\Delta X)_0$[mg·mL^{-1}]	0.6(0-24h)	0.5(0-24h)	0.6(0-24h)
$Y_{H2/SG}$[-]	1.26	2.68	1.92
$Y_{X/S}$[mg μmol^{-1}]	0.231(0-24h)	0.556(0-24h)	0.545(0-24h)
$Y_{L/SG}$[-]	1.27	0.0515	0.05
$Y_{A/SG}$[-]	4.60	8.93	4.03

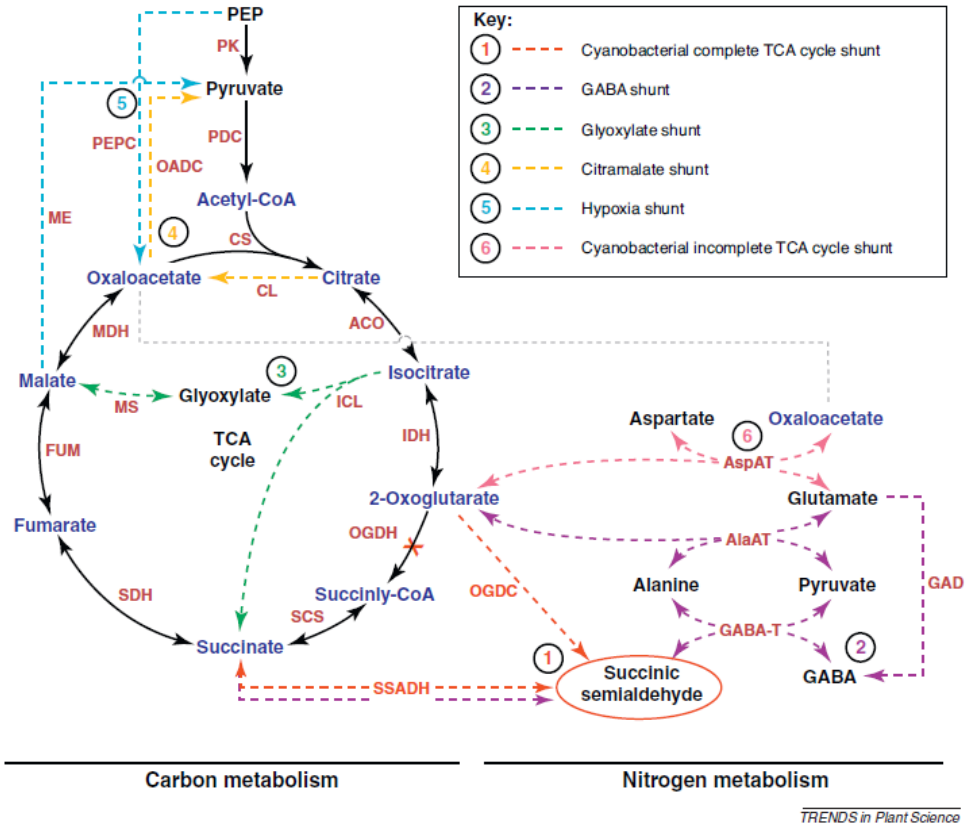

Figure 4.1 Incomplete TCA cycle (Steinhauser et al.,2012). TCA cycle in cyanobacteria is incomplete because of the lack the enzyme 2-oxoglutarate dehydrogenase (OGDH) (1) The TCA cycle variant – red broken arrows; the GABA shunt, broken violet arrows; the glyoxylate shunt, green broken arrows; the citramalate shunt, yellow broken arrows; the TCA cycle shunt observed under hypoxia, light-blue broken arrows; and the closing reaction (without glyoxylate shunt) of the incomplete cyanobacterial TCA cycle, pink broken arrows. TCA cycle intermediates are colored blue, whereas bypass intermediates are colored black. Enzymes are depicted in brown. ACO, aconitase; AlaAT, alanine aminotransferase; AspAT, aspartate aminotransferase; CL, citratelyase; CS, citrate synthase; FUM, fumarase; GABA-T, GABA aminotransferase; GAD, glutamate decarboxylase; ICL, isocitrate lyase; IDH, isocitrate dehydrogenase; MDH, malate dehydrogenase; ME, malic enzyme; MS, malate synthase; OADC, oxaloacetate decarboxylase; OGDC, 2-oxoglutarate decarboxylase; OGDH, 2-oxoglutarate dehydrogenase complex; PDC, pyruvate dehydrogenase complex; PEPC, phosphoenolpyruvate carboxylase; PK, pyruvate kinase; SCS, succinyl CoA ligase; SDH, succinate dehydrogenase; SSADH, succinic semialdehyde dehydrogenase.

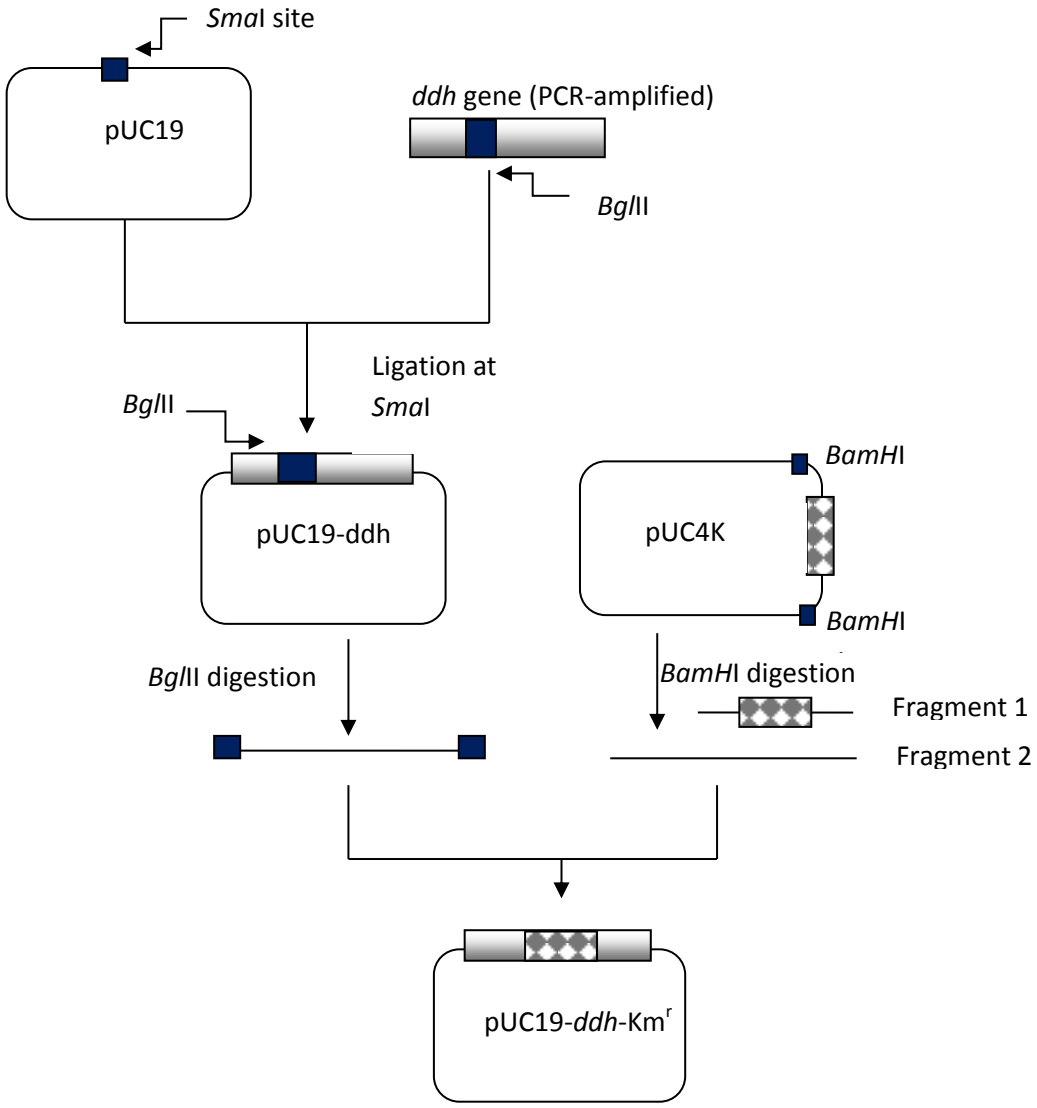

Figure 4.2 Overall strategies to construct pUC19-*ddh*-Km^r

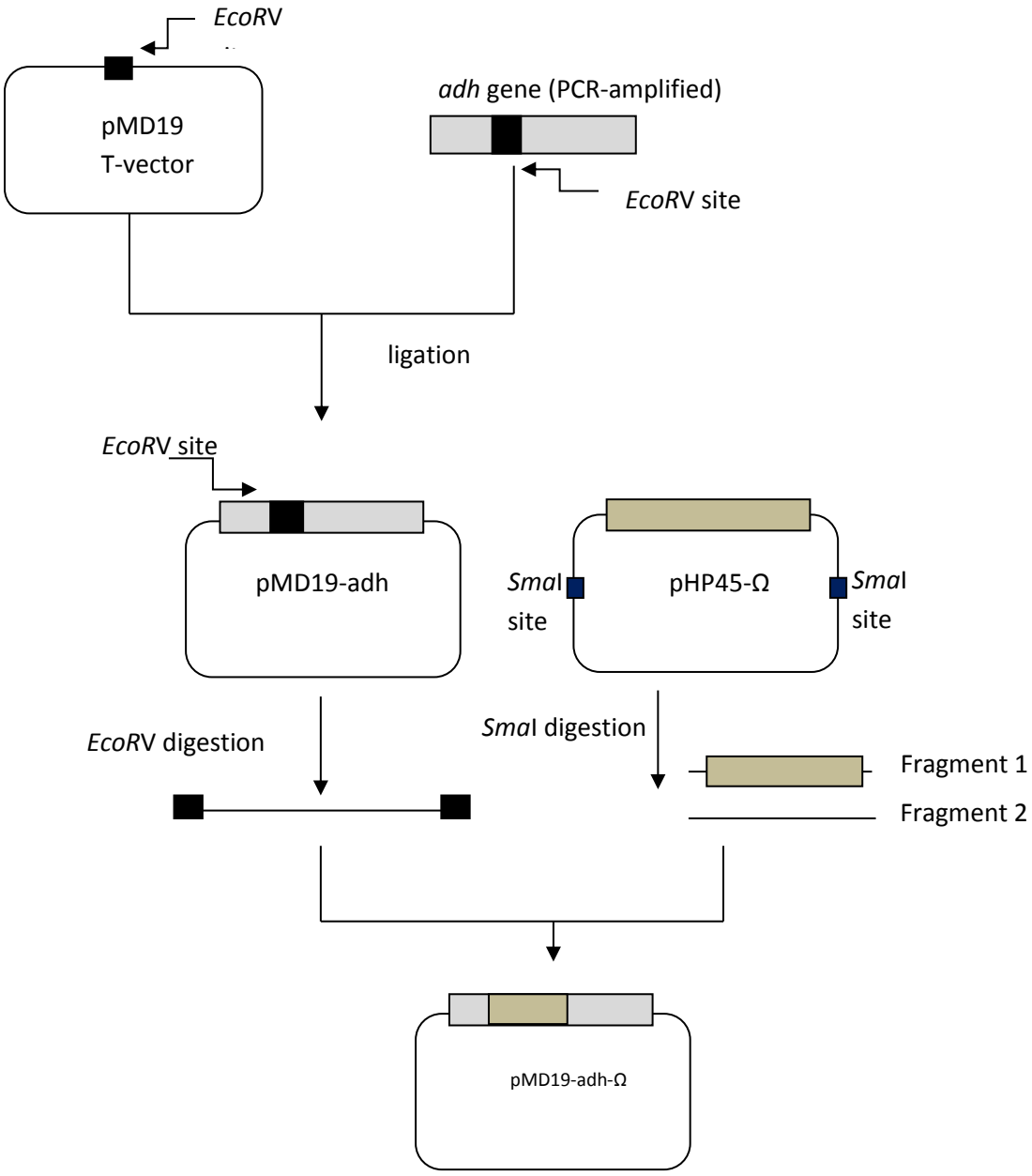

Figure 4.3 Overall strategies to construct pMD19-*adh*-Ω

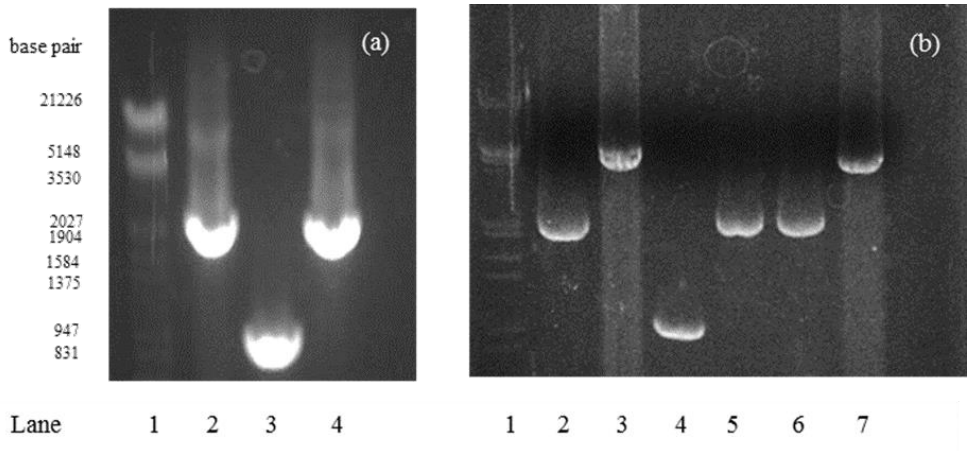

Figure 4.4 Agarose-gel electrophoretic analyses of PCR products for evaluating the achievement of (a) Δddh mutation and (b) ΔadhΔddh mutation

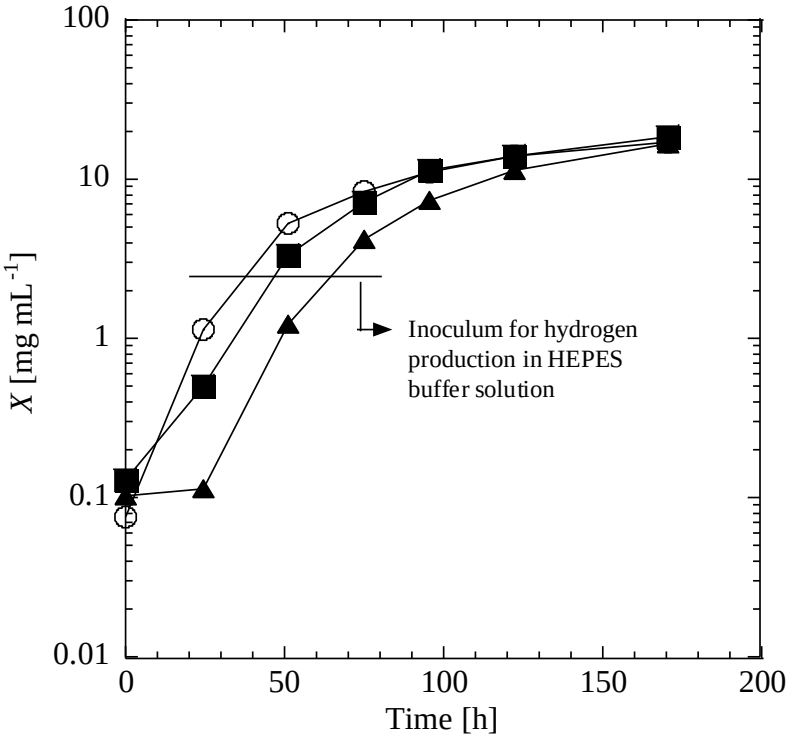

Figure 4.5 Photoautotrophic growth curves of GT strain (○), Δddh mutant (■) and ΔadhΔddh mutant (▲) on antibiotic-free BG-11 medium. The horizontal line pointing the level of X at 2.58 mg mL^{-1} represents the culture-harvesting time when OD_{730} of cell suspensions is 7.

Pre-culture cells of GT strain, Δddh mutant and ΔadhΔddh mutant for the inocula of main cultures shown in above curves were grown on BG-11 medium, BG-11 medium with 60 mg mL^{-1} kanamycin and BG-11 medium with both 60 mg mL^{-1} kanamycin and 2.5 mg mL^{-1} streptomycin, respectively. Harvested preculture cells were washed by sterilized distilled-water to remove antibiotics prior to main culture.

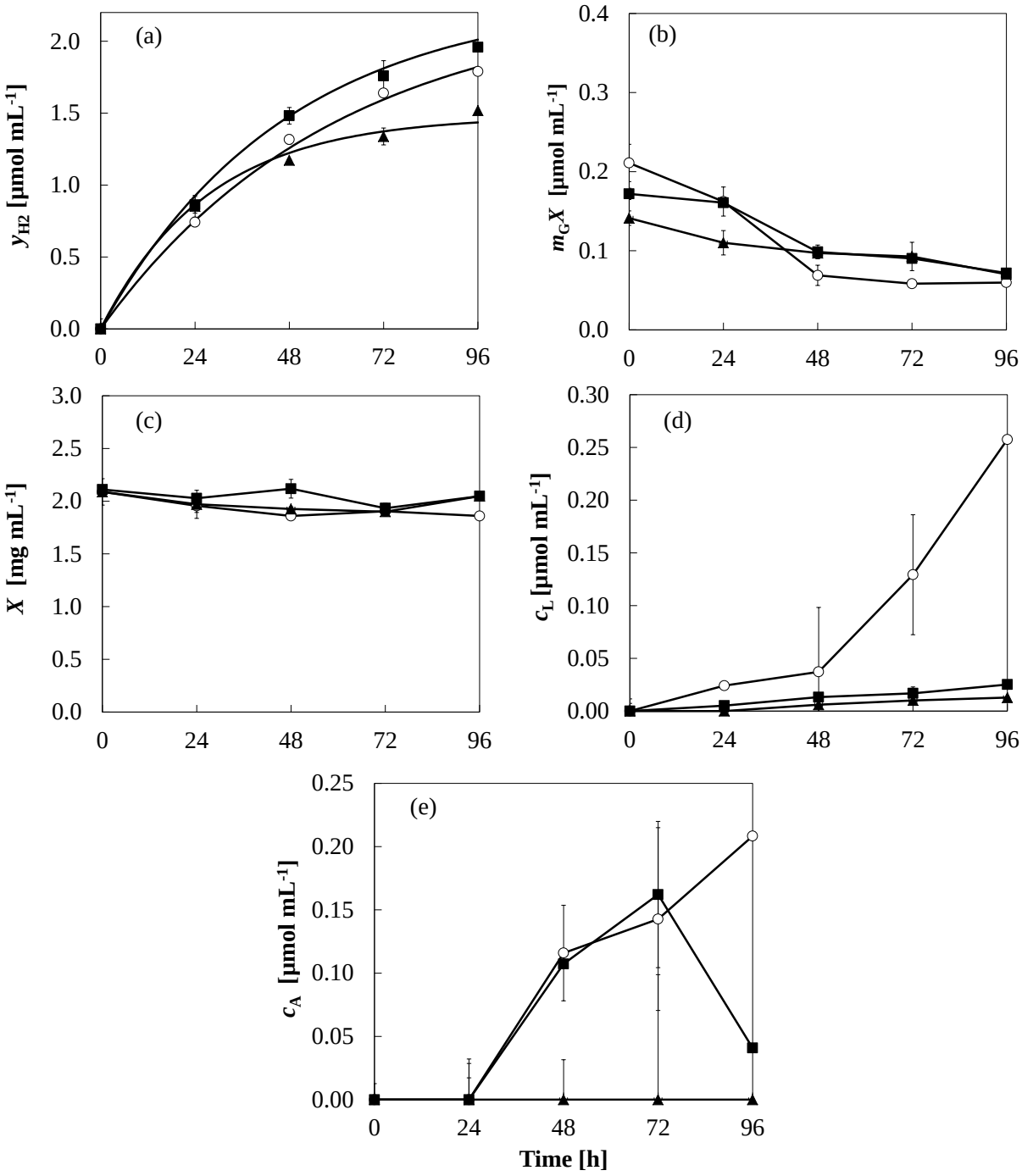

Figure 4.6 Time courses of culture variables for dark anaerobic hydrogen production of cells of GT strain (○), Δddh mutant (■) and ΔadhΔddh mutant (▲) in HEPES buffer solutions. Quantities measured include the moles per culture volume of (a) hydrogen and (b) the moles of endogenous glucose in glycogen, and the concentrations of (c) dry cell weight, (d) lactate and (e) acetate. Experiments were carried out in duplicate

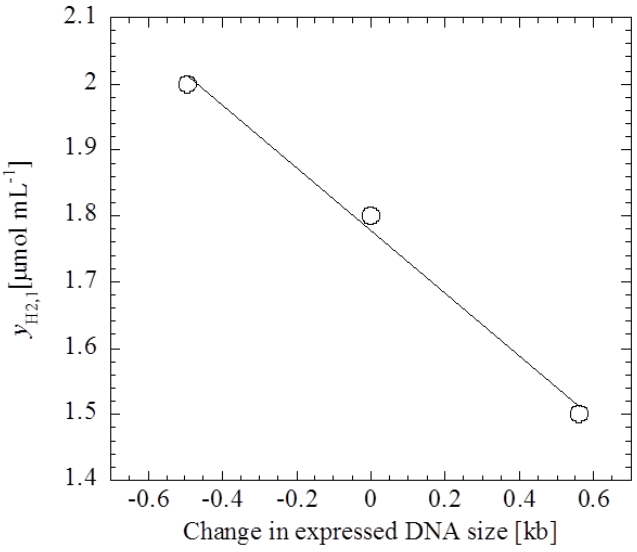

Figure 4.7 Plots of $y_{H2,1}$ against change in the expressed DNA size

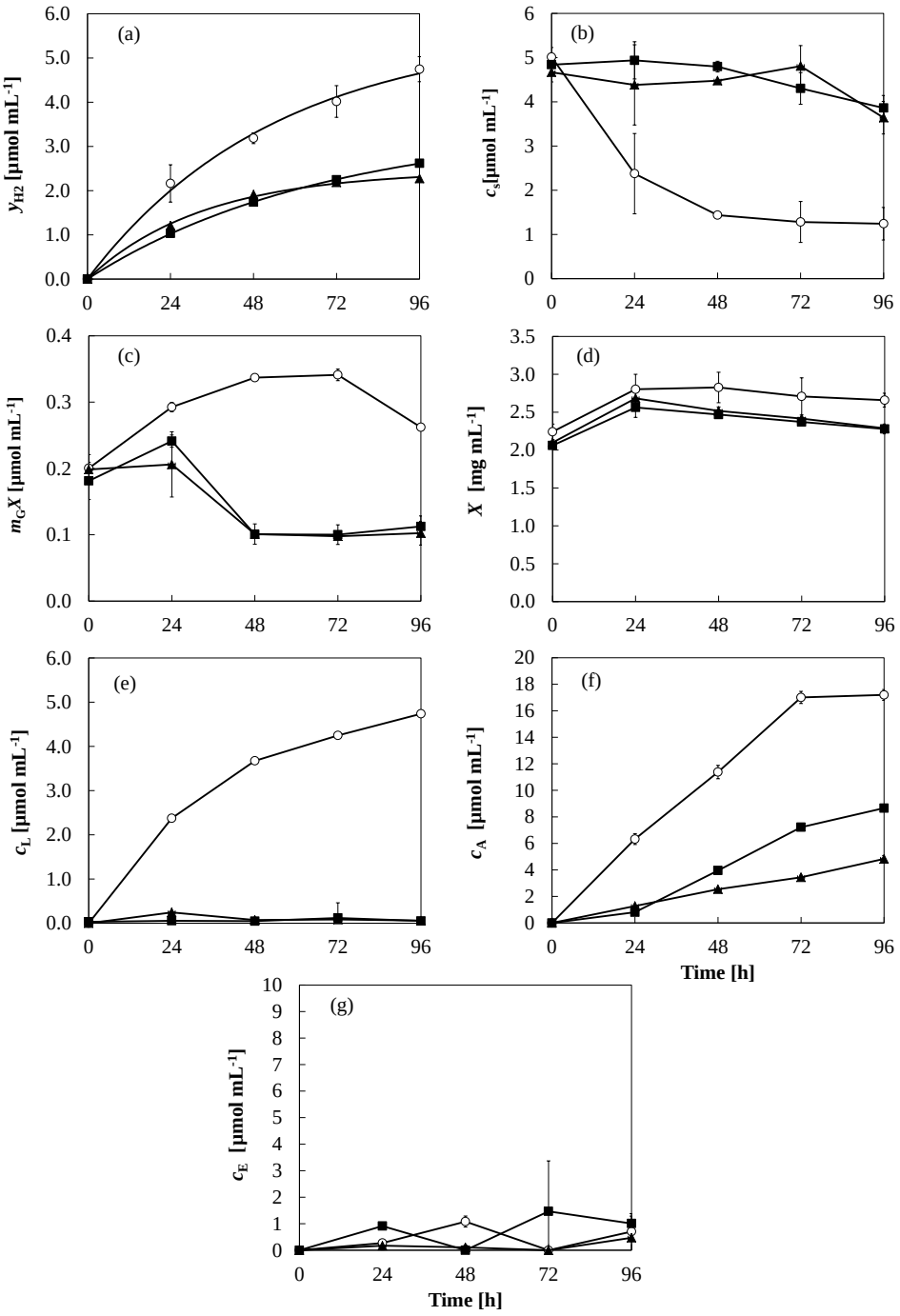

Figure 4.8 Time courses of culture variables for dark anaerobic hydrogen production of cells of GT strain (○), Δddh mutant (■) and ΔadhΔddh mutant (▲) in HEPES buffer solutions supplemented with 5 µmol·mL^{-1} glucose. Quantities measured include (a) the moles of hydrogen per culture volume, (b) the concentration of exogenous glucose, (c) the moles of endogenous glucose in glycogen per culture volume, (d) the concentration of cell mass, (e) the concentration of lactate, (f) the concentration of acetate and (g) the concentration of ethanol. Experiments were carried out in duplicate

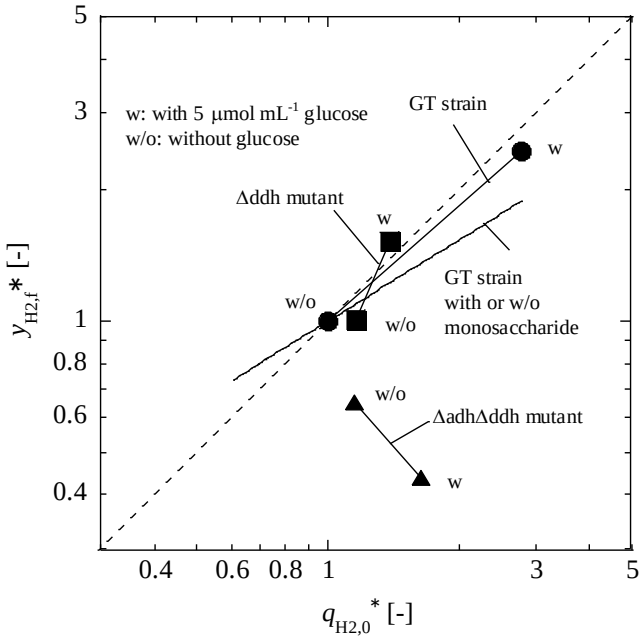

Figure 4.9 Relation between initial specific H_2 production rate and attainable level of H_2

$q_{H2,0}^{*}=q_{H2,0}/(q_{H2,0})_{ref}$; $y_{H2,f}^{*}=y_{H2,f}/(y_{H2,f})_{ref}$; ref, run with logarithmically growing cells

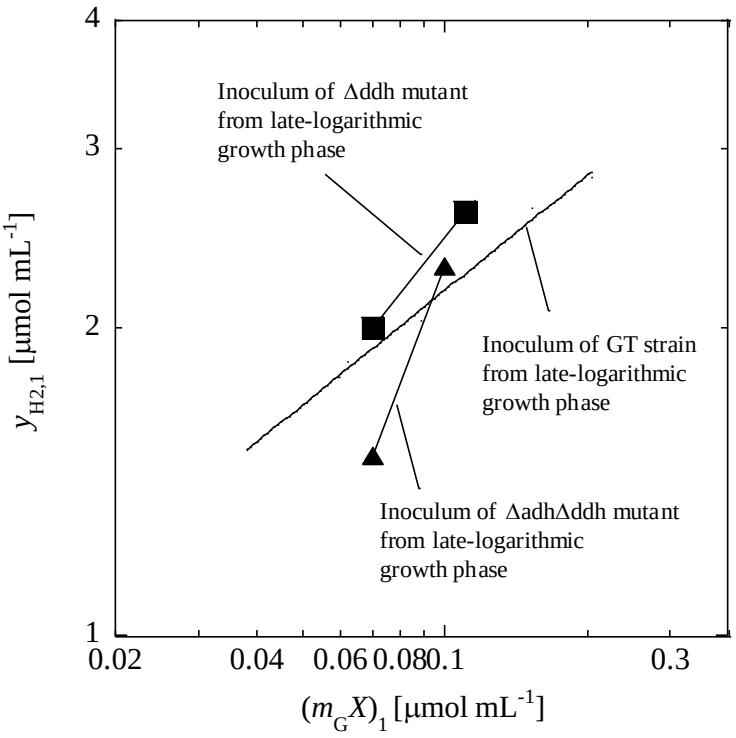

Figure 4.10 Relation between $(m_G X)_1$ and y_{H1} in runs with GT strain, Δddh mutant and ΔadhΔddh mutant in HEPES buffer solution with or without glucose

Chapter 4: References

Brown SA, Whiteley M (2009) Characterization of the L-lactate dehydrogenase from *Aggregatibacter actinomycetemcomitans*. PLoS ONE. 4(11)e7864

Chongsuksantikul A, Asami K, Yoshikawa S, Ohtaguchi K (2014) Dark Anaerobic Hydrogen Production in the Mutants of *Synechocystis* sp. Strain PCC6803-GT Defective in Lactate Dehydrogenase Activity and/or Alcohol Dehydrogenase Activity, Incubated in Buffer Solutions With or Without Glucose. International Journal of Biology 7 (1):p33

Cooley JW, Vermaas WF (2001) Succinate dehydrogenase and other respiratory pathways in thylakoid membranes of *Synechocystis* sp. strain PCC 6803: capacity comparisons and physiological function. Journal of bacteriology 183 (14):4251-4258

Dehring U, Kramer D, Ziegler K (2012) Selection of ADH in genetically modified cyanobacteria for the production of ethanol. United States Patent,

Gao Z, Zhao H, Li Z, Tan X, Lu X (2012) Photosynthetic production of ethanol from carbon dioxide in genetically engineered cyanobacteria. Energy and Environmental Science 5 (12):9857-9865

McNeely K, Xu Y, Bennette N, Bryant DA, Dismukes CG. (2010) Redirecting Reductant Flux into Hydrogen Production via Metabolic Engineering of Fermentative Carbon Metabolism in a Cyanobacterium. Applied and Environmental Microbiology 76:5032-5038

ADH5 alcohol dehydrogenase 5 (class III), chi polypeptide (2012) http://www.ncbi.nlm.nih.gov/sites/entrez?Db=gene&Cmd=ShowDetailView&TermToSearch=128#gene-top.

Prentki P, Krisch HM (1984) In vitro insertional mutagenesis with a selectable DNA fragment. Gene 29 (3):303-313.

Steinhauser D, Fernie AR, Araújo WL (2012) Unusual cyanobacterial TCA cycles: not broken just different. Trends in Plant Science 17 (9):503-509

Takemura T, Akiyama K, Umeno N, Tamai Y, Ohta H, Nakamura K (2009) Asymmetric reduction of a ketone by knockout mutants of a cyanobacterium. Journal of Molecular Catalysis B: Enzymatic 60 (1–2):93-95.

Vidal R, López-Maury L, Guerrero MG, Florencio FJ (2009) Characterization of an Alcohol Dehydrogenase from the Cyanobacterium *Synechocystis* sp. Strain PCC 6803 That Responds to Environmental Stress Conditions via the Hik34-Rre1 Two-Component System. Journal of Bacteriology 191 (13):4383-4391.

Yamamoto T, Chongsuksantikul A, Asami K, Ohtaguchi K (2012) Improvement of anaerobic production of hydrogen in the dark by genetic mutation strains of *Synechocystis* sp. strain PCC 6803. Journal of Biochemical Technology 4 (2): 600-603

Yanisch-Perron C, Vieira J, Messing J (1985) Improved M13 phage cloning vectors and host strains: nucleotide sequences of the M13mpl8 and pUC19 vectors. Gene 33 (1):103-119

Yu Y, You L, Liu D, Hollinshead W, Tang YJ, Zhang F (2013) Development of *Synechocystis* sp. PCC 6803 as a phototrophic cell factory. Marine drugs 11 (8):2894-2916

Chapter 5

Fructose Effects on Hydrogen Production

5.1 Problem Definition and General Consideration

The study in chapter 2 has concluded that, among monosaccharides, glucose and fructose largely promote dark anaerobic H_2 production in a glucose tolerant mutant of *Synechocystis* sp. strain (GT strain) cells in HEPES buffer solution. Fructose, along with glucose and sucrose, are three key sugars for photolithotrophs. No improvement in H_2 production is observed in sucrose. Attainable level of the amount of H_2 per cell suspended buffer solution ($y_{H2,f}$) with fructose and that with glucose are comparable. H_2 production in glucose is accompanied by high consumption of exogenous glucose and high production of dry cell weight, lactate and acetate, while that in fructose is accompanied by low consumption of fructose and low production of dry cell weight, lactate and acetate. Therefore dark anaerobic H_2 production in buffer solution with fructose is further studied in this chapter.

Figure 5.1 shows the calculated time courses of the number of moles of H_2 per culture volume in dark anaerobic incubation of GT strain (solid line), Δddh mutant (broken line) and ΔadhΔddh mutant (long dashed short dashed line) in HEPES buffer solution and GT strain in 28 μmol mL^{-1} fructose in HEPES buffer solution. Inoculum cells are assumed to be obtained from late logarithmic growth phase when X is 2.58 mg mL^{-1}. Initial H_2 production rate of Δddh mutant or ΔadhΔddh mutant is higher than that of GT strain, hence genetic modification is confirmed to be effective to shift the initial content of NAD(P)H. The attainable level of y_{H2} ($y_{H2,f}$) of Δddh mutant is comparable with that of GT strain and that of ΔadhΔddh mutant is lower than that of GT strain or Δddh mutant. The genetic mutation from GT strain to ΔadhΔddh mutant is so sensitive to result $y_{H2,f}$. Curves of GT strain shows that addition of fructose is extremely effective to increase both initial H_2 production rate and attainable level of y_{H2}. The X versus time data in dark anaerobic incubation in chapters 2-4 suggest that H_2 production without cell death results high attainable level in y_{H2}. The data of chapter 3 shows that inoculum from logarithmic growth phase performs H_2 production with extremely low specific death rate (K_d). The study of chapter 4 has shown that the uptake of fructose isomer glucose by Δddh mutant and ΔadhΔddh mutant is blocked. The possibility exists that H_2

production of GT strain, Δddh mutant and ΔadhΔddh mutant, from logarithmic growth phase, in the presence of fructose seems to be a good possibility to activate H_2 production.

Fructose is an extremely soluble ketohexose that exists in a cyclized form of hemiacetal fructofuranose in solution. The fructofuranose has the anomeric carbon directly bonding to two oxygen atoms in the forms of a free OH group and an OR group. This anomeric carbon is susceptible to be oxidized via a redox reaction, hence ketohexose fructose is classified into a reducing sugar. If H_2 production on NiFe-hydrogenase is the cellular response against redox unbalance, then a possibility exists that the presence of fructose in cellular environment affects H_2 production

Bidirectional NiFe-hydrogenase activity that, under the absence of oxygen and highly reductive condition, serves to provide a terminal electron sink and reduce excess protons and NAD(P)H by evolving H_2 (Ducat et al. 2011). Stresses caused by the nitrate or sulfate limitations are effective to trigger H_2 production in a unicellular non-nitrogen-fixing cyanobacterium *Synechocystis* sp. strain PCC 6803 (Antal et al. 2006; Yamamoto et al. 2012). Eliminating nitrate from medium constituents is established to be a key for dark H_2 production, which is supported by an observation that a deletion mutant of the genes encoding both nitrate reductase and nitrite reductase significantly enhanced production (Baebprasert et al. 2011). Inhibitor addition to block of a certain electron sink pathway that is competitive to NiFe-hydrogenase is applied to increase H_2 production (Burrows et al. 2011).

Experimental observation in chapter 2 showed fructose consumption by GT strain (Fig.2.6). Exogenous glucose and fructose are known to be transported through facilitated diffusion *via* a glucose-fructose permease (the product of the *glc*P transport gene) (Joset et al. 1988). Previous works show that *Synechocystis* sp. strain PCC6714 transports glucose via permease with K_m of about 0.4 $\mu mol \cdot mL^{-1}$ (Beauclerk and Smith 1978) and fructose inhibits the uptake of glucose slightly (Flores and Schmetterer 1986). The K_m for fructose consumption of *Anabaena variabilis* is reported to be approximately 0.16 $\mu mol \cdot mL^{-1}$ that does not change in the light versus dark (Haury and Spiller 1981). Although sensing mechanism in GT strain for glucose is not defined, growth arrested cells are known to respond to glucose at the level of post-translational modifications or modulation of enzyme activities and phosphorylate the transported glucose to glucose 6-phosphate on glucokinase (Kahlon et al. 2006). Glucose 6-phosohate is further decomposed mainly in the oxidative pentose

phosphate (OPP) pathway. Fructose inhibits photoautotrophic growth of a culture of *Synechocystis* sp. strain PCC 6714 but, cannot result in a toxic effect on the chemoheterotrophic growth of the strain on 5 μmol·mL^{-1} glucose in the light (Kahlon et al. 2006). Genome sequence of *Synechocystis* sp. strain PCC 6803 represents a potential-coding regions for fructokinase (Qry match, 18.4%) in ORF slr1448 (Kaneko et al. 1996). Glycogen accumulation in a heterocystous cyanobacterium *Anabaena azollae* is reported to be increased by fructose (Rozen et al. 1986). A recent work on higher plant *Arabidopsis thaliana* suggests that fructose is a signaling molecule regulating growth and development and that fructokinase plays a putative regulatory role in fructose signaling (Cho and Yoo 2011). However fructose signal transaction pathway is yet unsolved.

Thus, the primary purposes of the study in this chapter were (1) to elucidate the effect of fructose on dark anaerobic H_2 production in GT strain in HEPES buffer solution, (2) to compare the dark anaerobic H_2 production in GT strain, Δddh mutant and ΔadhΔddh mutant in HEPES buffer solution with or without 50 μmol mL^{-1} fructose, and (3) to perform a conceptual design of bioreactor to produce biofuel H_2.

5.2 Materials and methods

(a) Strains

Strains utilized in experiments are the glucose tolerant of *Synechocystis* sp. strain (GT strain) and its derivatives defective of genes coding for D-lactate dehydrogenase genes (Δddh mutant) and defective of genes coding for both alcohol dehydrogenase genes and D-lactate dehydrogenase genes (ΔadhΔddh mutant).

(b) Cultivation and fermentation techniques

For studying the effect of initial fructose concentration on dark anaerobic H_2 production, cells of GT strain were utilized. For cell preparation, cells of GT strain were grown photoautotrophically for 3 d in BG-11 medium (initial pH 7.8) at 34°C, aerated by 6 % CO_2 in air and illuminated by fluorescent lamps at 100 μmol photon s^{-1} m^{-2} photosynthetic photon flux density (PPFD). Utilizing the culture with OD_{730} at 3 (*X*, 1.11 mg mL^{-1}), cells at the end of logarithmic growth were collected by centrifugation at 1000 g and 25°C for 10 min. The cell pellets were first washed by 50 μmol mL^{-}

[1] HEPES buffer plus 18 μmol mL^{-1} $NaNO_3$ and then washed again by pure HEPES (4-(2-hydroxyethyl)-1-piperazineethanesulfonic acid) buffer (pH 7.8) solution. The washed cells were collected by centrifugation.

In the second stage of indirect biophotolysis, cells were re-suspended and incubated in 10 mL of 50 μmol mL^{-1} HEPES buffer (pH 7.8) solutions without or with 18 μmol mL^{-1} $NaNO_3$, without or with 5, 25, 50, 60, 70 and 110 μmol mL^{-1} fructose and with 18 μmol mL^{-1} $NaNO_3$ plus 50 μmol mL^{-1} fructose in 32 mL glass test tubes with butyl rubber caps. The initial dry cell weight concentration was set at 2 mg mL^{-1} (OD_{730}=5.4) and cell suspension was purged with nitrogen gas for a few minutes to remove oxygen molecules. Incubation was carried out under the dark anaerobic conditions with shaking at 145 rpm in a reciprocating shaker. The reciprocating distance was 40 mm and the horizontal angle was about 30°. Dark incubation in this study was slightly modified with a daily pulse of dim light. All experiments were carried out in duplicate.

For studying the effect of fructose on dark anaerobic H_2 production of GT strain, Δddh mutant and ΔadhΔddh mutant, cells of GT strain, Δddh mutant and ΔadhΔddh mutant were grown photoautotrophically on antibiotic-free BG-11 medium (initial pH 7.8) that was aerated by 6% carbon dioxide in air in clear Pyrex glass test tube (TE-32, AGC TECHNO GLASS Co. Ltd.) at 34 ºC in water bath, surface of which was exposed to fluorescent lamps with a PPFD of 100 μmol-photons m^{-2} s^{-1}. Growth was monitored by measuring OD_{730} of cell suspension. Cultures of OD_{730} at 3 (X, 1.11 mg mL^{-1}) were centrifuged at 25 ºC, 3000 rpm for 10 min. The cell pellets were washed, re-suspended and incubated in 10 mL of 50 μmol mL^{-1} HEPES buffer (pH 7.8) solution with 50 μmol mL^{-1} fructose in 32 mL glass test tube with butyl rubber cap. The initial dry cell mass weight concentration was set at 2 mg mL^{-1}. Other fermentation condition was same as described above.

(c) Analysis

The number of moles per culture volume of H_2 (y_{H2}), fructose (c_S), endogenous glucose ($m_G X$), lactate (c_L) and acetate (c_A) and the dry cell weight per culture volume (X) were analyzed as described in the section 2.2.

5.3 Results and discussion

(a) Effect of initial concentration of fructose on dark anaerobic H_2 production in GT strain

It has been shown that dark anaerobic H_2 production in unicellular cyanobacterium is elevated by fructose (chapter 2) and blocked by elimination of nitrate from the medium (Ohtaguchi et., 1995) or by disruption of genes coding for nitrate reductase (Baebprasert et al. 2011) which is a major electron consumption. This pathway competes NAD(P)H with NiFe-hydrogenase in dark anaerobic condition. The first experiment in this chapter was performed with GT strain to compare effect of nitrate and fructose towards H_2 production by cells.

Figure 5.2 compares the initial H_2 production rates of dark anaerobically incubated cells of GT strain in HEPES buffer solutions (a) without nitrate and fructose, (b) without nitrate and with 50 $\mu mol \cdot mL^{-1}$ fructose, (c) with 18 $\mu mol \cdot mL^{-1}$ $NaNO_3$ and without fructose, and (d) with 50 $\mu mol \cdot mL^{-1}$ fructose and 18 $\mu mol \cdot mL^{-1}$ $NaNO_3$. The H_2 production data of runs without fructose support the reported conclusion that H_2 production is inhibited by nitrate because of the NAD(P)H competition between nitrate assimilation and H_2 production (Baebprasert et al. 2011). The result of run without nitrate shows that fructose elevates dark anaerobic H_2 productions in GT strain. The initial H_2 production rate in run with fructose is 3.5 times that without fructose. It is especially noteworthy that addition of fructose on nitrate solution results in H_2 production. The positive effect of fructose on the dark anaerobic H_2 production in the presence of nitrate is found to overcome the inhibitory effect of nitrate. This observation appears to be the first description on the dark anaerobic H2 production in GT strain in the presence of nitrate. Fructose appears to brock intracellularly the consumption of NAD(P)H by nitrate reductase.

Figure 5.3 shows the time courses of (a) the number of moles of H_2 per culture volume (y_{H2}) , (b) the concentration of fructose (c_S), (c) the number of moles of endogenous glucose per culture volume ($m_G X$), (d) the concentration of dry cell weight (X), (e) the concentration of lactate (c_L) and (f) the concentration of acetate (c_A), measured in runs, performed by incubating GT strain in nitrate-free HEPES buffer solutions without fructose and with 5, 25, 50, 60, and 70 $\mu mol \cdot mL^{-1}$ fructose (c_{S0}) under the dark anaerobic condition. To elucidate relations of H_2 production to fructose utilization, acid evolution, endogenous glycogen metabolism and dry cell weight production, culture variables concerning these mechanisms are totally monitored.

Table 5.1 summarizing the effect of change in initial fructose concentration on culture characteristic variables observed in runs without and with 5, 25, 50, 60 and 70 μmol·mL^{-1} fructose. Culture parameters states at 0 h and 120 h are shown by subscript 0 and 1 respectively.

Fig.5.3 (a) shows that H_2 production starts right after inoculation, irrespective of varying c_{S0}. The y_{H2} versus time data of run without fructose are interpreted by Eq.(2.18) as described in chapters 2-4. The data on solid line calculated by Eq.(2.18) with parameters $r_{H2,0}$, 0.0284 μmol mL^{-1} h^{-1}; and k, 0.0136 h^{-1} fits well observed values. The attainable level in y_{H2} ($y_{H2,f}$=$r_{H2,0}$/k) is calculated as 2.09 μmol·mL^{-1}. The observed y_{H2} at 120 h ($y_{H2,1}$) of run without fructose is 1.7 μmol·mL^{-1}. The $y_{H2,f}$ of this run is 91.6% of that shown in Fig.5.1. Kinetic behavior of H_2 production shows remarkable difference between cells from logarithmic growth phase and late-logarithmic growth phase. This drop is due to the inoculum growth phase shift from late-logarithmic growth phase to logarithmic growth phase. Fructose effect is found to be stressed in logarithmically growing cells.

Fructose is found to elevate the number of moles of H_2 per culture volume at 120 h by increasing the initial H_2 production rate, and stabilizing it after 72 h. Of special interest is the stable and highest production of H_2 when initial fructose concentration (c_{S0}) is between 50 and 83 μmol·mL^{-1}.The r_{H2} is not time-varied and same as the $r_{H2,0}$ at 0.0927 μmol·mL^{-1}h^{-1} .The y_{H2} versus time data for runs with 50, 60 and 70 μmol·mL^{-1} fructose are fitted by Eq.(2.21), and the fitted relation is given by:

$$y_{H2} = r_{H2,0}t = 0.0927t \qquad (5.1).$$

NiFe-hydrogenase mediated H_2 production at high fructose concentration is found to be interpreted by zero-th order kinetics. The number of moles of H_2 per culture volume at 120 h ($y_{H2,1}$) of run with 50-70 μmol·mL^{-1} fructose is 11.1 μmol·mL^{-1} that is 6.54 times that without fructose. The additional experiments showed that the range of fructose that supports Eq.(5.1) is from 50 to 83 μmol mL^{-1}. Such linear relation is also seen in run with 25 μmol mL^{-1} fructose. The r_{H2} (=$r_{H2,0}$) of this run is 0.059 μmol mL^{-1}h^{-1}. The upper limit of c_{S0} for the stable H_2 production was observed at 110 μmol·mL^{-1}.

Different from runs with 25-100 μmol mL^{-1} fructose, the y_{H2} versus time data for runs with c_{S0} at 5 μmol·mL^{-1} in the first about 72 h represent the time courses similar to those shown in chapters 2

and 3. The result of run with 5 μmol·mL^{-1} fructose shows that the y_{H2} is slightly higher than that of run without fructose in the first about 72 h. The H_2 production curve in the first about 72 h is well fitted by Eq.(2.18) with parameters $r_{H2,0}$, 0.0422 μmol mL^{-1} h^{-1}; and k, 0.0202 h^{-1}. Of additional interest in Fig.5.3 is the acceleration of H_2 production at about 72 h. If r_{H2} is constant at $r_{H2,SHT}$ after this shift and t_{SHT} is the time of acceleration, then H_2 production of this run is interpreted by:

$$y_{H2} = \frac{r_{H2,0}}{k}\{1-\exp(-kt)\} \qquad \text{for } t \le t_{SHT}$$

$$y_{H2} = r_{H2,SHT}(t-t_{SHT}) + [\frac{r_{H2,0}}{k}\{1-\exp(-kt_{SHT})\}] \quad \text{for } t \ge t_{SHT} \qquad (5.2)$$

Fitting the data of this run results in that parameters $r_{H2,SHT}$ and t_{SHT} are 1.64 μmol mL^{-1}h^{-1} and 76.6 h, respectively. H_2 production rate of runs with 5 μmol·mL^{-1} fructose became almost similar to that of runs with 50-70 μmol·mL^{-1} fructose.

The result of run with 25 μmol·mL^{-1} fructose shows that effect of fructose is obvious right after inoculation. After about 72 h, r_{H2} of this run increases with time. The y_{H2} versus time of this run is interpreted by:

$$y_{H2} = r_{H2,0}t \qquad \text{for } t \le t_{SHT}$$

$$y_{H2} = r_{H2,SHT}(t-t_{SHT}) + r_{H2,0}t_{SHT} \qquad \text{for } t \ge t_{SHT} \qquad (5.3)$$

Fitting the data of this run results that parameters $r_{H2,SHT}$ and t_{SHT} are 5.17 μmol mL^{-1}h^{-1} and 81.9 h, respectively, since $r_{H2,0}$ is 0.0631 μmol mL^{-1}h^{-1}.

The initial H_2 production rates ($r_{H2,0}$) for runs with c_{S0} at 0, 5 and 25 μmol·mL^{-1} are 0.0285, 0.0422 and 0.059 μmol·mL^{-1} h, respectively. The $r_{H2,0}$ for runs with c_{S0} at no less than 50 μmol·mL^{-1} is constant at 0.0927 μmol·mL^{-1}h^{-1} (Table 5.1) that is 3.25-fold increase from run without fructose.

Figure 5.4 shows the effect of c_{S0} on the initial specific H_2 production rate $q_{H2,0}$(=$r_{H2,0}/X_0$), the initial specific consumption rate of fructose (q_{S0}) and the number of moles of H_2 per culture volume at 120h ($y_{H2,1}$). Fructose increased the q_{S0} and the $y_{H2,1}$. Effect of fructose on $y_{H2,1}$ is associated with that of q_{S0}. Linear relation is seen between $q_{H2,0}$ and c_{S0} when c_{S0} is between 5 and 50 μmol mL^{-1}.

The $q_{H2,0}$ and $y_{H2,1}$ are almost constant at 0.0488 μmol $mg^{-1}h^{-1}$ and 10.4 μmol mL^{-1}, respectively, when c_{S0} is no less than 50 μmol mL^{-1}, Fructose is found to increase initial cellular content of NAD(P)H.

Eqs.(5.2) and (5.3) and observations in chapters 2-4 suggests that H_2 production in GT strain, Δddh mutant and ΔadhΔddh mutant is a response to the intermittent accumulation of NAD(P)H. First intermittent accumulation occurs when photoautotrophically growing cells on BG-11 medium in the presence of O_2 is exposed to dark anaerobic HEPES buffer solution with or without monosaccharides. Cells that face the high oxidative stress instantaneously accumulate NAD(P)H to load a subsequent stress to inoculum cells. NiFe-hydrogenase works as a discharge mechanism of NAD(P)H and H_2 is generated. This process appears to be an action to keep a redox homeostasis. Second intermittent accumulation occurs when generated $NAD(P)^+$ by H_2 production reaction exceeds the limit for cell survival. Metabolic network for redox homeostasis after first intermittent NAD(P)H accumulation is reformulated at around 72-96 h. This event accelerates H_2 production. After this event, H_2 production at high rate proceeds to keep second redox homeostasis. When c_{S0} is no less than 5 μmol mL^{-1}, H_2 production proceeds on the kinetics of Eq.(5.1) even at 120 h, hence attainable level ($y_{H2,f}$) is not predicted from experimental data. The relative values $y_{H2,f}$* and $y_{H2,f}^+$ cannot be discussed in this chapter.

Figure 5.3 (b) shows that fructose consumption is not high as glucose consumption shown in Fig.4.8, however, small amount of fructose is assimilated from 0 to 24 h and after 96 h by GT strain when c_{S0} is between 5 and 50 μmol mL^{-1} and after 48 h when c_{S0} is 60 μmol mL^{-1}. In Fig.5.4, initial specific fructose uptake rate (q_{S0}) is plotted against c_{S0}. The q_{S0} is zero at low fructose concentration (c_{S0}<5) and high fructose concentration (50< c_{S0}) but linearly increase with c_{S0} when c_{S0} is between 5 and 50 μmol mL^{-1}.The K_m cannot be evaluated from this curve, however, this curve suggests that it should be no less than 5 μmol mL^{-1}. Low affinity of fructose to fructokinase in our experiment appears to be caused by limitation of ATP that is imperative for activation of fructokinase, since HEPES buffer solution lacks any phosphate ions.

Even though initial rate q_{S0} is small, curves in Fig.5.2(b) clearly shows the decrease in exogenous fructose concentration in 120 h reaction, except for run with 70 μmol mL^{-1} fructose, which shows no consumption of fructose. The amount of assimilated fructose ($-\Delta c_S=c_{S0}-c_{S1}$) is plotted against c_{S0} in Figure 5.4. When fructose concentration increases, consumption of fructose

increases except for c_{S0} at 70 μmol mL^{-1}. Result of run with 25 μmol mL^{-1} fructose also deviates from the linear line.

Figure 5.3 (c) shows that, in the presence of fructose, the amount of endogenous glucose per culture volume ($m_G X$) increased in the first 24 h, decreased drastically from 24 to 48 h, and then decreased with very small rate or kept constant after 48 h. The $m_G X$ in run with glucose showed the increase in $m_G X$ for 72 h (Fig.4.8(c)), however, Fig.5.3(c) shows it for only 24 h. The $m_G X$ of inoculum cells was fixed at 0.16 μmol·mL^{-1} by collecting the cells from the photoautotrophic culture of OD_{730} at 3. The $m_G X$ for run with c_{S0} at 0, 5, 25, 50, 60 and 70 μmol mL^{-1} increased right after dark incubation, reached the maximum value $(m_G X)_{max}$ of 0.22, 0.24, 0.27, 0.32, 0.36 and 0.33 μmol·mL^{-1} at 24 h in run with c_{S0} at 0, 5, 25, 50, 60 and 70 μmol mL^{-1}, respectively, rapidly decreased from 24 to 48 h, and then approached to the stable level after 48 h. The $m_G X$ at 120 h $(m_G X)_1$ for runs with c_{S0} at 0, 5, 25, 50, 60 and 70 μmol mL^{-1} are 0.06, 0.09, 0.15, 0.17, 0.19 and 0.18 μmol mL^{-1}, respectively. The $(m_G X)_{max}$ increases 1.64-fold from run without fructose by adding 60 μmol·mL^{-1} fructose. For run without fructose, it is difficult to consider any carbon source for this glycogen synthesis other than endogenous carbonaceous compounds such as amino acids in protein, fatty acids in membrane lipid and derivatives of poly-β-hydroxybutyrate (PHB). Turnover of cell constituting materials is known to activate many NAD(P)H-generating enzymes.

Glycogen contents in terms of endogenous glucose are drastically decomposed between 24 and 48 h. Of special interest is that the amount of this drop $(=(m_G X)_{max} - (m_G X)_1)$ is unrelated to initial fructose concentration, and is about 0.16 ± 0.04 μmol mL^{-1}. Glycolysis is found to be independent from the presence of exogenous fructose. When the degradable glycogen is assimilated, glycolysis is terminated. The amount of endogenous glucose per culture volume is found to be always higher in the presence of fructose than in the absence of fructose.

Glycogen decomposition is known to generate NADH. The H_2 production rate between 24 h and 48 h in run with 25 μmol·mL^{-1} fructose is 0.0604 μmol·mL^{-1}h^{-1} that is 2.39 times that in run without fructose, hence the H_2 production rate after 24 h is found to be independent from the amount of NADH generated by glycolysis. Considering that the amount of endogenous glucose per culture volume is increased by increasing initial fructose concentration and that the amount of assimilated endogenous glucose per culture volume after 24 h is not affected by initial fructose

concentration, it is found that the amount of endogenous glucose per culture volume after 24 h is always higher in run with fructose than in run without fructose.

The time course data of dry cell weight concentration (X) versus time is shown in Figure 5.3(d). Observations of run without or with 25 μmol L^{-1} fructose show that X in run without fructose decreases slightly with time, whereas it in run with fructose slightly increases in the first 24 h and in the period between 72 and 120 h.

In **Figure 5.5**, the amount of increase in dry cell weight concentration ($(\Delta X)_1=X_1-X_0$) is plotted against c_{S0}. The increase in $(\Delta X)_1$ is associated with the increase in $(-\Delta c_S)_1$, which is observed at c_{S0} from 5 to 60 μmol L^{-1}. There are remarkably few data available in previous works regarding the heterotrophic growth of GT strain on fructose, the relation between $(-\Delta c_S)_1$ and (ΔX) in Fig.5.5 suggests the high possibility of a limited heterotrophic growth of GT strain on fructose under the dark anaerobic condition. This research is carried out to find the condition to elevate H_2 production, hence cells were incubated not in BG-11 medium but in HEPES buffer solution that contained only HEPES and KOH for pH adjustment. A cessation of fructose assimilation is seen between 24 and 72 h. The unreacted fructose concentration in this period is 23.9±0.56 μmol·mL^{-1}. Combination of the curves for fructose concentration and dry cell weight concentration versus time in Figure 5.3b eminently demonstrates the limited heterotrophic growth on fructose in the first 24 h and in the period between 72 and 120 h. This discontinuous heterotrophic growth on fructose suggests that GT strain appear to respond on cell cycle events to the initial shift of cellular environment to dark anaerobic condition with fructose. The yield of endogenous glucose from fructose ($=r_{G0}/(-r_{S0})$) is calculated as 0.0279 ± 0.0146, which is quite low. Fructose is not mainly turned to endogenous glucose.

Figure 5.6 shows the relation between the number of moles of H_2 per culture volume at 120 h ($y_{H2,1}$) and the number of moles of endogenous glucose per culture volume at 120 h ($(m_G X)_1$). There seems to be a linear correlation, defined by Eq.(2.40). Best fit to the data results that parameters are k_5, 152 μmol $^{-0.52}$$mL^{0.52}$;and k_6, 1.52. The sensitivity of $y_{H2,1}$ to $(m_G X)_1$ of run with cells of GT strain from logarithmic growth phase increased 4.08-fold over that from late-logarithmic growth phase. For inoculum from logarithmic growth, fructose is found to elevate the amount of H_2 per culture volume. To keep high level in the amount of endogenous glucose per culture volume appears to be of prime importance to result in high H_2 production in GT strain.

In the absence of fructose, lactate concentration (c_L) was extremely low and reached only 0.2 μmol·mL^{-1} at 120 h, whereas, in the presence of fructose, lactate synthesis in GT strain continuously occurred during 120 h. The lactate production rate after 48 h was similar to the H_2 production rate. **Figure 5.7** relates y_{H2} and c_L in runs with GT strain in HEPES buffer solution with or without fructose. The level of c_L is seen to be the same order of magnitude of y_{H2}. Increase in c_L in the presence of fructose suggests that exogenous fructose is an additional carbon source for lactate production. The amount of intracellular lactate was not detectable level. There is a drastic change in the slope of the curve when c_L approaches to 1.8 μmol mL^{-1}. The drastic change in NAD(H)P at t_{SHT} corresponds to the point where slope of c_L versus y_{H2} curve data occurs.

Different from lactate, acetate concentration (c_A) rose to a maximum level at 72 h and then decreased. The highest c_A is 0.2 μmol·mL^{-1}. The activated production of H_2 in the presence of 50-83 μmol·mL^{-1} fructose is found to be accompanied by the elevated assimilation of fructose (Figure 5.3b), the elevated initial synthesis of glycogen (Figure 5.3c), followed by the assimilation of endogenous glucose after 24 h and the elevated production of lactate (Figure 5.3e). Because of the insufficiency of required elements for normal cell growth, a small portion of assimilated fructose is directed to cell growth (Figure 5.3d). When cells are exposed to fructose in buffer solution, the initial glycogen synthesis is activated, while the subsequent glycogen decomposition was not affected by initial concentration of fructose (Figure 5.3c).

The assimilation of endogenous glucose is obvious between 24 h and 48 h, hence the instantaneous fractional yield of H_2 on endogenous glucose $Y_{H2/G}$ that is defined by the amount of H_2 produced per amount of endogenous glucose utilized in this period is evaluated and listed in Table 5.1.

Glucose 6-phosphate is an intermediate both in gluconeogenesis pathway and glycolysis pathway. If glucose 6-phosphate is catabolized in the oxidative pentose phosphate (OPP) pathway and if both NADPH and ATP are required in this pathway, theoretical conversion of 1 mole glucose 6-phosphate to 5/3 mole pyruvate is accompanied by the generation of 2 mole NADPH and 5/3 mole NADH. When 1 mole pyruvate is completely converted to 3 mole carbon dioxide, this reaction yields 4 mole NADH and 1 mole $FADH_2$. If all of NAD(P)H generated in these pathways are directed to NiFe-hydrogenase, potential yields of H_2 in the pathway from glucose 6-phosphate to pyruvate and from glucose 6-phosphae to carbon dioxide are estimated as 3.67 and 12, respectively.

The yield of H_2 for run without fructose in Table 5.1 is slightly lower than the theoretical yield from glucose 6-phosphate to pyruvate, and that for runs with 50-70 $\mu mol \cdot mL^{-1}$ fructose is much higher than the theoretical yield from glucose 6-phosphate to carbon dioxide. Our observation suggests that NAD(P)H for H_2 production are supplied not only from glycogen degradation but also from turnover of proteins, membrane lipid and PHB. This turnover appears to be accompanied by glycolysis. The observed lactate level was high at high initial fructose concentration. High concentration fructose appears to activate NiFe-hydrogenase and lactate dehydrogenase to discharge excess reductant generated in the incomplete tricarboxylic acid (TCA) cycle and in the pathways for turnover of above components. The positive effect of fructose on H_2 production in this result suggests that fructose transport through cellular membrane is of prime importance to elevate H_2 production.

Chapters 2 and 4 reported the elevation of dark anaerobic H_2 production in GT strain by adding glucose in HEPES buffer solution. H_2 production in cells under glucose fermentation is different from that in fructose fermentation because cells extensively utilize glucose for cell division and thus, more cell population results in more H_2 production. In fructose under dark anaerobic condition, cells utilize fructose for endogenous glucose buildup rather than limited cell growth. This endogenous glucose accumulation is followed by the endogenous glucose break down by glycolysis that triggers many intracellular associated turnover reactions against cell constituting components. Cells gain more electrons through glycolysis and associated turnover reactions. This is partially supported by the increase in lactate concentration in runs with fructose since lactate is one of key carbon terminal compounds. Since fructose inhibited photoheterotrophic growth, our observation suggests that fructose might suppress an important pathway or mechanism related to light mode of life. Interestingly, this growth inhibition was not observed under dark anaerobic mode of life. Suppression of specific mechanism by fructose might be a key for redirection of more electrons to H_2ase enzyme.

(b) Effect of 50 $\mu mol\ mL^{-1}$ fructose on dark anaerobic H_2 production in GT strain, Δddh mutant and ΔadhΔddh mutant

One of the primary objectives of the study in this chapter was to stabilize long-term H_2 production in genetically modified Δddh mutant and ΔadhΔddh mutant of glucose tolerant derivative of *Synechocystis* sp. strain PCC 6803 (GT strain) utilizing fructose. Experimental data

above show that fructose largely elevates the dark anaerobic H_2 production of GT strain cells from logarithmic growth phase and that optimum fructose concentration regarding H_2 production is 50 μmol mL^{-1}, and that, in the absence of fructose, the initial H_2 production rate of Δddh mutant prepared from late-logarithmic growth phase in photosynthesis is higher than that of GT strain. Dark anaerobic incubation of those cells in the presence of glucose also shows that the rate of H_2 production by Δddh mutant is higher than that of GT strain Therefore, a series of dark anaerobic H_2 production experiments were performed in which cells of Δddh mutant and ΔadhΔddh mutant from logarithmic growth phase were incubated in HEPES buffer solution without or with 50 μmol mL^{-1} fructose. **Figure 5.8** shows that H_2 production yield from endogenous glucose degradation is highest when initial fructose concentration is 60 μmol mL^{-1}.

Figure 5.9 shows the time courses of dark anaerobic H_2 production in GT strain, Δ*ddh* mutant and Δ*adh*Δ*ddh* mutant, from logarithmic growth phase, in HEPES buffer solution with or without 50 μmol mL^{-1} fructose. The amount of H_2 produced from unit volume of solution (y_{H2}), the amount of endogenous glucose in glycogen of a unit volume ($m_G X$), dry cell weight per solution volume (X), the concentrations of fructose, lactate and acetate were determined.

The curves of y_{H2} versus time in Figure 5.9(a) show that fructose increased initial H_2 production rate and stabilized and accelerated H_2 production rate after the initial stage. The initial H_2 production rates ($r_{H2,0}$) in GT strain, Δddh mutant and ΔadhΔddh mutant, which were 0.025, 0.015 and 0.020 μmol mL^{-1} h^{-1}, respectively, in the absence of fructose, were increased to 0.091, 0.109 and 0.129 μmol mL^{-1} h^{-1}, respectively, in the presence of fructose. Fructose is found to largely enhance H_2 production activity of NiFe-hydrogenase activity. The H_2 production in GT strain in fructose solution shown in Figure 5.9(a) is related by Eq.(2.21) and well fitted by Eq.(5.1).

The y_{H2} versus time data of run with Δddh mutant and ΔadhΔddh mutant in 50 μmol mL^{-1} fructose is similar to the result of run with GT strain in 25 μmol·mL^{-1} fructose that was well fitted by Eq.(5.3). Best fitting the data with Eq.(5.3) results the parameters $r_{H2,0}$, 0.104 μmol $mL^{-1}h^{-1}$; t_{SHT}, 86.8 h; and $r_{H2,SHT}$, 0.216 μmol $mL^{-1}h^{-1}$ for Δddh mutant, and $r_{H2,0}$, 0.123 μmol $mL^{-1}h^{-1}$; t_{SHT}, 68.2 h; and $r_{H2,SHT}$, 0.203 μmol $mL^{-1}h^{-1}$. Solid lines for calculated data of y_{H2} by Eq.(5.3) and those parameters show good fits to the observed variables. Results of t_{SHT} is so far suggested that shift of metabolic network occurs earlier when initial H_2 production rate is higher. The t_{SHT} of this work is from 68.2 to 86.8 h. In Fig.5.3, maximum initial H_2 production rate ($r_{H2,0}$) was 0.0927 μmol·$mL^{-1}h^{-1}$.

When ΔadhΔddh mutant mutant is incubated in 50 μmol mL^{-1} fructose, initial rate increased 1.33-fold over best run with GT strain in fructose. After second reformation of metabolic network for redox homeostasis at t_{SHT}, H_2 production rate shows 2.19-fold increase over the maximum $r_{H2,0}$ of Fig.5.3.

The relation between the initial specific H_2 production rate ($q_{H2,0}$) and initial fructose concentration (c_{S0}) of runs with GT strain, Δddh mutant and ΔadhΔddh mutant is shown in **Figure 5.10**. In the presence of 50 μmol mL^{-1} fructose, q_{S0} values of cells of GT strain, Δddh mutant and ΔadhΔddh mutant from logarithmic growth phase are 0.092, 0 and 0.031 μmol $mL^{-1}h^{-1}$. Similar to runs with Δddh mutant, from late-logarithmic growth phase, in HEPES buffer solution with glucose shown in chapter 4, initial uptake of fructose by Δddh mutant is blocked.

Figure 5.11 compares $(-\Delta c_S)_1$, $(\Delta X)_1$ of runs with GT strain, Δddh mutant and ΔadhΔddh mutant. Even though q_{S0} is zero in Δddh mutant and ΔadhΔddh mutant, fructose is eminently consumed by those mutants during 120 h incubation. The amount of consumed fructose by Δddh mutant and that by ΔadhΔddh mutant is comparable. The $(-\Delta c_S)_1$ appears to be defined by the activity of lactate dehydrogenase. The total amount of assimilated fructose by mutants is 1.64 times that of GT strain. The $(\Delta X)_1$ of GT strain and that of Δddh mutant is comparable, while that of ΔadhΔddh mutant is higher than that of GT strain and Δddh mutant. The NAD(P)H content in ΔadhΔddh mutant in fructose solution is so high that additional metabolism to discharge extra electrons for the reproduction of biomaterials appears to occur in ΔadhΔddh mutant.

Figure 5.12 shows a relation between $(m_G X)_1$ and y_{H1} in runs with GT strain in HEPES buffer solution with or without fructose. Straight broken lines in the graph show the relations of Eq.(2.40) for cells of GT strain from logarithmic growth phase and late-logarithmic growth phase. If plots of data for runs with .Δddh mutant and ΔadhΔddh mutant are also interpreted by Eq.(2.40), parameters are estimated as k_5, 7970; k_6, 3.66 for Δddh mutant and k_5, 8510; k_6, 3.45 for ΔadhΔddh mutant. Calculated results are shown by solid lines. Two solid lines are almost parallel. Sensitivity to fructose is found to be highest in ΔadhΔddh mutant, second highest in .Δddh mutant and lowest in GT strain. Sensitivity of H_2 production to the amount of endogenous glucose per culture volume of Δddh mutant and that of ΔadhΔddh mutant from logarithmic growth phase are found to be comparable, and are 2.27-2.41-folds higher than that of GT strain from logarithmic growth phase. It

is found that, in the presence of fructose, elimination of lactate dehydrogenase genes makes H_2 production ability of cells to be extremely sensitive to the variation in the amount of endogenous glucose. The $y_{H2,1}$ of run with ΔadhΔddh mutant is higher than that of Δddh mutant. Elimination of alcohol dehydrogenase genes appears to shift up the activity of NAD(P)H accumulation reactions that are not led by glycolysis.

The time course data of c_S in Figure 5.9(b) confirms the initial small uptake of fructose by GT strain (q_{S0}) which was shown in Fig.5.4, while no uptake by Δddh mutant and ΔadhΔddh mutant. The relation between c_{S0} and q_{S0} is shown in Fig.5.4. This observation is similar to the block of glucose uptake in Δddh mutant and ΔadhΔddh mutant shown in 4.8(b). Fructose appears to be consumed by cells of GT strain, Δddh mutant and ΔadhΔddh mutant for maintaining dry cell weight stability. The consumption of fructose by GT, Δddh and ΔadhΔddh strains were comparable. Consumption of fructose during 120 h was 5.1-8.4 μmol mL^{-1}. High H_2 production of those cells in the presence of fructose was not likely resulted from direct fructose consumption.

In Figure 5.9(c), the time courses of the amount per culture volume of glycogen in terms of endogenous glucose (m_G) were displayed. In the first 24 h of dark incubation in HEPES buffer solution without or with fructose, the m_G increased in GT strain, Δddh mutant and ΔadhΔddh mutant. This amount of endogenous glucose is corresponding to consumption of fructose. The peak value of m_G of runs with fructose is higher than that without fructose. The ΔadhΔddh mutant converted more fructose to endogenous glucose than GT strain and Δddh mutant. The glycogen content dropped during dark anaerobic fermentation. The highest drop in $m_G X$ from 24 h to 120 h was 0.183 μmol mL^{-1} that was observed in run with ΔadhΔddh mutant in fructose solution. H_2 generated in this run is 25.5 times that estimated from the theoretical yield of NAD(P)H in glycolysis. Cells used fructose for gluconeogenesis in the first 24 h then for glycolysis from glycogen after 24 h. At the end of fermentation, all strains had the same level of glycogen content.

In Figure 5.9(d), the time courses of the dry cell weight concentration of cyanobacterium cells (X) were illustrated. The dry cell weight concentration of GT strain, Δddh mutant and ΔadhΔddh mutant slowly decreased with time during 120 h in the absence of fructose. The aqueous solution for cell suspension was consisted of milliQ grade water and HEPES-KOH for pH buffering. Nitrate was totally removed from the system. The buffer solution is confirmed to be insufficient to support cell viability of GT strain, Δddh mutant and ΔadhΔddh mutant. In the presence of fructose, the X of

GT strain increased in the first 24 h, was constant between 48 h and 72 h and increased again after 72 h, the *X* of Δddh mutant was constant in the first 48 h, increased between 48 h and 72 h, decreased between 72 h and 96 h and increased after 96 h, and the *X* of ΔadhΔddh mutant was constant for the first 72 h and increased after 72 h. The dry cell weight concentrations of GT strain, Δddh mutant and ΔadhΔddh mutant at 120 h were higher than the initial concentrations. Curves for runs with fructose in Fig. 5.9 (c) and (d) show that GT strain, Δddh mutant and Δ*adh*Δ*ddh* mutant are capable of limited heterotrophic growth on fructose in HEPES buffer solution. In the presence of fructose, the *X* at 120 h was highest in runs with GT strain and Δddh mutant and lowest that with ΔadhΔddh mutant. It is observed that growth period of Δddh mutant is later than that of GT strain, and that of ΔadhΔdh mutant is later than that of Δddh mutant. Instability of dry cell weight concentration in dark anaerobic nitrate-free HEPES buffer solution was suppressed by fructose. This result shows that fructose supports cell viability in the dark anaerobic condition.

The total increase in dry cell weight concentration $(\Delta X)_1$ is plotted in Fig.5.11. The increase in $(\Delta X)_1$ by genetic modification is found to be accompanied by the increase in $(-\Delta c_S)_1$. This plot support above view that GT strain, Δddh mutant and ΔadhΔddh mutant can utilize fructose and represent limited heterotrophic growth.

In Figure 5.9(e), the time courses of lactate concentration (c_L) are shown. The production of lactate by GT strain in the presence of fructose is extremely high. Lactate production of GT strain in the presence of fructose was activated at 72 h. At 120 h, lactate concentration of run with GT strain, which was 0.204 μmol mL^{-1} in buffer solution, increased to 9.02 μmol mL^{-1} in the presence of fructose. Photosynthetic growth for cell preparation and dark anaerobic incubation were performed in the absence of antibiotics, hence the observation of trace amount lactate in runs with Δ*ddh* mutant and Δ*adh*Δ*ddh* mutant shows the drop of phenotype of lactate dehydrogenase deficiency.

Figure 5.13 is a plot showing a relation between y_{H2} and c_L in runs with GT strain, Δ*ddh* mutant and ΔadhΔddh mutant in HEPES buffer solution with or without fructose. Since lactate dehydrogenase activity is absent in Δddh mutant and ΔadhΔddh mutant, the c_L of mutants are zero even though the sample solution contains extremely low population of phenotype deficient strain. Among the plotted data, only those for GT strain in HEPES buffer solution with 50 μmol mL^{-1} fructose shows a meaningful relation between c_L and y_{H2}, which confirms the relation in Figure 5.7.

In Figure 5.9(f), the time courses of acetate concentration (c_A) were plotted. Acetate concentrations of runs with fructose were higher than those without fructose, and increased drastically during 48-72 h. In the presence of fructose, acetate concentration was highest in GT strain, second highest in Δddh mutant and lowest in ΔadhΔddh mutant. Acetate concentrations were highest during 48-72 h then the concentration dropped. The peaks of acetate concentration in runs with buffer solutions were 0.062, 0.162, and 0 μmol mL^{-1} for GT strain, Δddh mutant and ΔadhΔddh mutant, respectively, and those with buffer solutions with fructose were 1.21, 0.847 and 0.394 μmol mL^{-1} for them, respectively. The concentration of acetate after 72 h was extremely low. The consumption of acetate is highest in run with GT strain, second highest in run with Δddh mutant and lowest in run with ΔadhΔddh mutant. This order is reverse of that of H_2 production, while close to that of dry cell weight production. It suggests that acetate consumption after the peak seems related to late cell growth

Ethanol concentrations in runs without or with fructose were not at detectable level. Our previous report shows the ethanol production of GT strain, Δ*ddh* mutant and Δ*adh*Δ*ddh* mutant are 0.70, 1.01 and 0.47 μmol mL^{-1}, respectively, in the presence of glucose after 96 h. hence fructose fermentation of above strains appears to be different from glucose fermentation.

High production of H_2, endogenous glucose and acetate were observed if fructose was present. This observation raised very interesting points concerning participation of fructose in NAD(P)H production or redirection of NAD(P)H in the dark. The slight higher fructose consumption by mutants could be the reason that mutants took long time for cell growth therefore cell kept utilizing more carbon source. However at 120 h, difference of final dry cell weight concentrations among three strains was not large. Mutants consumed more fructose while produced less acid than GT strain. More trials are required to find the products from acetate.

Cellular state variables of GT strain, Δddh mutant and ΔadhΔddh mutant are summarized in Table 5.2, The initial H_2 production rates of Δddh mutant and ΔadhΔddh mutant increased 3-fold to 7-fold over GT strain when fructose was present. H_2 production from mutant lacking both *ddh* and *adh* genes yielded extremely high amount of H_2.

In the presence of fructose, the amount per culture volume of H_2 produced from GT strain was extremely high when logarithmic growth phase cells were incubated in dark anaerobic condition. Quite important phenomenon found from this observation is that cells prepared from logarithmic

growth phase are capable of expressing a stable high reductive state under the cellular exposure to fructose.

The deletion of the genes coding for competitive enzymes of NiFe-hydrogenase was effective for increasing the initial H_2 production rate of cells prepared from late-logarithmic growth phase. If fructose is present, mutant cells prepared not from late-logarithmic growth phase but from logarithmic growth phase produce highest amount of H_2. The selection of growth phase affects H_2 production in mutants greatly. The presence of fructose significantly activates H_2 production in mutants.

Figure 5.14 shows an effect of genetic modification upon yield of H_2 on endogenous glucose for glycolysis ($Y_{H2/G}$). In the absence of fructose, the highest $Y_{H2/G}$ of 6.63 is seen in GT strain and the lowest $Y_{H2/G}$ of 5.81 is seen in Δddh mutant. Contrary to the expectation, elimination of lactate dehydrogenase results in the decrease in the yield of H_2 from endogenous glucose. The order of magnitude of $Y_{H2/G}$ is close to the theoretical yield. In the presence of fructose, $Y_{H2/G}$ values are extremely high in GT strain, Δddh mutant and ΔadhΔddh mutant. The NAD(P)H for NiFe-hydrogenase in the presence of fructose is found to be supplied mainly by pathways other than glycolysis pathway. If the $Y_{H2/G}$ of three strains are compared, elimination of lactate dehydrogenase activity is found to elevate NAD(P)H supply by other pathways.

The overview of the data shown in Fig.5.9 indicates that genetic perturbation of redox status that is brought by disruption of genes coding for lactate dehydrogenase and alcohol dehydrogenase plays an integral part to increase H_2 production. Deletion of lactate dehydrogenase activity and alcohol dehydrogenase activity results not only redirection of NAD(P)H molecule for lactate dehydrogenase and alcohol dehydrogenase to NiFe-hydrogenase but also reforming the redox homeostasis networks. The increased amount of H_2 is higher than that expected by above redirection of NAD(P)H. Genetically modified mutants appear to represent a cellular state under the added load of mutation. Fructose plays the other integral part to increase H_2 production. Dry cell weight concentration of mutants is supported by fructose as that of GT strain. In the presence of fructose, cells of GT strain, Δddh mutant and ΔadhΔddh mutant express the redox balance systems to constantly make-up NAD(P)H molecules utilized by NiFe-hydrogenase. The supernumerary NAD(P)H synthesis in mutants appear to trigger the second reformation of the redox balance systems at t_{SHT}. This reformation contributes to further increase the amount of H_2 per culture volume. The second reformation occurs when acetate production is changed to acetate assimilation.

(c) Conceptual design of bioreactor for H_2 production

Biological data obtained in this work is applied for the conceptual design of dark anaerobic bioreactor to produce fuel H_2. In experiments, HEPES buffer solution with a pH at 7.8 was utilized; however, to reduce the cost of buffer solution, the replacement of HEPES buffer solution by PBS (phosphate buffered saline; NaCl, 8.0 kg m^{-3} ; KCl, 0.20 kg m^{-3} ; Na_2HPO_4, 1.44 kg m^{-3}; KH_2PO_4, 0.24 kg m^{-3}; pH7.4) solution is assumed. In experiment, point mutagenesis was applied to construct ΔadhΔddh mutant that is defective of lactate dehydrogenase activity and alcohol dehydrogenase activity. For considering industrialization, ΔadhΔddh mutant is assumed to be obtained by mutagenesis. The data obtained in this work for the point-mutagenesis-derived ΔadhΔddh mutant in HEPES buffer solution are assumed to be applicable for the calculation of dark anaerobic H_2 production in mutagenesis-derived ΔadhΔddh mutant in PBS solution.

Figure 5.15 shows a conceptual design of dark anaerobic bioreactor for ΔadhΔddh mutant. The employment of 5,000 m^3 anaerobic biogas bioreactor (Harvestore, 2014) is assumed in this work. The bioreactor is a cylindrical stirred tank with standard dimensions. The working volume is typically 70-80% of the total volume, hence this graph assumes the 4,000 m^3 working volume. The headspace volume is 1,000 m^3. If height (*H*) per diameter (*D*) is 0.4, then size of bioreactor is *D*, 25.2 m; *H*, 10.1 m. Channel is equipped inside the anaerobic bioreactor, for which PBS buffer solution with 50 mol m^{-3} (=50 μmol mL^{-1}) fructose is fed with plug flow reactor operation. Flow rate of buffer solution is 33.3 m^3 h^{-1} in order to set the mean residence time of fluid at 120 h. From Table 5.2, the number of moles of H_2 at 120 h is predicted as 18.7 mol m^{-3}(=18.7 μmol mL^{-1}). Production rate is 623 (=(33.3)(18.7)) mol h^{-1}. Gas phase contains CO_2 that is removed by NaOH to form Na_2CO_3 in absorber that is equipped at the gas outlet. This byproduct is returned to photobioreactor in which CO_2 and HCO_3^- are assimilated by ΔadhΔddh mutant. At the liquid outlet, ΔadhΔddh mutant is separated by continuous centrifugal and it is directed to fertilizer. The separated PBS buffer solution in supernatant is returned to the mixing tank where concentrated newly fed inoculum is suspended in nitrate-free PBS buffer solution. The spent cells can be utilized in for growth cultivation in photosynthesis. In order to control pH and buffer concentration, the makeup is added up into buffer solution return.

If operation time of a unit is 300d y^{-1}, then annual H_2 production from a unit is 4,480,000(=(623)(24)(300)) mol y^{-1}.=100,000 Nm^3 y^{-1}. The amount of H_2 to fill-up a 156L tank of FCV was shown to be 4,880 moles (chapter 1). Hence annually produced H_2 from one unit of

bioreactor is found to fill-up the tank of 918 (=4480000/4880) FCVs. H_2 production rate of Japan in 2014 is 140,000,000Nm^3, hence one unit is found to have a potential to support 0.1% of national demand of fuel H_2. The proposed cyanobacterial H_2 production doesn't require any consumption of natural gas, oil and other fossil fuel, hence it appears to be a very promising technological approach.

(d) Proposed method to activate dark anaerobic H_2 production with a unicellular cyanobacterium

Figure 5.16 is a proposed method to elevate dark anaerobic H_2 production utilizing unicellular cyanobacterium. The method is based on the approach of this work. Knowledge from previous work contributes to initiate the approach. Condition for H_2 production in GT strain had been established at the beginning of this work. Problem to achieve activated H_2 production was decomposed into four sub-problems. Experiments have been directed by a mathematical model. Feedback has been made utilizing results of experiments for solving sub-problems. In this work, the glucose tolerant mutant of *Synechocystis* sp. strain PCC6803 has been a material for a strain of experimental approach. Redox homeostasis of this strain appears to be a model of that of unicellular cyanobacteria, hence this graph can be useful to search for condition on the optimum H_2 production of other strains.

5.4 Summary

The study in this chapter was made (1) to elucidate the effect of fructose on dark anaerobic H_2 production in GT strain in HEPES buffer solution, (2) to compare the dark anaerobic H_2 production in GT strain, Δddh mutant and ΔadhΔddh mutant in HEPES buffer solution with or without 50 μmol mL^{-1} fructose, and (3) to perform a conceptual design of bioreactor to produce biofuel H_2. Results are summarized as follows.

1. Cells consumed fructose for endogenous glucose accumulation and dry cell weight production. Affinity to fructose was extremely low compared to glucose consumption.

2. Fructose was one of important factors that can save or provide reductive compound for H_2 production via H_2ase. The best concentration of fructose for H_2 production was 50 μmol· mL^{-1}.

3. The H_2 production of the glucose tolerant mutant of *Synechococystis* sp. strain PCC6803 in dark anaerobic HEPES buffer solution is found to be largely elevated by supply of fructose and elimination of dehydrogenase genes.

4. Dark anaerobic 120 h incubation of a mutant lacking both lactate dehydrogenase genes and alcohol dehydrogenase genes in HEPES buffer solution with fructose is found to increase the amount of H_2 per culture volume 11-fold over that without fructose.

5. Conceptual design of the dark anaerobic production of H_2 is challenged. One unit of 5,000m3 biogas production facility is estimated to be able to produce 100,000 Nm^3 H_2 per year that can support to fill up the tank of 918 FCVs. Baseline of the research for biofuel H_2 production is created.

6. A method to activate dark anaerobic H_2 production in unicellular cyanobacterium is proposed.

Table 5.1 Kinetic parameters for H_2 production in GT strain in HEPES buffer solution with 0-70 μmol mL^{-1} fructose. Logarithmically growing cells were used. $q^*_{H2,0}$, $q_{H2,0}/(q_{H2,0})_{w/o}$; $y^*_{H2,f}$, $y_{H2,f}/(y_{H2,f})_{w/o}$; and $k^*=k/(k)_{w/o}$. $y_{H2,1}$, c_{L1}, c_{A1}, observed number of moles of H_2, lactate and acetate per culture volume at 120 h. m_{G1}, X_1, observed m_G and X at 120 h; $\Delta(m_GX)_0$, observed increase in m_GX during first 24 h; $\Delta(-m_GX)_1$, observed decrease in m_GX from 24 h to 120 h; H_2 production; $y_{H2/G}=y_{H2,1}/\Delta(m_GX)_1$;Subscripts 0,initial; 1,120h;f,attainable state; SHT, shift in redox state; S, fructose; G, endogenous glucose; L, lactate; A, acetate; w/o, without fructose. Reference run is run without monosaccharide and with GT strain from late-logarithmic growth phase shown in Table 4.7. $(q_{H2,0})_{ref}$, 0.0147 μmol $mg^{-1}h^{-1}$; $(y_{H2,f})_{ref}$, 2.28 μmol mL^{-1}; k_{ref}, 0.0167h^{-1};$K_{d,ref}$,0.00105h^{-1}.

	c_{S0}[μmol mL^{-1}]					
	w/o	5	25	50	60	70
X_0 [mg·mL^{-1}]	2.1	1.9	2.0	1.9	1.9	1.9
$r_{H2,0}$ [μmol·mL^{-1}·h^{-1}]	0.0285	0.0422	0.0631	0.0927	0.0927	0.0927
$q_{H2,0}$ [μmol·mg^{-1}·h^{-1}]	0.0136	0.0222	0.0316	0.0488	0.0488	0.0488
t_{SHT}[h]	nd	76.6	81.9	nd	nd	nd
$r_{H2,SHT}$ [μmol·mL^{-1}·h^{-1}]	nd	1.64	5.17	nd	nd	nd
$q_{H2,SHT}$ [μmol·mg^{-1}·h^{-1}]	nd	0.863	2.59	nd	nd	nd
$q^*_{H2,0}$ [-]	0.925	1.51	2.01	3.32	3.32	3.32
$y_{H2,f}$ [μmol·mL^{-1}]	2.10	no less than 5.4	no less than 8.1	no less than 10.8	no less than 10.6	no less than 10.4
$y^*_{H2,f}$ [-]	0.956	no less than 2.37	no less than 3.55	no less than 4.74	no less than 4.65	no less than 4.56
k [h^{-1}]	0.0136	0.0202 (0-76.6h) nd (after 76.6h)	nd	nd	nd	nd
k^*[-]	0.814	1.21 (0-72h) 0(after 72h)	nd	nd	nd	nd
q_{S0}[μmol·mg^{-1}·h^{-1}]	0	0.0390	0.0369	0.0838	0.0303	0.0333
K_d [h^{-1}]	0.000710	0.000345 (24-96h)	0.00641 (24-120h)	0	0	0

$y_{H2,1}$[μmol·mL^{-1}]	1.70	5.4	8.1	10.8	10.6	10.4
m_{G1} [μmol·mg^{-1}]	0.0298	0.0386	0.0730	0.0690	0.0790	0.0707
X_1 [mg·mL^{-1}]	1.9	2.2	2.1	2.5	2.4	2.5
$(m_G X)_1$[μmol· ·mL^{-1}]	0.0566	0.0849	0.153	0.173	0.190	0.177
$c_{L,1}$ [μmol·mL^{-1}]	0.2	3.0	5.4	8.8	9.0	10.4
$c_{A,1}$[μmol·mL^{-1}]	0.0	0.0	0.1	0.2	0.2	0.2
$\Delta(m_G X)_1$[μmol·mL^{-1}]	0.4	0.5	1.6	2.2	2.4	2.0
$Y_{H2/G}$[-]	3.2	3.8	8.9	14.1	12.5	11.7

Table 5.2 Kinetic parameters for H_2 production in GT strain, Δddh mutant and ΔadhΔddh mutant in HEPES buffer solution with or without 50 μmol mL^{-1} fructose. Logarithmically growing cells were used. $q^{*}_{H2,0}$, $q_{H2,0}/(q_{H2,0})_{w/o}$; $y^{*}_{H2,f}$, $y_{H2,f}/(y_{H2,f})_{w/o}$; and $k^{*}=k/(k)_{w/o}$. $y_{H2,1}$, c_{L1}, c_{A1}, observed number of moles of H_2, lactate and acetate per culture volume at 120 h. m_{G1}, X_1, observed m_G and X at 120 h;$\Delta(m_GX)_0$, observed increase in m_GX during first 24 h; $\Delta(-m_GX)_1$, observed decrease in m_GX from 24 h to 120 h; H_2 production; $y_{H2/G}=y_{H2,1}/\Delta(m_GX)_1$;Subscripts 0,initial; 1,120h;f,attainable state; SHT, shift in redox state; S, fructose; G, endogenous glucose; L, lactate; A, acetate; w/o, without fructose. Reference run is run without monosaccharide and with GT strain from late-logarithmic growth phase shown in Table 4.7. $(q_{H2,0})_{ref}$, 0.0147 μmol $mg^{-1}h^{-1}$; $(y_{H2,f})_{ref}$, 2.28 μmol mL^{-1}; k_{ref}, 0.0167h^{-1};$K_{d,ref}$,0.00105h^{-1}.

	Strain					
	GT strain		Δddh mutant		ΔadhΔddh mutant	
c_{S0}[μmol mL^{-1}]	0	50	0	50	0	50
X_0 [mg·mL^{-1}]	2.1	1.9	2.2	2.2	2.0	2.0
$r_{H2,0}$ [μmol·mL^{-1}·h^{-1}]	0.0252	0.0911	0.0150	0.104	0.0200	0.129
$q_{H2,0}$ [μmol·mg^{-1}·h^{-1}]	0.0119	0.0479	0.00682	0.0495	0.010	0.0645
t_{SHT}[h]	nd	nd	nd	86.8	nd	68.2
$r_{H2,SHT}$ [μmol·mL^{-1}·h^{-1}]	nd	1.64	5.17	nd	nd	nd
$q_{H2,SHT}$ [μmol·mg^{-1}·h^{-1}]	nd	nd	nd	6.02	nd	4.91
$q^{*}_{H2,0}$ [-]	0.810	3.26	0.464	3.37	0.680	4.39
$y_{H2,f}$ [μmol·mL^{-1}]	1.67	no less than 10.8	1.30	no less than 16.2	1.68	no less than 18.7
$y^{*}_{H2,f}$ [-]	0.732	no less than 4.74	0.570	no less than 7.11	0.737	no less than 8.20
k [h^{-1}]	0.0151	nd	0.0115	nd	0.0119	nd
k^{*}[-]	0.904	nd	0.782	nd	0.810	nd
q_{S0}[μmol·mg^{-1}·h^{-1}]	0	0.0853	0	0	0	0
K_d [h^{-1}]	0(0-48h); 0.00103(48-120h)	0	0.000741	0	0.00106	0
μ[h^{-1}]	0	0.00149	0	0(0-72h);	0	0(0-72h);

				0.000978(76-120h)		0.00255 (72-120h)
$y_{H2,1}$[μmol·mL^{-1}]	1.66	10.8	1.00	16.2	1.42	18.7
m_{G1} [μmol·mg^{-1}]	0.0298	0.0695	0.0439	0.0736	0.0411	0.0753
X_1 [mg·mL^{-1}]	1.91	2.41	1.96	2.50	1.96	2.26
$(m_G X)_1$[μmol· ·mL^{-1}]	0.0569	0.167	0.0860	0.184	0.0806	0.170
$c_{L,1}$ [μmol·mL^{-1}]	0.204	9.02	0.016	0.019	0.017	0.015
$c_{A,1}$[μmol·mL^{-1}]	0.0495	0.223	0.0623	0.203	0.0	0.152
$\Delta(-c_S)_1$[μmol·mL^{-1}]	0	5.2	0	8.2	0	8.5
$\Delta(m_G X)_1$[μmol·mL^{-1}]	0.16	0.15	0.11	0.09	0.15	0.18
$Y_{H2/G}$[-]	6.63	57.5	5.82	151	6.2	86.6

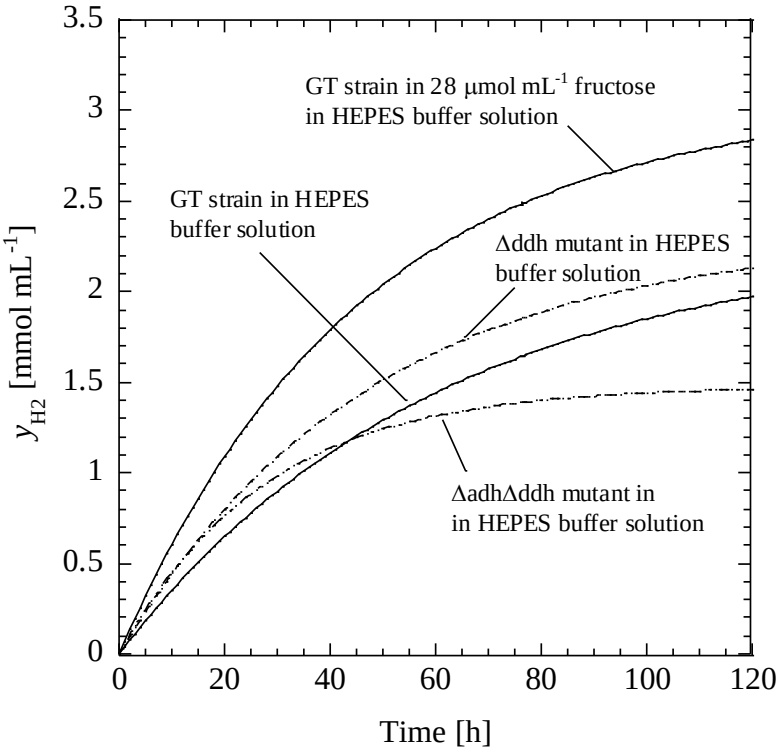

Figure 5.1 Simulation of dark anaerobic H_2 production in GT strain, Δddh mutant and ΔadhΔddh mutant in HEPES buffer solution and GT strain in HEPES buffer solution with 28 μmol mL^{-1} fructose. Inoculum cells are from late-logarithmic growth phase when X is 2.58 mg mL^{-1}. The model parameters $r_{H2,0}$ and k of runs without fructose and with fructose are obtained from Table 4.7 and Table 2.3, respectively.

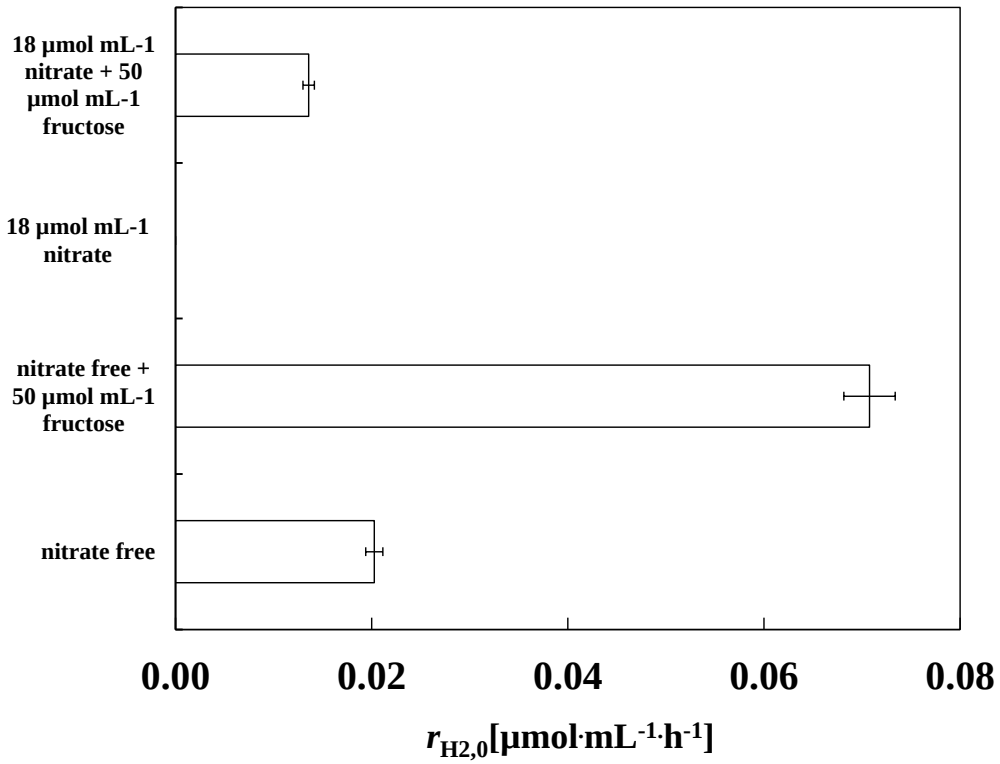

Figure 5.2 Effect of nitrate and fructose on the initial H_2 production rate in GT strain. The H_2 production was evaluated by the measurements of the amount of H_2 per culture volume after 48 h incubation of cells in HEPES buffer solutions (a) without nitrate or fructose, (b) without nitrate and with 50 µmol·mL^{-1} fructose, (c) with 18 µmol·mL^{-1} $NaNO_3$ and without fructose, and (d) with 50 µmol·mL^{-1} fructose and 18 µmol·mL^{-1} $NaNO_3$. All experiments were carried out in duplicate.

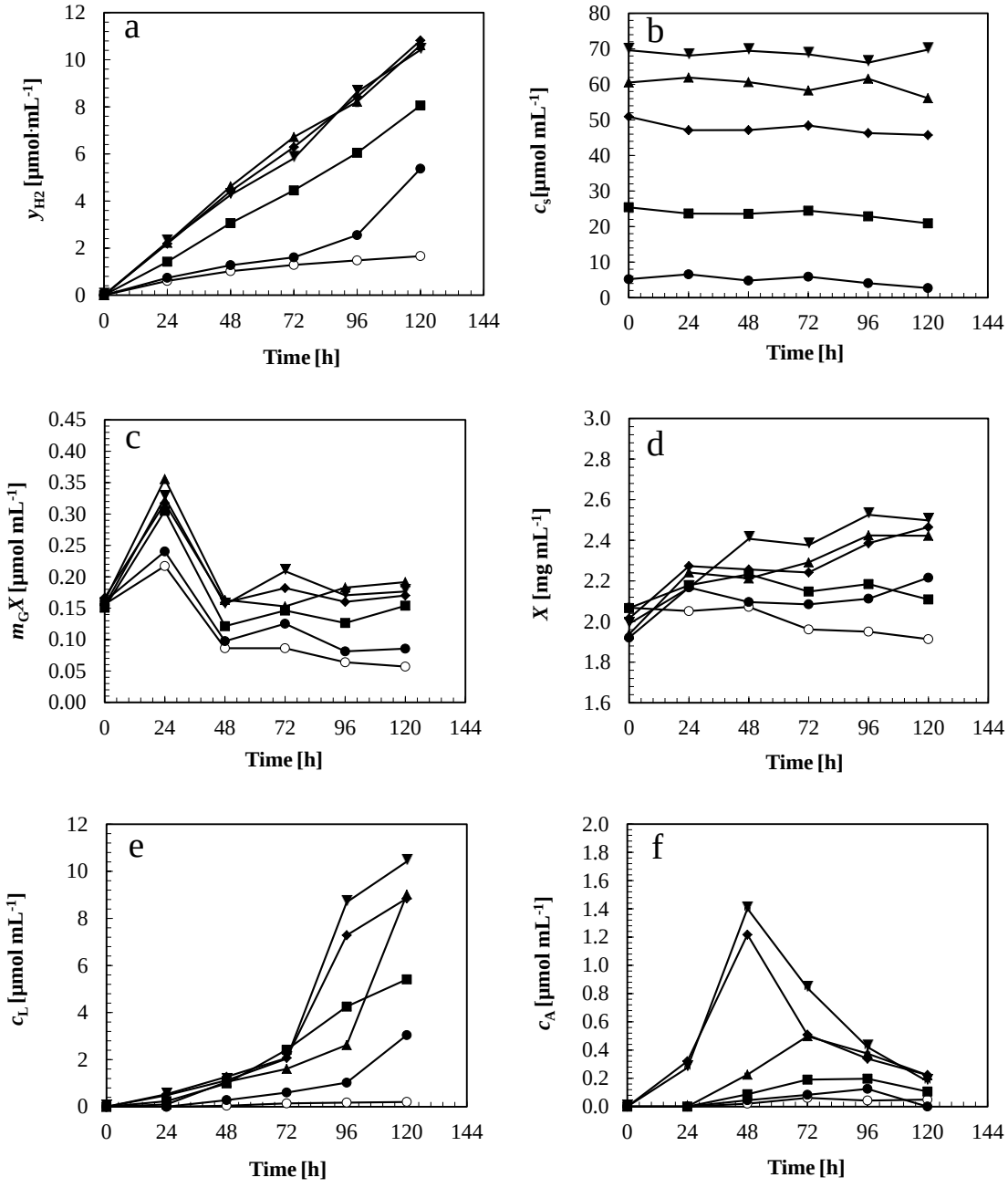

Figure 5.3 Time courses of (a) the number of moles of H_2 per culture volume, (b)the concentration of fructose, (c) the number of moles of endogenous glucose per culture volume, (d) the concentration of dry cell weight (X), (e) the concentrations of lactate and (f) the concentration of acetate of the dark anaerobic incubation of cells of GT strain in nitrate-free HEPES buffer solutions with 0 (○), 5(●), 25(■), 50(◆), 60(▲) or 70 (▼) μmol·mL^{-1} fructose.

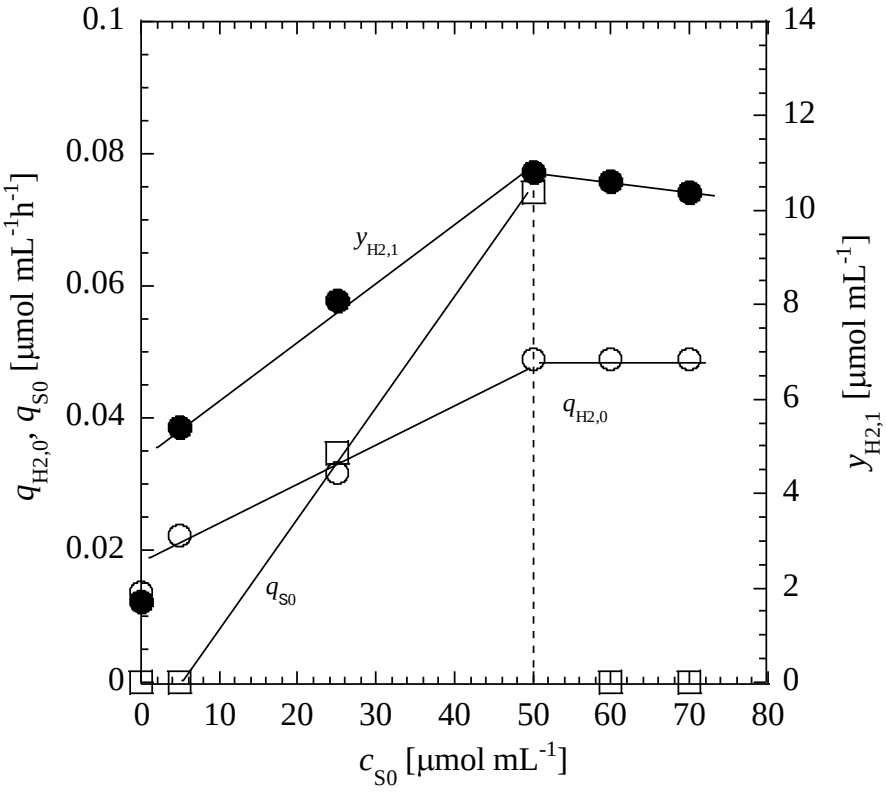

Figure 5.4 Effect of initial fructose concentration (c_{S0}) upon initial specific H_2 production rate ($q_{H2,0}$) initial specific fructose uptake rate (q_{S0}) and the number of moles of H_2 per culture volume at 120 h ($y_{H2,1}$)

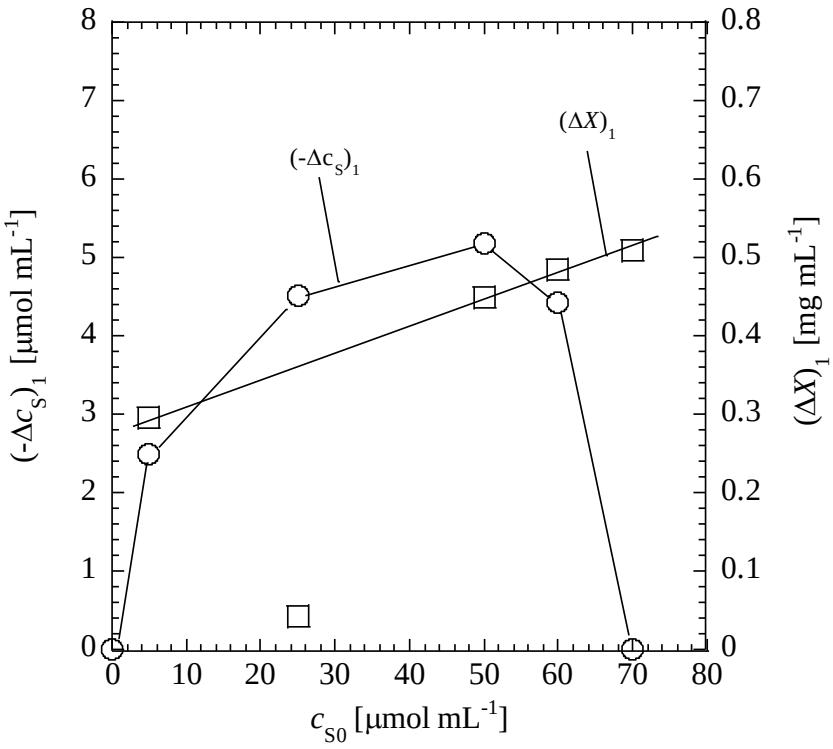

Figure 5.5 Effect of initial fructose concentration (c_{S0}) upon total consumption of fructose $(-\Delta c_S)_1$ and total reproduction of dry cell weight $(\Delta X)_1$ from 0 to 120h. $(-\Delta c_S)_1=c_{S0}-c_{S1}$; $(DX)1=X_1-X_0$

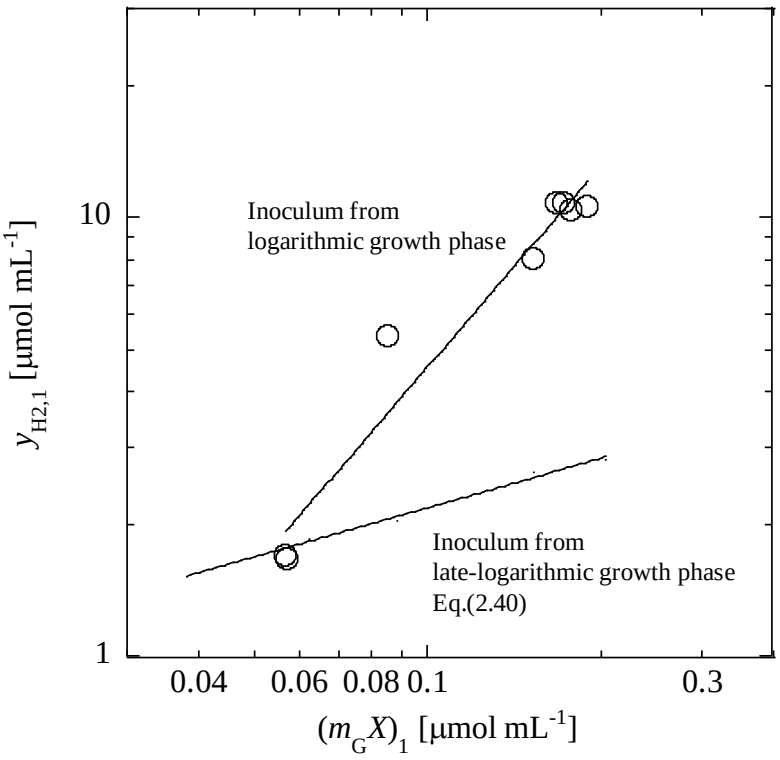

Figure 5.6 Relation between $(m_G X)_1$ and y_{H1} in runs with GT strain in HEPES buffer solution with or without fructose

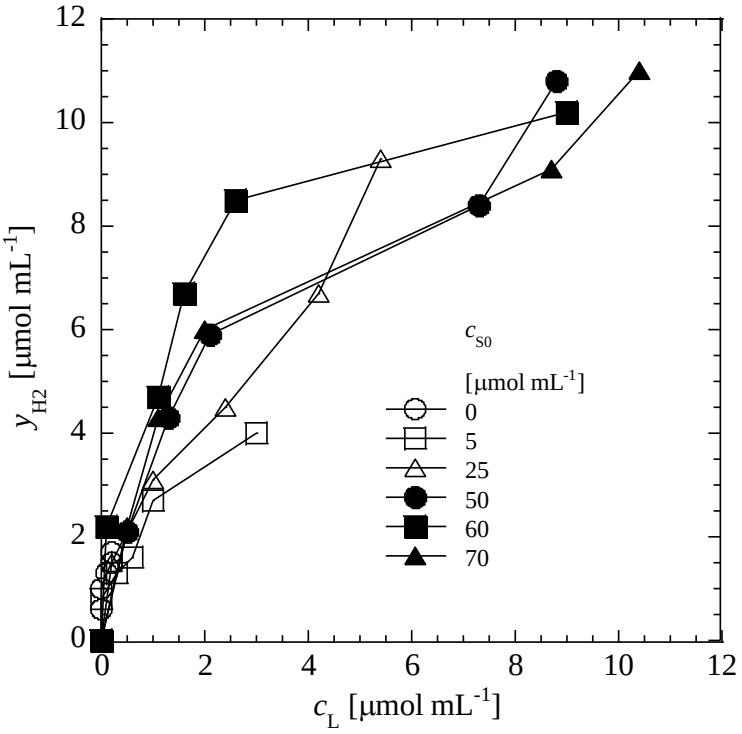

Figure 5.7 Relation between c_L and y_{H2} in runs with GT strain in HEPES buffer solution with or without fructose

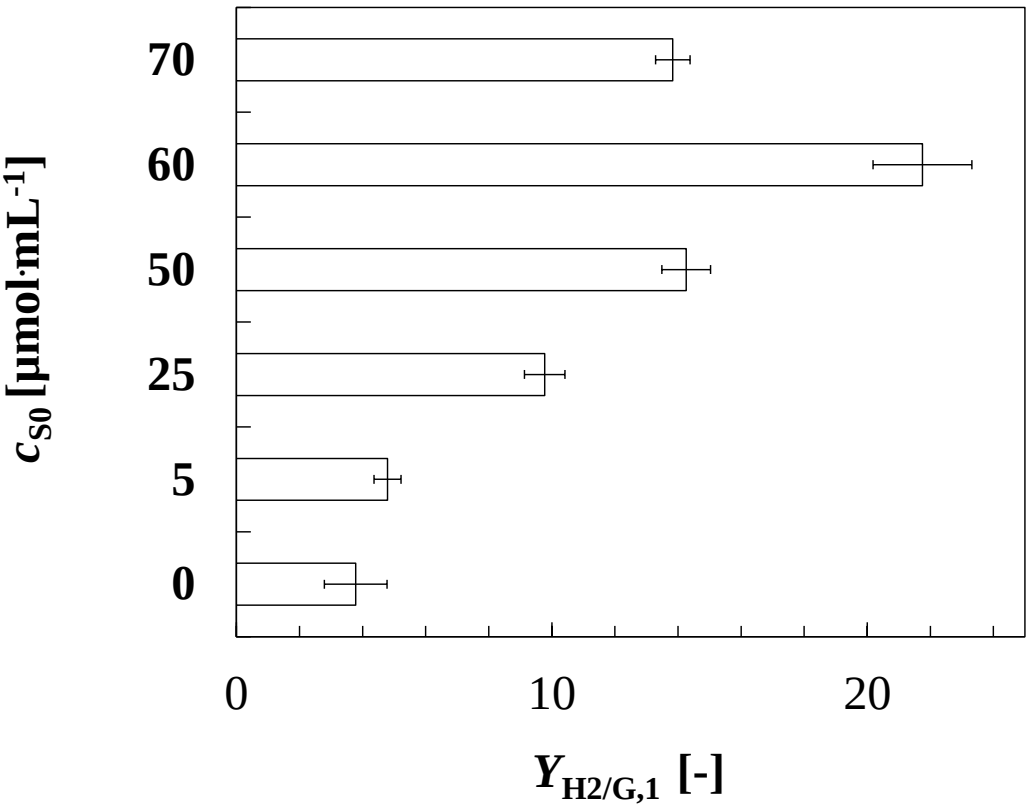

Figure 5.8 Effect of initial fructose concentration upon yield of H_2 on endogenous glucose for glycolysis. $Y_{H2/G}=(y_{H2,1}-y_{H2}(24))/(m_G X)_{24}-(m_G X)_1)$ in the period between 24 h and 120 h

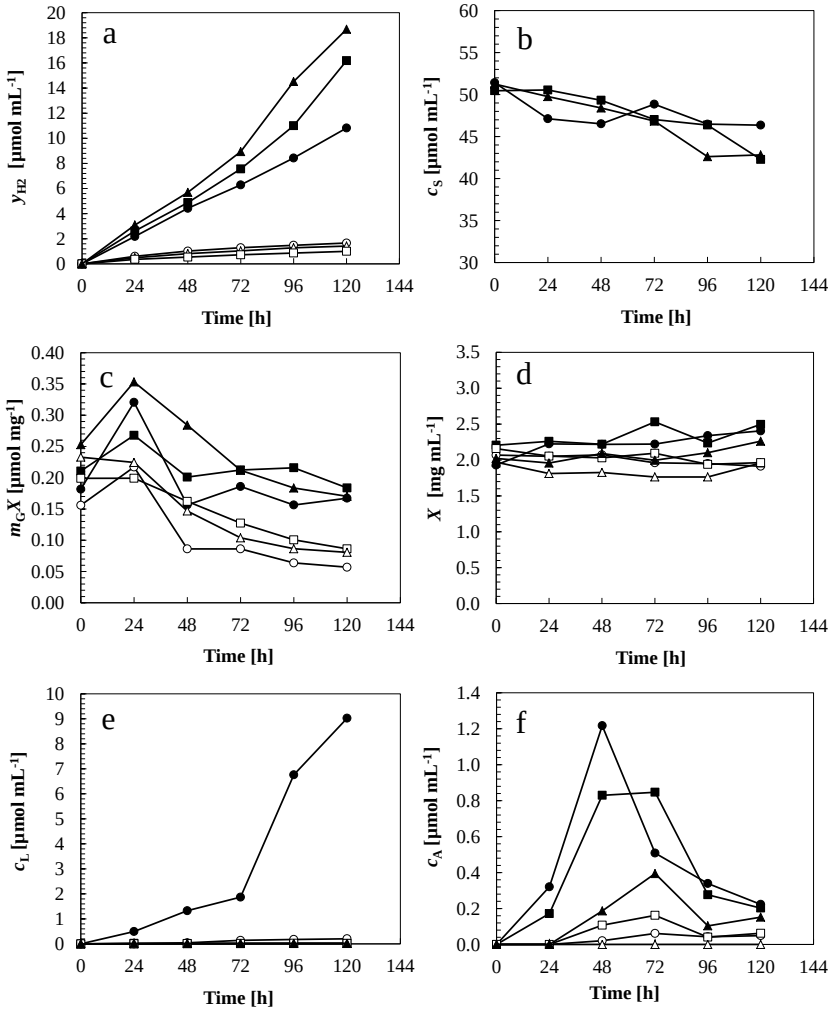

Figure 5.9 Time courses of culture variables for dark anaerobic hydrogen production in cells of GT strain, Δ*ddh* mutant and Δ*adh*Δ*ddh* mutant without or with 50 µmol mL^{-1} fructose in HEPES buffer solution. GT strain (○, ●); Δ*ddh* mutant (□, ■); and Δ*adh*Δ*ddh* mutant(△, ▲). Open keys, runs without fructose; solid keys, runs with fructose. Quantities measured include (a) the moles of hydrogen per culture volume (y_{H2}), (b) the concentration of exogenous fructose (c_S), (c) the moles of endogenous glucose in glycogen per culture volume (m_GX), (d) the concentration of dry cell weight (X), (e) the concentration of lactate (c_L), (f) the concentration of acetate (c_A) and (g) the concentration of ethanol (c_E). Experiments were carried out in duplicate

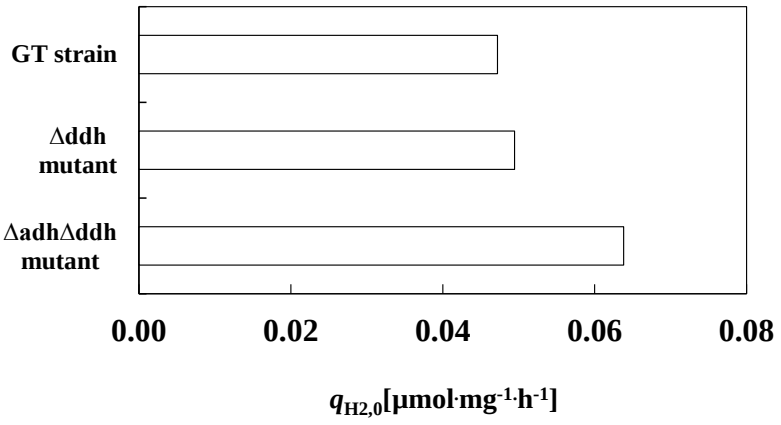

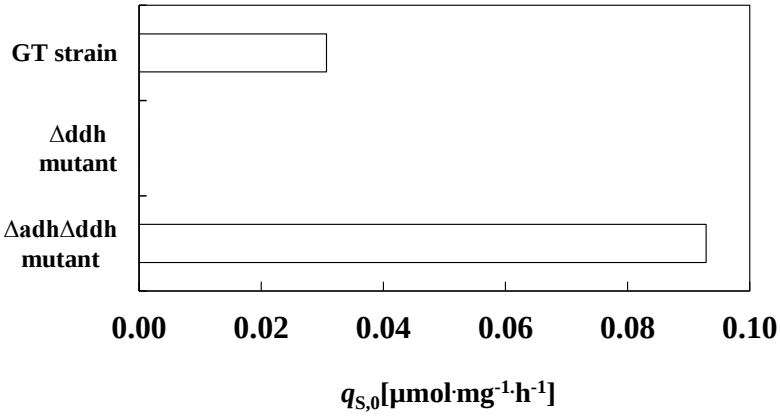

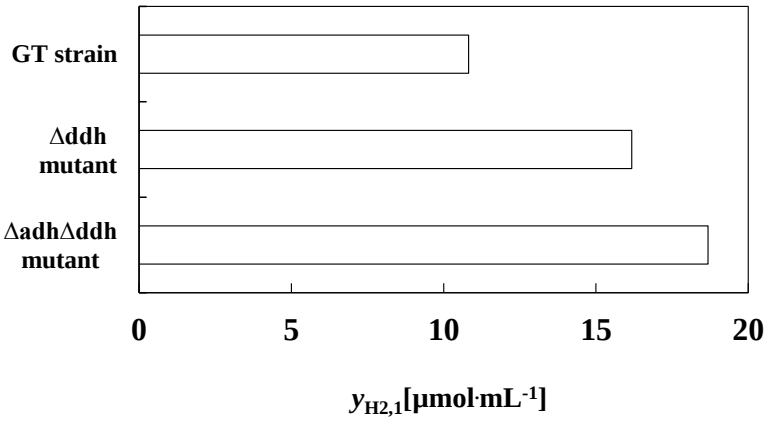

Figure 5.10 Effect of genetic modification upon initial specific H_2 production rate ($q_{H2,0}$) initial specific fructose uptake rate (q_{S0}) and the number of moles of H_2 per culture volume at 120 h ($y_{H2,1}$)

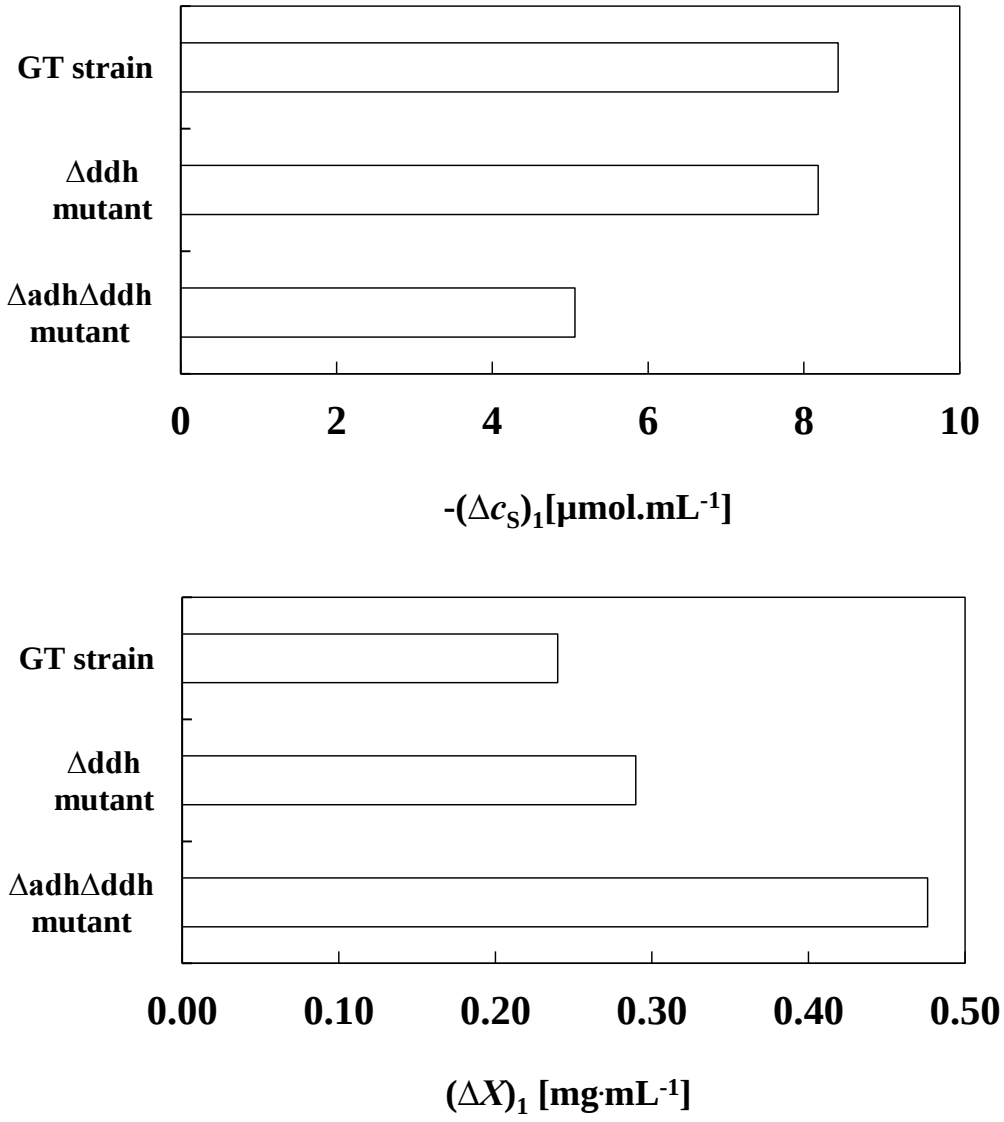

Figure 5.11 Effect of genetic modification upon total consumption of fructose -$(\Delta c_S)_1$ and total reproduction of dry cell weight $(\Delta X)_1$ from 0h to 120h. $(-\Delta c_S)_1=c_{S0}-c_{S1}$; $(\Delta X)_1=X_1-X_0$

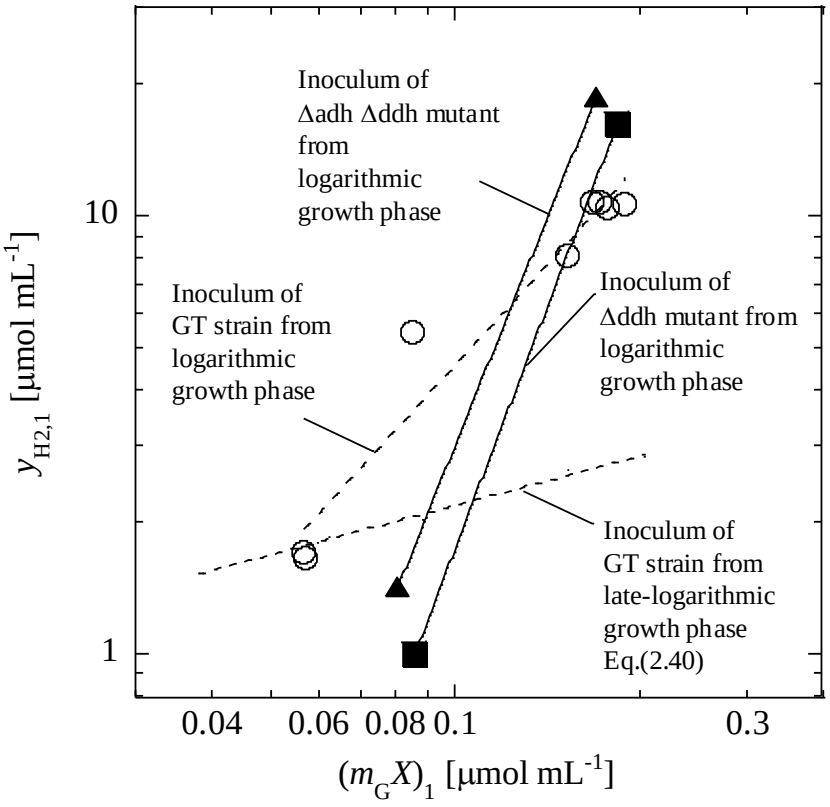

Figure 5.12 Relation between $(m_G X)_1$ and y_{H1} in runs with GT strain in HEPES buffer solution with or without fructose

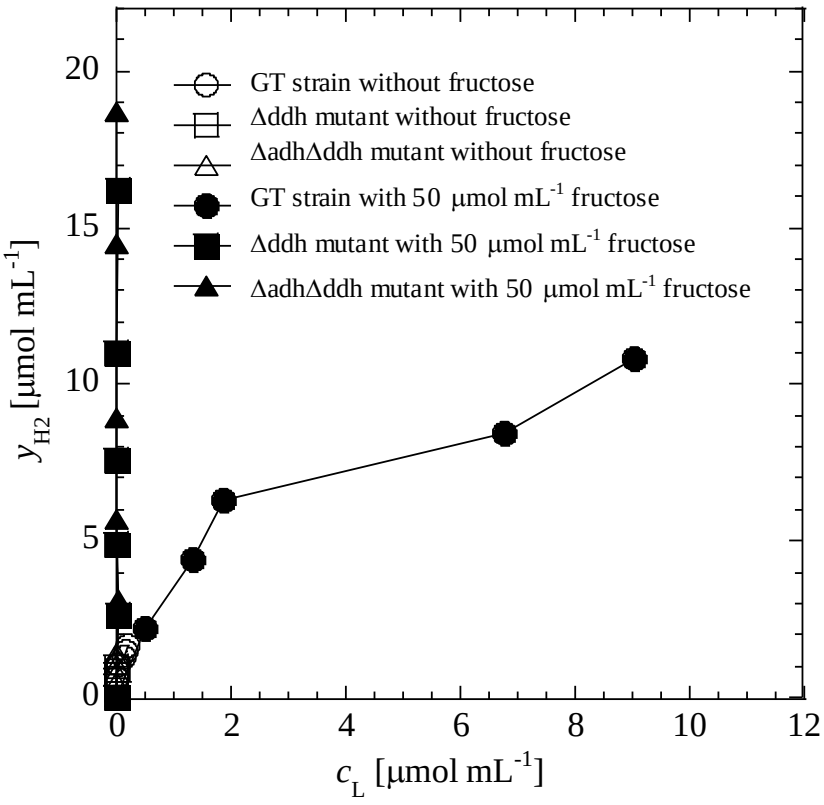

Figure 5.13 Relation between c_L and y_{H2} in runs with GT strain, Δ*ddh* mutant and Δ*adh*Δ*ddh* mutant in HEPES buffer solution with or without fructose

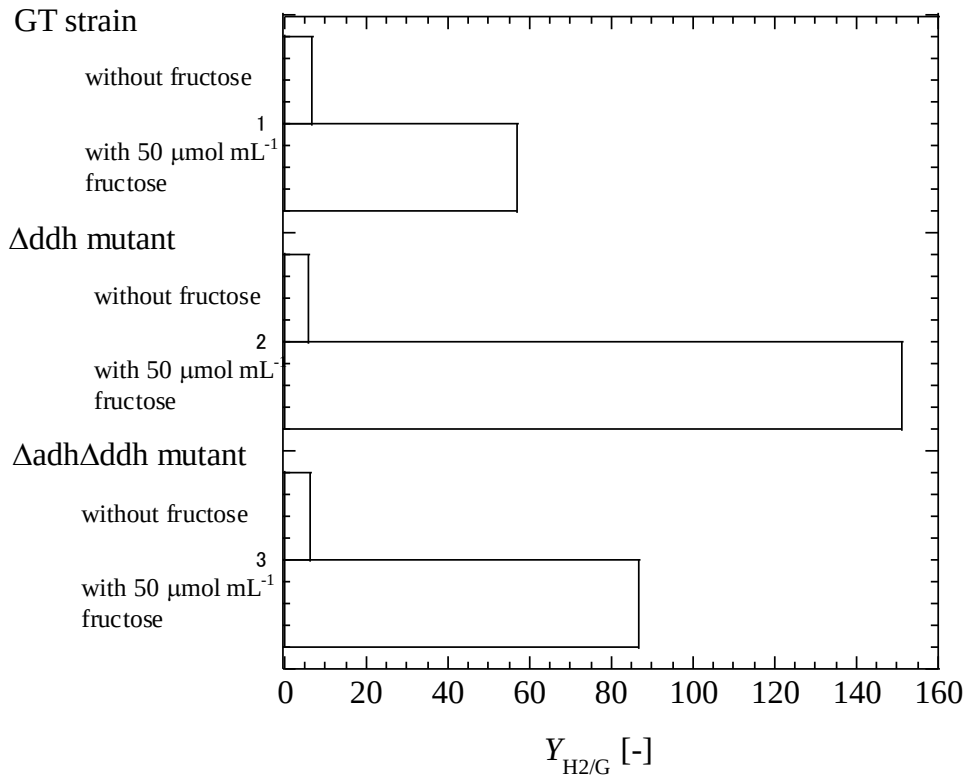

Figure 5.14 Effect of genetic modification upon yield of H_2 on endogenous glucose for glycolysis. $Y_{H2/G}=(y_{H2,1}-y_{H2}(24))/(m_G X)_{24}-(m_G X)_1)$ in the period between 24 h and 120 h

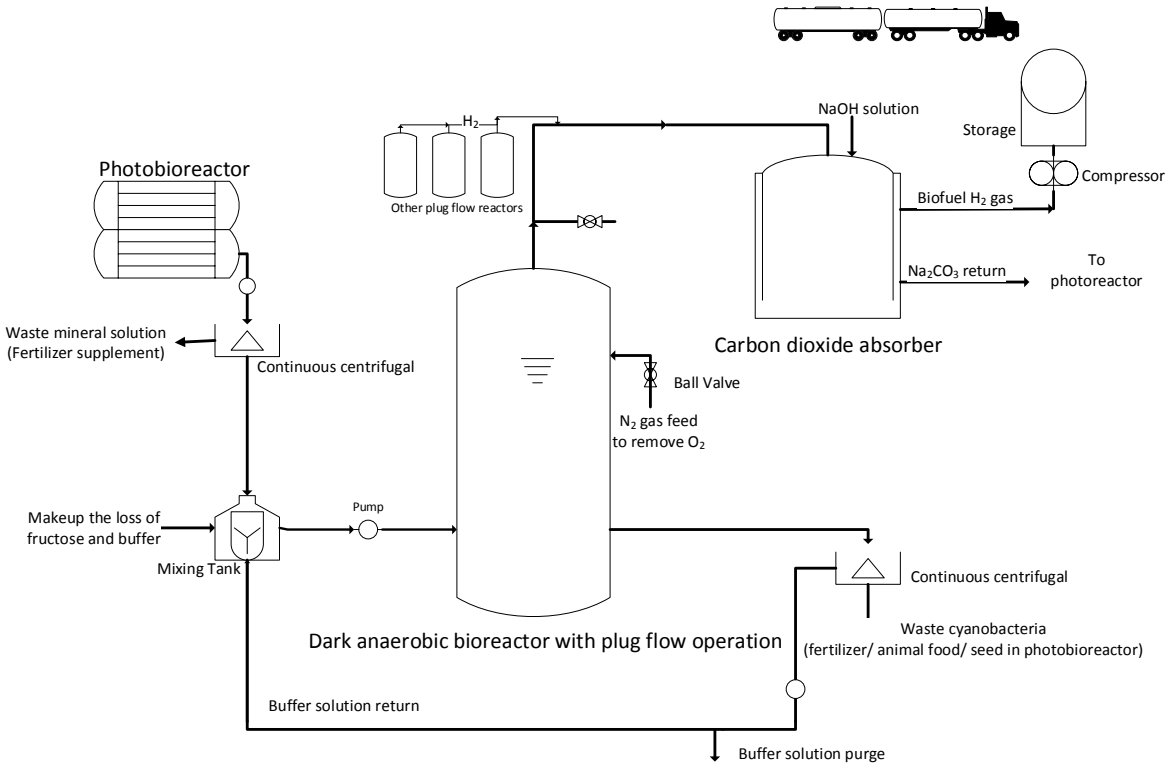

Figure 5.15 Conceptual design of dark anaerobic bioreactor to produce biofuel H_2

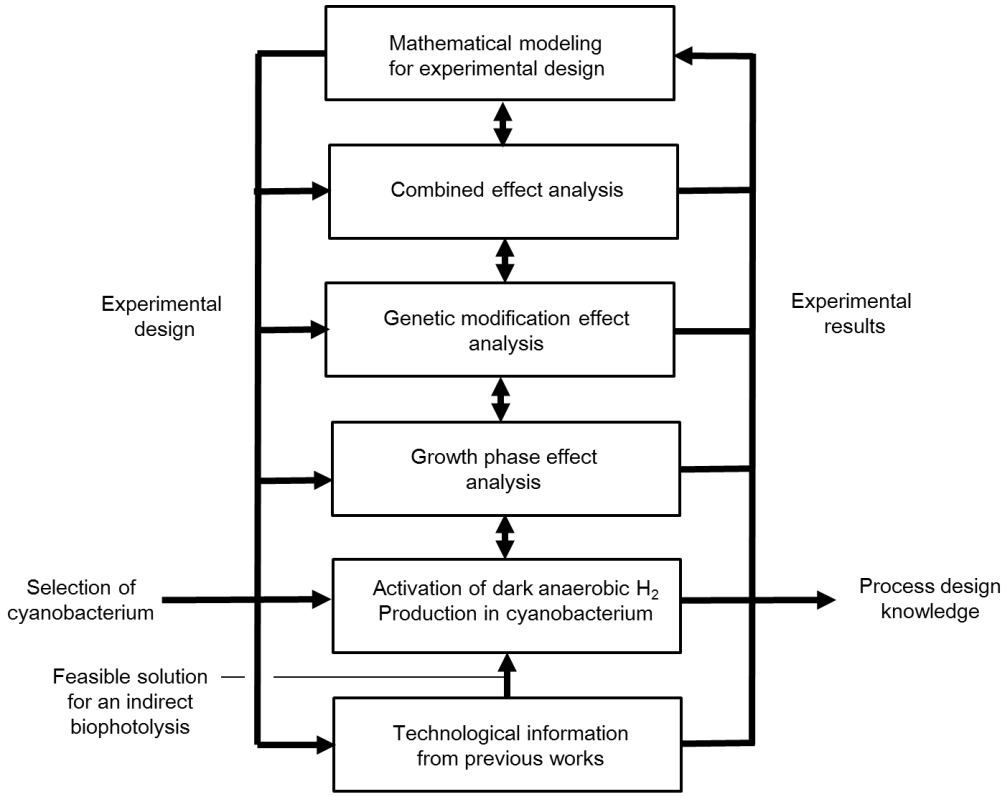

Figure 5.16 Proposed methods to elevate dark anaerobic H_2 production utilizing unicellular cyanobacterium

Chapter 5: References

Antal TK, Oliveira P, Lindblad P (2006) The bidirectional hydrogenase in the cyanobacterium *Synechocystis* sp. strain PCC 6803. Internaional Journal of Hydrogen Energy 31 (11):1439-1444

Baebprasert W, Jantaro S, Khetkorn W, Lindblad P, Incharoensakdi A (2011) Increased H_2 production in the cyanobacterium *Synechocystis* sp. strain PCC 6803 by redirecting the electron supply via genetic engineering of the nitrate assimilation pathway. Metabolic Engineering 13 (5):610-616

Beauclerk A, Smith A (1978) Transport of D-glucose and 3-O-methyl-D-glucose in the cyanobacteria *Aphanocapsa* 6714 and *Nostoc* strain Mac. European Journal of Biochemistry 82:187-197

Burrows EH, Chaplen FWR, Ely RL (2011) Effects of selected electron transport chain inhibitors on 24-h hydrogen production by *Synechocystis* sp. PCC 6803. Bioresource Technology 102 (3):3062-3070

Cho Y, Yoo S (2011) Signaling role of fructose mediated by FINS1/FBP in *Arabidopsis thaliana*. PLOS Genetics 7 (1):1-10

Ducat DC, Sachdeva G, Silver PA (2011) Rewiring hydrogenase-dependent redox circuits in cyanobacteria. Proceedings of the National Academy of Sciences 108 (10):3941-3946.

Flores E, Schmetterer G (1986) Interaction of fructose with the glucose permease of the cyanobacterium *Synechocystis* sp. strain PCC 6803. Journal of Bacteriology 166 (2): 693-696

Haury J, Spiller H (1981) Fructose uptake and influence on growth of the nitrogen fixation of *Anabaena variabilis*. Journal of Bacteriology 147:227-235

Joset F, Buchou T, Zhang CC, Jeanjean R (1988) Physiological and genetic analysis of the glucose-fructose permeation system in two Synechocystis species. Archives of Microbiology 149 (5):417-421

Kahlon S, Beeri K, Ohkawa H, Hihara Y, Murik O, Suzuki I, Ogawa T, Kaplan A (2006) A putative sensor kinase, Hik31, is involved in the response of *Synechocystis* sp. strain PCC 6803 to the presence of glucose. Microbiology 152 (3):647-655

Kaneko T, Sato S, Kotani H, Tanaka A, Asamizu E, Nakamura Y, Miyajima N, Hirosawa M, Sugiura M, Sasamoto S, Kimura T, Hosouchi T, Matsuno A, Muraki A, Nakazaki N, Naruo K, Okumura S, Shimpo S, Takeuchi C, Wada T, Watanabe A, Yamada M, Yasuda M, Tabata S (1996) Sequence Analysis of the Genome of the Unicellular Cyanobacterium *Synechocystis* sp. Strain PCC6803. II. Sequence Determination of the Entire Genome and Assignment of Potential Protein-coding Regions. DNA Research 3(3):109-136

Ohtaguchi K OA, Takahashi N, Ogawa M and Koide K (1995) Kinetics of hydrogen production by the photolithotroph *Synechococcus leopoliensis*, . IONICS 21:69-72

Rozen A, Arad H, Schonfeld M, Tel-Or E (1986) Fructose supports glycogen accumulation, heterocysts differentiation, N_2 fixation and growth of the isolated cyanobiont *Anabaena azollae*. . Archieves of Microbiol 145:187-190

Yamamoto T, Asami K, Ohtaguchi K (2012) Anaerobic production of hydrogen in the dark by *Synechocystis* sp. strain PCC 6803: effect of photosynthesis media for cell preparation. Journal of Biochemical Technology 3 (4):344-348

Chapter 6

Concluding Remarks

6.1 Conclusions

This thesis has described the methods to enhance a dark anaerobic H_2 production in unicellular cyanobacteria using a glucose tolerant mutant of *Synechocystis* sp. strain PCC 6803 (GT strain) as a model organism. Indirect biophotolysis was performed. In a reference run, cells of GT strain was photoautotrophically grown in the first stage, and then cells were dark anaerobically incubated in HEPES buffer solution for molecular hydrogen (H_2) production. At the end of enhancement method purposed in this thesis, no less than 8.58-fold increase in H_2 production was accomplished over the reference run that had been optimized in previous works, This has increased the possibility of biological H_2 production process using cyanobacteria to take place. Experimental approach of this study was supported by a mathematical modeling for dark anaerobic H_2 production.

Summarizations of this thesis are shown below.

(1) Principal parameters to develop the maximum dark anaerobic production of H_2 with defined cyanobacteria are i) the selection of monosaccharide additives to increase initial amount of reductive compounds; ii) the characterization of growth phase in photosynthesis; iii) the genetic modification by metabolic engineering approach; and iv) the integration of all three platforms for dark anaerobic H_2 production (Chapter 1).

(2) The addition of exogenous reducing sugar to dark anaerobic HEPES buffer solution is useful to increase initial H_2 production activity of NiFe-hydrogenase in GT strain.

(3) Glucose and fructose are characterized as monosaccharides that bring cells to elevate the attainable level of the number of moles of H_2 per culture volume at no less than 1.40 times that of reference run. In dark anaerobic condition, different from glucose, fructose elevates H_2 production without a notable amount of assimilation of fructose. (Chapter 2).

(4) Mathematical model for the kinetics of dark anaerobic H_2 production is formulated based on the global redox balance within a cell. Relative cellular content of NAD(P)H are evaluated utilizing the model (Chapter 2, 3, 4, 5).

(5) Relations between the attainable level of the number of moles of H_2 per culture volume and the initial H_2 production rate, and between the final level of the number of moles of H_2 per culture volume and the final level of the number of moles of endogenous glucose per culture volume are developed. The H_2 production of GT strain in dark anaerobic HEPES buffer solution is found to be elevated by limiting glycogen decomposition, cell breakage and hydrogenase deactivation under stresses (nitrate deprivation and dark anaerobic). The shift-up of the amount of stored glycogen is of utmost importance to elevate H_2 production (Chapter 2).

(6) A large portion of electrons for H_2 production on NiFe-hydrogenase are supplied not only by glycolysis to generate acetate but also by other degradation reactions. Glycolysis is associated with such decomposition reactions, and useful as a marker of the progress of global decomposition reactions (Chapters 2, 3).

(7) Reductive wing of incomplete TCA cycle is important in mixotrophic growth under dark anaerobic condition (Chapter 2).

(8) Dark anaerobic H_2 production in NiFe-hydrogenase of GT strain HEPES buffer solution is strongly dependent on the growth phase of inoculum cells in the first stage of biophotolysis (Chapter 3).

(9) Cell death during dark anaerobic incubation can be limited by the use of cells from logarithmic growth phase (Chapter 3).

(10) Cells from stationary phase contain high amount of endogenous glucose and they are useful to achieve high amount of stored glycogen at the end of H_2 production. Different from expectation, H_2 production is not affected by glycogen content. Glycogen content effect is found to be a growth phase dependent phenomenon (Chapter 3).

(11) Metabolic engineering approach to introduce a perturbation in redox homeostasis of GT strain is made. Mutants defective the genes coding for lactate dehydrogenase (Δddh mutant) and for both lactate dehydrogenase and alcohol dehydrogenase (ΔadhΔddh mutant) are constructed. The initial H_2 production of mutants are slightly higher than that of GT strain (Chapter 4).

(12) Among GT strain, Δddh mutant and ΔadhΔddh mutant in HEPES buffer solution with or without glucose, GT strain in the presence of glucose is capable of producing the highest attainable level of the number of moles of hydrogen per culture volume due to heterotrophic growth by assimilating exogenous glucose and producing endogenous glucose, lactate and acetate (Chapter 4).

(13) Glucose elevates H_2 production in GT strain and Δddh mutant, while lowers it in ΔadhΔddh mutant. Glucose is assimilated by GT strain. Assimilation of glucose is blocked by the elimination of the genes coding for lactate dehydrogenase (Chapter 4).

(14) Under dark anaerobic incubation, Δddh mutant and ΔadhΔddh mutant are sensitive to the cellular exposure to glucose (Chapter 4).

(15) Cells of GT strain, Δddh mutant and ΔadhΔddh mutant slowly consumed exogenous fructose for endogenous glucose accumulation and dry cell weight production. Affinity to fructose is extremely low compared to glucose consumption (Chapter 5).

(16) Fructose is an important factor that activates cells to save or provide reductive compound for H_2 production on NiFe-hydrogenase. The best concentration of fructose for H_2 production is 50 μmol mL^{-1} (Chapter 5).

(17) H_2 production in the presence of high concentration fructose is accelerated during dark anaerobic incubation (Chapter 5).

(18) Mutants, Δddh mutant and ΔadhΔddh mutant are very sensitive to fructose to elevate H_2 production. Combined effect of fructose addition and genetic modification is observed (Chapter 5).

(19) Dark anaerobic 120 h incubation of a mutant lacking both lactate dehydrogenase genes and alcohol dehydrogenase genes, from logarithmic growth phase, in HEPES buffer solution with fructose is found to increase the amount of H_2 per culture volume no less than 8.2-fold over that with cells from late-logarithmic growth phase and without fructose (Chapter 5) .

(20) Conceptual design of the dark anaerobic production of H_2 is challenged. One unit of 5,000m3 biogas production facility is estimated to be able to produce 100,000 Nm^3 H_2 per year that can support to fill up the tank of 918 FCVs. Baseline of the research for biofuel H_2 production is created (Chapter 5).

(21) A method to activate dark anaerobic H_2 production in unicellular cyanobacterium is proposed (Chapter 5).

Selection of the fructose supplement for fermentation with *Synechocystis* sp. strain PCC 6803 cells is the most important factor to increase H_2 production. This study has proposed a better way of H_2 production by using genetically modified cyanobacterium cells and fructose as carbon source. H_2 production by logarithmical phase aged GT, Δddh and Δadhddh strains on 50 μmol mL^{-1} fructose yields 10.8 mmoles, 16.2 mmoles and 18.7 mmoles H_2 per L after 120 h fermentation respectively.

6.2 Future Works

The present findings appear to contribute a technology for activating dark anaerobic H_2 production in cyanobacteria. For future works, the following experimental design is recommended.
1. Study on the effect of long run operation upon H_2 production

Dark anaerobic H_2 production in GT strain, Δddh mutant and ΔadhΔddh mutant in HEPES buffer solution with fructose of this study was monitored up to 120 h. After 68-2-86.8 h, acceleration of H_2 production was observed. At 120 h, high rate production of H_2 was not quitted. For future development of process, H_2 production after 120 h needs to be studied.

2. Exploitation of a mutant lacking both lactate dehydrogenase and alcohol dehydrogenase (ΔadhΔddh mutant) utilizing mutagenesis.

In this study, ΔadhΔddh mutant was developed using recombinant DNA technique. H_2 production in ΔadhΔddh mutant in fructose solution results in marked impression for industrialization. Since application of genetic modified organism is highly regulated, it is required to develop similar mutant using mutagenesis or UV radiation techniques.

3. Evaluation of H_2 production in PBS solution.

HEPES buffer solution was used in this study. However, considering cost performance of buffer solution, it is recommended to elucidate dark anaerobic H_2 production in PBS solution.

Appendix-1

Hydrogen production from non-renewable sources

Current industrial H_2 production applies this technology. Technology is well-established. Natural gas, oil and coal are resources; hence it represents a high risk of abundant CO_2 emission to the atmosphere. Additional problem is that the amount of fossil sources on the earth is limited.

Steam methane reforming: Steam reforming of natural gas at 973-1373 K with Ni based catalyst generates H_2 in the form of syngas:

$$CH_4+H_2O \rightarrow CO+3H_2 \qquad \text{(A1.1).}$$

This endothermic reaction outlet gas from the reformer contains 10% CO.

Exothermic water gas shift reaction at 633 K further generates H_2 by stripping the oxygen atom from the steam and oxidizing CO to CO_2:

$$CO+ H_2O \rightarrow CO_2 +H_2 \qquad \text{(A1.2).}$$

Outlet gas from the water gas shift reactor contains 2000 ppm CO.

Removal of CO, CO_2 and other impurities is performed after water gas shift reactor. Concentration of CO at the outlet of this process is no more than 100 ppm.

The efficiency of H_2 production is about 80%. Steam methane reforming is the least expensive method to generate industrial H_2. Commercial bulk H_2 including H_2 for ammonia synthesis is produced by steam reforming. Steam reforming has drawbacks such as consuming fossil fuels stocks and generating CO_2 from carbonaceous compounds of fossil fuels.

Partial oxidation of hydrocarbons: Partial oxidation also generates H_2-rich syngas from heavy hydrocarbons including diesel fuel and residual oil:

$$C_nH_m+ \frac{n}{2} O_2 \rightarrow nCO + \frac{m}{2} H_2 \qquad \text{(A1.3).}$$

This method shares above drawbacks with steam reforming.

Coal gasification: Basic equation in coal gasification is given by:

$$Coal \rightarrow C_nH_m +H_2+Char(C) \qquad \text{(A1.4).}$$

$$C+O_2 \rightarrow CO_2 \quad \text{(A1.5)},$$

$$C+\frac{1}{2}O_2 \rightarrow CO \quad \text{(A1.6)},$$

$$C+CO_2 \rightarrow 2CO \quad \text{(A1.7)},$$

$$C+H_2O \rightarrow CO+H_2 \quad \text{(A1.8)},$$

$$C+2H_2O \rightarrow CO_2+2H_2 \quad \text{(A1.9)}$$

$$CO+H_2O \rightarrow CO_2+H_2 \quad \text{(A1.10)}$$

and

$$C+2H_2 \rightarrow CH_4 \quad \text{(A1.11)}.$$

Equation (A1.4) shows the thermal decomposition of coal. Equations (A1.5) and (A1.6) show a complete oxidation and partial oxidation of carbon, respectively. Equations (A1.7) and (A1.8) are key reactions. Coal is reacted with air or O_2 plus steam in the first reactor. Generated gas is purified to remove sulfur containing components. Then shift reaction shown by Eq.(A1.10) is performed. After CO_2 removal, pure H_2 is obtained. Coal is abundant hence it has a possibility to replace natural gas and oil as a feedstock for H_2 production.

Appendix-2

Hydrogen production from renewable sources

Biomass gasification and biomass pyrolysis utilizes biomass as a source. They produce CO_2, however, when the organism of biomass was alive, it assimilated atmospheric CO_2. Hence carbon neutral mechanism supports these technologies. Other technologies split the water to form H_2. Electrolysis, thermolysis and biocatalyzed electrolysis require the energy other than solar energy. There is a potential to produce CO_2. Biological conversion is supported by carbon neutral mechanism.

Biomass gasification: Biological material derived from living organisms or recently living organism is named biomass. Examples of biomass are plant scraps, switch grass, garbage and human waste materials. Gasification of biomass generates H_2 from organic compounds.

Biomass pyrolysis: High-temperature gasifying converts biomass into a gas. The H_2 rich vapor is condensed in pyrolysis oil that is used to steam reform to generate H_2. The yield is 12-17% H_2 by dry weight of biomass.

Electrolysis: A direct electric current (DC) is utilized to split water to H_2 and O_2:

$$2H_2O \rightarrow 2H_2 + O_2 \qquad \text{(A2.1).}$$

At the cathode (negatively charged terminal), the electricity enters the water. The electricity passes through the water and reaches to the anode (positively charged terminal). High grade pure H_2 for use in the electronics, pharmaceutical and food industries is collected at the cathode. The supply of power is important to generate H_2. If sustainable energy is available for the electrolysis, then this technology can produce H_2 as a renewable energy.

Biocatalyzed electrolysis: It is an electrolytic process that electrically connects the oxidation of organic compound at a biological anode to the reduction of H^+ at the cathode to evolve H_2 (Rozendal et al. 2006). If acetate is utilized half reactions and net reaction are given by

Anode: $CH_3COO^- + 4H_2O \rightarrow 2HCO_3^- + 9H^+ + 8e^-$ (A2.2)

Cathode: $8H^+ + 8e^- \rightarrow 4H_2$ (A2.3)

Net: $CH_3COO^- + 4H_2O \rightarrow 2HCO_3^- + H^+ + 4H_2$ (A2.4)

Thermolysis: H_2 and O_2 are produced from water at no less than 2773 K. However, it is not easy to block back reaction.

Photocatalytic water splitting: Artificial photosynthesis utilizing catalyst has a potential to generate H_2 according to Eq. (A2.1). Highest water splitting rate of 9.7 mmol h^{-1} is observed with UV-based photocatalyst $NaTaO_3$:La. The catalyst $K_3Ta_3B_2O_{12}$ shows a water splitting rate of 1.21 mmol h^{-1}. The highest quantum yield of 5.9% in visible light is achieved by $(Ga_{0.82}Zn_{0.18})(N_{0.82}O_{0.18})$. The study on photocatalytic water splitting is ongoing (Maeda and Domen, 2010). Although this photocatalytic water splitting has high potential for future H_2 energy, the material used in the system is extreme expensive. Bulk gallium nitride (GaN) is very expensive today, costing about $1,900 or more for a two-inch substrate.

Dark fermentation: Dark fermentation does not require light. The theoretical maximum yields are 2-4 moles H_2 per mole of glucose consumption, depending on butyrate or acetate produced as final fermentative products. Chemical equations representing the stoichiometry for the conversion of glucose to lactate and that to acetate are shown by

$$C_6H_{12}O_6 \rightarrow CH_3CH_2CH_2COOH + 2CO_2 + 2H_2 \quad \text{(A2.5)}$$

$$C_6H_{12}O_6 + 2H_2O \rightarrow 2CH_3COOH + 2CO_2 + 4H_2 \quad \text{(A2.6)}$$

The actual yield of H_2 from glucose in *Escherichia coli* is very low because H_2 production is mediated only in the formate formation reaction by formate hydrogen lyase (FHL) complex that is composed of hydrogenase 3 and formate dehydrogenase-H (FdhF) (Axley et al., 1990). *Escherichia coli* is capable of converting only electrons available at the pyruvate node to H_2, and is unable to use the electrons generated during glycolysis. **Figure A2.1** shows the genetically modified *E.coli* for H_2 production through heterologous expression of NiFe-hydrogenase (the soluble NAD-dependent hydrogenase of *Ralstonia eutropha* (SH hydrogenase)) (Ghosh et al., 2013). This work reported the success of 2 moles H_2 production per mole of glucose consumed, close to the theoretical maximum. Final H_2 levels that were achieved for 120 h were between 1.0 and 1.8 μmol mL^{-1}.

H_2 production by a soluble FeFe-hydrogenase in *Clostridium* species has also been studied (Hallebeck, 2008). Different from the metabolism shown in Fig.A2.1, pyruvate is further converted to acetyl-CoA, CO_2 and reduced ferredoxin by pyruvate ferredoxin oxidoreductase (PFOR). Electrons are directly transferred from reduced ferredoxin to FeFe-hydrogenase. If H_2 partial pressure is low, the NADH from glycolysis is reoxidized possibly by a NADH-dependent FeFe-hydrogenase.

The constraint of those dark fermentations is that they require carbon sources for growth and cell activity, whereas, cyanobacteria requires only small nutrition, solar light (energy), water (electron), mineral salts and CO_2 in the air for their growth in photosynthetic. The power of solar light reaching to the earth surface is so vast and infinite. The absence of light energy utilization for molecular energy rather than high carbon substrate consumption puts this system into a high-cost process.

Direct biophotolysis: Direct biophotolysis is a fermentative conversion of organic compounds to hydrogen in the presence of light. It requires absorption of sunlight by the biochemical of interest. Gaffron discovered photobiological H_2 evolution in unicellular green algae *Scenedesmus* after being kept in dark anaerobic condition (Gaffron 1939). Green algae utilize photosynthetically generated electrons for the reduction of H^+ to H_2. Illumination enhanced the H_2 generation. The enzyme responsible for this H_2 evolution is a bidirectional hydrogenase. Photobiological H_2 production is the biological splitting of the water into H_2 and O_2.

$$2H_2O + \text{light energy} \rightarrow 2H_2 + O_2 \quad \text{(A2.7)}$$

Direct biophotolysis is also studied by other researchers (Mathews and Wang 2009; Oh et al. 2011). In microalgae, Fd (ferredoxin) acts as an electron donor to FeFe-hydrogenase (about 48 kDa) and reversibly facilitates the formation of H_2 from H^+.

$$2H^+ + 2Fd^- \rightarrow H_2 + 2Fd \quad \text{(A2.8)}$$

Sulfur deprivation in algae cultivation onsets H_2 production from O_2 production. Hydrogen production rate is 0.446-0.536 μmol mL^{-1} h^{-1}(=10-12 mL L^{-1} h^{-1}). Photobiological H_2 production is still in research stage. Sunlight conversion efficiency is reported to be 24%.

Purple non-sulfur bacteria (PNSB) such as *Rhodobacter*, *Rhodopseudomonas* produce H_2 in photo-fermentation (nitrogen deficiency condition) by nitrogenase utilizing organic or inorganic acids as substrates. The reaction is illustrated by

$$CH_3COOH + 2H_2O + \text{light energy} \rightarrow 4H_2 + 2CO_2 \quad \text{(A2.9)}$$

Some researchers are working on cheap compound using organic waste as substrates.

Besides algae and PNSB, cyanobacteria are well known to perform direct biophotolysis to generate H_2 from solar light energy.

Figure A2.2 shows a direct biophotolysis of unicellular cyanobacterium (Yu and Takahashi 2007). A direct biophotolysis takes place through action of the complete photosynthetic apparatus in the water. Water is spitted at PSII and the ferredoxin-reducing photosystem PSI. Even though, solar energy conversion to H_2 production is high, the H_2 production is inhibited by O_2. Due to O_2 generation during

photosynthesis suppress hydrogenase from H_2 production. A reversible hydrogenase accepts electron from reduced ferrodoxin to generate H_2 by the general reaction.

Indirect biophotolysis: Indirect biophotolysis occurs when a species other than the biochemical of interest absorbs sunlight and initiates a series of bioreaction that result in the transformation of the biochemical. The inhibition of O_2 on FeFe-hydrogenase and NiFe-hydrogenase is eliminated utilizing two stage incubation method. In the first stage, algae and cyanobacteria are photoautotrophically grown under the light to evolve O_2. Carbohydrates are accumulated within cell. In the second stage, cells are exposed to dark anaerobic condition. Dark fermentation utilizes intracellularly accumulated carbohydrates. The combination of the first and second stages are shown by:

$$12H_2O+6CO_2 \rightarrow C_6H_{12}O_6+6O_2 \quad \text{(A2.10)}$$

$$C_6H_{12}O_6+12H_2O \rightarrow 12H_2+6CO_2 \quad \text{(A2.11).}$$

Gaffron and Rubin observed the dark evolution of H_2 in *Scenedesmus* (Gaffron and Rubin 1942). They demonstrated that after a period of dark anaerobic 'adaptation', the green alga *Scenedesmus obliquus* produced H_2 in the dark. After that, several algae and cyanobacteria have been studied to observe hydrogen evolution. Indirect biophotolysis is promising for H_2 production process because there is no O_2 generation to suppress hydrogenase. The specific H_2 evolution activities of reversible hydrogenases are higher than those of nitrogenase-base. Therefore systems based on bidirectional hydrogenases present the most likely approach to practical development.

For indirect biophotolysis, photosynthesis stage is important to prepare cellular states suitable for dark anaerobic H_2 production. If this technology can be realized, cyanobacterial fuel is renewable, clean and sustainable for future. It can be genetically modified to produce valuable substance such as isoprene, ethanol, sugar, and lactate (Ducat et al. 2011). However, several obstacles must be overcome to put cyanobacteria to be economically commercialized. From recent knowledge, cyanobacteria have been known as origin of photosynthesis organism. Fossil stromatolites (microbial communities mat) can be dated back to 3.5 Gya (Giga years ago) (Blankenship 1992). Photosynthetic organisms may have been among the very earliest life forms on the primitive earth. Global Oxygen accumulation in the atmosphere and oceans are from production of O_2 by photosynthesis. Photosynthesis of cyanobacteria still recently plays a major role in the conversion of carbon dioxide to biological energy storage materials on earth. Photosynthesis efficiency calculated by the combination of energy losses in light absorption and the

initial chemical reactions results in a maximal overall energetic efficiency estimated at about 11% (Brenner et al. 2006) which is much higher than plants (mostly less than 1%)

Cyanobacteria produce H_2 both from direct and indirect photolysis as shown in **Figure A2.3**. For indirect photolysis, cyanobacteria can produce H_2 from two ways of indirect photolysis, first, H_2 production directly from bidirectional hydrogenase (non-nitrogen fixation) and second H_2-production from nitrogenase (nitrogen fixation). The electron donors for the H_2 producing enzymes are ferredoxin (nitrogenase and FeFe-hydrogenases) and NAD(P)H (NiFe-hydrogenases). The illustration of this gaph shows the differences of two types of indirect photolysis hydrogenase. Many strategies of research have been done on H_2 production enhancement; from condition optimization to genetic engineered bacteria to increase desired products. H_2 production by hydrogenase of cyanobacteria has been elevated by many approaches. Classical optimization of pH, temperature, media composition and gas phase could change H_2 fermentation productivity significantly (Burrows et al. 2008; Antal and Lindblad 2005). Eco-metabolism further includes dark fermentation of anaerobic bacteria. Isolation and elevation of H_2 production activity of some species contribute to the H_2 production technology.

Figure A2.4 illustrates the nitrogenase-mediated H_2 production in N_2-fixing cyanobacteria. Filamentous cyanobacterium *Anabaena* strains are the representative of N_2-fixing cyanobacteria producing H_2 production as shown in below equation. However, both systems are limited by the O_2 sensitivity of enzyme because photosynthetic H_2 production of water splitting generates O_2.

Presence of N_2:

$$N_2 + 8H^+ + 8e^+ + 16ATP \xrightarrow{Mo-nitrogenase} 2NH_3 + H_2 + 16ADH + 16Pi \quad \text{(A2.12)}$$

Absence of N_2:

$$8H^+ + 8e^+ + 16ATP \rightarrow 4H_2 + 16ADH + 16Pi \quad \text{(A2.13)}$$

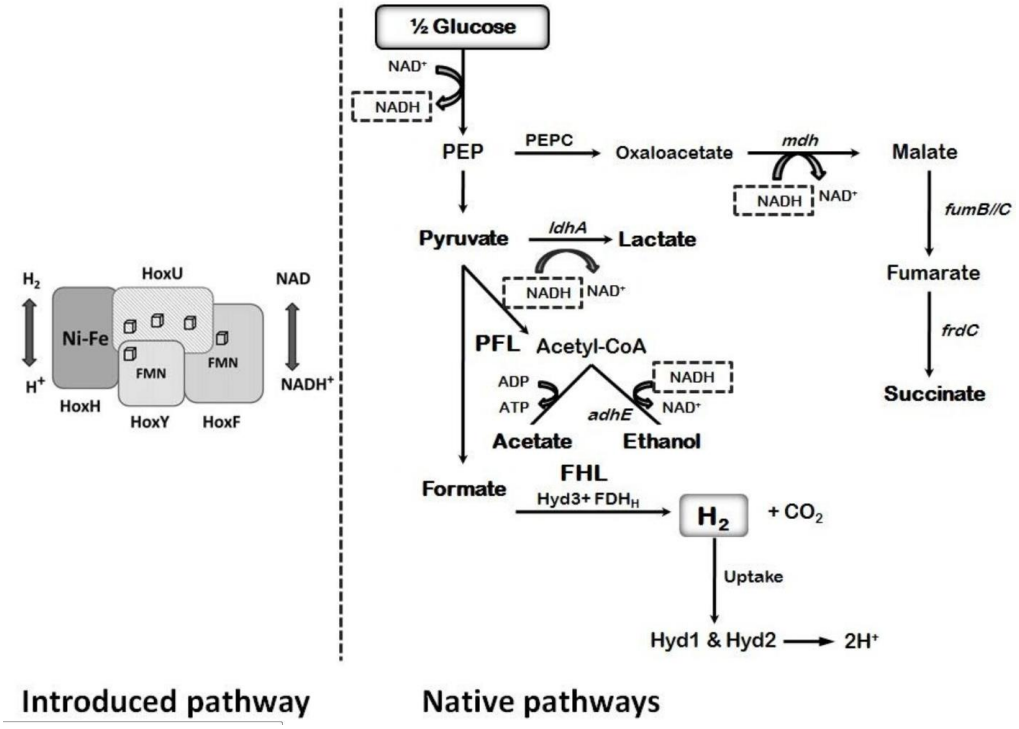

Figure A2.1 Genetically modified *Escherichia coli* to utilize NADH from glycolysis for H_2 production (Ghosh et al., 2013)

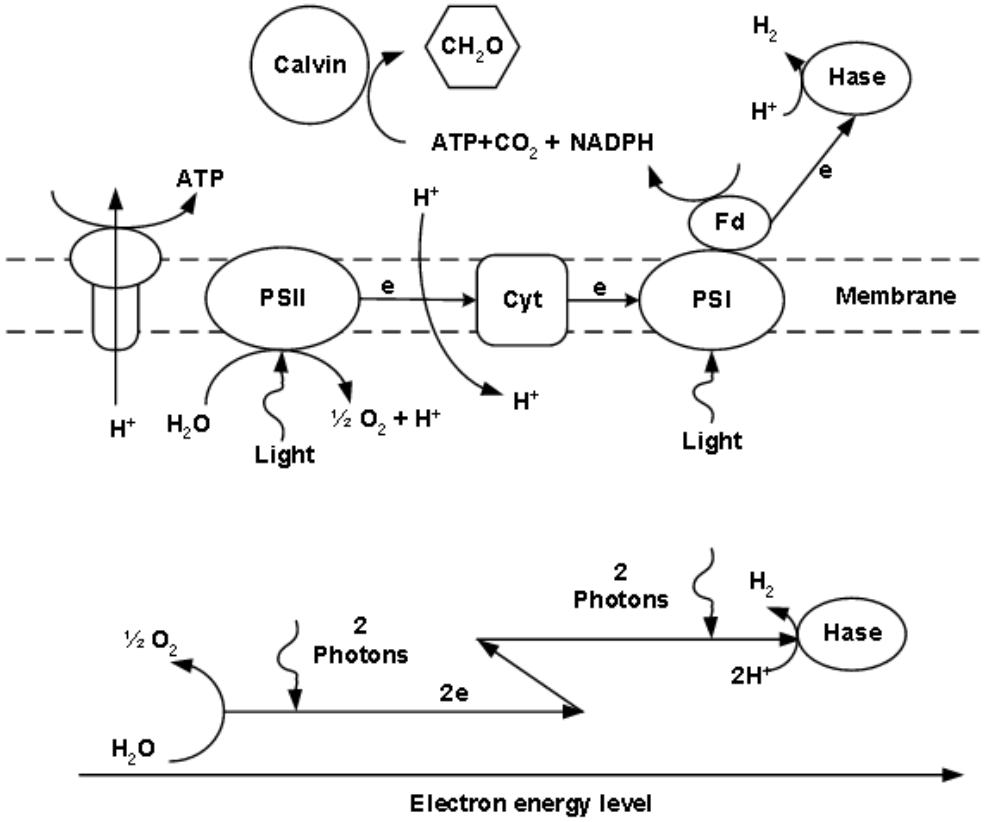

Figure A2.2 H_2 production based on direct biophotolysis (Yu and Takahashi 2007)

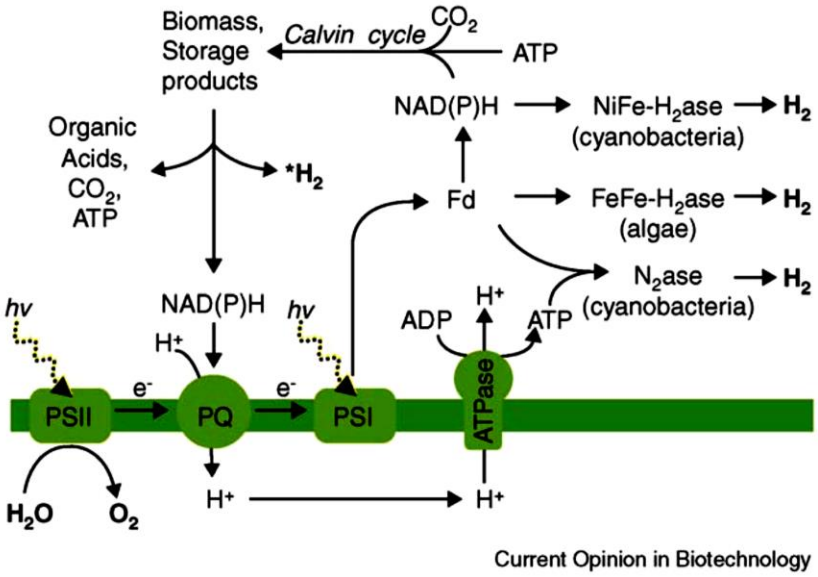

Figure A2.3 Direct and indirect biophotolysis to generate H_2 (McKinlay and Harwood 2010)

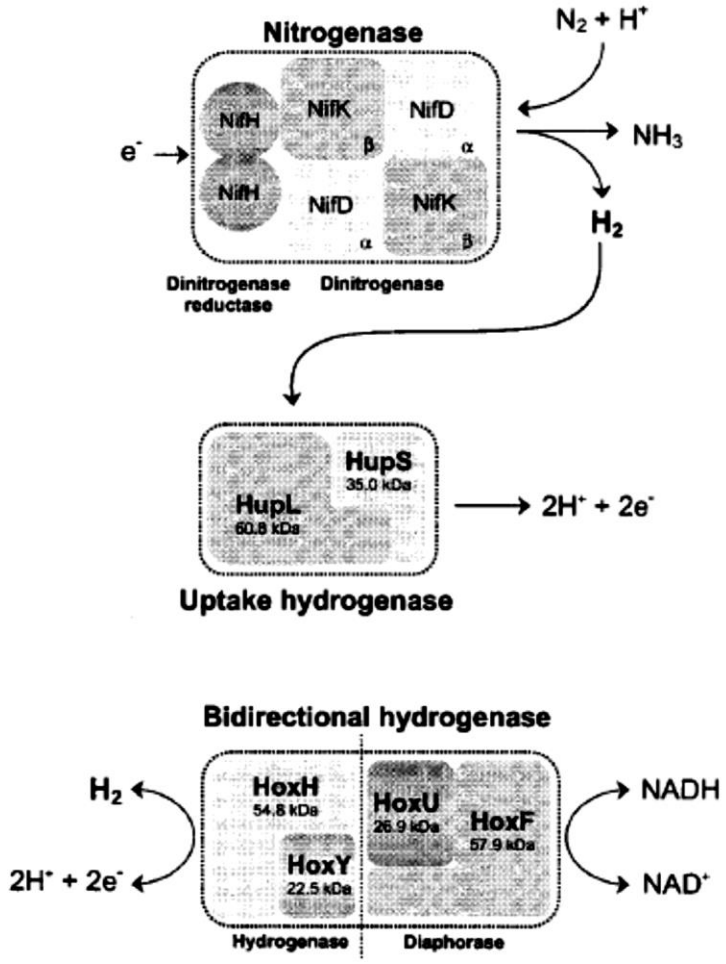

Figure A2.4 Enzymes directly involved in hydrogen metabolism in cyanobacteria. (Tamagnini et al. 2002)

Appendix-3
Metabolic map for *Synechocystis* sp. strain PCC6803

(1) Starch and sucrose metabolism

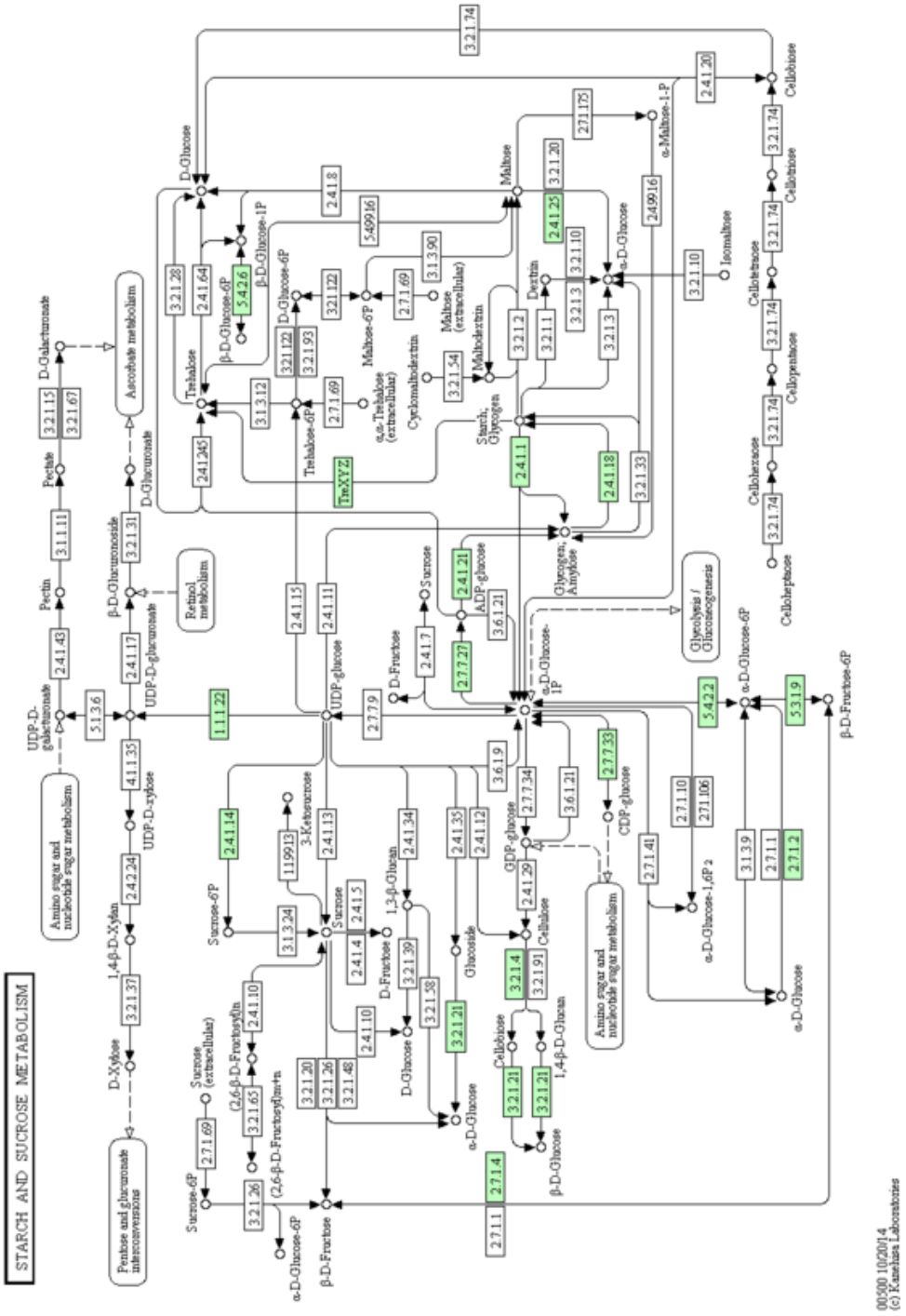

Figure A3.1 Starch and sucrose metabolism in *Synechocystis* sp. strain PCC6803 shown in KEGG Pathway Database (http://www.genome.jp/kegg-bin/show_pathway?syn00500)

(2) Glycolysis/Gluconeogenesis

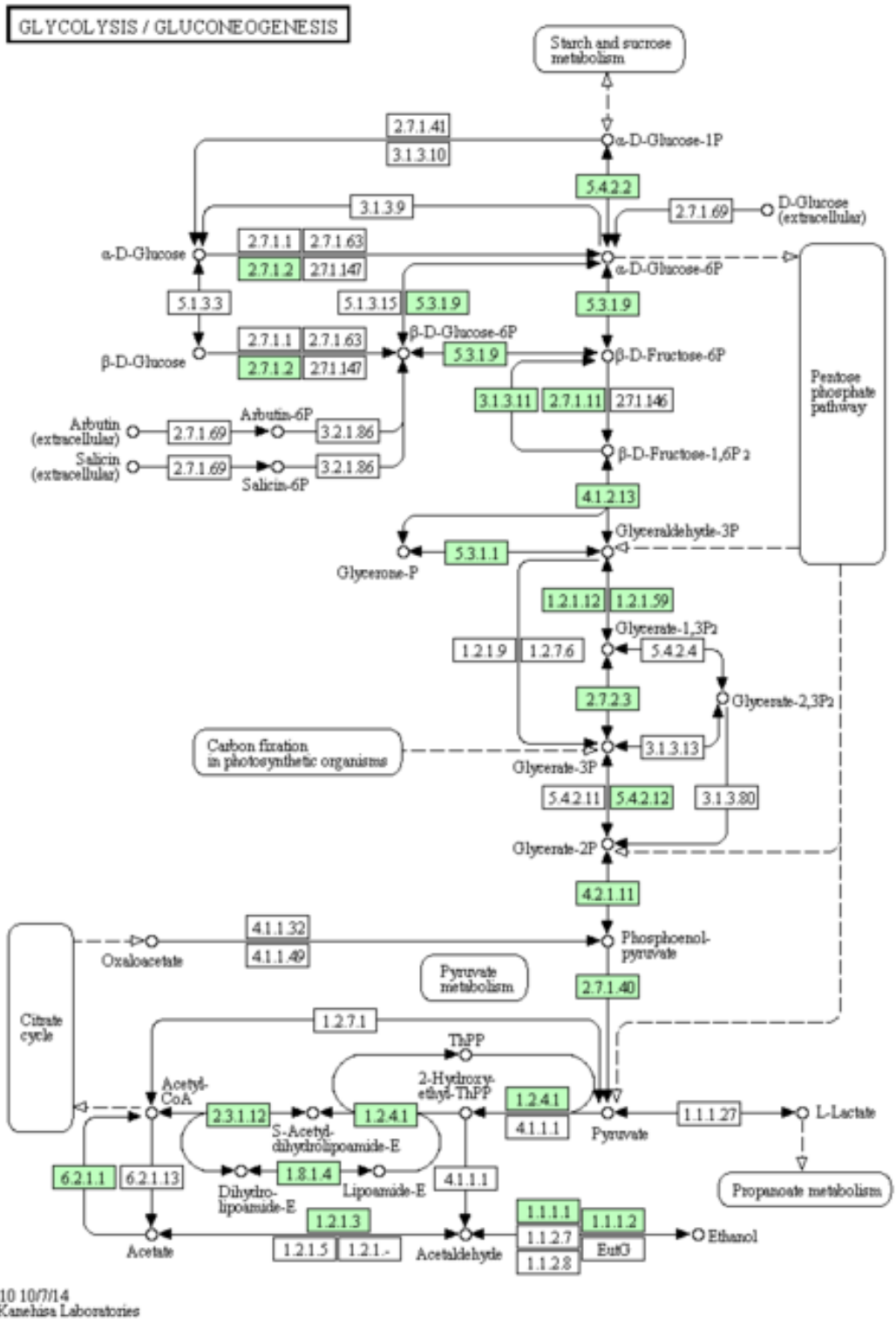

Figure A3.2 Glycolysis/Gluconeogenesis in *Synechocystis* sp. strain PCC6803 shown in KEGG Pathway Database (http://www.genome.jp/kegg-bin/show_pathway?syn00010)

(3) Pentose phosphate pathway

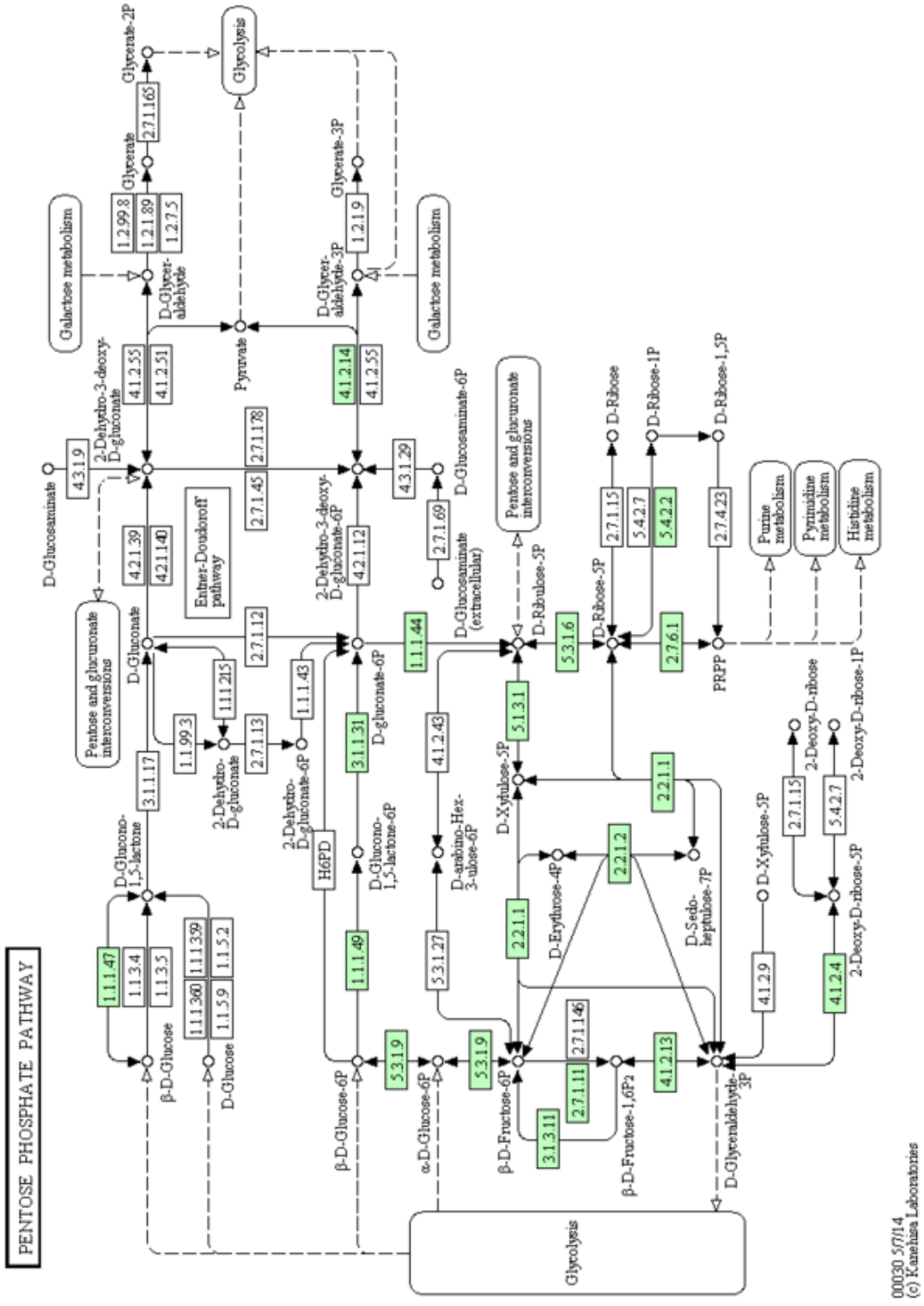

Figure A3.3 Pentose phosphate pathway in *Synechocystis* sp. strain PCC6803 shown in KEGG Pathway Database (http://www.genome.jp/kegg-bin/show_pathway?syn00030)

(4) Pyruvate metabolism

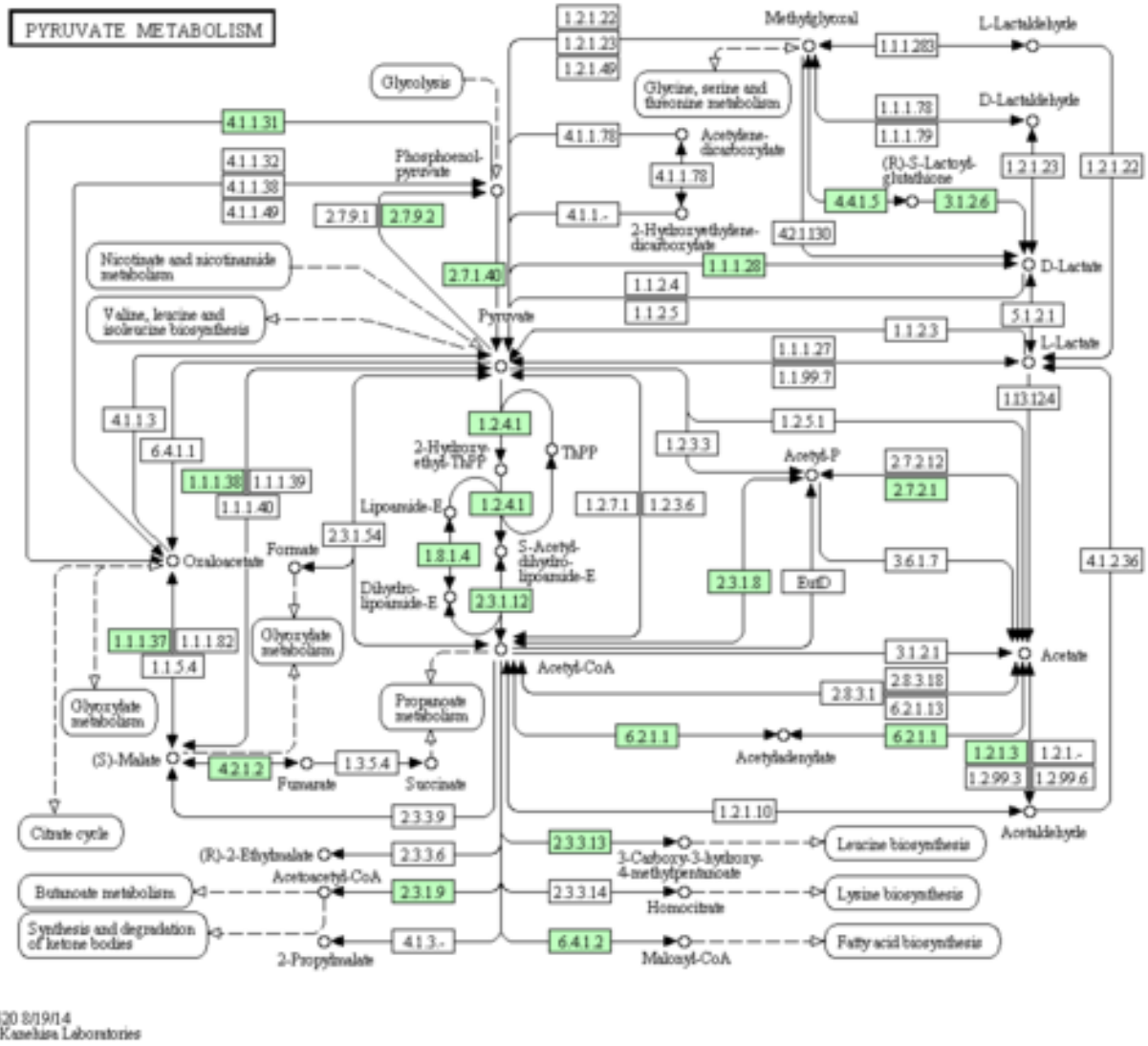

Figure A3.4 Pyruvate metabolism in *Synechocystis* sp. strain PCC6803 shown in KEGG Pathway Database (http://www.genome.jp/kegg-bin/show_pathway?syn00620)

(5) Fructose and mannose metabolism

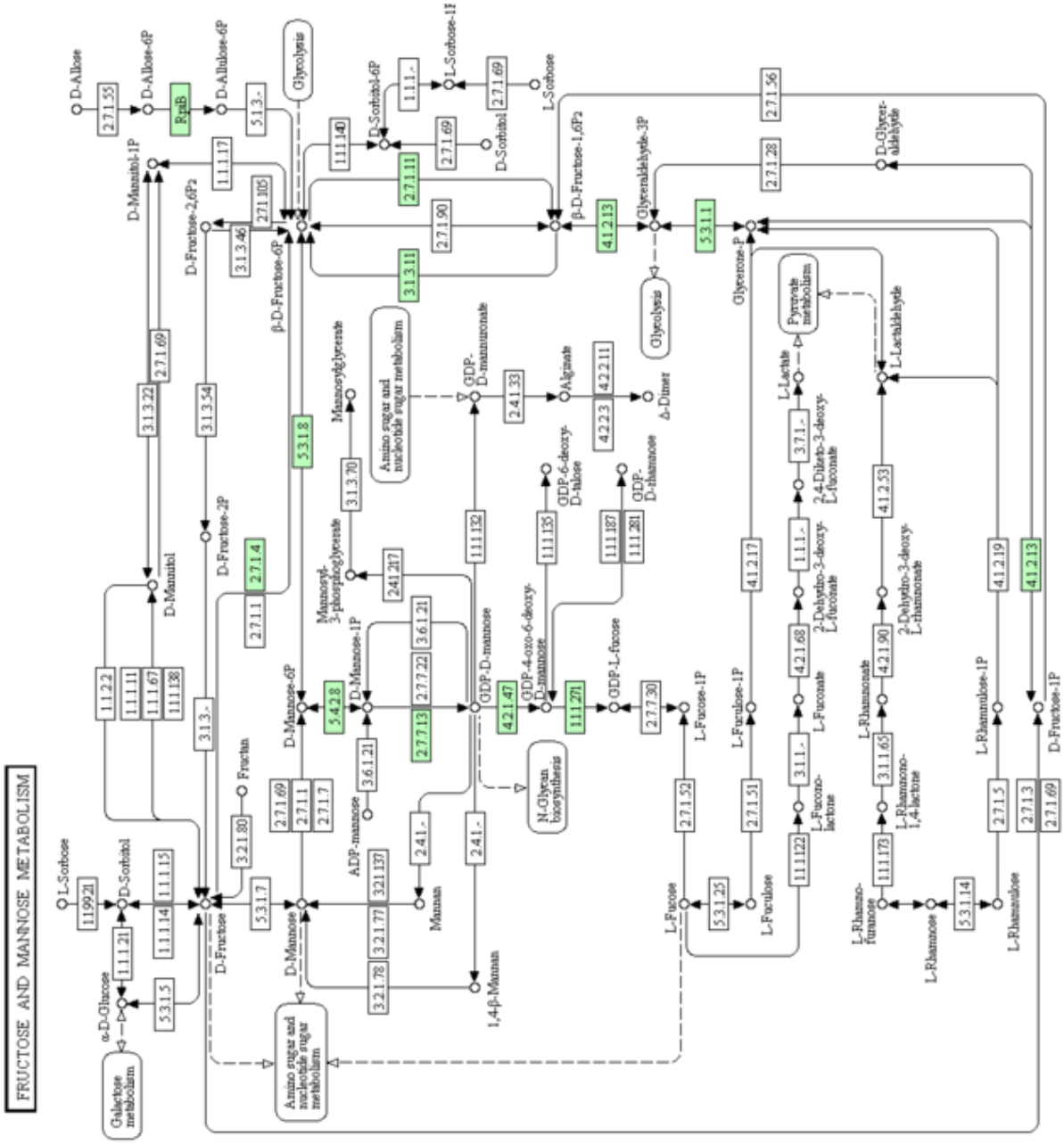

Figure A3.5 Fructose and mannose metabolism in *Synechocystis* sp. strain PCC6803 shown in KEGG Pathway Database (http://www.genome.jp/kegg-bin/show_pathway?syn00051)

(6) Galactose metabolism

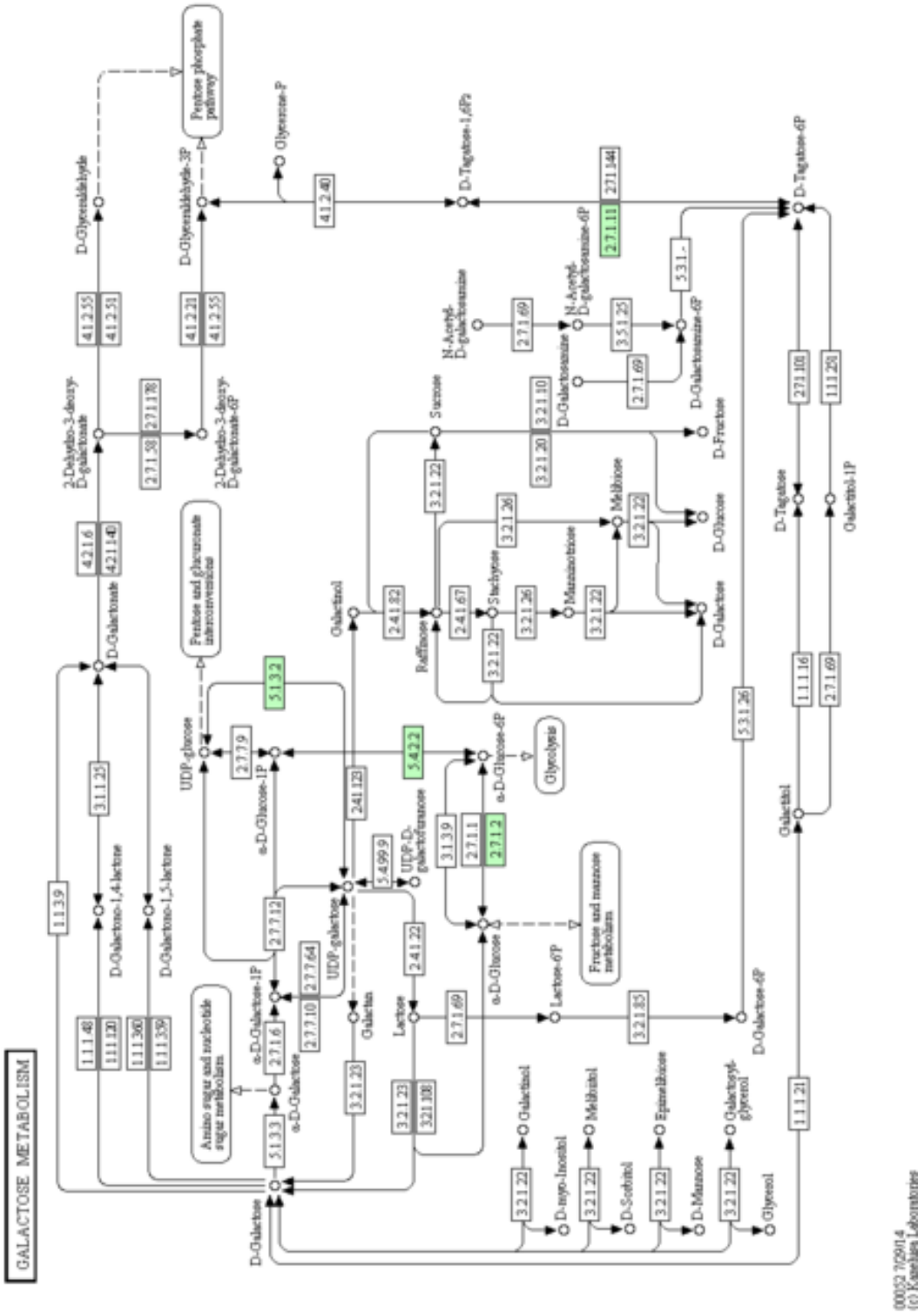

Figure A3.6 Galactose metabolism in *Synechocystis* sp. strain PCC6803 shown in KEGG Pathway Database (http://www.genome.jp/kegg-bin/show_pathway?syn00052)

(7) Pentose and glucuronate interconversions

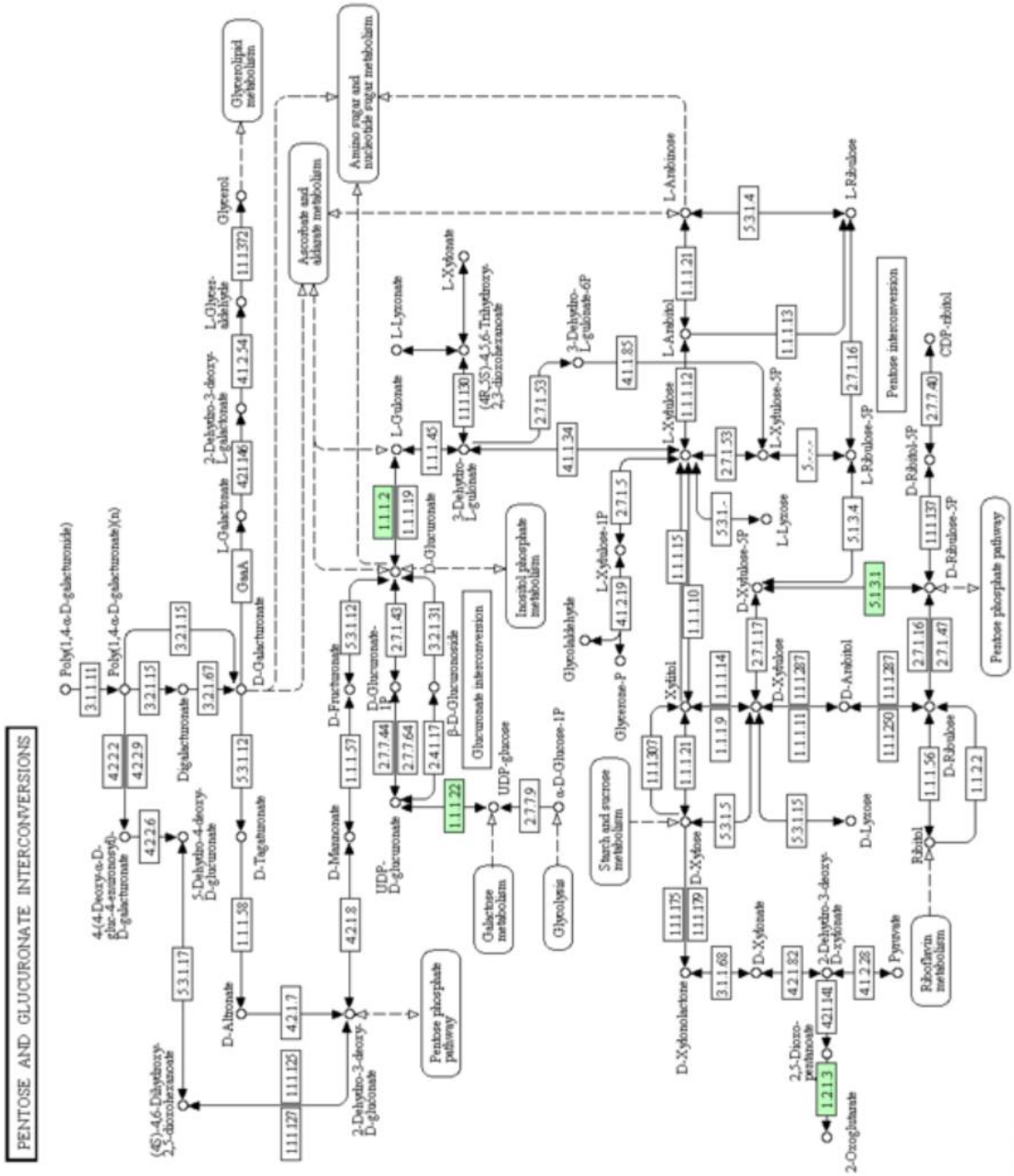

Figure A3.7 Pentose and glucuronate interconversions in *Synechocystis* sp. strain PCC6803 shown in KEGG Pathway Database (http://www.genome.jp/kegg-bin/show_pathway?syn00040)

Appendix-4

Extracellular pigment production from *Synechocystis* sp. strain PCC6803

GT strain cells release reddish orange protein during being kept in HEPPES buffer solution containing glucose under dark-anaerobic condition (**Figure A4.1**). The pigment was able to pass through ultrafilter membrane. This pigment is well dissolved in water. The pigment is known to be involved in cell photoprotection. Possible reasons of this coloration are dark-light stress, nitrogen starvation or anaerobic condition. Absorbance spectrum of the supernatant is shown in **Figure A4.2**.

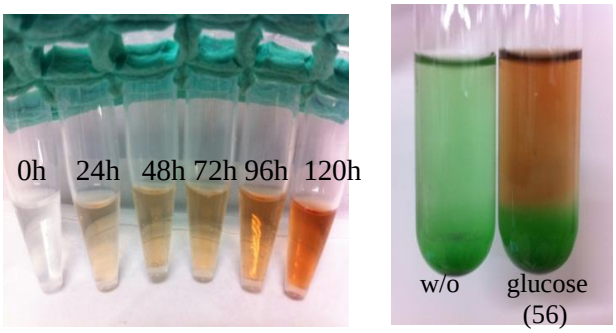

Figure A4.1 Supernatant of cell suspension of GT strain that is dark anaerobically incubated in HEPPES buffer solution with 56 µmol mL^{-1} glucose. Left picture shows color change of isolated supernatant from 0, 24, 48, 72, 96 and 120 h. Right-hand-side picture shows supernatants in working test tube after 120 h fermentation. Test tube was kept standing for several hours for cell sedimentation.

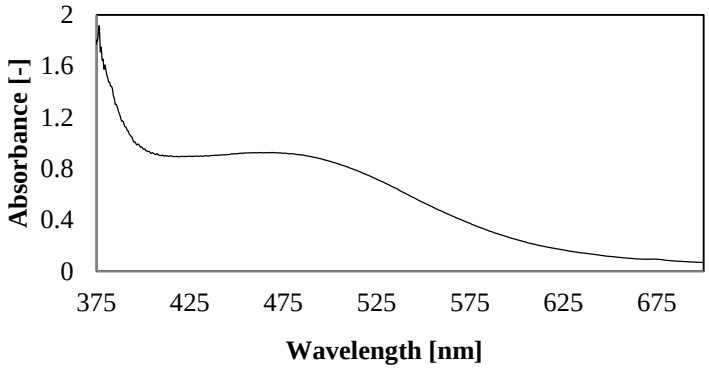

Figure A4.2 Spectrum of peak at 470 nm of supernatant of cell suspension of GT strain in buffer solution. Dark anaerobic incubation of GT strain was made in HEPES buffer solution with 28 µmol mL^{-1} glucose for.96 h.

Appendix: References

Antal TK, Lindblad P (2005) Production of H2 by sulphur-deprived cells of the unicellular cyanobacteria *Gloeocapsa alpicola* and *Synechocystis* sp. PCC 6803 during dark incubation with methane or at various extracellular pH. Journal of Applied Microbiology 98 (1):114-120

Axley M.J, Grahame DA, Stadtman TC (1990) *Escherichia coli* formate-hydrogen lyase. Purification and properties of the selenium-dependent formate dehydrogenase component. Journal of Bioogical. Chemistry 265: 18213–18218.

Blankenship R (1992) Origin and early evolution of photosynthesis. Photosynth Res 33 (2):91-111.

Brenner MP, Bildsten L, Dyson F, Fortson N, Garwin R, Grober R, Hemley R, Hwa T, Joyce G, Katz J (2006) Engineering microorganisms for energy production. DTIC Document,

Burrows EH, Chaplen FWR, Ely RL (2008) Optimization of media nutrient composition for increased photofermentative hydrogen production by *Synechocystis* sp. PCC 6803. International Journal of Hydrogen Energy 33 (21):6092-6099

Ghosh D, Bisaillon A, Hallenbeck PC (2013) Increasing the metabolic capacity of Escherichia coli for hydrogen production through heterologous expression of the *Ralstonia eutropha*. Biotechnology for biofuels. 6:122

Gaffron H (1939) Reduction of carbon dioxide with molecular hydrogen in green algae. Nature 143 (3614):204-205

Gaffron H, Rubin J (1942) Fermentative and Photochemical Production of Hydrogen in Algae. The Journal of General Physiology 26 (2):219-240

Hallebeck,PC (2008) Fermentative hydrogen production: Principles, progress, and prognosis. International Journal of Hydrogen Energy. 34:7379-7389

McKinlay JB, Harwood CS (2010) Photobiological production of hydrogen gas as a biofuel. Current Opinion in Biotechnology 21 (3):244-251

Maeda K, Domen K (2010) Photocatalytic Water Splitting: Recent Progress and Future Challenges. The Journal of Physical Chemistry Letters 1 (18):2655-2661

Mathews J, Wang G (2009) Metabolic pathway engineering for enhanced biohydrogen production. International Journal of Hydrogen Energy 34 (17):7404-7416

Oh Y-K, Raj SM, Jung GY, Park S (2011) Current status of the metabolic engineering of microorganisms for biohydrogen production. Bioresource Technology 102 (18):8357-8367.

Rozendal RA, Hamelers HVM, Euverink GJW, Metz SJ, Buisman CJN (2006) Principle and perspectives of hydrogen production through biocatalyzed electrolysis. International Journal of Hydrogen Energy 31 (12):1632-1640

Tamagnini P, Axelsson R, Lindberg P, Oxelfelt F, Wünschiers R, Lindblad P (2002) Hydrogenases and Hydrogen Metabolism of Cyanobacteria. Microbiology and Molecular Biology Reviews 66 (1):1-20. doi:10.1128/mmbr.66.1.1-20.2002

Yu J, Takahashi P (2007) Biophotolysis-based hydrogen production by cyanobacteria and green microalgae. Communicating Current Research and Educational Topics and Trends in Applied Microbiology 1:79-89